Dynamics of the Coronavirus Replicative Structures

Marne Casper Hagemeijer

Cover design by Robert Bakelaar
Printed by Proeftschriftmaken.nl
ISBN: 978-90-393-5667-8

Aan mijn ouders

Dynamics of the Coronavirus Replicative Structures

Dynamiek van de Coronavirus Replicatie Structuren
(met een samenvatting in het Nederlands)

PROEFSCHRIFT

ter verkrijging van de graad van doctor aan de Universiteit Utrecht
op gezag van de rector magnificus, prof. dr. G.J. Van der Zwaan, ingevolge
het besluit van het college voor promoties in het openbaar te verdedigen op
donderdag 27 oktober 2011 des middags te 12.45 uur

door

Marne Casper Hagemeijer

geboren op 29 juni 1983 te 's-Gravenhage

Promotor: Prof. dr. P.J.M. Rottier
Co-promotor: Dr. C.A.M. de Haan

Contents

Chapter 1

General Introduction

Viruses are small infectious agents able to cause a variety of diseases in all living organisms. The word *virus* comes from Latin and means venom or poison. This notion of viruses originates from the late nineteenth century when Dmitrii Ivanovsky and Martinus Beijerinck independently reported that tobacco mosaic disease (TMD), an infection of tobacco plants, was caused by a "*contagium vivum fluidum*", which means contagious living liquid (5, 53). With the observation that these infectious agents are unable to replicate independently but require a host to multiply themselves, the initial concept of a virus was established and is now considered the foundation of the field of virology [reviewed in (37, 38)].

Our understanding of viruses has increased considerably since the discovery of the first virus, tobacco mosaic virus (TMV), in 1898. Nowadays, we know that viruses are not living organisms as they lack any means of energy generation or metabolism. Consequently, viruses depend entirely on the machinery of the infected host cell to produce progeny and to evolve. They are obligate intracellular parasites that can be defined structurally as (cellular-derived) molecular assemblies build of proteins, nucleic acids, lipids, and carbohydrates. When compared to other organisms, they are relatively simple by (i) the size and nature of their genomes, (ii) their morphology, (iii) coding strategies, and (iv) tropisms (37, 38). Yet, they are complicated for their complex replication strategies, adaptive features and pathogenic mechanisms. The characteristics of viruses have been used for their classification leading to a division based on order, family, subfamily, genus and species (49). Alternatively, a division was made according to the way by which viral messenger RNAs (mRNAs) are generated in infected cells (2).

The most abundant viruses in nature are those of which the genetic material consists of a positive single-stranded RNA (+ ssRNA) genome. To this category of viruses significant human pathogens belong, with poliovirus (PV), hepatitis C virus (HCV) and the severe acute respiratory syndrome (SARS)-coronavirus (CoV) as notorious examples. A distinctive common feature of + ssRNA viruses is the replication of their genomes in the cytoplasm of the host cell, a process that is associated with rearranged cellular membranes. Such cytoplasmic organelle-like membranous structures have been described among others for + ssRNA family members of the *Picornaviridae*, *Flaviviridae*, *Togaviridae*, *Arteriviridae*, *Bromoviridae*, *Nodaviridae,* and the *Coronaviridae* [reviewed in (23, 24, 73)]. These membrane rearrangements seem to be beneficial for (i) sequestering and concentrating all viral and cellular components necessary for viral RNA synthesis and (ii) to provide a protective microenvironment against virus-elicited host defense mechanisms.

The various membrane rearrangements of the + ssRNA viruses range in size from 40 to 400 nm, contain lipids that are derived from various cellular compartments and demonstrate an impressively diverse plethora of morphologies that include, among others, clusters of vesicles for the *Picorna-* and *Togaviridae*, spherule-like invaginations for the *Bromoviridae* and *Nodaviridae*, vesicle packets and membranous webs for the *Flaviviridae* and double-membrane vesicles and convoluted membrane assemblies for the *Arteri-* and *Coronaviridae* [reviewed in (23, 24, 73)]. Although the elucidation of the biogenesis and functioning of these virus-induced membrane structures is an active field of research, still not much is known with respect to the mechanisms underlying the assembly, dynamics and RNA synthesizing activity of the CoV membrane-associated replication complexes.

THE *CORONAVIRINAE*

The *Coronaviridae* are a family of evolutionary related + ssRNA viruses that together with the *Arteriviridae* and the *Roniviridae*, belong to the order of the *Nidovirales*. A taxonomical revision has recently been proposed to divide the *Coronaviridae* family into two subfamilies, the *Coronavirinae* and the *Torovirinae*. The *Coronavirinae* comprise the genera *Alpha-*, *Beta-*, and *Gamma coronaviruses*, while the *Torovirinae* consist of the genera *Toro-* and *Bafiniviruses* (17) (Fig. 1A).

Historically, CoVs have been recognized as important infectious agents to domestic livestock, poultry and companion animals. In contrast to the animal viruses, human CoVs (HCoVs) have been associated with relatively mild upper and lower respiratory tract infections, including ordinary common colds. However, in 2002 the outbreak of a novel HCoV in China, causing severe fatal atypical pneumonia in infected individuals, demonstrated that HCoVs were also able to induce severe life-threatening disease to humans. This virus was called the SARS-CoV (31, 62) and emerged in the human population from an animal reservoir, probably originating from bats, with palm civet cats probably acting as intermediate hosts (46, 66).

Architecture of the Coronavirion

CoVs are eveloped pleiomorphic viruses with varying size (80 – 120 nm in diameter) and shape. The mouse hepatitis virus strain A59 (MHV-A59), the prototype CoV that has been used in the studies described in this thesis, has a spherical shape and a relatively homogenous size of 85 nm in diameter (3). A schematic representation of the coronavirion is depicted in Fig. 1B. The

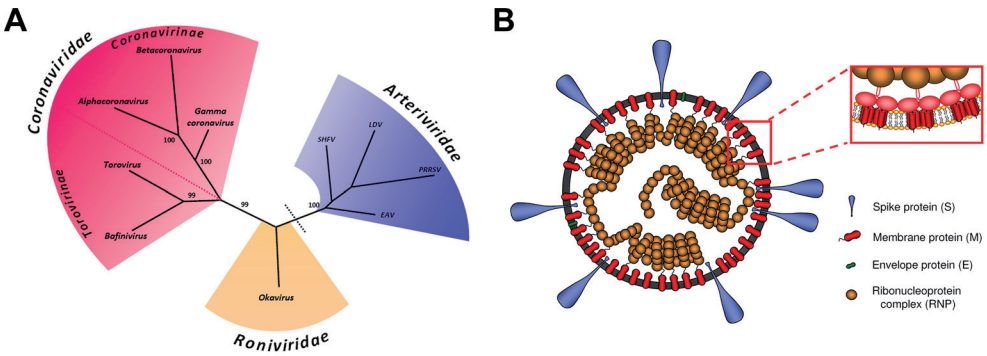

Figure 1. *Nidovirales* phylogeny and model of the coronavirion. (A) The evolutionary relationships between the *Corona-*, *Roni-*, and *Arteriviridae*. Shown is an unrooted maximum parsimonious tree based upon multiple nucleotide sequence alignments of the RNA-dependent RNA polymerase – Helicase region of representative members of the Nidoviruses. *Picture kindly provided by Raoul de Groot and adapted from (41).* (B) Schematic representation of the MHV-A59 particle. The envelope contains three membrane proteins: the spike (S), membrane (M) and envelope (E) protein. The interior harbors the genomic RNA that is encapsidated by multiple nucleocapsid (N) proteins thereby forming the ribonucleoprotein (RNP) complex. The inset shows that the C-terminal domain of M forms an additional layer that coats the interior of the lipid membrane and interacts with the RNP. *Picture kindly provided by Berend Jan Bosch and adapted from (3).*

lipid envelope harbors three integral membrane proteins: the triple-spanning membrane (M) protein, the small hydrophobic envelope (E) protein, and the spike (S) class I fusion glycoprotein. Certain *betacoronaviruses* contain an additional structural protein, the hemagglutinin-esterase (HE) envelope membrane protein that contains sialic acid binding and acetyl esterase activities. However, in MHV-A59 the HE gene has been lost from the genome during *in vitro* passaging of the virus indicating that its function was apparently not beneficial under these conditions (67).

The S proteins are present as trimers in the virion membrane and is the major determinant for cell tropism and responsible for receptor binding and entry by mediating fusion of viral and cellular membranes (7). The M protein is the most abundant component of the coronavirion envelope. It is important for virus assembly by functioning as a scaffold, thereby interacting with all components of the envelope and orchestrating virion assembly [reviewed in (19)]. The E protein, which is only present in minor amounts in the viral lipid bilayer and which has been shown to exhibit ion channel activity (70, 109), is also important for virus production (104).

The only structural protein not present in the viral envelope is the nucleocapsid (N) protein. This multifunctional protein is present in the interior of the virion and by being the capsid protein its major function is

to package the genomic RNA into a helical nucleocapsid structure, termed the ribonucleoprotein (RNP) complex. The RNP complex is densely packed, which is probably necessary because of the enormous size of the RNA genome, and is located underneath the viral envelope (3) interacting with the carboxy-terminal domain of the M protein (64).

Coronavirus genome organization and gene expression

Among the + ssRNA viruses, CoVs clearly distinguish themselves by carrying the most complex and largest genomes, which range in size from ~26 to 32 kb (42). Despite the variation in size, the overall genome organization of the various CoVs is quite conserved. The genome contains all the genetic information to direct both *replication*, the synthesis of full-length genomic RNA, and *transcription*, the (discontinuous) production of subgenomic mRNAs (85).

The linear + ssRNA genome of CoVs is 3' polyadenylated and has a 5' cap structure, thereby mimicking cellular mRNAs. The 5' and 3' ends of the genome contain untranslated regions (UTRs) with *cis*-acting elements that are important for replication and transcription. Two-thirds of the genome consists of two large open reading frames (ORFs), ORF1a and ORF1b. The remaining 3' one-third part encodes the structural proteins interspersed with sequences encoding some accessory proteins. A schematic picture of the MHV-A59 genome is shown in Fig. 2A.

Translation of ORF1a and ORF1b generates two very large replicase polyproteins, pp1a and pp1ab. The latter is synthesized via a -1 ribosomal frameshift mechanism mediated by a pseudoknot structural element at the end of ORF1a (10, 11). These replicase polyproteins are extensively processed by viral proteinases, resulting in the generation of sixteen nonstructural proteins (nsps) that together (with the N protein, see next section) form the replication-transcription complexes (RTCs). A schematic representation of the CoV replicase polyprotein is shown in Fig. 2B.

The structural and the accessory proteins are expressed from a nested set of 3' coterminal subgenomic (sg) mRNAs that are generated via discontinuous transcription during subgenome-length minus-strand RNA synthesis (84). The RNA-dependent RNA polymerase (RdRp) copies the genomic positive-sense RNA into a negative-sense template until it reaches a transcription-regulation sequence (TRS). At this point, RNA synthesis may either continue or the RdRp may relocate to the 5' end of the genome and complete the negative-sense sgRNA. These negative-sense sgRNAs serve as templates for the synthesis of the corresponding positive-sense sgRNAs. As a result,

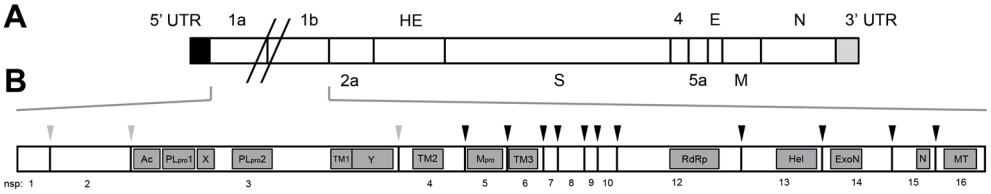

Figure 2. MHV-A59 genome and replicase polyprotein organization. (A) The linear + ssRNA genome is approximately ~32 kb in size. A 5' cap structure and a 3' poly(A) tail are present, together with UTRs. Two-thirds of the genome encodes the two large ORFs, ORF1a and ORF1b, which encode the nonstructural proteins (nsps). The remaining one-third of the genome encodes the structural proteins (HE, S, E, M and N), interspaced by the group-specific proteins (2a, 4, 5a). (B) Viral proteinases residing in nsp3 ($PL1_{PRO}$ and $PL2_{PRO}$; grey arrowheads indicate cleavage sites) and nsp5 (M^{PRO}; black arrowheads indicate cleavage sites) respectively, process pp1ab into 16 nsps. Hydrophic regions reside in nsp3, nsp4 and nsp6 (TM1, TM2 and TM3, respectively). Predicted and identified RNA(-modifying) enzymes are indicated: the RNA-dependent RNA polymerase (RdRP; nsp12), the helicase (Hel; nsp13), the exonuclease (ExoN), the uridylate-specific endoribonuclease (N), and the methyl transferase (MT). *Adapted from (42).*

the positive-sense sgRNAs form a nested set of mRNAs, which extend for different lengths from a common 3' terminus while also having a common 5' end, which is known as the leader sequence. Generally, only the 5' first unique gene of each sgRNA is translated [reviewed in (85)].

The coronavirus infection cycle

The CoV infection cycle can be divided into several steps: (i) attachment and entry, (ii) replication and transcription, and (iii) assembly and release. A description of each of these steps is given in the following sections and illustrated in Fig. 3.

The first step of the infection is for the virion to gain access to a susceptible host cell. The amino-terminal S1 domain of the viral S glycoprotein (63) binds to the cellular receptor, which for MHV-A59 is the murine carcinoembryonic antigen-related cell adhesion molecule 1 (CEACAM1) (32, 108), after which the virion enters the cell via the clathrin-mediated endocytic pathway (35). Viral attachment by the S1 subunit triggers a conformational change in the S protein, which exposes the membrane-anchored S2 subunit that is responsible for viral and cellular membrane fusion (110). The merging of these membranes results in the release of the RNP complex into the cytoplasm of the infected cell.

Translation of the genome results in the synthesis of pp1a and pp1ab. These two large polyproteins are processed by viral proteinases [reviewed in (114)] into sixteen nsps. Together with the N protein (8, 28, 101, 105) and yet to be

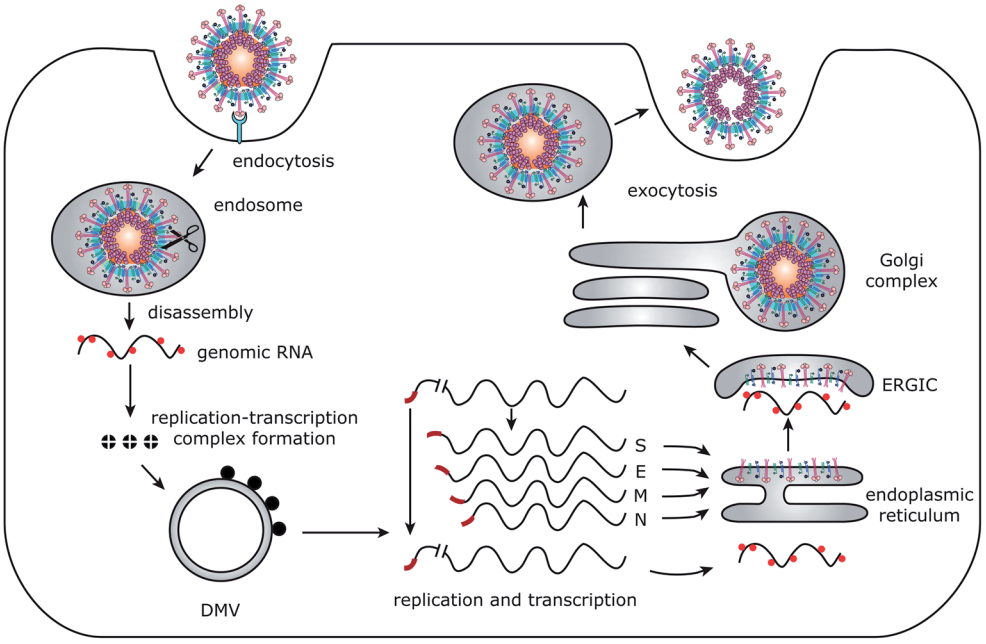

Figure 3. MHV-A59 infection cycle. The MHV-A59 virion binds to the cellular CEACAM1 receptor after which it is taken up via endocytosis. Fusion of the endosomal and viral membranes releases the genomic RNA into the cytoplasm of the cell. Translation of the genome results in the generation of pp1a and pp1ab, which are processed into 16 nsps. These nsps induce the formation of double-membrane vesicles (DMVs) with which replication-transcription complexes are associated. Replication and transcription results in the synthesis of genomic and subgenomic RNAs, the latter are translated into the structural proteins S, E, M, and N. The (full-length) genomic RNA is encapsidated by multiple copies of the N protein and meets the structural proteins at the ER-to-Golgi intermediate compartment (ERGIC). Here, new virions are formed via budding after which they are released from the cell via the secretory pathway. *Adapted from (20).*

identified cellular host proteins, the nsps and/or their precursor proteins form the CoV RTCs. Once the RTCs are formed, the full-length + ssRNA genome is copied into negative strands that serve as templates for the synthesis of the plus-sense full-length genomic RNA and of the sgRNAs, as described above. Minus- and plus-strand RNA synthesis is already detected at 75 to 90 min post infection (p.i.) (85). Minus-strand synthesis, of which the resulting RNA species are mainly present as double-stranded (ds) intermediates because of their association with plus-strand RNA molecules, peaks at 5 to 6 h p.i., after which their synthesis declines but does not stop (83). The plus-stranded RNAs are produced in a 50- to 100-fold excess over their minus-strand counterparts (82, 85).

The final step of the CoV life cycle is the assembly of the virion components, i.e. genomic RNA, N, M, E, and S, into a new viral particle and its subsequent release from the cell. The genomic RNA is encapsidated

in the cytoplasm by multiple copies of the N protein (19), thereby forming the helical RNP. Whether the RNP complex is generated at the replicative structures and subsequently transported to the sites of viral budding, the ER-to-Golgi intermediate compartment (ERGIC), or whether formation of the RNP occurs at the ERGIC itself is presently unknown. The viral envelope is acquired by budding of the RNP through the lipid bilayer of the ERGIC (59, 95). The M protein is the key player in assembly as it interacts with all other virion components, as already mentioned earlier. After budding, the virus particle is released from the cell via the secretory pathway.

THE CORONAVIRUS REPLICATION MACHINERY

Processing of the CoV polyprotein(s) by the viral proteinases

To generate the functional CoV replication complexes, the replicase polyproteins pp1a and pp1ab have to be proteolytically processed to liberate the sixteen individual protein products. Cleavage of pp1a and pp1ab is performed by two viral proteinases that reside in nsp3 and nsp5: the papain-like proteases ($PL1_{PRO}$ and $PL2_{PRO}$) located in nsp3 and the chymotrypsin-like cysteine proteinase ($3CL^{PRO}$), *or* main protease [M^{PRO}], present in nsp5.

The first proteins to be released from pp1a and/or pp1ab are nsp1 to nsp3. Cotranslational cleavage by $PL1_{PRO}$ between nsp1|nsp2 liberates the mature nsp1 protein (p28) and generates the nsp2/3 precursor protein (p250 or p290) (26, 27, 44), whereas cleavage between nsp2|nsp3 releases nsp2 (p65) (44, 47). Processing of the nsp3|nsp4 cleavage site by $PL2_{PRO}$ releases the nsp3 protein (p210) (44, 57). The remaining nsps located downstream of nsp3, i.e., nsp4 to nsp16, are released by nsp5 ($3CL^{PRO}$; p27). First, an ORF1a-expressed large nsp4-nsp10 precursor protein (p150) is generated (57, 88), which is processed into the individual mature proteins (8, 22, 57, 68, 88) by nsp5. Also the ORF1b-encoded nsps are processed by nsp5 into functional subunits (25). It is thought that the intermediate and precursor polyproteins may somehow be involved in the temporal regulation of plus and/or minus sense viral RNA synthesis (22, 86, 114).

The CoV RNA-dependent RNA polymerases: nsp8 and nsp12

Once released in the cytoplasm of the infected cell, replication of the positive-sense CoV genome has to be initiated. Eukaryotic cells do not possess the machinery that is required for this essential step in the CoV life cycle. As a consequence, CoV encode the enzymatic functions necessary for replication and transcription in their genome.

The key replicative enzyme involved in genome replication is the RNA-dependent RNA polymerase (RdRp), which is present in nsp12; this enzymatic function is genetically conserved throughout the order of the *Nidovirales* (42). The nsp12 protein is able to utilize both homo- and heteropolymeric RNAs as template but its RdRp activity is dependent on primers to copy the viral RNA (100). These primers might be produced by a non-canonical RdRp activity that has been described for the nsp8-encoded 'RNA primase', as this protein is able to produce short oligonucleotides complementary to the RNA genome (48). Nsp8 has been shown to form together with nsp7 a hexadecameric complex, consisting of eight copies of each protein, thereby forming a channel that can harbor RNA and may serve as a processivity factor for nsp12 (111).

The auxiliary troops: RNA-modifying enzymes

CoVs possess the largest genomes among the + ssRNA viruses (42). They encode a large number of additional RNA-modifying enzymes, which are often not present in other RNA viruses. These additional enzymatic activities are probably required to ensure proper RNA synthesis and might account for their large size.

Unwinding of (ribo)nucleic acids is mediated by helicases. The CoV nsp13 protein contains a superfamily 1 helicase domain with an amino-terminal zinc-binding domain that is important for the unwinding activity of duplex RNA (and DNA) in a 5'-to-3' direction (89, 90, 99). The resulting single-strands probably serve as templates for RNA synthesis. The multifunctional nsp13 protein additionally possesses nucleotide triphosphatase activity (51, 52, 89) and is likely to be involved in removal of one of the terminal phosphate groups at the 5' end of the positive-sense RNAs, which is the first step in the formation of the 5' cap structure. Although the enzyme that subsequently adds the guanine to the terminal phosphates (guanylyl transferase) has not been identified yet, nsp14 has been shown to exert S-adenosyl-L-methionine (AdoMet)-dependent (guanine-N7)-methyltransferase (N7-MTase) activity (15). Finally, the cap-1 structure is formed by the AdoMet-dependent (nucleoside-2'O)-methyltransferase (2'O-MTase) activity that is present in nsp16 (21), for which the latter needs to form a complex with nsp10 (9, 69).

The CoV genome also encodes some enzymatic functions not found in other RNA viruses. In addition to the cap N7-MTase activity, nsp14 has metal ion-dependent 3'-to-5' exoribonuclease (ExoN) activity (74) and contains a *nidoviral* uridylate-specific endoribonuclease (NendoU; nsp15) (50), both able to degrade ssRNA and dsRNA (6, 50). While the function of the NendoU activity in the CoV infection cycle is not known, it appears that the ExoN

activity is required to ensure high replication fidelity of the extremely large CoV genome (33).

CoVs possess several other RNA-binding proteins. Nsp9, which contains an oligosaccharide/oligonucleotide (OB)-like fold that was not reported earlier for RNA viruses (34), is able to (non-specifically) bind ssRNA (34, 98). Dimerization of this protein, although not important for RNA binding, is essential for viral growth (72). Also nsp10 possesses RNA-binding properties. Twelve subunits of nsp10 assemble into a spherical dodecameric structure (97) that is able to bind (ss)RNA molecules, mediated by two zinc-finger domains (54, 71). Mutations engineered near the zinc-finger domains resulted in a decrease of viral RNA synthesis (30).

Fighting the host immune response

Several nsps synthesized by CoVs play a role in the evasion of the anti-viral response of the host. Whereas nsp1 degrades host mRNAs (56), including those of the type I interferon (IFN) system (76), thus suppressing innate immune responses (107, 115), the $PL2_{PRO}$ activity of nsp3 inhibits phosphorylation and nuclear translocation of IFN-regulatory factor 3 (IRF-3) (29) by either deubiquitination and binding to IRF-3 (113) or by delaying dissociation of TANK-binding kinase-1 (TBK1) (106). Another activity exhibited by nsp3, that of ADP-ribose-1"-monophosphatase (ADRP), also interferes with innate responses as the lack of this activity gave rise to increased type I IFN responses (36, 65). The nsp1 protein can induce cell cycle arrest in the G_0/G_1 phase (14) and by interacting with the 40S ribosomal subunit induce the modification of cellular mRNA cap structures and translational host shut-off (55).

Membrane anchors and inducers of the replicative structures

The primary structures of three nsps, i.e., nsp3, nsp4, and nsp6, contain hydrophobic stretches and these proteins are therefore predicted to be integral membrane proteins. Indeed, for the nsp3 and nsp4 proteins of SARS-CoV (47, 78) and MHV (58, 78) membrane association has been demonstrated. The nsp3 protein is co-translationally inserted into the endoplasmic reticulum (ER) membrane and becomes *N*-glycosylated (58). The nsp4 protein when expressed *in trans*, is inserted into the ER, becomes *N*-glycosylated, and relocalizes upon infection to the RTCs (78). This protein is essential for viral replication although the carboxy-terminal domain and the fourth predicted hydrophobic domain are not required (94). However, detailed information on the membrane anchoring, topology and processing of these (putative) transmembrane domain containing nsps is lacking, even while these proteins

are likely to play an important role in the biogenesis of the membranous structures that are associated with virus replication and in the anchoring of the RTCs to these structures.

Additional RTC-associated proteins

The function of the nsp2 protein in CoV replication is not known. Deletion of the nsp2-encoding region from the genome resulted in a recombinant virus that was viable, albeit with reduced levels of replication and reduced titers (45). Despite its dispensability in cell culture, nsp2 is likely to have an important function because evolutionary pressure did not remove the genetic information coding for this protein from the CoV genome.

In addition to its structural role in the coronavirion, i.e. packaging of the genomic RNA into the RNP complex, the multifunctional nucleocapsid (N) protein is also important in coronavirus replication and has been detected in the perinuclear region of infected cells colocalizing with markers for the RTCs (8, 28, 101, 105). This RNA-binding protein is able to associate with high affinity to all CoV mRNA species (4, 75, 96). Interestingly, the absence of N greatly impairs CoV replication, while addition of the N protein *in trans* early in infection enhances CoV genomic RNA synthesis significantly (1, 87).

INTRACELLULAR MEMBRANE MODIFICATIONS

Organelle-like membranous replicative structures and RNA synthesis

During the work described in this thesis, several papers were published that characterized the membrane rearrangements observed in CoV-infected cells. The first detectable membrane rearrangements are 200 to 350 nm organelle-like structures that have been described for both MHV-A59 (43, 101) and the SARS-CoV (40, 92) and consist of spherical double lipid bilayers, termed double-membrane vesicles (DMVs; Fig. 4A and 4B). In between the clusters of DMVs, reticular convoluted membrane assemblies (CMs) are present (16, 60, 101). Later in infection large virion-containing vesicles (LVCVs) (40, 60, 77, 101), highly organized cubic membrane structures (40, 101) and condensed tubular bodies (16, 101) are formed. The latter two structures are likely a result of the overexpression of CoV structural proteins during infection and do not seem to be involved in CoV replication (101).

Electron tomography was used to show that in SARS-CoV infected cells the DMVs and CMs form an interconnected network that is also continuous with the ER (60). This latter observation is in agreement with previous reports describing DMVs in close proximity to the ER or continuous with it (40,

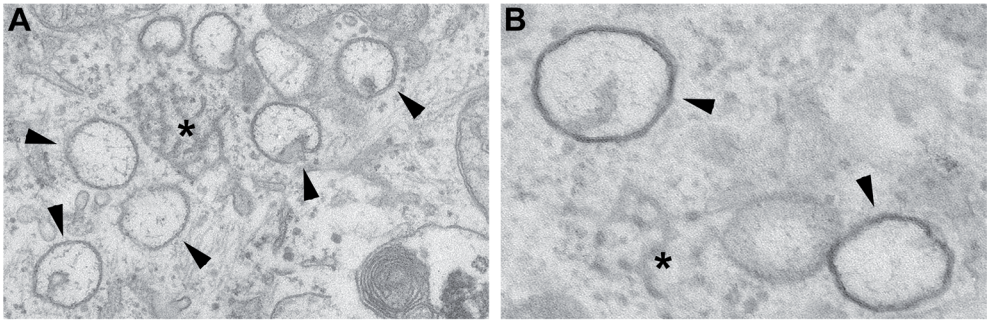

Figure 4. Ultrastructure of CoV-induced replicative structures. HELA-CEACAM1a cells infected with MHV-A59 and processed for EM. (A) Cytoplasmic vesicles that contain a double-lipid bilayer (DMVs) are indicated by the arrowheads. In between the clusters of DMVs, convoluted membrane (CM) assemblies are observed that consist of small networks of membranes (indicated by the asterisks). (B) A higher magnification clearly demonstrating the double lipid bilayer of the DMVs. *Pictures are kindly provided by Mustafa Ulasli and Fulvio Reggiori from the Cell Biology Department of the University Medical Center Utrecht, the Netherlands.*

43, 92). Moreover, (partial) colocalization of replicase proteins together with the ER resident protein disulfide isomerase (PDI) has been reported (92), while also the translocon subunit Sec61α was found to be redistributed to the replicative structures upon SARS-CoV infection (61). The combined data indicate that the ER is the most likely membrane donor for the DMVs, despite the absence of most conventional ER markers on these structures (78, 92, 101, 105).

The CoV replicative structures, i.e., DMVs and CMs, are associated with viral RNA synthesis, as the MHV and SARS-CoV nsps have been shown to localize to these structures (22, 40, 45, 60, 78, 79, 81, 91, 92, 101, 102). Newly synthesized viral RNA, visualized by 5-bromouridine 5'-triphosphate (BrUTP) labeling, colocalizes with antibodies recognizing either nsp5 or the C-terminal part of pp1a (102), and was observed in close proximity to the DMVs by immunoelectron microscopy in MHV-infected cells (43, 102). In addition, antibodies recognizing dsRNA, the presumed replicative intermediates, labeled the interior of the SARS-CoV-induced DMVs (60). Although CoV RNA synthesis appears to be protected by membranes (103) it is still unclear whether synthesis of nascent viral RNA occurs at sites of dsRNA accumulation, as no pores connecting the interior of the coronavirus DMVs with the cytoplasm have been detected.

Involvement of cellular pathways in DMV biogenesis

In agreement with the ER being the most likely membrane donor of the DMVs, an intimate association between the early secretory pathway

and CoV replication has been reported. Interference with this pathway by blocking protein export at ER exit sites in MHV-infected cells by treatment with the kinase inhibitor H89 or by overexpression of a dominant active Sar1 mutant resulted in inhibition of replication and RTC formation (78). Also treatment with Brefeldin A (BFA), an inhibitor of ER to Golgi trafficking, or knockdown of GBF1, inhibited MHV replication while reducing the number of DMVs (105). Similar results were published for SARS-CoV infected cells treated with BFA and it was noticed that the inner and outer membranes of the DMVs were separated in BFA-treated cells (61), which probably explains the observed inhibition of viral replication.

Initial ultrastructural studies have revealed that the morphology of the DMVs resembles those of autophagosomes in that both structures have a double lipid bilayer, which is suggestive of an autophagosomal lipid origin of the CoV DMVs. However, conflicting data on this topic have been published. Thus, early studies revealed a colocalization between the autophagosomal protein marker microtubule-associated protein light-chain 3 (LC3/Atg8) with the replicative structures (80, 112); moreover, viral replication was impaired and DMVs were not detected in the absence of the essential autophagy protein Atg5 (80). Others were, however, unable to reproduce the colocalization data (18, 92), whereas the requirement of Atg5 seemed to be cell type specific (112). More recently, coronavirus replication was also shown not to be affected in autophagy-deficient cells lacking Atg7 (81). In contrast to autophagosomes, CoV replicative structures were shown to recruit the non-lipidated form of LC3, while they were not decorated with ectopically expressed GFP-LC3. Similar findings have been reported for EDEMosomes (12, 13), ER-derived vesicles that transport ER chaperones to lysosomes. As the EDEMosome cargo proteins EDEM1 and OS-9 were also detected on the CoV replicative structures, it was proposed that CoVs hijack EDEMosomes for their replication (81).

AIM AND OUTLINE OF THE THESIS

The last few decades have provided coronavirologists with exciting new findings with respect to functions and structures of individual replicase proteins and regarding the characterization of the CoV-induced membranous structures. Nonetheless, fundamental questions concerning the biogenesis of the DMVs, the functioning of the nsps in RTC assembly, membrane anchoring and viral RNA synthesis, and the precise location of RNA synthesis remain to be elucidated.

Essentially nothing is known about the induction of the membranous replicative structures in CoV-infected cells and how the individual nsps and other necessary constituents are recruited to these sites. It is, however, likely that the (putative) transmembrane-containing nsps not only function in the membrane anchoring of the RTCs but also induce the formation of the membranous structures. The involvement of these nsps in the formation of replication complexes is supported by the fact that for the related arterivirus equine arteritis virus (EAV), the mere coexpression of the counterparts of nsp3 and nsp4, i.e., nsp2 and nsp3, is sufficient for the induction of DMVs (93). Furthermore, mutations in MHV nsp4 impaired DMV formation (39). Yet, the topology of nsp3, 4 and 6 had not been established. As this was expected to provide valuable insight into the role of these proteins in the formation of the DMVs, chapter 2 centers on establishing an experimentally verified topology model of the complete coronavirus replicase polyprotein.

One of the fundamental aspects that have so far been ignored is the dynamics of the CoV replicative structures and of the individual proteins present at the RTCs in living cells. To obtain more insight into the dynamics of the replicative structures, three replication-associated proteins were studied: (i) the cytoplasmic nsp2 protein (chapter 3), (ii) the transmembrane protein nsp4 (chapter 5), and (iii) the structural N protein (chapter 4). Real-time imaging of recombinant viruses expressing fluorescently-tagged versions of these proteins was performed, in combination with live-cell imaging approaches including fluorescent recovery after photobleaching (FRAP) and fluorescent loss in photobleaching (FLIP). The results revealed information about the mobility of the CoV replicative structures, about the different diffusional mobilities of the proteins when associated to these structures and about the continuity of the membranes of the ER with those harboring the replicative structures. In addition, we studied the interaction of nsp4 with the other transmembrane–containing nsps and its ability to induce membrane rearrangements (chapter 5).

The assembly of the CoV RTCs in infected cells serves one major purpose: the synthesis of viral genomic RNA. Although the CoV replicative structures, i.e DMVs and CMs, are associated with the generation of viral RNA, the exact location of this process remains a mystery. To get more insight into this aspect of the CoV infection cycle, CoV nascent RNA synthesis was investigated in time using a novel click chemistry approach (chapter 6). The observations reveal that the colocalization of nascent and dsRNA species and nsps changes in time, indicating that dsRNA foci not necessarily correspond with sites of active RNA synthesis.

The final chapter of this thesis provides a summarizing discussion in which the data of chapter 2 to 6 are discussed in a broader perspective against the available literature on + ssRNA virus-induced membrane modifications, replication complex formation, and dynamics of replicative structures and individual replication-associated proteins.

REFERENCES

1. Almazan, F., C. Galan, and L. Enjuanes. 2004. The Nucleoprotein Is Required for Efficient Coronavirus Genome Replication. J. Virol. 78:12683-12688. doi: 10.1128/JVI.78.22.12683-12688.2004.

2. Baltimore, D. 1971. Expression of animal virus genomes. Microbiol. Mol. Biol. Rev. 35:235-241.

3. Barcena, M., G. T. Oostergetel, W. Bartelink, F. G. Faas, A. Verkleij, P. J. Rottier, A. J. Koster, and B. J. Bosch. 2009. Cryo-electron tomography of mouse hepatitis virus: Insights into the structure of the coronavirion. Proc. Natl. Acad. Sci. U. S. A. 106:582-587. doi: 10.1073/pnas.0805270106.

4. Baric, R. S., G. W. Nelson, J. O. Fleming, R. J. Deans, J. G. Keck, N. Casteel, and S. A. Stohlman. 1988. Interactions between coronavirus nucleocapsid protein and viral RNAs: implications for viral transcription. J. Virol. 62:4280-4287.

5. Beijerinck, M. W. 1898. Concerning a contagium vivum fluidum as a cause of the spot-disease of tobacco leaves. Verh. Akad. Wet. Amsterdam. II:3-21.

6. Bhardwaj, K., J. Sun, A. Holzenburg, L. A. Guarino, and C. C. Kao. 2006. RNA recognition and cleavage by the SARS coronavirus endoribonuclease. J. Mol. Biol. 361:243-256. doi: 10.1016/j.jmb.2006.06.021.

7. Bosch, B. J., and P. J. M. Rottier. Nidovirus Entry into Cells, p. 157. in Nidoviruses. ASM; Blackwell distributor, Washington, D.C.; Oxford, 2008, S. Perlman, T. Gallagher, and E. J. Snijder (eds.).

8. Bost, A. G., R. H. Carnahan, X. T. Lu, and M. R. Denison. 2000. Four Proteins Processed from the Replicase Gene Polyprotein of Mouse Hepatitis Virus Colocalize in the Cell Periphery and Adjacent to Sites of Virion Assembly. J. Virol. 74:3379-3387. doi: 10.1128/JVI.74.7.3379-3387.2000.

9. Bouvet, M., C. Debarnot, I. Imbert, B. Selisko, E. J. Snijder, B. Canard, and E. Decroly. 2010. In vitro reconstitution of SARS-coronavirus mRNA cap methylation. PLoS Pathog. 6:e1000863. doi: 10.1371/journal.ppat.1000863.

10. Bredenbeek, P. J., C. J. Pachuk, A. F. Noten, J. Charite, W. Luytjes, S. R. Weiss, and W. J. Spaan. 1990. The primary structure and expression of the second open reading frame of the polymerase gene of the coronavirus MHV-A59; a highly conserved polymerase is expressed by an efficient ribosomal frameshifting mechanism. Nucleic Acids Res. 18:1825-1832.

11. Brierley, I., P. Digard, and S. C. Inglis. 1989. Characterization of an efficient coronavirus ribosomal frameshifting signal: Requirement for an RNA pseudoknot. Cell. 57:537-547. doi: DOI: 10.1016/0092-8674(89)90124-4.

12. Cali, T., C. Galli, S. Olivari, and M. Molinari. 2008. Segregation and rapid turnover of EDEM1 by an autophagy-like mechanism modulates standard ERAD and folding activities. Biochem. Biophys. Res. Commun. 371:405-410. doi: 10.1016/j.bbrc.2008.04.098.

13. Cali, T., O. Vanoni, and M. Molinari. 2008. The endoplasmic reticulum crossroads for newly synthesized polypeptide chains. Prog. Mol. Biol. Transl. Sci. 83:135-179. doi: 10.1016/S0079-6603(08)00604-1.

14. Chen, C. J., K. Sugiyama, H. Kubo, C. Huang, and S. Makino. 2004. Murine coronavirus nonstructural protein p28 arrests cell cycle in G0/G1 phase. J. Virol. 78:10410-10419. doi: 10.1128/JVI.78.19.10410-10419.2004.

15. Chen, Y., H. Cai, J. Pan, N. Xiang, P. Tien, T. Ahola, and D. Guo. 2009. Functional screen reveals SARS coronavirus nonstructural protein nsp14 as a novel cap N7 methyltransferase. Proc. Natl. Acad. Sci. U. S. A. 106:3484-3489. doi: 10.1073/pnas.0808790106.

16. David-Ferreira, J. F., and R. A. Manaker. 1965. An Electron Microscope Study of the Development of a Mouse Hepatitis Virus in Tissue Culture Cells. J. Cell Biol. 24:57-78.

17. de Groot, R., J. Ziebuhr, L. L. Poon, P. Woo, P. Talbot, P. J. Rottier, K. V. Holmes, R. S. Baric, Perlman S, L. Enjuanes, and A. E. Gorbalenya. 2008. Revision of the family Coronaviridae. Taxonomic proposal to the ICTV Executive Committee.

18. de Haan, C. A., and F. Reggiori. 2008. Are nidoviruses hijacking the autophagy machinery? Autophagy. 4:276-279.

19. de Haan, C. A., and P. J. Rottier. 2005. Molecular interactions in the assembly of coronaviruses. Adv. Virus Res. 64:165-230. doi: 10.1016/S0065-3527(05)64006-7.

20. De Haan, C. A. M., and P. J. M. Rottier. 2006. Hosting the severe acute respiratory syndrome coronavirus: specific cell factors required for infection. Cell. Microbiol. 8:1211-1218. doi: 10.1111/j.1462-5822.2006.00744.x.

21. Decroly, E., I. Imbert, B. Coutard, M. Bouvet, B. Selisko, K. Alvarez, A. E. Gorbalenya, E. J. Snijder, and B. Canard. 2008. Coronavirus nonstructural protein 16 is a cap-0 binding enzyme possessing (nucleoside-2'O)-methyltransferase activity. J Virol. 82:8071-84.

22. Deming, D. J., R. L. Graham, M. R. Denison, and R. S. Baric. 2007. Processing of open reading frame 1a replicase proteins nsp7 to nsp10 in murine hepatitis virus strain A59 replication. J. Virol. 81:10280-10291. doi: 10.1128/JVI.00017-07.

23. den Boon, J. A., and P. Ahlquist. 2010. Organelle-like membrane compartmentalization of positive-strand RNA virus replication factories. Annu. Rev. Microbiol. 64:241-256. doi: 10.1146/annurev.micro.112408.134012.

24. den Boon, J. A., A. Diaz, and P. Ahlquist. 2010. Cytoplasmic viral replication complexes. Cell. Host Microbe. 8:77-85. doi: 10.1016/j.chom.2010.06.010.

25. Denison, M. R., P. W. Zoltick, J. L. Leibowitz, C. J. Pachuk, and S. R. Weiss. 1991. Identification of polypeptides encoded in open reading frame 1b of the putative polymerase gene of the murine coronavirus mouse hepatitis virus A59. J. Virol. 65:3076-3082.

26. Denison, M. R., S. A. Hughes, and S. R. Weiss. 1995. Identification and characterization of a 65-kDa protein processed from the gene 1 polyprotein of the murine coronavirus MHV-A59. Virology. 207:316-320. doi: 10.1006/viro.1995.1085.

27. Denison, M. R., and S. Perlman. 1986. Translation and processing of mouse hepatitis virus virion RNA in a cell-free system. J. Virol. 60:12-18.

28. Denison, M. R., W. J. Spaan, Y. van der Meer, C. A. Gibson, A. C. Sims, E. Prentice, and X. T. Lu. 1999. The putative helicase of the coronavirus mouse hepatitis virus is processed from the replicase gene polyprotein and localizes in complexes that are active in viral RNA synthesis. J. Virol. 73:6862-6871.

29. Devaraj, S. G., N. Wang, Z. Chen, Z. Chen, M. Tseng, N. Barretto, R. Lin, C. J. Peters, C. T. Tseng, S. C. Baker, and K. Li. 2007. Regulation of IRF-3-dependent innate immunity by the papain-like protease domain of the severe acute respiratory syndrome coronavirus. J. Biol. Chem. 282:32208-32221. doi: 10.1074/jbc.M704870200.

30. Donaldson, E. F., A. C. Sims, R. L. Graham, M. R. Denison, and R. S. Baric. 2007. Murine hepatitis virus replicase protein nsp10 is a critical regulator of viral RNA synthesis. J. Virol. 81:6356-6368. doi: 10.1128/JVI.02805-06.

31. Drosten, C., S. Günther, W. Preiser, d. W. van, H. Brodt, S. Becker, H. Rabenau, M. Panning, L. Kolesnikova, R. A. M. Fouchier, A. Berger, A. Burguière, J. Cinatl, M. Eickmann, N. Escriou, K. Grywna, S. Kramme, J. Manuguerra, S. Müller, V. Rickerts, M. Stürmer, S. Vieth, H. Klenk, A. D. M. E. Osterhaus, H. Schmitz, and H. W. Doerr. 2003. Identification of a Novel Coronavirus in Patients with Severe Acute Respiratory Syndrome. N. Engl. J. Med. 348:1967-1976. http://dx.doi.org/10.1056/NEJMoa030747.

32. Dveksler, G. S., M. N. Pensiero, C. B. Cardellichio, R. K. Williams, G. S. Jiang, K. V. Holmes, and C. W. Dieffenbach. 1991. Cloning of the mouse hepatitis virus (MHV) receptor: expression in human and hamster cell lines confers susceptibility to MHV. J. Virol. 65:6881-6891.

33. Eckerle, L. D., X. Lu, S. M. Sperry, L. Choi, and M. R. Denison. 2007. High fidelity of murine hepatitis virus replication is decreased in nsp14 exoribonuclease mutants. J. Virol. 81:12135-12144. doi: 10.1128/JVI.01296-07.

34. Egloff, M. P., F. Ferron, V. Campanacci, S. Longhi, C. Rancurel, H. Dutartre, E. J. Snijder, A. E. Gorbalenya, C. Cambillau, and B. Canard. 2004. The severe acute respiratory syndrome-coronavirus replicative protein nsp9 is a single-stranded RNA-binding subunit unique in the RNA virus world. Proc. Natl. Acad. Sci. U. S. A. 101:3792-3796. doi: 10.1073/pnas.0307877101.

35. Eifart, P., K. Ludwig, C. Bottcher, C. A. M. de Haan, P. J. M. Rottier, T. Korte, and A. Herrmann. 2007. Role of Endocytosis and Low pH in Murine Hepatitis Virus Strain A59 Cell Entry. J. Virol. 81:10758-10768. doi: 10.1128/JVI.00725-07.

36. Eriksson, K. K., L. Cervantes-Barragan, B. Ludewig, and V. Thiel. 2008. Mouse hepatitis virus liver pathology is dependent on ADP-ribose-1"-phosphatase, a viral function conserved in the alpha-like supergroup. J. Virol. 82:12325-12334. doi: 10.1128/JVI.02082-08.

37. Fields, B. N., D. M. Knipe, P. M. Howley, and D. E. Griffin. 2001. Fields' virology. Wolters Kluwer/ Lippincott Williams & Wilkins, Philadelphia, Pa.; London.

38. Flint, S. J., Enquist, L. W., Racaniello, V. R., and Skalka, A.M., Principles of virology., ASM; Blackwell distributor, Washington, D.C.; Oxford, 2009.

39. Gadlage, M. J., J. S. Sparks, D. C. Beachboard, R. G. Cox, J. D. Doyle, C. C. Stobart, and M. R. Denison. 2010. Murine hepatitis virus nonstructural protein 4 regulates virus-induced membrane modifications and replication complex function. J. Virol. 84:280-290. doi: 10.1128/JVI.01772-09.

40. Goldsmith, C. S., K. M. Tatti, T. G. Ksiazek, P. E. Rollin, J. A. Comer, W. W. Lee, P. A. Rota, B. Bankamp, W. J. Bellini, and S. R. Zaki. 2004. Ultrastructural characterization of SARS coronavirus. Emerg. Infect. Dis. 10:320-326.

41. Gorbalenya, A. E., Genomics and Evolution of the Nidovirales, p. 15. in Nidoviruses. ASM; Blackwell distributor, Washington, D.C.; Oxford, 2008, S. Perlman, T. Gallagher, and E. J. Snijder (eds.).

42. Gorbalenya, A. E., L. Enjuanes, J. Ziebuhr, and E. J. Snijder. 2006. Nidovirales: Evolving the largest RNA virus genome. Virus Res. 117:17-37. doi: DOI: 10.1016/j.virusres.2006.01.017.

43. Gosert, R., A. Kanjanahaluethai, D. Egger, K. Bienz, and S. C. Baker. 2002. RNA replication of mouse hepatitis virus takes place at double-membrane vesicles. J. Virol. 76:3697-3708.

44. Graham, R. L., and M. R. Denison. 2006. Replication of murine hepatitis virus is regulated by papain-like proteinase 1 processing of nonstructural proteins 1, 2, and 3. J. Virol. 80:11610-11620. doi: 10.1128/JVI.01428-06.

45. Graham, R. L., A. C. Sims, S. M. Brockway, R. S. Baric, and M. R. Denison. 2005. The nsp2 replicase proteins of murine hepatitis virus and severe acute respiratory syndrome coronavirus are dispensable for viral replication. J Virol. 79:13399-411.

46. Guan, Y., B. J. Zheng, Y. Q. He, X. L. Liu, Z. X. Zhuang, C. L. Cheung, S. W. Luo, P. H. Li, L. J. Zhang, Y. J. Guan, K. M. Butt, K. L. Wong, K. W. Chan, W. Lim, K. F. Shortridge, K. Y. Yuen, J. S. Peiris, and L. L. Poon. 2003. Isolation and characterization of viruses related to the SARS coronavirus from animals in southern China. Science. 302:276-278. doi: 10.1126/science.1087139.

47. Harcourt, B. H., D. Jukneliene, A. Kanjanahaluethai, J. Bechill, K. M. Severson, C. M. Smith, P. A. Rota, and S. C. Baker. 2004. Identification of severe acute respiratory syndrome coronavirus replicase products and characterization of papain-like protease activity. J. Virol. 78:13600-13612. doi: 10.1128/JVI.78.24.13600-13612.2004.

48. Imbert, I., J. C. Guillemot, J. M. Bourhis, C. Bussetta, B. Coutard, M. P. Egloff, F. Ferron, A. E. Gorbalenya, and B. Canard. 2006. A second, non-canonical RNA-dependent RNA polymerase in SARS coronavirus. EMBO J. 25:4933-4942. doi: 10.1038/sj.emboj.7601368.

49. International Committee on Taxonomy of Viruses, C. Fauquet, and International Union of Microbiological Societies. Virology Division. 2005. Virus taxonomy : classification and nomenclature of viruses : eighth report of the International Committee on the Taxonomy of Viruses. Elsevier Academic Press, San Diego, Calif. ; London.

50. Ivanov, K. A., T. Hertzig, M. Rozanov, S. Bayer, V. Thiel, A. E. Gorbalenya, and J. Ziebuhr. 2004. Major genetic marker of nidoviruses encodes a replicative endoribonuclease. Proc. Natl. Acad. Sci. U. S. A. 101:12694-12699. doi: 10.1073/pnas.0403127101.

51. Ivanov, K. A., V. Thiel, J. C. Dobbe, Y. van der Meer, E. J. Snijder, and J. Ziebuhr. 2004. Multiple enzymatic activities associated with severe acute respiratory syndrome coronavirus helicase. J. Virol. 78:5619-5632. doi: 10.1128/JVI.78.11.5619-5632.2004.

52. Ivanov, K. A., and J. Ziebuhr. 2004. Human coronavirus 229E nonstructural protein 13: characterization of duplex-unwinding, nucleoside triphosphatase, and RNA 5'-triphosphatase activities. J. Virol. 78:7833-7838. doi: 10.1128/JVI.78.14.7833-7838.2004.

53. Ivanvosky, D. 1892. Concerning the mosaic disease of the tobacco plant. Acad Imp Sci Bull. 35:67-70.

54. Joseph, J. S., K. S. Saikatendu, V. Subramanian, B. W. Neuman, A. Brooun, M. Griffith, K. Moy, M. K. Yadav, J. Velasquez, M. J. Buchmeier, R. C. Stevens, and P. Kuhn. 2006. Crystal structure of nonstructural protein 10 from the severe acute respiratory syndrome coronavirus reveals a novel fold with two zinc-binding motifs. J. Virol. 80:7894-7901. doi: 10.1128/JVI.00467-06.

55. Kamitani, W., C. Huang, K. Narayanan, K. G. Lokugamage, and S. Makino. 2009. A two-pronged strategy to suppress host protein synthesis by SARS coronavirus Nsp1 protein. Nat. Struct. Mol. Biol. 16:1134-1140. doi: 10.1038/nsmb.1680.

56. Kamitani, W., K. Narayanan, C. Huang, K. Lokugamage, T. Ikegami, N. Ito, H. Kubo, and S. Makino. 2006. Severe acute respiratory syndrome coronavirus nsp1 protein suppresses host gene expression by promoting host mRNA degradation. Proc. Natl. Acad. Sci. U. S. A. 103:12885-12890. doi: 10.1073/pnas.0603144103.

57. Kanjanahaluethai, A., and S. C. Baker. 2000. Identification of mouse hepatitis virus papain-like proteinase 2 activity. J. Virol. 74:7911-7921.

58. Kanjanahaluethai, A., Z. Chen, D. Jukneliene, and S. C. Baker. 2007. Membrane topology of murine coronavirus replicase nonstructural protein 3. Virology. 361:391-401.

59. Klumperman, J., J. K. Locker, A. Meijer, M. C. Horzinek, H. J. Geuze, and P. J. Rottier. 1994. Coronavirus M proteins accumulate in the Golgi complex beyond the site of virion budding. J. Virol. 68:6523-6534.

60. Knoops, K., M. Kikkert, S. H. E. Van Den Worm, J. C. Zevenhoven-Dobbe, Y. Van Der Meer, A. J. Koster, A. M. Mommaas, and E. J. Snijder. 2008. SARS-coronavirus replication is supported by a reticulovesicular network of modified endoplasmic reticulum. PLoS Biology. 6:1957-1974.

61. Knoops, K., C. Swett-Tapia, S. H. E. van den Worm, A. J. W. te Velthuis, A. J. Koster, A. M. Mommaas, E. J. Snijder, and M. Kikkert. 2010. Integrity of the Early Secretory Pathway Promotes, but Is Not Required for, Severe Acute Respiratory Syndrome Coronavirus RNA Synthesis and Virus-Induced Remodeling of Endoplasmic Reticulum Membranes. J. Virol. 84:833-846. doi: 10.1128/JVI.01826-09.

62. Ksiazek, T. G., D. Erdman, C. S. Goldsmith, S. R. Zaki, T. Peret, S. Emery, S. Tong, C. Urbani, J. A. Comer, W. Lim, P. E. Rollin, S. F. Dowell, A. Ling, C. D. Humphrey, W. Shieh, J. Guarner, C. D. Paddock, P. Rota, B. Fields, J. DeRisi, J. Yang, N. Cox, J. M. Hughes, J. W. LeDuc, W. J. Bellini, and L. J. Anderson. 2003. A Novel Coronavirus Associated with Severe Acute Respiratory Syndrome. N. Engl. J. Med. 348:1953-1966. http://dx.doi.org/10.1056/NEJMoa030781.

63. Kubo, H., Y. K. Yamada, and F. Taguchi. 1994. Localization of neutralizing epitopes and the receptor-binding site within the amino-terminal 330 amino acids of the murine coronavirus spike protein. J. Virol. 68:5403-5410.

64. Kuo, L., and P. S. Masters. 2002. Genetic evidence for a structural interaction between the carboxy termini of the membrane and nucleocapsid proteins of mouse hepatitis virus. J. Virol. 76:4987-4999.

65. Kuri, T., K. K. Eriksson, A. Putics, R. Zust, E. J. Snijder, A. D. Davidson, S. G. Siddell, V. Thiel, J. Ziebuhr, and F. Weber. 2011. The ADP-ribose-1"-monophosphatase domains of SARS-coronavirus and Human coronavirus 229E mediate resistance to antiviral interferon responses. J. Gen. Virol. . doi: 10.1099/vir.0.031856-0.

66. Li, W., Z. Shi, M. Yu, W. Ren, C. Smith, J. H. Epstein, H. Wang, G. Crameri, Z. Hu, H. Zhang, J. Zhang, J. McEachern, H. Field, P. Daszak, B. T. Eaton, S. Zhang, and L. F. Wang. 2005. Bats are natural reservoirs of SARS-like coronaviruses. Science. 310:676-679. doi: 10.1126/science.1118391.

67. Lissenberg, A., M. M. Vrolijk, A. L. W. van Vliet, M. A. Langereis, J. D. F. de Groot-Mijnes, P. J. M. Rottier, and R. J. de Groot. 2005. Luxury at a Cost? Recombinant Mouse Hepatitis Viruses Expressing the Accessory Hemagglutinin Esterase Protein Display Reduced Fitness In Vitro. J. Virol. 79:15054-15063. doi: 10.1128/JVI.79.24.15054-15063.2005.

68. Lu, X., Y. Lu, and M. R. Denison. 1996. Intracellular and in vitro-translated 27-kDa proteins contain the 3C-like proteinase activity of the coronavirus MHV-A59. Virology. 222:375-382. doi: 10.1006/viro.1996.0434.

69. Lugari, A., S. Betzi, E. Decroly, E. Bonnaud, A. Hermant, J. C. Guillemot, C. Debarnot, J. P. Borg, M. Bouvet, B. Canard, X. Morelli, and P. Lecine. 2010. Molecular mapping of the RNA Cap 2'-O-methyltransferase activation interface between severe acute respiratory syndrome coronavirus nsp10 and nsp16. J. Biol. Chem. 285:33230-33241. doi: 10.1074/jbc.M110.120014.

70. Madan, V., J. Garcia Mde, M. A. Sanz, and L. Carrasco. 2005. Viroporin activity of murine hepatitis virus E protein. FEBS Lett. 579:3607-3612. doi: 10.1016/j.febslet.2005.05.046.

71. Matthes, N., J. R. Mesters, B. Coutard, B. Canard, E. J. Snijder, R. Moll, and R. Hilgenfeld. 2006. The non-structural protein Nsp10 of mouse hepatitis virus binds zinc ions and nucleic acids. FEBS Lett. 580:4143-4149. doi: 10.1016/j.febslet.2006.06.061.

72. Miknis, Z. J., E. F. Donaldson, T. C. Umland, R. A. Rimmer, R. S. Baric, and L. W. Schultz. 2009. Severe acute respiratory syndrome coronavirus nsp9 dimerization is essential for efficient viral growth. J. Virol. 83:3007-3018. doi: 10.1128/JVI.01505-08.

73. Miller, S., and J. Krijnse-Locker. 2008. Modification of intracellular membrane structures for virus replication. Nat. Rev. Microbiol. 6:363-374. doi: 10.1038/nrmicro1890.

74. Minskaia, E., T. Hertzig, A. E. Gorbalenya, V. Campanacci, C. Cambillau, B. Canard, and J. Ziebuhr. 2006. Discovery of an RNA virus 3'->5' exoribonuclease that is critically involved in coronavirus RNA synthesis. Proc. Natl. Acad. Sci. U. S. A. 103:5108-5113. doi: 10.1073/pnas.0508200103.

75. Molenkamp, R., and W. J. Spaan. 1997. Identification of a specific interaction between the coronavirus mouse hepatitis virus A59 nucleocapsid protein and packaging signal. Virology. 239:78-86. doi: 10.1006/viro.1997.8867.

76. Narayanan, K., C. Huang, K. Lokugamage, W. Kamitani, T. Ikegami, C. T. Tseng, and S. Makino. 2008. Severe acute respiratory syndrome coronavirus nsp1 suppresses host gene expression, including that of type I interferon, in infected cells. J. Virol. 82:4471-4479. doi: 10.1128/JVI.02472-07.

77. Ng, M. L., S. H. Tan, E. E. See, E. E. Ooi, and A. E. Ling. 2003. Proliferative growth of SARS coronavirus in Vero E6 cells. J. Gen. Virol. 84:3291-3303.

78. Oostra, M., E. G. te Lintelo, M. Deijs, M. H. Verheije, P. J. Rottier, and C. A. de Haan. 2007. Localization and membrane topology of coronavirus nonstructural protein 4: involvement of the early secretory pathway in replication. J Virol. 81:12323-36.

79. Prentice, E., J. McAuliffe, X. Lu, K. Subbarao, and M. R. Denison. 2004. Identification and characterization of severe acute respiratory syndrome coronavirus replicase proteins. J Virol. 78:9977-86.

80. Prentice, E., W. G. Jerome, T. Yoshimori, N. Mizushima, and M. R. Denison. 2004. Coronavirus Replication Complex Formation Utilizes Components of Cellular Autophagy. Journal of Biological Chemistry. 279:10136-10141. doi: 10.1074/jbc.M306124200.

81. Reggiori, F., I. Monastyrska, M. Verheije H., T. Calì, M. Ulasli, S. Bianchi, R. Bernasconi, C. de Haan A.M., and M. Molinari. 2010. Coronaviruses Hijack the LC3-I-Positive EDEMosomes, ER-Derived Vesicles Exporting Short-Lived ERAD Regulators, for Replication. Cell Host & Microbe. 7:500.

82. Sawicki, D., T. Wang, and S. Sawicki. 2001. The RNA structures engaged in replication and transcription of the A59 strain of mouse hepatitis virus. J. Gen. Virol. 82:385-396.

83. Sawicki, S. G., and D. L. Sawicki. 1986. Coronavirus minus-strand RNA synthesis and effect of cycloheximide on coronavirus RNA synthesis. J. Virol. 57:328-334.

84. Sawicki, S. G., and D. L. Sawicki. 1995. Coronaviruses use discontinuous extension for synthesis of subgenome-length negative strands. Adv. Exp. Med. Biol. 380:499-506.

85. Sawicki, S. G., D. L. Sawicki, and S. G. Siddell. 2007. A contemporary view of coronavirus transcription. J Virol. 81:20-9.

86. Sawicki, S. G., D. L. Sawicki, D. Younker, Y. Meyer, V. Thiel, H. Stokes, and S. G. Siddell. 2005. Functional and genetic analysis of coronavirus replicase-transcriptase proteins. PLoS Pathog. 1:e39. doi: 10.1371/journal.ppat.0010039.

87. Schelle, B., N. Karl, B. Ludewig, S. G. Siddell, and V. Thiel. 2005. Selective replication of coronavirus genomes that express nucleocapsid protein. J. Virol. 79:6620-6630. doi: 10.1128/JVI.79.11.6620-6630.2005.

88. Schiller, J. J., A. Kanjanahaluethai, and S. C. Baker. 1998. Processing of the coronavirus MHV-JHM polymerase polyprotein: identification of precursors and proteolytic products spanning 400 kilodaltons of ORF1a. Virology. 242:288-302. doi: 10.1006/viro.1997.9010.

89. Seybert, A., A. Hegyi, S. G. Siddell, and J. Ziebuhr. 2000. The human coronavirus 229E superfamily 1 helicase has RNA and DNA duplex-unwinding activities with 5'-to-3' polarity. RNA. 6:1056-1068.

90. Seybert, A., C. C. Posthuma, L. C. van Dinten, E. J. Snijder, A. E. Gorbalenya, and J. Ziebuhr. 2005. A complex zinc finger controls the enzymatic activities of nidovirus helicases. J Virol. 79:696-704.

91. Shi, S. T., J. J. Schiller, A. Kanjanahaluethai, S. C. Baker, J. W. Oh, and M. M. Lai. 1999. Colocalization and membrane association of murine hepatitis virus gene 1 products and De novo-synthesized viral RNA in infected cells. J Virol. 73:5957-69.

92. Snijder, E. J., Y. van der Meer, J. Zevenhoven-Dobbe, J. J. Onderwater, J. van der Meulen, H. K. Koerten, and A. M. Mommaas. 2006. Ultrastructure and origin of membrane vesicles associated with the severe acute respiratory syndrome coronavirus replication complex. J Virol. 80:5927-40.

93. Snijder, E. J., H. van Tol, N. Roos, and K. W. Pedersen. 2001. Non-structural proteins 2 and 3 interact to modify host cell membranes during the formation of the arterivirus replication complex. J. Gen. Virol. 82:985-994.

94. Sparks, J. S., X. Lu, and M. R. Denison. 2007. Genetic analysis of Murine hepatitis virus nsp4 in virus replication. J Virol. 81:12554-63.

95. Stertz, S., M. Reichelt, M. Spiegel, T. Kuri, L. Martinez-Sobrido, A. Garcia-Sastre, F. Weber, and G. Kochs. 2007. The intracellular sites of early replication and budding of SARS-coronavirus. Virology. 361:304-315. doi: 10.1016/j.virol.2006.11.027.

96. Stohlman, S. A., R. S. Baric, G. N. Nelson, L. H. Soe, L. M. Welter, and R. J. Deans. 1988. Specific interaction between coronavirus leader RNA and nucleocapsid protein. J. Virol. 62:4288-4295.

97. Su, D., Z. Lou, F. Sun, Y. Zhai, H. Yang, R. Zhang, A. Joachimiak, X. C. Zhang, M. Bartlam, and Z. Rao. 2006. Dodecamer structure of severe acute respiratory syndrome coronavirus nonstructural protein nsp10. J. Virol. 80:7902-7908. doi: 10.1128/JVI.00483-06.

98. Sutton, G., E. Fry, L. Carter, S. Sainsbury, T. Walter, J. Nettleship, N. Berrow, R. Owens, R. Gilbert, A. Davidson, S. Siddell, L. L. Poon, J. Diprose, D. Alderton, M. Walsh, J. M. Grimes, and D. I. Stuart. 2004. The nsp9 replicase protein of SARS-coronavirus, structure and functional insights. Structure. 12:341-353. doi: 10.1016/j.str.2004.01.016.

99. Tanner, J. A., R. M. Watt, Y. B. Chai, L. Y. Lu, M. C. Lin, J. S. Peiris, L. L. Poon, H. F. Kung, and J. D. Huang. 2003. The severe acute respiratory syndrome (SARS) coronavirus NTPase/helicase belongs to a distinct class of 5' to 3' viral helicases. J. Biol. Chem. 278:39578-39582. doi: 10.1074/jbc.C300328200.

100. te Velthuis, A. J., J. J. Arnold, C. E. Cameron, S. H. van den Worm, and E. J. Snijder. 2010. The RNA polymerase activity of SARS-coronavirus nsp12 is primer dependent. Nucleic Acids Res. 38:203-214. doi: 10.1093/nar/gkp904.

101. Ulasli, M., M. H. Verheije, C. A. de Haan, and F. Reggiori. 2010. Qualitative and quantitative ultrastructural analysis of the membrane rearrangements induced by coronavirus. Cell. Microbiol. 12:844-861. doi: 10.1111/j.1462-5822.2010.01437.x.

102. van der Meer, Y., E. J. Snijder, J. C. Dobbe, S. Schleich, M. R. Denison, W. J. Spaan, and J. K. Locker. 1999. Localization of mouse hepatitis virus nonstructural proteins and RNA synthesis indicates a role for late endosomes in viral replication. J. Virol. 73:7641-7657.

103. van Hemert, M. J., S. H. van den Worm, K. Knoops, A. M. Mommaas, A. E. Gorbalenya, and E. J. Snijder. 2008. SARS-coronavirus replication/transcription complexes are membrane-protected and need a host factor for activity in vitro. PLoS Pathog. 4:e1000054. doi: 10.1371/journal.ppat.1000054.

104. Vennema, H., G. J. Godeke, J. W. Rossen, W. F. Voorhout, M. C. Horzinek, D. J. Opstelten, and P. J. Rottier. 1996. Nucleocapsid-independent assembly of coronavirus-like particles by co-expression of viral envelope protein genes. EMBO J. 15:2020-2028.

105. Verheije, M. H., M. Raaben, M. Mari, E. G. Te Lintelo, F. Reggiori, F. J. van Kuppeveld, P. J. Rottier, and C. A. de Haan. 2008. Mouse hepatitis coronavirus RNA replication depends on GBF1-mediated ARF1 activation. PLoS Pathog. 4:e1000088.

106. Wang, G., G. Chen, D. Zheng, G. Cheng, and H. Tang. 2011. PLP2 of mouse hepatitis virus A59 (MHV-A59) targets TBK1 to negatively regulate cellular type I interferon signaling pathway. PLoS One. 6:e17192. doi: 10.1371/journal.pone.0017192.

107. Wathelet, M. G., M. Orr, M. B. Frieman, and R. S. Baric. 2007. Severe acute respiratory syndrome coronavirus evades antiviral signaling: role of nsp1 and rational design of an attenuated strain. J. Virol. 81:11620-11633. doi: 10.1128/JVI.00702-07.

108. Williams, R. K., G. S. Jiang, and K. V. Holmes. 1991. Receptor for mouse hepatitis virus is a member of the carcinoembryonic antigen family of glycoproteins. Proc. Natl. Acad. Sci. U. S. A. 88:5533-5536.

109. Wilson, L., C. Mckinlay, P. Gage, and G. Ewart. 2004. SARS coronavirus E protein forms cation-selective ion channels. Virology. 330:322-331. doi: DOI: 10.1016/j.virol.2004.09.033.

110. Yoo, D. W., M. D. Parker, and L. A. Babiuk. 1991. The S2 subunit of the spike glycoprotein of bovine coronavirus mediates membrane fusion in insect cells. Virology. 180:395-399.

111. Zhai, Y., F. Sun, X. Li, H. Pang, X. Xu, M. Bartlam, and Z. Rao. 2005. Insights into SARS-CoV transcription and replication from the structure of the nsp7-nsp8 hexadecamer. Nat. Struct. Mol. Biol. 12:980-986. doi: 10.1038/nsmb999.

112. Zhao, Z., L. B. Thackray, B. C. Miller, T. M. Lynn, M. M. Becker, E. Ward, N. N. Mizushima, M. R. Denison, and H. W. Virgin 4th. 2007. Coronavirus replication does not require the autophagy gene ATG5. Autophagy. 3:581-585.

113. Zheng, D., G. Chen, B. Guo, G. Cheng, and H. Tang. 2008. PLP2, a potent deubiquitinase from murine hepatitis virus, strongly inhibits cellular type I interferon production. Cell Res. 18:1105-1113. doi: 10.1038/cr.2008.294.

114. Ziebuhr, J., E. J. Snijder, and A. E. Gorbalenya. 2000. Virus-encoded proteinases and proteolytic processing in the Nidovirales. J. Gen. Virol. 81:853-879.

115. Zust, R., L. Cervantes-Barragan, T. Kuri, G. Blakqori, F. Weber, B. Ludewig, and V. Thiel. 2007. Coronavirus non-structural protein 1 is a major pathogenicity factor: implications for the rational design of coronavirus vaccines. PLoS Pathog. 3:e109. doi: 10.1371/journal.ppat.0030109.

Chapter 2

Topology and Membrane Anchoring of the Coronavirus Replication Complex: Not All Hydrophobic Domains of nsp3 and nsp6 Are Membrane Spanning

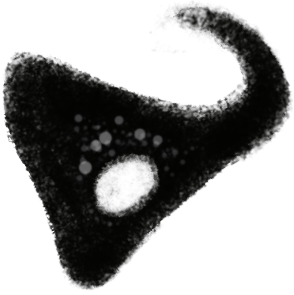

Monique Oostra, **Marne C. Hagemeijer**, Michiel van Gent, Cornelis P. J. Bekker, Eddie G. te Lintelo, Peter J. M. Rottier, and Cornelis A. M. de Haan

Virology Division, Department of Infectious Diseases and Immunology, Faculty of Veterinary Medicine, Utrecht University, Utrecht, the Netherlands

Journal of Virology, Dec. 2008, p. 12392–12405 Vol. 82, No. 24

ABSTRACT

Coronaviruses express two very large replicase polyproteins, the 16 autoproteolytic cleavage products of which collectively form the membrane-anchored replication complexes. How these structures are assembled is still largely unknown, but it is likely that the membrane-spanning members of these nonstructural proteins (nsps) are responsible for the induction of the double-membrane vesicles and for anchoring the replication complexes to these membranes. For 3 of the 16 coronavirus nsps —nsp3, nsp4, and nsp6— multiple transmembrane domains are predicted. Previously we showed that, consistent with predictions, nsp4 occurs in membranes with both of its termini exposed in the cytoplasm (M. Oostra et al., J. Virol. 81:12323-12336, 2007). Strikingly, however, for both nsp3 and nsp6, predictions based on a multiple alignment of 27 coronavirus genome sequences indicate an uneven number of transmembrane domains. As a consequence, the proteinase domains present in nsp3 and nsp5 would be separated from their target sequences by the lipid bilayer. To look into this incongruity, we studied the membrane disposition of nsp3 and nsp6 of the severe acute respiratory syndrome coronavirus and murine hepatitis virus by analyzing tagged forms of the proteins expressed in cultured cells. Contrary to the predictions, in both viruses, both proteins had their amino terminus, as well as their carboxy terminus, exposed in the cytoplasm. We established that two of the three hydrophobic domains in nsp3 and six of the seven in nsp6 are membrane spanning. Subsequently, we verified that in nsp4, all four hydrophobic domains span the lipid bilayer. The occurrence of conserved non-membrane-spanning hydrophobic domains in nsp3 and nsp6 suggests an important function for these domains in coronavirus replication.

INTRODUCTION

Positive-strand RNA viruses induce the formation of cytoplasmic membrane structures in their host cells to accomplish the efficient replication of their genomes. These structures probably facilitate the orchestration of the replication process and the recruitment of the components required for RNA synthesis and may shield the RNA intermediates from recognition by the host cell's defense mechanisms. The membranes of these structures can be acquired from different cellular compartments. In many virus families, such as *Picorna-*, *Flavi-*, and *Bromoviridae*, the RNA replication complex is associated with membranes derived from the endoplasmic reticulum (ER). However, endosomes and lysosomes (*Togaviridae*), peroxisomes and chloroplasts (*Tombusviridae*), and mitochondria (*Nodaviridae*) are also used as membrane donors [for a review, see reference (44)]. In general, viral nonstructural proteins (nsps) are responsible for the assembly of the replication complex at these specific cellular organelles and for the observed membrane rearrangements.

Coronaviruses are enveloped, plus-strand RNA viruses belonging to the family *Coronaviridae* that, together with the *Arteri-* and *Roniviridae*, belong to the order *Nidovirales*. With sizes ranging between 27 and 32 kb, coronaviruses possess the largest genomes among all known RNA viruses. The 5' two-thirds of the coronaviral genome is occupied by open reading frames (ORFs) that encode the viral replicase. The remaining part of the genome codes for the structural proteins, which invariably comprise at least the spike (S), envelope (E), membrane (M), and nucleocapsid (N) proteins, and for a variable number of accessory proteins. Except for the replicase ORFs, all genes are translated from subgenomic mRNAs, which are generated by a process of discontinuous transcription [for a recent review, see reference (45)]. The viral replicase is encoded by the two most 5' ORFs on the genomic RNA, ORF1a and ORF1b, which are translated into two very large precursor polyproteins, pp1a and pp1ab, comprising approximately 4,000 and 7,000 amino acids, respectively. pp1ab is translated only after a -1 frameshift induced by a slippery sequence at the end of ORF1a, which only occurs in a fraction of translational events (5).

The replicase polyproteins are processed by virus-encoded proteinases to produce 16 mature nsps (19, 63). nsp1, -2, and -3 are released through cleavage by a papain-like proteinase, one or two functional copies of which are contained within nsp3; all other cleavages are performed by the 3C-like main proteinase located in nsp5 (2, 11, 17, 55, 64). pp1a, which contains the first 11 nsps, including the proteinases, is three to five times more abundantly produced than pp1ab, which additionally gives rise to nsp12 to

nsp16 (13). Functions involving the actual replication and transcription of the viral genome have been assigned to several of the orf1b-encoded nsps, like RNA-dependent RNA polymerase (RdRp) activity in nsp12, helicase activity in nsp13, exonuclease activity in nsp14, endoribonuclease activity in nsp15, and methyltransferase activity in nsp16 (3, 7, 9, 25–27, 43, 63). Except for the proteases, the functions of the orf1a-encoded nsps are less clearly defined. ADP-ribose-1-monophosphatase activity has been identified in nsp3, whereas in nsp8 a second RdRp activity was discovered (24, 42). nsp7 and nsp8 together were shown to form a hexadecameric complex able to bind nucleic acids and suggested to function as a processivity factor for the RdRp (62). nsp9 and nsp10 were also found to bind nucleic acids, while nsp10, which contains two zinc-finger domains, might additionally be somehow involved in the processing of the polyproteins (12, 31, 52).

The nsps collectively assemble into membrane-associated complexes that constitute the sites of *de novo* viral RNA synthesis (47, 58). The virus-encoded N protein and possibly several cellular proteins are also recruited to these sites (4, 46). The replication complexes are found in the perinuclear region of the host cell anchored to double-membrane vesicles (DMVs) (6, 20, 48). The origin of the membranes in these structures has not unambiguously been established. Several cellular pathways and organelles, such as the ER, Golgi complex, endosomal/lysosomal system, and autophagic pathway, have been implicated in the formation of the replication complexes (40, 47, 48, 57). However, recent studies indicate the ER to be the most likely lipid donor compartment (37, 48).

Essentially nothing is known about how the membrane-anchored replication complexes are induced and assembled and how the individual nsps and other necessary constituents are recruited to these sites. Coronavirus ORF1a encodes three nsps —nsp3, nsp4, and nsp6— that are predicted to contain transmembrane domains. It is likely that these proteins not only function in the membrane anchoring of the multisubunit replication complex but also induce the formation of the membrane structures. The membrane association of mouse hepatitis virus (MHV) and severe acute respiratory syndrome-associated coronavirus (SARS-CoV) nsp3 has been demonstrated previously (22, 28). In addition, the membrane association, as well as the topology, of nsp4 of these two viruses has been resolved (37). The involvement of these nsps in the formation of replication complexes is supported by the fact that for the related arterivirus equine arteritis virus (EAV), coexpression of the counterparts of nsp3 and nsp4, i.e., nsp2 and nsp3, is sufficient for the induction of DMVs (49). Furthermore, mutations in MHV nsp4 or EAV nsp3 impaired DMV formation (8, 39).

In this study, we wanted to fill a gap in the existing knowledge of coronaviruses by establishing an experimentally verified topology model of the complete coronavirus replicase polyprotein. When transmembrane predictions (51) were performed on the entire ORF1a region based on the multiple alignment of 27 coronavirus sequences, with representatives from each of the different coronavirus groups (present as reference sequences [RefSeq] in the NCBI CoreNucleotide database), some discrepancies were observed (Fig. 1). For nsp4, four transmembrane domains were predicted, which is in agreement with our previous experimental data that showed that both termini are located on the cytoplasmic face of the membrane (37). However, for both nsp3 and nsp6, an uneven number of transmembrane domains was predicted, three and seven, respectively, resulting in a model in which the proteinases, present in nsp3 and nsp5, would be separated from some of their target sequences by the lipid bilayer. Furthermore, this prediction places nsp1, nsp2, and most of nsp3 on the luminal side of the membrane, which is unlikely as pp1a lacks an amino-terminal signal sequence. In addition, several studies have shown that nsp1 and nsp2, as well as a number of nsps downstream of nsp6, localize to the cytosol (6, 21, 22, 57). To solve these discrepancies, we focused on the topology and membrane integration of the hydrophobic nsps, particularly nsp3 and nsp6. To strengthen our conclusions, the nsps of both

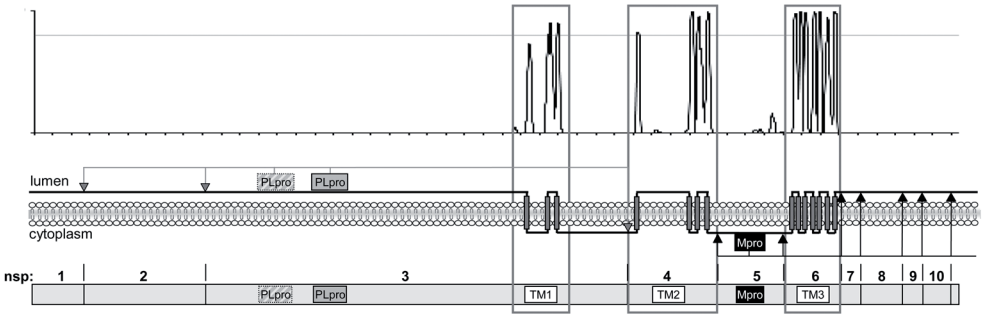

Figure 1. pp1a transmembrane domain prediction based on multiple alignment. The presence of transmembrane domains in the pp1a precursor was predicted (51) on the basis of a multiple alignment of 27 different coronavirus sequences with representatives from each of the different groups (RefSeq in the NCBI CoreNucleotide database). The resulting hydrophobicity plot is shown in the upper panel, with peaks reaching the threshold (dotted line) representing predicted membrane-spanning domains. The black line in the middle panel represents the protein and shows, based on the known topology of nsp4 (37), its predicted localization on the lumenal or cytoplasmic side of the membrane, which is symbolized by the gray bar. At the bottom, a schematic representation of pp1a is shown in which the regions containing the putative transmembrane (TM) domains, the papain-like protease (PLpro, two in MHV and one in SARS-CoV), and the main protease (Mpro) are highlighted. The protease cleavage sites are indicated by arrowheads, with the nsp3-encoded PLpro cleavage sites in gray and the nsp5-encoded Mpro cleavage sites in black.

MHV and SARS-CoV were studied. Contrary to the predictions, in each virus both nsp3 and nsp6 appeared to have the amino terminus as well as the carboxy terminus exposed on the cytoplasmic side of the membrane. We show that in both nsp3 and nsp6, not all of the predicted transmembrane domains are used as such. In nsp3, only two, and in nsp6, only six of the predicted transmembrane domains actually span the lipid bilayer. These results raise the question of why coronaviruses have conserved hydrophobic domains in their nsps that do not function as membrane-spanning domains.

MATERIALS AND METHODS

Cells, viruses, and antibodies. OST7-1 cells, obtained from B. Moss (16), were maintained as monolayer cultures in Dulbecco's modified Eagle's medium (DMEM) (Cambrex Bio Science Verviers) containing 10% fetal calf serum (FCS) (Bodinco B.V.), 100 IU of penicillin per ml, and 100 μg of streptomycin per ml (referred to as culture medium). Recombinant vaccinia virus encoding the bacteriophage T7 RNA polymerase (vTF7-3) was also obtained from B. Moss (18).

Rabbit polyclonal antisera directed against the enhanced green fluorescentprotein (EGFP) or the influenza virus hemagglutinin (HA) tag were obtained from ICL. Rabbit antiserum recognizing the C-terminal domain of the MHV membrane (M) protein (anti-M_C) has been described previously (30), while mouse monoclonal antibody against the amino terminus of MHV M (J1.3 or anti-M_N) was provided by J. Fleming (53).

Plasmid constructions. First, a plasmid was created in which all gene fragments could be cloned behind a T7 promoter in frame with the sequence encoding the EGFP tag. To this end, the pEGFP-N3 vector (Clontech) was digested with EcoRI and NotI, of which the latter restriction site was filled in with Klenow polymerase (Invitrogen) and this fragment was cloned into the EcoRI and BamHI-digested pTUG31 vector (59), of which the BamHI restriction site was also filled in with Klenow polymerase (Invitrogen), thereby creating pTug-EGFP. An *N*-glycosylation site was created in the EGFP gene by performing site-directed mutagenesis with the QuikChange site-directed mutagenesis kit (Stratagene) according to the manufacturer's instructions on pEGFP-N3 with primers 3212 and 3213. This mutated EGFP gene was cloned into the pTUG31 vector similar to the wild-type EGFP gene, thereby creating pTug-$EGFP^{glyc}$. For the sequences and locations on the viral genomes of all of the primers used, see Table 1.

The SARS-CoV nsp gene fragments were obtained by reverse transcriptase-PCR amplification of viral RNA isolated from SARS-CoV isolate 5688 (*29*) with primers 3072 and 3073 for nsp3 ($nsp3_s$) and primers 3070 and 3071 for nsp6 ($nsp6_s$). The MHV nsp gene fragments were obtained by reverse transcription-PCR amplification of viral genomic RNA isolated from MHV strain A59 with primers 3632 and 2933 for nsp3 ($nsp3_m$) and primers 2974 and 2975 for nsp6 ($nsp6_m$). The PCR products were cloned into the pGEM-T Easy vector (Promega), and their sequences were confirmed by sequence analysis. Site-directed mutagenesis to mutate the *N*-glycosylation sites was performed on the pGem-T Easy constructs containing the nsp3 gene fragments with primers 3354 and 3355 for SARS-CoV nsp3 and primers 3630 and 3631 for MHV nsp3. The nsp gene fragments were cloned into the pTug-EGFP or pTug-$EGFP^{glyc}$ vector by digesting the pGem-T Easy constructs with EcoRI and BamHI and cloning the fragments obtained into the EcoRI-BamHI-digested pTug-EGFP and pTug-$EGFP^{glyc}$ vectors. The plasmids created encode the different nsps fused C terminally to the wild-type or mutant EGFP tag. The same EcoRI-BamHI nsp3 and nsp6 fragments were also cloned into the EcoRI-BamHI-digested pTUG31 vector together with a primer dimer of primers 3050 and 3051, resulting in plasmids encoding the nsps C terminally fused to a HA tag. In these latter constructs, as well as in the pTug construct encoding MHV nsp6 fused to $EGFP^{glyc}$ (pTug-$nsp6_m$-$EGFP^{glyc}$), an MHV M (M_N) tag-encoding sequence was inserted in front of the nsps by cloning a primer dimer of primers 3019 and 3020, coding for the 10-residue amino-terminal sequence of the MHV M protein (MSSTTQAPEP), into the XhoI-EcoRV-restricted plasmids, thereby creating constructs that encode nsps tagged at both termini.

MHV nsp6 lacking the first hydrophobic domain ($nsp6_m\Delta HD1'$) was amplified by PCR with primers 3566 and 2975. The PCR product was cloned into the pGEM-T Easy vector (Promega), and the sequence was confirmed by sequence analysis. A fragment was obtained by digestion with EcoRV and BamHI and cloned into the EcoRV-BamHI-digested pTugM_N-$nsp6_m$-$EGFP^{glyc}$ plasmid, thereby creating a construct containing MHV nsp6 without the first hydrophobic domain fused N terminally to the MHV M tag and C terminally to the EGFP tag containing the *N* glycosylation site.

Progressive C-terminal deletion mutant forms lacking one or more hydrophobic domains were made for both nsp3 and -6. PCRs were performed with the same forward primers as described before; for the reverse primers used, see Table 1. For nsp3, the PCRs were performed on the constructs with the mutated *N* glycosylation sites. The PCR products were cloned into

the pGEM-T Easy vector (Promega), and the sequences were confirmed by sequence analysis. Fragments were obtained by digestion with EcoRI and BamHI and cloned into the EcoRI-BamHI-digested pTug-EGFP^{glyc} vector.

By using combinations of the primers used to create the C-terminal deletions and primers for N-terminal deletions, the sequences encoding each of the hydrophobic domains of MHV nsp6 were also amplified separately. These sequences were cloned into the pGEM-T Easy vector (Promega) and confirmed by sequence analysis. Fragments were obtained by digestion with EcoRV and BamHI and cloned into the EcoRV-BamHI-digested pTugM_N-nsp6$_m$-EGFP^{glyc} plasmid, thereby creating constructs encoding the MHV nsp6 fragments fused N terminally to the MHV M tag and C terminally to the EGFP tag containing the *N* glycosylation site.

The construct containing SARS-CoV nsp4 in which the *N* glycosylation site had been removed by mutation has been described previously (37). This construct was used to create C-terminal deletion mutants lacking one to three of the hydrophobic domains. PCRs were performed with primer 3648 and primer 3848, 3650, or 3651; the products were cloned into the pGEM-T Easy vector (Promega); and the sequences were confirmed by sequence analysis. Fragments were obtained by digestion with EcoRI and BamHI and cloned into the EcoRI-BamHI-digested pTug-EGFP^{glyc} vector.

The construct containing MHV nsp4 has also been described previously (37). The glycosylation sites in MHV nsp4 were mutated by performing sequential site-directed mutagenesis reactions with primers 3758 and 3759 and primers 3760 and 3761. The construct with the mutated glycosylation sites was used to create C-terminal deletion mutants by performing PCRs with primer 2890 and primer 3847, 3756, or 3757. The PCR products were cloned into the pGEM-T Easy vector (Promega), and the sequences were confirmed by sequence analysis. Fragments were obtained by digestion with EcoRI and BamHI and cloned into the EcoRI-BamHI-digested pTug-EGFP^{glyc} vector.

The constructs encoding the equine arterivirus (EAV) membrane protein N-terminally extended with the M_N tag (EAV M + 9A) (10) and the 8a protein C-terminally tagged with the EGFP tag with or without the *N* glycosylation site (36) have been described previously.

Infection and transfection. Subconfluent monolayers of OST7-1 cells grown in 10-cm^2 tissue culture dishes were inoculated with vTF7-3 at a multiplicity of infection of 10 for 1 h, after which the medium was replaced with a transfection mixture consisting of 0.5 ml of DMEM without FCS but containing 10 μl Lipofectin (Invitrogen) and 5 μg of each selected construct. After a 5-min incubation at room temperature, 0.5 ml of DMEM was

added and incubation was continued at 37°C. At 3 h post infection (p.i.), the medium was replaced with culture medium. Where indicated, tunicamycin (5 μg/ml) or brefeldin A (6 μg/ml) was added to the culture medium at 3 h p.i.

Metabolic labeling and immunoprecipitation. Prior to labeling, the cells were starved for 30 min in cysteine- and methionine-free modified Eagle's medium containing 10 mM HEPES (pH 7.2) and 5% dialyzed FCS. This medium was replaced with 1 ml of a similar medium containing 100 μCi of ^{35}S *in vitro* cell-labeling mixture (Amersham), after which the cells were further incubated for the indicated time periods. After labeling, the cells were washed once with phosphate-buffered saline (PBS) containing 50 mM Ca^{2+} and 50 mM Mg^{2+} and then lysed on ice in 1 ml of lysis buffer (0.5 mM Tris [pH 7.3], 1 mM EDTA, 0.1 M NaCl, 1% Triton X-100) per 10-cm^2 dish. The lysates were cleared by centrifugation for 5 min at 15,000 rpm and 4°C.

Coupled *in vitro* transcription and translation reactions were performed with the TNT coupled reticulocyte lysate system from Promega, according to manufacturer's instructions, in the presence of ^{35}S *in vitro* labeling mixture (Amersham) but without the use of microsomal membranes.

Radioimmunoprecipitations were performed essentially as described previously (35); 200-μl aliquots of the cell lysates or 5-μl volumes of *in vitro* translation reaction mixtures were diluted in 1 ml detergent buffer (50 mM Tris [pH 8.0], 62.5 mM EDTA, 1% NP-40, 0.4% sodium deoxycholate, 0.1% sodiumdodecyl sulfate [SDS]) containing antibodies (2 μl rabbit anti-EGFP or rabbit anti-HA serum or 25 μl of J1.3 monoclonal anti-MHV M serum). The immunoprecipitation mixtures were incubated overnight at 4°C. The immune complexes were adsorbed to Pansorbin cells (Calbiochem) for 60 min at 4°C and subsequently collected by centrifugation. The pellets were washed three times by resuspension and centrifugation with RIPA buffer (10 mM Tris [pH 7.4], 150 mM NaCl, 0.1% SDS, 1% NP-40, 1% sodium deoxycholate). The final pellets were suspended in Laemmli sample buffer (LSB) and heated at 95°C for 1 min before analysis by SDS-polyacrylamide gel electrophoresis (PAGE) with 10 to 15% polyacrylamide gels.

Where indicated, immunoprecipitates were treated with peptide–*N*-glycosidaseF (PNGaseF; New England BioLabs). To this end, the final immunoprecipitation pellets were suspended in PBS instead of LSB, 2 μl PNGaseF was added, and the samples were incubated at 37°C for 2 h. Before analysis by SDS-PAGE, 0.5 volume of a three-times-concentrated solution of LSB was added to the samples, which were then heated at 95°C for 1 min.

Immunofluorescence microscopy. OST7-1 cells grown on glass coverslips were fixed at the indicated times post infection with 3%

Table 1. Sequence, polarity, position and purpose of primers used in this study

Primer	Sequence (5' to 3')*	Polarity	Position on viral genome	Purpose
3212	GCGACGTAAACGGCacCAAGTTCAGCGTG	+	-	EGFP +Nglyc
3213	CACGCTGAACTTGgtGCCGTTTACGTCGC	-	-	EGFP +Nglyc
3050	gatccTACCCATACGACGTGCCCGACTATGCCtag	+		HA tag
3051	gatcctaGGCATAGTCGGGCACGTCGTATGGGTAg	-		HA tag
3019	tcgagattATGAGTAGTACTACGCAAGCCCCAGAGCCAgat	+		M_N tag
3020	atcTGGCTCTGGGGCTTGCGTAGTACTACTCATaatc	-		M_N tag
3072	gaattc gatatcaccatgGCTGCTTATGTGGAAA	+	6482-6500	$nsp3_s$ C-2kb.
3073	ttaggatccACCACCCTTGAGTGAGATT	-	8484-8466	$nsp3_s$ C-2kb.
3354	GCGTTAGAGAATTGTATCTTAATTCGTaTcACGTTACTA CTATGGATTTCTG	+	6989-7040	$nsp3_s$ ΔN-glyc
3355	CAGAAATCCATACTAGTAACGTgAtACGAATTAAGATAC AATTCTCTAACGC	-	7040-6989	$nsp3_s$ ΔN-glyc
3460	ggatccATGAACATAGCTCTTCCATA	-	7392-7373	$nsp3_s$ ΔC-term
3461	ggatccCCAAGAATTGCTGATGAAATG	-	7284-7264	$nsp3_s$ ΔHD3
3576	ggatccCAATTCTCTAACGCCATTAC	-	7002-6983	$nsp3_s$ ΔHD2-3
3632	gaattc gatatcatgAAGTATGTGGTTTGGACTG	+	6717-6735	$nsp3_m$ C-2kb.
2933	ggatccTCCTTTAAGAGAGAACGGTG	-	8717-8698	$nsp3_m$ C-2kb.
3630	GAAGTTCGTTTTGTgcTGGAAGTATGGTATG	+	7255-7285	$nsp3_m$ ΔN-glyc
3631	CATACCATACTTCCAgcACAAAACGAACTTC	-	7285-7255	$nsp3_m$ ΔN-glyc
3633	ggatccAGTCTCCAGCATAAAGAA	-	7514-7497	$nsp3_m$ ΔHD5
3634	ggatccAAATAGGCTAATATAGTCAA	-	7391-7372	$nsp3_m$ ΔHD4-5
3635	ggatccAGGCAAATAGAAGTCACTC	-	7145-7127	$nsp3_m$ ΔHD3-5
3636	ggatccATTAAACGTCTGTAAGGCA	-	7043-7025	$nsp3_m$ ΔHD2-5
3070	gaattc gatatcaccatgGGTAAGTTCAAGAAAATTGT	+	10903-10922	$nsp6_s$
3071	ttaggatccCTGTACAGTAGCAACCTTGA	-	11772-11753	$nsp6_s$
2974	gatatcatgAGCAAGCGCACAAGAGTTATAAAAGG	+	11118-11143	$nsp6_m$
2975	ggatccTTGGATCTGAGATACTTCAATGACTG	-	11978-11953	$nsp6_m$
3350	ggatccCTGCGGTACGTCTGTGAAG	-	11726-11708	$nsp6_m$ ΔHD7
3351	ggatccGGATGTGAGGAACAATAG	-	11621-11604	$nsp6_m$ ΔHD6-7
3572	ggatccGTCGTGGTTTATGCTACGC	-	11519-11501	$nsp6_m$ ΔHD5-7
3573	ggatccTACAGCAGGGACAAAGTGTG	-	11432-11413	$nsp6_m$ ΔHD4-7
3574	ggatccATGCTTATGCTTGATCAACA	-	11306-11287	$nsp6_m$ ΔHD3-7
3575	ggatccGGTAGTAACATACATAAACATA	-	11234-11213	$nsp6_m$ ΔHD2-7
3566	gatatcatgagcaagcgcacaagaTATGTTACTACCCATATGTT	+	11223-11242	$nsp6_m$ ΔHD1
3567	gatatcatgagcaagcgcacaagaAAGCATAAGCATTTGTATT	+	11295-11313	$nsp6_m$ ΔHD1-2
3568	gatatcatgAAACAGAGTTTTAGAGGTC	+	11376-11394	$nsp6_m$ ΔHD1-3
3569	gatatcatgagcaagcgcacaagaCGTAGCATAAACCACGAC	+	11502-11519	$nsp6_m$ ΔHD1-4
3570	gatatcatgAATTTAGAGGAAGAGGTACT	+	11586-11605	$nsp6_m$ ΔHD1-5
3571	gatatcatgAATGTCTTGTACTTCACAGA	+	11697-11716	$nsp6_m$ ΔHD1-6
3648	gaattcaccatgAAGATTGTTAGTACTTGTTTT	+	8485-8505	$nsp4_s$
3848	ttaggatccTCCCGGCAGAAAGCTGTA	-	9504-9487	$nsp4_s$ ΔHD4
3650	ttaggatccGTTGTACTCACCAAAAACAC	-	9420-9401	$nsp4_s$ ΔHD3-4
3651	ttaggatccGCCAACAGCACTAAAAACAC	-	8874-8855	$nsp4_s$ ΔHD2-4
3758	GGTGTTATGCACgcTGCCTCTCTGTA	+	9234-9259	$nsp4_m$ ΔN-glyc1
3759	TACAGAGAGGCAgcGTGCATAACACC	-	9259-9234	$nsp4_m$ ΔN-glyc1
3760	CTGCTTTAATTTTgcTCGTTCATGGGT	+	9416-9442	$nsp4_m$ ΔN-glyc2
3761	ACCCATGAACGAgcAAAATTAAAGCAG	-	9442-9416	$nsp4_m$ ΔN-glyc2
2890	gatatcatgGCTGTTTTTAGTAGAATGTTAC	+	8721-8742	$nsp4_m$
3847	ttaggatccACAAGCATATAAACAAGACA	-	9749-9730	$nsp4_m$ ΔHD4
3756	ttaggatccAGTGTAGTCACCAAAGGCACG	-	9653-9633	$nsp4_m$ ΔHD3-4
3757	ttaggatccCATAACACCCCCTGTATAAC	-	9242-9223	$nsp4_m$ ΔHD2-4

* Coding sequences are shown in uppercase, lowercases indicate nucleotides added for cloning purposes with restriction enzyme recognition sites underlined.

paraformaldehyde for 1 h at room temperature. The fixed cells were washed with PBS and permeabilized with either 0.1% Triton X-100 for 10 min at room temperature or 0.5 μg/ml digitonin (diluted in 0.3 M sucrose–25 mM $MgCl^{2+}$–0.1 M KCl–1 mM EDTA–10 mM PIPES [pH 6.8]) for 5 min at 4°C. Next, the permeabilized cells were washed with PBS and incubated

for 15 min in blocking buffer (PBS–10% normal goat serum), followed by a 45-min incubation with antibodies directed against HA or against the C- or N-terminal domain of MHV M. After four washes with PBS, the cells were incubated for 45 min with either fluorescein isothiocyanate-conjugated goat anti-rabbitimmunoglobulin G antibodies (ICN) or Cy5-conjugated donkey anti-mouse immunoglobulin G antibodies (Jackson Laboratories). After four washes with PBS, the samples were mounted on glass slides in FluorSave (Calbiochem). The samples were examined with a confocal fluorescence microscope (Leica TCS SP2).

RESULTS

Processing of nsp3 and nsp6.

We started our studies of nsp3 and nsp6 by analyzing the co- and posttranslational modifications of the two proteins from both SARS-CoV and MHV. To this end, gene fragments encoding nsp3 and nsp6 of both viruses were cloned into the pTUG31 vector behind a T7 promoter and fused to an EGFP tag, since no antibodies to the proteins themselves were available. As the full-length nsp3-encoding genome segments are very large (approximately 6 kb) and difficult to clone, only the 3'-terminal 2-kb fragments, which encode all of the hydrophobic domains, were cloned. nsp3 of both SARS-CoV and MHV contains potential *N* glycosylation sites (NXS/T) in front of the first hydrophobic domain, between the first and second hydrophobic domains, and behind the third hydrophobic domain (Fig. 1 shows the localization of the hydrophobic domains). The glycosylation sites between the first and second hydrophobic domains, two for SARS-CoV and one for MHV, have previously been shown to be functional (22, 28). No potential *N* glycosylation sites were identified in the sequence of MHV nsp6, while for SARS-CoV nsp6, an *N* glycosylation site was predicted between the fifth and sixth hydrophobic domains.

We studied the expression and processing of the nsps by *in vitro* translation and by using the recombinant vaccinia virus bacteriophage T7 RNA polymerase (vTF7-3) expression system. OST7-1 cells were infected with vTF7-3, transfected with plasmids containing the nsp3-EGFP or nsp6-EGFP gene, and labeled with [^{35}S]methionine from 5 to 6 h p.i. The cells were lysed and processed for immunoprecipitation with a rabbit polyclonal antiserum directed to the EGFP tag. In parallel, *in vitro* translations were performed with the TNT coupled reticulocyte lysate system from Promega in the absence of membranes to analyze the electrophoretic mobility of the

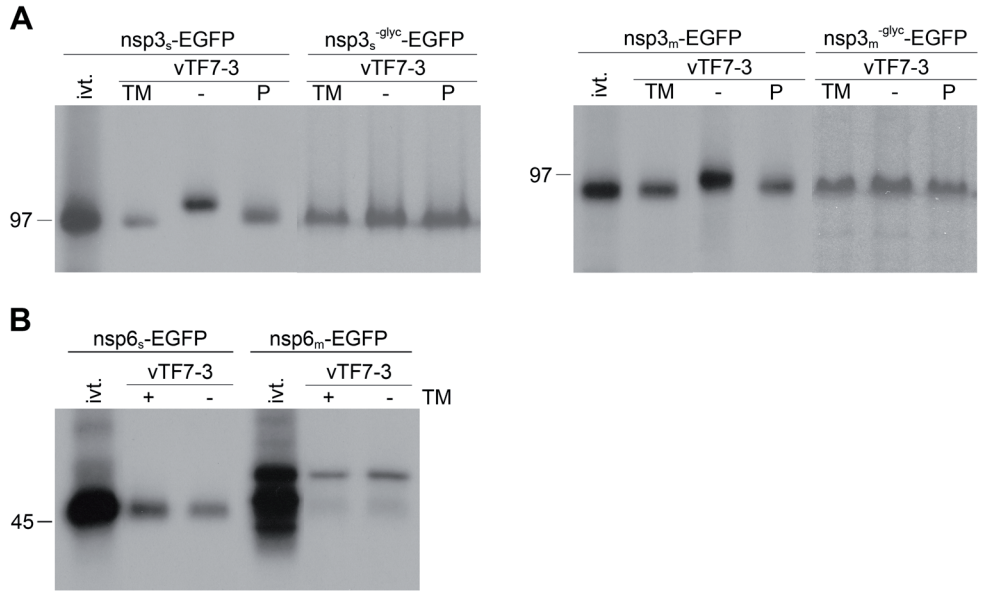

Figure 2. Processing of SARS-CoV and MHV nsp3 and nsp6. vTF7-3-infected OST7-1 cells were transfected with the indicated constructs. The cells were labeled with [^{35}S]methionine from 5 to 6 h p.i., lysed, and processed for immunoprecipitation with antiserum directed to the EGFP tag, followed by SDS-PAGE. (A) Cells were transfected with SARS-CoV or MHV nsp3-EGFP (nsp3$_s$-EGFP or nsp3$_m$-EGFP, respectively)-encoding constructs without or with mutation (–glyc) of the *N* glycosylation sites in the presence (TM) or absence (– and P) of tunicamycin. The constructs with intact glycosylation sites were also transcribed and translated *in vitro* with the TNT coupled reticulocyte lysate system from Promega (ivt.). After immunoprecipitations, the samples were mock (TM, –) or PNGaseF (P) treated. (B) Cells were transfected with SARS-CoV or MHV nsp6-EGFP (nsp6$_s$-EGFP and nsp6$_m$-EGFP, respectively)-encoding constructs in the presence (+) or absence (–) of tunicamycin (TM). The same constructs were also transcribed and translated *in vitro* with the TNT coupled reticulocyte lysate system from Promega (ivt.). The positions and masses (in kilodaltons) of protein size markers are indicated at the left. Only the relevant portion of the gels is shown.

non-processed proteins. To demonstrate the presence of the *N*-linked sugars on the nsps, the proteins were expressed in the presence and absence of tunicamycin, which is an inhibitor of *N*-linked glycosylation, and/or the *N*-linked glycans were enzymatically removed with PNGaseF.

As shown in Fig. 2A, the electrophoretic mobility of nsp3 expressed in OST7-1 cells in the presence of tunicamycin was similar to that of the *in vitro*-translated product, whereas the protein expressed in the absence of tunicamycin migrated slower. Treatment of this latter protein with PNGaseF shifted its electrophoretic mobility to that of the *in vitro*-translated product and of the protein expressed in the presence of tunicamycin. This result confirms the addition of *N*-linked glycans to nsp3, as has been demonstrated previously (22, 28). Next, the *N* glycosylation sites between the first and

second hydrophobic domains were mutated and these proteins, in fusion with EGFP (nsp3^{-glyc}-EGFP), were also expressed in the presence and absence of tunicamycin and/or treated with PNGaseF. The presence of tunicamycin or treatment with PNGaseF did not influence the electrophoretic mobility of these mutant proteins (Fig. 2A). This clearly demonstrates that the *N* glycosylation sites between the first and second hydrophobic domains are the only *N*-glycan attachment sites. The other potential sites are likely inaccessible, probably because they are located on the cytoplasmic side of the membrane.

vTF7-3-expressed nsp6 of both viruses comigrated in the gel with the corresponding *in vitro*-translated products, both in the presence and in the absence of tunicamycin (Fig. 2B). Also, some lower-molecular-weight products were observed after the *in vitro* translation of MHV nsp6, which probably resulted from translation initiation at more downstream start codons. Apparently, nsp6 of SARS-CoV or MHV is not *N* glycosylated, indicating that the putative glycosylation site in the region between the fifth and sixth hydrophobic domains of SARS-CoV nsp6 is either located on the cytoplasmic side of the membrane or not accessible for glycosylation for other reasons. Furthermore, it appeared that both nsp6 fusion proteins migrated with lower mobility in the gel than predicted on the basis of their amino acid sequences. Similar results have been obtained before for other highly hydrophobic proteins (37, 41).

Membrane topology of nsp3 and nsp6.

In order to elucidate the membrane topology of SARS-CoV and MHV nsp3 and nsp6, we studied the disposition of their amino and carboxy termini. Therefore, the proteins were C or N terminally extended with tags containing potential glycosylation sites. The C termini of the proteins were fused to an EGFP tag in which an *N* glycosylation site had been created (EGFP^{glyc}). As a control, we used a fusion protein generated earlier which essentially consists of a cleavable signal sequence fused to the same tag (8a-EGFP) (36). For nsp3, the tag was fused to either the SARS-CoV or the MHV gene fragment in which the *N* glycosylation sites between the first and second hydrophobic domains had been disabled by mutation (nsp3^{-glyc}) to allow discrimination between glycosylation of the tag and that of nsp3 itself. The fusion proteins were expressed with the vTF7-3 expression system in the presence and absence of tunicamycin. *N* glycosylation of the C-terminal EGFP tag would demonstrate that the carboxy terminus of the protein is located on the lumenal side of the membrane.

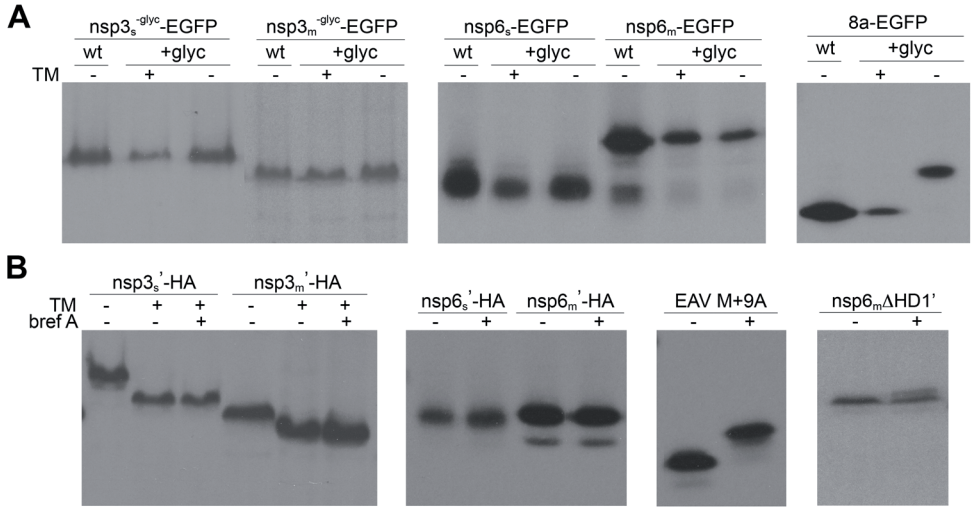

Figure 3. Glycosylation of tagged SARS-CoV and MHV nsp3 and nsp6. vTF7-3-infected OST7-1 cells were transfected with the indicated constructs. The cells were labeled with [^{35}S]methionine from 5 to 6 h p.i., lysed, and processed for immunoprecipitation, followed by SDS-PAGE. (A) Cells were transfected with constructs encoding SARS-CoV or MHV nsp3 or nsp6 or encoding the SARS-CoV orf8a protein (8a), each fused either to a wild-type EGFP tag (wt) or to an EGFP tag with an *N* glycosylation site (+glyc). The proteins were expressed in the presence (+) or absence (–) of tunicamycin (TM). Immunoprecipitations were performed with rabbit antiserum directed to the EGFP tag. (B) Cells were transfected with constructs encoding SARS-CoV or MHV nsp3 or nsp6 with a C-terminal HA tag and an N-terminal M_N tag (') or with a construct encoding the EAV M protein with the same M_N tag (EAV M + 9A). MHV nsp6 lacking the first hydrophobic domain (nsp6$_m$HD1') contains the N-terminal M_N tag in combination with a C-terminal EGFP tag. The cells were incubated in the presence (+) or absence (–) of brefeldin A (bref A) and or tunicamycin (TM). Immunoprecipitations were performed with rabbit antiserum directed to the HA tag or, for EAV M, with monoclonal antibody J1.3 (directed against the M_N tag). Only the relevant portions of the gels are shown.

For each of the proteins (nsp3 or nsp6), a similar electrophoretic mobility was observed regardless of the EGFP tag used (i.e., with or without the *N* glycosylation site) or the presence of tunicamycin (Fig. 3A). The control protein, 8a, behaved as expected. In the presence of tunicamycin, the protein with the EGFP^{glyc} tag migrated with the same mobility as the protein with the wild-type tag in the absence of tunicamycin, whereas in the absence of tunicamycin the protein with the EGFP^{glyc} tag migrated slower (Fig. 3A). The results demonstrate that the carboxy termini of nsp3 and nsp6 of both SARS-CoV and MHV are located on the cytoplasmic side of the membrane.

To examine the disposition of the nsp3 and nsp6 amino termini, the N-terminal 10-residue sequence of the MHV M protein (M_N), which contains a well-defined *O* glycosylation motif, was fused to the amino terminus of each nsp. The functionality of this tag was previously demonstrated after fusion to

the EAV type III M protein, resulting in EAV M + 9A (10). This protein has a N_{exo}/C_{endo} topology and is retained in the ER. Yet it became *O* glycosylated upon the addition of brefeldin A, a drug which causes the redistribution of Golgi enzymes, including the ones involved in *O* glycosylation, to the ER. By a similar approach, the location of the N termini of nsp3 and nsp6 was assessed. The nsp fusion proteins, containing the N-terminal M_N and a C-terminal HA tag, were expressed with the vTF7-3 expression system in OST7-1 cells in the presence or absence of brefeldin A and/or tunicamycin. Tunicamycin was added to the cells expressing the nsp3 fusion protein to prevent its *N* glycosylation, as this could obscure the detection of its *O* glycosylation.

As shown in Fig. 3B, the EAV M + 9A control protein showed a shift in electrophoretic mobility when it was expressed in the presence of brefeldin A. In contrast, the electrophoretic mobilities of the nsp3 and nsp6 fusion proteins were unaffected by the addition of brefeldin A. As expected, the presence of tunicamycin did prevent the addition of *N*-linked sugars to nsp3. These results indicate that the amino termini of SARS-CoV and MHV nsp3 and nsp6 are not accessible to enzymes that mediate the addition of *O*-linked sugars, which is most likely explained by the cytoplasmic exposure of these termini, although misfolding of the amino terminal tag as the cause can also not be ruled out completely. We do not consider the latter explanation very likely, since the presence of two proline residues in the tag has previously been demonstrated to induce a conformation favorable for glycosylation (10). Indeed, when the first hydrophobic domain of MHV nsp6 was removed, the resulting protein carrying the amino-terminal tag (now in combination with a C-terminal EGFP tag) did become modified by *O*-linked sugars in the presence of brefeldin A, as shown by the appearance of an extra band which runs at a slightly higher position in the gel. The difference in electrophoretic mobility between the glycosylated and unglycosylated protein species is smaller for the nsp6 mutant than for the EAV M protein because of the much higher molecular weight of EGFP-tagged nsp6 (Fig. 3B).

The localization of the amino and carboxy termini of each nsp was also determined by immunofluorescence assays. In these experiments, nsps were used that were tagged at both ends, containing the N-terminal M_N and a C-terminal HA extension. OST7-1 cells were infected with vTF7-3 and transfected with plasmids encoding the fusion proteins. The cells were fixed at 6 h p.i. with 3% paraformaldehyde and permeabilized under strictly controlled conditions with either Triton X-100, which permeabilizes all cellular membranes, or digitonin, which selectively permeabilizes the plasma membrane. The type III MHV M protein, which has a known N_{exo}/C_{endo}

topology and localizes to the Golgi compartment, was used as a control. A rabbit polyclonal antibody directed to the C terminus and a mouse monoclonal antibody directed to the N terminus were used to detect this protein after the use of each of the permeabilization methods. As expected, the antibody directed to the C terminus detected the protein after Triton X-100 permeabilization, as well as after digitonin permeabilization, whereas the antibody directed to the N terminus only detected the protein after permeabilization with Triton X-100 and not after treatment with digitonin, thereby validating the assay conditions (Fig. 4).

Similar experiments were performed for SARS-CoV and MHV nsp3 and nsp6, with the exception that a different rabbit antiserum, directed against the C-terminal HA tag, was used. Both nsp3 and nsp6 appeared to localize in a reticular pattern reminiscent of the ER, as observed at higher magnification (data not shown). After permeabilization with Triton X-100 or digitonin, cells were stained with the rabbit antibody directed to the C terminus and the mouse antibody directed to the N terminus. The results, shown in Fig. 4, demonstrate that the amino and carboxy termini of both nsp3 and nsp6 are located on the cytoplasmic face of the membrane and confirm the results obtained with the biochemical experiments shown in Fig. 3. Furthermore, the localization of the nsp3 amino terminus on the cytoplasmic face of the membrane is in agreement with the observed *N* glycosylation in the region between the first and second transmembrane domains.

Membrane integration of nsp3.

The above results show that both nsp3 and nsp6 have a N_{endo}/C_{endo} membrane topology, indicating that both nsps have an even number of transmembrane domains. This is not in agreement with the three and seven transmembrane domains that are predicted for nsp3 and nsp6, respectively. Therefore, we examined which of the predicted transmembrane domains are indeed used as such. To this end, constructs were made that encode progressive C-terminal deletion mutant forms of the nsps, lacking one or more hydrophobic domains, fused to the $EGFP^{glyc}$ tag.

As SARS-CoV nsp3 appeared to be *N* glycosylated between the first two of its three predicted transmembrane domains, it seems most likely that either the second or the third hydrophobic domain does not function as a membrane-spanning domain. Mutant forms were made in which the C-terminal hydrophilic tail was deleted or in which the C-terminal deletion was extended to include either the third hydrophobic domain or both the third and second hydrophobic domains (Fig. 5A). These deletion mutant forms,

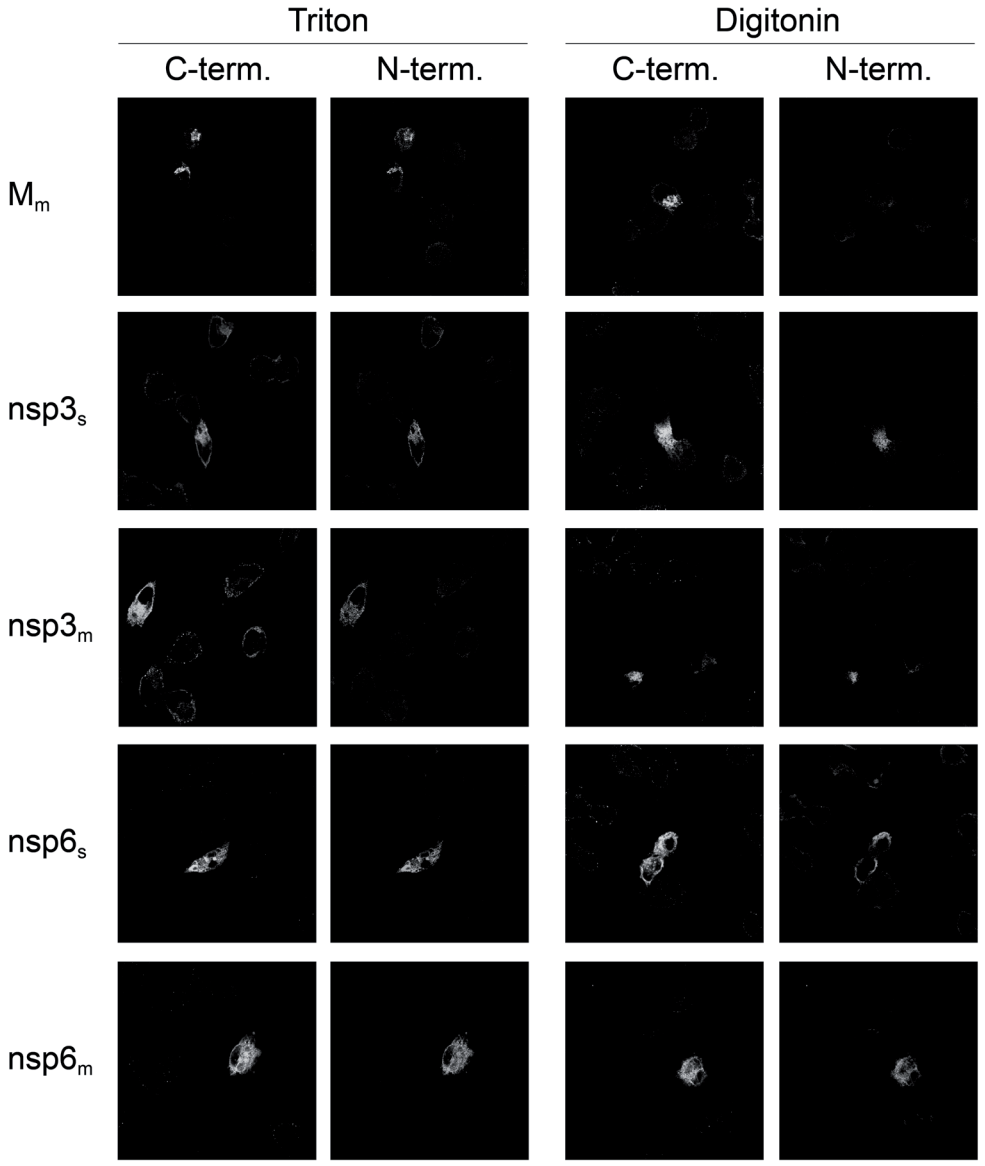

Figure 4. Membrane topology of SARS-CoV and MHV nsp3 and nsp6. vTF7-3-infected OST7-1 cells were transfected with constructs encoding the proteins indicated at the left. The cells were fixed at 6 h p.i. and permeabilized with Triton X-100 (left two columns) or digitonin (right two columns). Immunofluorescence analysis was performed with antibodies against the C-terminal (C-term.) tag, anti-M_C for M_M and anti-HA for the nsps (first and third columns), or against the N-terminal (N-term.) tag, J1.3 (anti-M_N, second and fourth columns).

which were fused to the $EGFP^{glyc}$ tag, additionally carried the mutations that disrupt the *N* glycosylation motifs between the first and second hydrophobic domains.

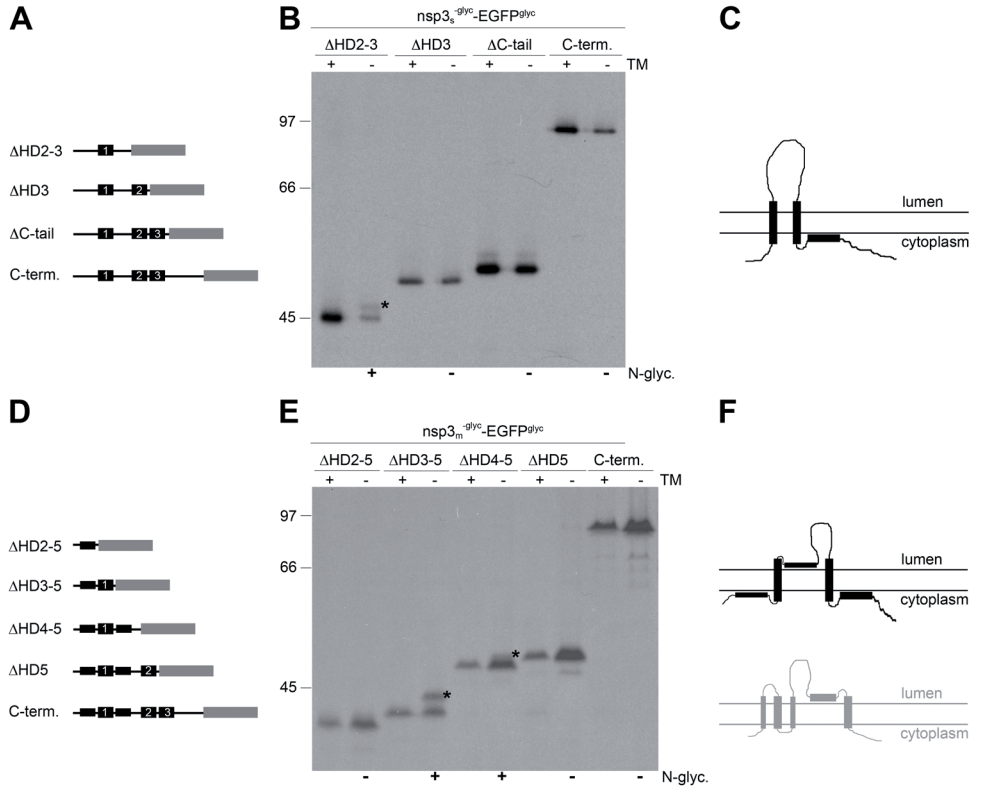

Figure 5. Membrane integration of deletion mutant forms of SARS-CoV and MHV nsp3. (A, D) Schematic representations of the C-terminal (C-term.) deletion mutant forms of SARS-CoV (A) and MHV (D) nsp3, with the hydrophobic domains presented as black rectangles and the EGFP^{glyc} tag in gray. The corresponding hydrophobic domains in the two proteins are indicated by numbers. (B, E) vTF7-3-infected OST7-1 cells were transfected with the indicated constructs and expressed in the presence (+) or absence (–) of tunicamycin (TM). The cells were labeled with [^{35}S]methionine from 5 to 6 h p.i., lysed, and processed for immunoprecipitation with anti-EGFP antiserum followed by SDS-PAGE. The positions and masses (in kilodaltons) of the protein size markers are indicated at the left. The asterisks indicate the position of the glycosylated protein species. Below the panels, the observed presence or absence of *N* glycosylation is indicated by a plus or a minus sign, respectively. (C, F) Models of the membrane structures of SARS-CoV (C) and MHV (F) nsp3, with the hydrophobic domains presented as black rectangles. For comparison, the MHV nsp3 model proposed by Baker and coworkers is shown below in gray.

vTF7-3-infected OST7-1 cells were transfected with constructs encoding the different fusion proteins and labeled from 5 to 6 hp.i. in the presence or absence of tunicamycin. The cells were lysed and processed for immunoprecipitation with the anti-EGFP serum. As shown in Fig. 5B, complete removal of the hydrophilic C terminus of nsp3 (ΔC-tail) does not affect the glycosylation of the fusion protein, as expected. When the third hydrophobic domain was additionally deleted, the fusion protein still remained

indifferent to tunicamycin and was thus not glycosylated, indicating that this third hydrophobic domain did not function as a transmembrane domain (Fig. 5B). However, when the second hydrophobic domain was deleted as well, an extra protein species with a slightly lower electrophoretic mobility appeared after expression in the absence of tunicamycin compared to in its presence (Fig. 5B). Although the protein was only partially glycosylated, this result demonstrates that the carboxy-terminal EGFP tag fused to this mutant form of nsp3 is translocated to the lumenal side of the membrane. As nsp3ΔHD2-3 was the only mutant form that became modified by *N*-linked sugars, we conclude that SARS-CoV nsp3 spans the lipid bilayer only twice and that the third hydrophobic domain does not function as a transmembrane domain (Fig. 5C).

The transmembrane domain predictions for MHV nsp3 are somewhat different from those for SARS-CoV nsp3. Several programs predict the presence of five rather than three transmembrane domains. Three of these correspond to those in SARS-CoV nsp3, but additional hydrophobic domains are located immediately up- and downstream of the first domain (Fig. 5D). However, not all programs predict these additional hydrophobic domains to be membrane spanning (28). Earlier work by Baker and coworkers, with a combination of *in vitro* translations, carbonate extraction assays, and proteinase K treatments, suggested that four of the five predicted hydrophobic domains functioned as transmembrane domains, with only the fourth domain (i.e., the one corresponding to the second hydrophobic domain in SARS-CoV nsp3) not spanning the lipid bilayer (28). As these results are in conflict with the results we obtained for SARS-CoV nsp3, we prepared a similar set of progressive C-terminal deletion mutant forms of MHV nsp3 lacking one, two, three, or four of the putative transmembrane domains and again fused to the $EGFP^{glyc}$ tag (Fig. 5D).

The different constructs were expressed with the vTF7-3 system in the presence or absence of tunicamycin. The EGFP tag was again not glycosylated when fused to the unmodified carboxy terminus of nsp3 or when the last hydrophobic domain(HD5) was deleted, consistent with the results obtained for SARS-CoV nsp3 (Fig. 5E). However, when the fourth hydrophobic domain was deleted as well, the fusion protein became partially glycosylated, as shown by the presence of a protein species the appearance of which was inhibited by tunicamycin (Fig. 5E), indicating that the EGFP tag had become translocated. The same result, though with more efficient glycosylation, was obtained when also the third hydrophobic domain was removed. Finally, additional deletion of the second hydrophobic domain, which corresponds

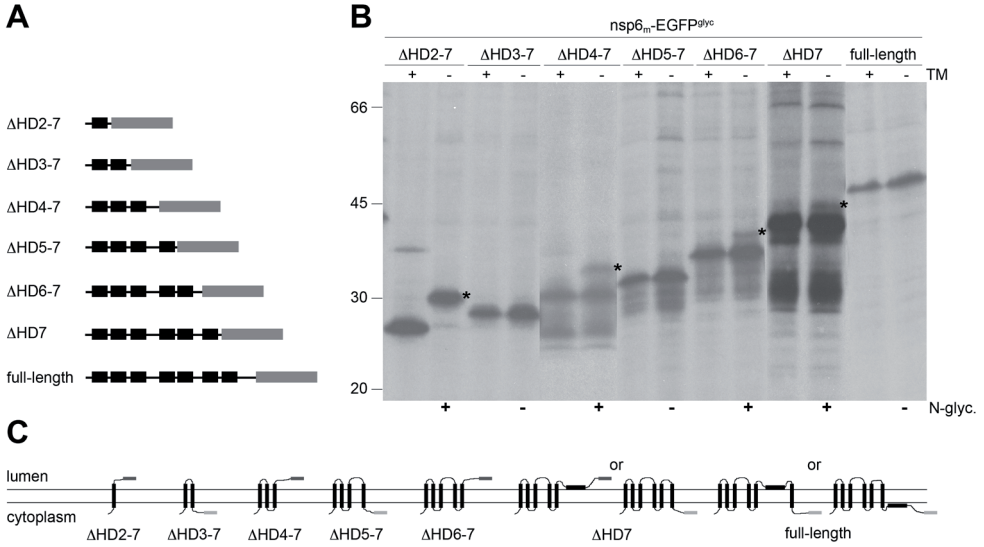

Figure 6. Membrane integration of deletion mutant forms of MHV nsp6. (A) Schematic representation of the MHV nsp6 C-terminal deletion mutant forms, with the hydrophobic domains presented in black and the EGFP^{glyc} tag in gray. (B) vTF7-3-infected OST7-1 cells were transfected with the constructs presented in panel A and expressed in the presence (+) or absence (–) of tunicamycin (TM). The cells were labeled with [^{35}S]methionine from 5 to 6 h p.i., lysed, and processed for immunoprecipitation with anti-EGFP antiserum, followed by SDS-PAGE. The positions and masses (in kilodaltons) of the protein size markers are indicated at the left. The asterisks indicate the positions of the glycosylated protein species. Below the gel, the observed presence or absence of *N* glycosylation is indicated by a plus or a minus sign, respectively. (C) Models of the membrane structures of the C-terminal deletion mutant forms of MHV nsp6. The hydrophobic domains are presented as black rectangles, and the EGFP tag is presented as a dark gray rectangle when glycosylated and in light gray when unglycosylated.

to the first hydrophobic domain of SARS-CoV nsp3, resulted in an unglycosylated protein as its electrophoretic mobility was not affected by the presence of tunicamycin (Fig. 5E). As nsp3ΔHD4-5 and nsp3ΔHD3-5 were the only MHV nsp3 mutant constructs that became modified by *N*-linked sugars, while the other mutants showed no trace of glycosylation, we conclude that MHV nsp3 integrates into the membrane similarly to SARS-CoV nsp3, with only two membrane-spanning domains at approximately the same positions in the protein (Fig. 5F).

Membrane integration of nsp6.

Transmembrane domain predictions for nsp6 yielded similar results for the MHV and SARS-CoV proteins, as well as for other coronaviruses shown in the multiple alignment of the ORF1a sequence. Because SARS-CoV nsp6 consistently appeared as a fuzzy band when analyzed by SDS-PAGE, which

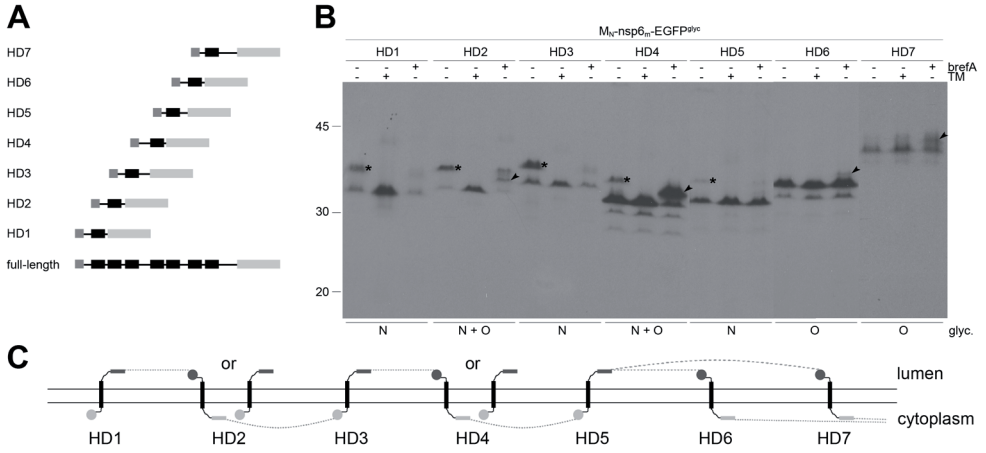

Figure 7. Membrane integration of MHV nsp6 hydrophobic domains. (A) Schematic representation of the MHV nsp6 constructs. (B) vTF7-3-infected OST7-1 cells were transfected with the constructs presented in panel A and expressed in the presence (+) or absence (–) of tunicamycin (TM) or brefeldin A (brefA). The cells were labeled with [^{35}S]methionine from 5 to 6 h p.i., lysed, and processed for immunoprecipitation with anti-EGFP antiserum, followed by SDS-PAGE. The positions and masses (in kilodaltons) of the protein size markers are indicated at the left. Only the relevant portion of the gel is shown. The asterisks indicate the position of the *N*-glycosylated protein species, and the arrowhead indicates that of the *O*-glycosylated protein species. Below the panels, the observed presence or absence of *N*- and or *O*-linked oligosaccharides is indicated. (C) Model of the membrane topologies of the nsp6 hydrophobic domains. The hydrophobic domains are presented as black rectangles, the EGFP^{glyc} tag is presented as a gray rectangle, and the M_N tag is presented as a gray circle. Dark gray rectangles or circles represent glycosylated tags, and light gray rectangles or circles represent unglycosylated tags. The dotted line connects the transmembrane domains in accordance with the full-length nsp6 structure, indicating that either the sixth or the seventh hydrophobic domain does not traverse the lipid bilayer.

will complicate the interpretation of our assay, we limited our focus to MHV nsp6. The observed cytoplasmic localization of both the amino and the carboxy termini of nsp6 implies the presence of an even number of transmembrane domains, although invariably seven such domains are predicted. Thus, as for nsp3, one of the predicted transmembrane domains is probably not used as such. To confirm this conclusion and identify this particular domain, we made progressive C-terminal deletion mutant constructs lacking one to six of the potential transmembrane domains and tagged once again with the EGFP^{glyc} tag (Fig. 6A) and evaluated these mutant constructs as before.

As shown in Fig. 6B, when only the first hydrophobic domain was present (ΔHD2-7), the clear electrophoretic mobility difference caused by tunicamycin indicated that the EGFP tag was glycosylated and thus present on the lumenal side of the membrane, implying that the first hydrophobic domain functions both as a signal sequence and as a transmembrane domain.

The mutant protein containing the first two hydrophobic domains (ΔHD3-7) remained unglycosylated, indicating that also the second hydrophobic domain spans the membrane. Mutant proteins with additional transmembrane domains continued to reveal alternatingly the appearance and disappearance of *N*-linked modifications, indicating that the predicted transmembrane domains are integrated in the lipid bilayer. However, when reaching the sixth hydrophobic domain, the regular succession was interrupted as this protein, ΔHD7, appeared to become glycosylated, though only marginally. The wild-type protein showed no sign of glycosylation. These observations lead to a model in which only six hydrophobic domains in MHV nsp6 are actually used as transmembrane domains. Our data appear to indicate that the sixth hydrophobic domain does not span the lipid bilayer; however, in view of the very inefficient glycosylation of the ΔHD7 mutant construct, we cannot fully exclude the possibility that the seventh hydrophobic domain is not membrane spanning (Fig. 6C).

The efficiency of glycosylation that we observed in this deletion assay appeared to decrease with increasing protein length. We have no clear explanation for this. Perhaps the accessibility of the glycosylation site differs between the different proteins, though this does not seem very likely, assuming that the EGFP moiety folds independently and similarly in all cases its glycosylation site is always presented in the same way. Alternatively, the longer proteins might adopt multiple alternative membrane topologies, though this is again not a very likely possibility since such behavior is not observed for ΔHD3-7, ΔHD5-7, and full-length nsp6, as judged by their complete lack of glycosylation. It seems more plausible that the functioning of the third, and particularly the fifth, hydrophobic domain as an internal signal sequence for membrane insertion is somehow hampered by the EGFP extension, resulting in decreased efficiency of tag translocation.

In view of these uncertainties and to obtain further evidence for our model, an additional set of mutant proteins was created in which each one of the MHV nsp6 hydrophobic domains was individually positioned between a C-terminal $EGFP^{glyc}$ tag and an N-terminal M_N tag containing an *O* glycosylation site (Fig. 7A). The HD1 protein is, in fact, identical to nsp6ΔHD2-7 (Fig. 6), except for the amino-terminal tag containing the *O* glycosylation site. The proteins were expressed with the vTF7-3 system in the presence and absence of brefeldin A or tunicamycin and analyzed as before (Fig. 7B). The fusion proteins containing hydrophobic domain 1, 2, 3, 4, or 5 appeared in two electrophoretic forms when expressed in the absence of any drug. The slower-migrating form of these was not observed

when tunicamycin had been applied, indicating that these proteins became *N* glycosylated. The proteins that contained either hydrophobic domain 2, 4, 6, or 7 exhibited a partial shift in electrophoretic mobility upon expression in the presence of brefeldin A, indicating that these proteins were modified by *O*-linked sugars. The addition of *O*-linked sugars was less efficient for the proteins containing either hydrophobic domain 6 or 7. Strikingly, the proteins that contained hydrophobic domain 2 or 4 were apparently able to adopt two alternative topologies, as both types of glycosylation were detected. These proteins are either *N* or *O* glycosylated, but not both, since in that case expression in the presence of brefeldin A would have resulted in an additional reduction in electrophoretic mobility relative to the *N*-glycosylated protein species. Thus, these proteins are still membrane associated. These results indicate that, in principle, all hydrophobic domains are able to individually mediate insertion into the membrane and to function as transmembrane domains, although with different efficiencies, where especially domains 6 and 7 were inserted with lower efficiency (Fig. 7C). All together, the results are consistent with our model in which nsp6 has both of its termini exposed on the cytoplasmic face of the membrane while spanning the lipid bilayer six times. Of the seven predicted transmembrane domains, the sixth or seventh is least likely to function as such.

Membrane integration of nsp4.

In view of the observations with nsp3 and nsp6, we wanted to complete these evaluations by similarly analyzing the membrane structure of the third viral membrane protein involved in anchoring the replication complex, nsp4. Our earlier study already revealed that both termini of this protein are oriented cytoplasmically and that the protein, both for SARS-CoV and for MHV, is *N* glycosylated in a region between the first two of its four hydrophobic domains, which led us to propose a tetraspanning structure (37). Yet, we could not exclude the possibility that actually two of the three carboxy-terminal hydrophobic domains are not membrane spanning. Hence, we constructed progressive C-terminal deletion mutant constructs of both MHV and SARS-CoV nsp4 in which the natural glycosylation sites had additionally been removed by mutagenesis and which were again fused to the EGFP^{glyc} tag (Fig. 8A and D). The proteins were expressed in the presence and absence of tunicamycin and analyzed as before.

The nsp4 mutant forms of both viruses gave similar results (Fig. 8B and E). Full-length nsp4-EGFP^{glyc} remained unglycosylated, as expected (37). When only the first hydrophobic domain was present (ΔHD2-4), the

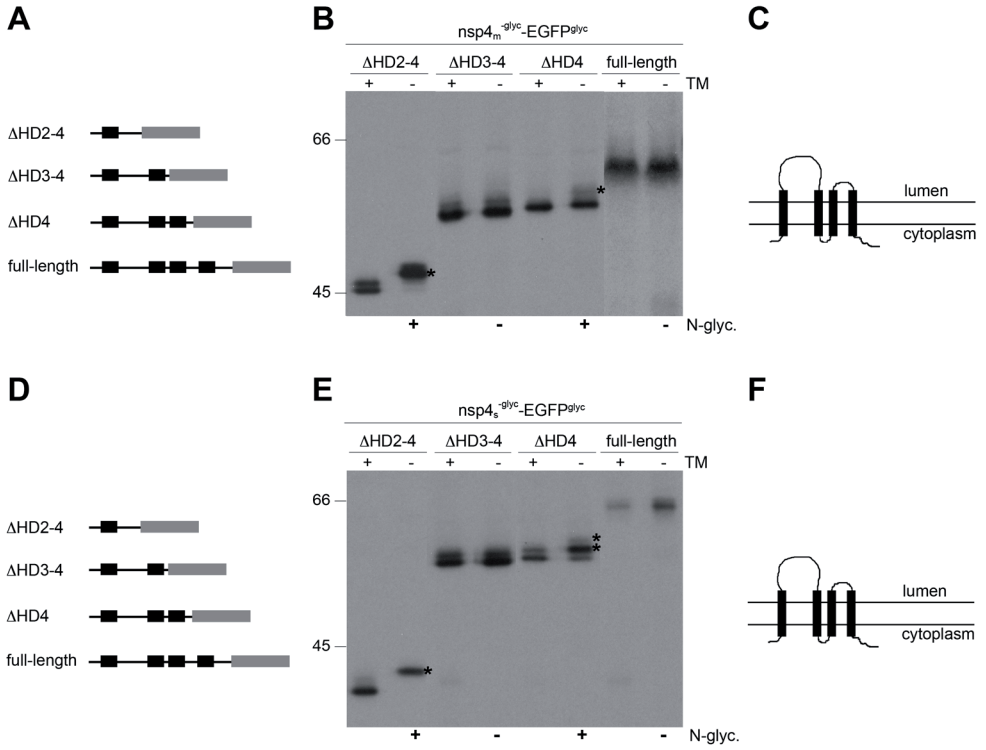

Figure 8. Membrane integration of deletion mutant forms of MHV and SARS-CoV nsp4. (A, D) Schematic representations of the MHV (A) and SARS-CoV (D) nsp4 C-terminal deletion mutant forms, with the hydrophobic domains presented as black rectangles and the EGFP^{glyc} tag shown in gray. (B, E) vTF7-3-infected OST7-1 cells were transfected with the indicated constructs and expressed in the presence (+) or absence (–) of tunicamycin (TM). The cells were labeled with [^{35}S]methionine from 5 to 6 h p.i., lysed, and processed for immunoprecipitation with anti-EGFP antiserum, followed by SDS-PAGE. The positions and masses (in kilodaltons) of the protein size markers are indicated at the left. Only the relevant portions of the gels are shown. The asterisks indicate the position of the glycosylated protein species. Below the panels, the observed presence or absence of *N* glycosylation is indicated by a plus or a minus sign, respectively (C, F). Models of the membrane structure of nsp4 of MHV (C) and SARS-CoV (F), with the hydrophobic domains presented as black rectangles.

fusion proteins became efficiently *N* glycosylated, as shown by the complete shift in electrophoretic mobility due to the presence of tunicamycin. This is again as expected and confirms that the first hydrophobic domain spans the lipid bilayer. When the first two hydrophobic domains were present (ΔHD3-4), the electrophoretic mobility was not influenced by the presence of tunicamycin. Since this fusion protein was not *N* glycosylated, its C terminus was located on the cytoplasmic side of the membrane, implying that also the second hydrophobic domain spans the lipid bilayer. *N* glycosylation was again observed, though especially for MHV nsp4 not very efficiently, when only

the fourth hydrophobic domain was deleted (ΔHD4), as demonstrated by the higher-molecular-weight band seen in the absence of tunicamycin but not in its presence, indicating that also the third and fourth hydrophobic domains span the membrane. For several nsp4 deletion mutant constructs, two rather than one tunicamycin-resistant protein species could be detected, which is explained by the partial removal of the first transmembrane domain by signal peptidase (37; data not shown). It appeared that signal peptidase cleavage of nsp4 was more efficient for the smaller deletion mutant proteins. *N* glycosylation of the SARS-CoV nsp4ΔHD4 mutant form combined with signal peptidase cleavage resulted in an electrophoretic mobility similar to that of the unglycosylated and uncleaved protein (hence the two asterisks in Fig. 8E, which indicate the position of the *N*-glycosylated protein species), similar to what has been observed previously (37). The results show that, in contrast to nsp3 and nsp6, all of the predicted transmembrane domains of nsp4 span the lipid bilayer (Fig. 8C and F).

DISCUSSION

Coronaviruses have exceptionally large RNA genomes and exhibit complex replication and transcription strategies. These processes take place at DMVs located in the perinuclear region of the host cell. Although the membranes of these structures are most likely derived from the ER, the way they are organized and modified to function as the scaffolds of the replication complexes is still largely unknown. Presumably, as has been demonstrated for other RNA viruses, the hydrophobic nsps are key organizers of the observed membrane rearrangements. All known members of the families *Coronaviridae* and *Arteriviridae* encode three nsps containing hydrophobic domains. Invariably, hydrophobic domains are present in the two nsps surrounding the 3C-like main proteinase encoded by nsp5 of coronaviruses and by nsp4 of arteriviruses, while additional hydrophobic domains are found in the large nsp immediately upstream of this cluster, which further contains the papain-like proteinase domains (19). For EAV, the coexpression of nsp2 and nsp3, which are the homologues of coronavirus nsp3 and nsp4, is sufficient to induce the formation of DMVs (49). Similar results, however, have so far not been reported for coronaviruses. In order to get more insight into the function of the coronavirus hydrophobic nsps, we studied the topology and membrane integration of these proteins. The results demonstrate that, similar to nsp4 (37), both nsp3 and nsp6 have a N_{endo}/C_{endo} topology with an even number of transmembrane domains, although for both proteins an uneven number

of transmembrane domains was predicted. The conservation of hydrophobic domains not actually serving as transmembrane domains suggests that these domains may play important roles in the formation, stabilization, or functioning of the replication complexes.

Membrane structures of complex multispanning proteins are notoriously difficult to establish. Ideally, one would like to probe the disposition of particular domains in such proteins by introducing or removing glycosylation sites and by using specific antisera raised to peptides corresponding to these domains. Removal of the glycosylation sites in the large luminal loops of nsp3 and nsp4 was relatively straightforward. Unfortunately, however, no glycosylation motifs occurred in the other, much smaller loops, and motifs introduced into such loops appeared to be nonfunctional (data not shown), probably because they are not accessible to the enzymes. As domain specific antibodies are not available —and are probably hard to generate due to the small size of most loops— we decided to use other frequently applied approaches, which involved tagging of the nsps with epitopes or EGFP carrying *O* or *N* glycosylation sites in combination with progressive deletions of hydrophobic domains. A potential drawback of these techniques is that the manipulation may affect the conformational behavior of the protein. Thus, deletion mutant proteins often appeared to be only partially glycosylated. While this might be taken as an indication that the protein can adopt more than one membrane topology, we do not consider this interpretation very likely. First of all, a large number of our mutant proteins did not become glycosylated at all and apparently do not adopt a dual topology. Furthermore, glycosylation was invariably observed for those deletion mutant proteins in which the glycosylatable tag replaced a lumenal loop with an authentic glycosylation site. It seems more likely that the partial glycosylation of the proteins is inherent to the type of approach and relates to their very hydrophobic nature and their often drastically modified state, which makes them prone to aggregation when expressed out of their natural context. Furthermore, we confirmed our results by performing the experiments with nsps of both SARS-CoV and MHV, which yielded essentially identical results.

We studied the topology and membrane integration of SARS-CoV and MHV hydrophobic nsps by expressing the proteins independently, i.e., out of their polyprotein context. Similar strategies have been employed before to study the membrane integration of viral nsps derived from large precursor proteins (33, 34, 37). Unlike for nsp4 and nsp6, we expressed only the C-terminal approximately 700 amino acids of nsp3, the part that contains all of the putative transmembrane domains. The full-size, approximately

2,000-amino-acid polypeptide would have been too large to detect the often subtle size differences inherent to our analytic approach. Moreover, it appeared difficult to express complete nsp3, presumably due to the presence of toxic sequences, as have also been reported by others to occur in approximately the same region of other coronavirus genomes (1, 60, 61). The N-terminal region of nsp3 lacking in our expression constructs does not contain any appreciable hydrophobic domains, and prediction programs do not identify any transmembrane domains in this region. Hence, we believe that the models obtained for the partial proteins apply as well to complete MHV and SARS-CoV nsp3.

By using biochemical and immunofluorescence assays, we demonstrated that in both SARS-CoV and MHV, nsp3 has a N_{endo}/C_{endo} topology. While this is inconsistent with the predicted number of transmembrane domains (Fig. 1), it is in agreement with a previous study on the topology of MHV nsp3 (28). A N_{endo}/C_{endo} topology obviously makes more sense than the predicted N_{exo}/C_{endo} orientation with respect to the localization of the PLpro domain and its substrates (Fig. 9). However, whereas previously four transmembrane domains were identified for MHV nsp3 (28), we found evidence for the presence of only two such domains in both of the nsps studied. We could not confirm the presence of additional membrane-spanning domains located immediately up- and downstream of the first transmembrane domain, nor were these additional domains predicted on the basis of the multiple alignment. Our study did confirm, however, the use of the previously identified *N*-linked glycosylation sites between the first and second transmembrane domains (22, 28). It further demonstrated that in both SARS-CoV and MHV, the second, but not the third predicted transmembrane domain of nsp3 is used. This result is in conflict with findings of Baker and coworkers, who identified the third rather than the second predicted transmembrane domain of MHV nsp3 as spanning the lipid bilayer (28). Their conclusion was mainly based on electrophoretic mobility measurements of hydrophobic nsp3 fragments obtained after proteinase K digestions. Hydrophobic proteins, including coronavirus nsp4 and nsp6, often exhibit anomalous migration in gels, and this might explain the different interpretations. Regardless of the number of transmembrane domains, it is striking that the first transmembrane domain in coronavirus pp1a and pp1ab is found only after more than 2,000 amino acids, while the polyproteins and mature nsp3 lack an identifiable signal sequence at the amino-terminal end. Apparently, the first hydrophobic domain of nsp3 is able to function as an internal signal sequence for membrane insertion, as we confirmed in our study.

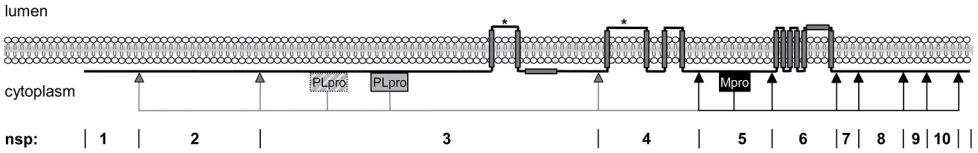

Figure 9. Model of the membrane disposition of coronavirus pp1a. The black line represents the protein, with the hydrophobic domains depicted as gray rectangles, and shows its localization with respect to the membrane. The proteases, papain-like protease (PLpro) and main protease (Mpro), and their cleavage sites (arrowheads) are indicated, with the PLpro cleavage sites in gray and the Mpro cleavage sites in black. The confirmed *N* glycosylation sites of the proteins are indicated by asterisks. In this model, the sixth hydrophobic domain of nsp6 does not span the lipid bilayer; however, we cannot exclude the possibility that the seventh rather than the sixth predicted transmembrane domain is not used as such.

Like nsp4 and nsp3, nsp6 of SARS-CoV and MHV appeared to have a N_{endo}/C_{endo} membrane topology. This is again inconsistent with the prediction, which identified seven transmembrane domains, compatible with a N_{endo}/C_{exo} topology. The experimentally established topology obviously makes more sense, as it positions all of the main proteinase cleavage sites on the same side of the membrane as the proteinase itself (Fig. 9). Demonstrating which of the hydrophobic domains in nsp6 actually served as transmembrane domains was not as straightforward as it was for nsp3. It appeared that, in principle, all seven domains have the capacity to function as signal sequences and membrane anchors, irrespective of their fate in the full-length protein. The combined observations appear to fit best a model in which nsp6 contains six transmembrane domains, with the sixth or seventh hydrophobic domain not spanning the lipid bilayer. The transmembrane prediction program SOSUI (http://bp.nuap.nagoya-u.ac.jp/sosui/sosuimenu0.html) also predicts seven transmembrane-spanning helices but additionally calculates that the hydrophobicity of the sixth domain, but not that of the others, is similar to the hydrophobicity of helices found in soluble proteins (23). This prediction hence supports the model in which the sixth putative transmembrane domain does not span the lipid bilayer.

Our experience with nsp3 and nsp6 prompted us to revisit also the membrane structure of nsp4. With four hydrophobic domains, the known N_{endo}/C_{endo} topology of this protein could, in principle, be achieved with either two or all of those as transmembrane domains. Our deletion assay led us to conclude that all four domains are membrane spanning. Remarkably, in MHV, the removal of the fourth domain was found by Sparks and coworkers (50) to yield a virus that grew in cultured cells with kinetics and to titers similar to those of the wild-type virus, although the kinetics of its RNA replication were

significantly delayed. Given the topological consequences of this deletion, one has to assume that in this mutant virus either the third hydrophobic membrane is not functioning as a transmembrane domain or, as the authors suggest, the effect of the deletion is compensated by the region between the third and fourth transmembrane domains, which is also somewhat hydrophobic. Mutant viruses lacking any of the other three hydrophobic domains of nsp4 could not be recovered.

Combining all of the information obtained for nsp3, -4, and -6 into one model, we arrive at the membrane structure of the pp1a precursor that is depicted in Fig. 9. As a result of the N_{endo}/C_{endo} topology of all three membrane-anchored nsps, the major part of the polyproteins, including all known functional domains, is located on the cytoplasmic side of the membrane. Of the entire approximately 4,400-amino-acid pp1a precursor, only six relatively short stretches are exposed lumenally, exceptions being the glycosylated polypeptides occurring between the first and second transmembrane domains of nsp3 and nsp4, which comprise some 80 and 250 residues, respectively. Interestingly, both of these polypeptide loops contain several highly conserved cysteine residues. Mutations in the lumenally exposed part of MHV nsp4 (and its EAV counterpart) were shown to affect DMV formation (8, 39).

Also, the pp1b precursor, which lacks membrane-spanning domains but carries cleavage sites processed by the nsp5-encoded main protease, and its cleavage products nsp12 to -16 end up cytoplasmically. This topological arrangement fits into a picture of the biogenesis of the replication complexes in which membrane proteins nsp3, -4 and -6, while still contained in the precursor, direct the formation of the membranous structures on which RNA replication is to take place. These proteins probably shape the platform onto which the subsequently appearing non-anchored cleavage products derived from pp1a and pp1b remain associated and to which cellular, as well as viral (e.g., N protein), components may additionally attach to generate the functional replication complex.

What role(s) the conserved non-membrane-spanning hydrophobic domains in nsp3 and -6 play in the formation and functioning of the complex remains to be established. A cytoplasmically exposed hydrophobic domain might serve as an interaction partner for other components of the complex, while the hydrophobic non-membrane-spanning domains might also contribute to the double-membrane configuration, for instance, by dipping into the hydrophobic phase of the membrane. The latter has been observed earlier for proteins containing amphipathic helices, showing that these domains can act as a wedge in the membrane and thereby induce curvature (32, 65).

The induction of membrane rearrangements to create sites for RNA replication and transcription in infected cells is not unique to coronaviruses but is common among plus strand RNA viruses. These viruses generally encode nsps that induce membrane rearrangements. These nsps can be integral membrane proteins, but this is not always the case. The occurrence of hydrophobic/amphipathic regions that do not span the bilayer but are peripherally associated with membranes is not an exception; it rather is a common theme. Interestingly, dengue virus, which also replicates on DMVs (56), encodes two nonstructural membrane proteins that, in addition to transmembrane domains, also contain hydrophobic domains that do not span the lipid bilayer (33, 34). The NS4A and NS4B proteins of this virus contain one and two hydrophobic domains, respectively, that do not function as transmembrane domains in the full-length protein. Yet, the non-membrane-spanning hydrophobic domain of NS4A is integrated into the membrane when expressed individually (33, 34), comparable to our observations with the hydrophobic domains of MHV nsp6. In the case of hepatitis C virus, which, like dengue virus, also belongs to the flavivirus family, the amphipathic helix contained in NS4B was shown to be required for the formation of replication sites (15). Likewise, the poliovirus 2C protein, which is able to induce the membrane rearrangements associated with RNA replication, also contains an essential amphipathic domain (14, 38, 54). In view of these observations, it is tempting to speculate that these similarities among the viral nonstructural membrane-associated proteins relate to their common ability to induce membrane rearrangements.

ACKNOWLEDGEMENTS

We thank Matthijs Raaben and Mijke Vogels for stimulating discussions. This work was supported by grants from The Netherlands Organization for Scientific Research (NWO-VIDI-700.54.421) and Utrecht University (High Potential) to C. A. M. de Haan and from the European Community (Frame VI, DISSECT PROJECT, SP22-CT-2004-511060) to P. J. M. Rottier.

REFERENCES

1. Almazán, F., J. M. Gonzalez, Z. Penzes, A. Izeta, E. Calvo, J. Plana-Duran, and L. Enjuanes. 2000. Engineering the largest RNA virus genome as an infectious bacterial artificial chromosome. Proc. Natl. Acad. Sci. USA 97:5516–5521.

2. Baker, S. C., K. Yokomori, S. Dong, R. Carlisle, A. E. Gorbalenya, E. V. Koonin, and M. M. Lai. 1993. Identification of the catalytic sites of a papain-like cysteine proteinase of murine coronavirus. J. Virol. 67:6056–6063.

3. Bhardwaj, K., L. Guarino, and C. C. Kao. 2004. The severe acute respiratory syndrome coronavirus Nsp15 protein is an endoribonuclease that prefers manganese as a cofactor. J. Virol. 78:12218–12224.

4. Bost, A. G., R. H. Carnahan, X. T. Lu, and M. R. Denison. 2000. Four proteins processed from the replicase gene polyprotein of mouse hepatitis virus colocalize in the cell periphery and adjacent to sites of virion assembly. J. Virol. 74:3379–3387.

5. Bredenbeek, P. J., C. J. Pachuk, A. F. Noten, J. Charite, W. Luytjes, S. R. Weiss, and W. J. Spaan. 1990. The primary structure and expression of the second open reading frame of the polymerase gene of the coronavirus MHV A59; a highly conserved polymerase is expressed by an efficient ribosomal frameshifting mechanism. Nucleic Acids Res. 18:1825–1832.

6. Brockway, S. M., C. T. Clay, X. T. Lu, and M. R. Denison. 2003. Characterization of the expression, intracellular localization, and replication complex association of the putative mouse hepatitis virus RNA-dependent RNA polymerase. J. Virol. 77:10515–10527.

7. Cheng, A., W. Zhang, Y. Xie, W. Jiang, E. Arnold, S. G. Sarafianos, and J. Ding. 2005. Expression, purification, and characterization of SARS coronavirus RNA polymerase. Virology 335:165–176.

8. Clementz, M. A., A. Kanjanahaluethai, T. E. O'Brien, and S. C. Baker. 2008. Mutation in murine coronavirus replication protein nsp4 alters assembly of double membrane vesicles. Virology 375:118–129.

9. Decroly, E., I. Imbert, B. Coutard, M. Bouvet, B. Selisko, K. Alvarez, A. E. Gorbalenya, E. J. Snijder, and B. Canard. 2008. Coronavirus nonstructural protein 16 is a Cap-0 binding enzyme possessing (nucleoside-2-O)-methyltransferase activity. J. Virol. 82:8071–8084.

10. de Haan, C. A., P. Roestenberg, M. de Wit, A. A. de Vries, T. Nilsson, H. Vennema, and P. J. Rottier. 1998. Structural requirements for O glycosylation of the mouse hepatitis virus membrane protein. J. Biol. Chem. 273:29905–29914.

11. Denison, M. R., A. C. Sims, C. A. Gibson, and X. T. Lu. 1998. Processing of the MHV-A59 gene 1 polyprotein by the 3C-like proteinase. Adv. Exp. Med.Biol. 440:121–127.

12. Donaldson, E. F., R. L. Graham, A. C. Sims, M. R. Denison, and R. S. Baric. 2007. Analysis of murine hepatitis virus strain A59 temperature-sensitive mutant TS-LA6 suggests that nsp10 plays a critical role in polyprotein processing. J. Virol. 81:7086–7098.

13. Dos Ramos, F., M. Carrasco, T. Doyle, and I. Brierley. 2004. Programmed -1 ribosomal frameshifting in the SARS coronavirus. Biochem. Soc. Trans.32:1081–1083.

14. Echeverri, A. C., and A. Dasgupta. 1995. Amino terminal regions of poliovirus 2C protein mediate membrane binding. Virology 208:540–553.

15. Elazar, M., P. Liu, C. M. Rice, and J. S. Glenn. 2004. An N-terminal amphipathic helix in hepatitis C virus (HCV) NS4B mediates membrane association, correct localization of replication complex proteins, and HCV RNA replication. J. Virol. 78:11393–11400.

16. Elroy-Stein, O., and B. Moss. 1990. Cytoplasmic expression system based on constitutive synthesis of bacteriophage T7 RNA polymerase in mammalian cells. Proc. Natl. Acad. Sci. USA 87:6743–6747.

17. Fan, K., L. Ma, X. Han, H. Liang, P. Wei, Y. Liu, and L. Lai. 2005. The substrate specificity of SARS coronavirus 3C-like proteinase. Biochem. Biophys. Res. Commun. 329:934–940.

18. Fuerst, T. R., E. G. Niles, F. W. Studier, and B. Moss. 1986. Eukaryotic transient-expression system based on recombinant vaccinia virus that synthesizes bacteriophage T7 RNA polymerase. Proc. Natl. Acad. Sci. USA 83:8122–8126.

19. Gorbalenya, A. E., L. Enjuanes, J. Ziebuhr, and E. J. Snijder. 2006. Nidovirales: evolving the largest RNA virus genome. Virus Res. 117:17–37.

20. Gosert, R., A. Kanjanahaluethai, D. Egger, K. Bienz, and S. C. Baker. 2002. RNA replication of mouse hepatitis virus takes place at double-membrane vesicles. J. Virol. 76:3697–3708.

21. Graham, R. L., A. C. Sims, S. M. Brockway, R. S. Baric, and M. R. Denison. 2005. The nsp2 replicase proteins of murine hepatitis virus and severe acute respiratory syndrome coronavirus are dispensable for viral replication. J. Virol.79:13399–13411.

22. Harcourt, B. H., D. Jukneliene, A. Kanjanahaluethai, J. Bechill, K. M.Severson, C. M. Smith, P. A. Rota, and S. C. Baker. 2004. Identification of severe acute respiratory syndrome coronavirus replicase products and characterization of papain-like protease activity. J. Virol. 78:13600–13612.

23. Hirokawa, T., S. Boon-Chieng, and S. Mitaku. 1998. SOSUI: classification and secondary structure prediction system for membrane proteins. Bioinformatics 14:378–379.

24. Imbert, I., J. C. Guillemot, J. M. Bourhis, C. Bussetta, B. Coutard, M. P. Egloff, F. Ferron, A. E. Gorbalenya, and B. Canard. 2006. A second, noncanonical RNA-dependent RNA polymerase in SARS coronavirus. EMBO J. 25:4933–4942.

25. Ivanov, K. A., T. Hertzig, M. Rozanov, S. Bayer, V. Thiel, A. E. Gorbalenya,and J. Ziebuhr. 2004. Major genetic marker of nidoviruses encodes a replicative endoribonuclease. Proc. Natl. Acad. Sci. USA 101:12694–12699.

26. Ivanov, K. A., V. Thiel, J. C. Dobbe, Y. van der Meer, E. J. Snijder, and J.Ziebuhr. 2004. Multiple enzymatic activities associated with severe acutere spiratory syndrome coronavirus helicase. J. Virol. 78:5619–5632.

27. Ivanov, K. A., and J. Ziebuhr. 2004. Human coronavirus 229E nonstructural protein 13: characterization of duplex-unwinding, nucleoside triphosphatase, and RNA 5'-triphosphatase activities. J. Virol. 78:7833–7838.

28. Kanjanahaluethai, A., Z. Chen, D. Jukneliene, and S. C. Baker. 2007. Membrane topology of murine coronavirus replicase nonstructural protein 3. Virology 361:391–401.

29. Kuiken, T., R. A. Fouchier, M. Schutten, G. F. Rimmelzwaan, G. van Amerongen, D. van Riel, J. D. Laman, T. de Jong, G. van Doornum, W. Lim, A. E. Ling, P. K. Chan, J. S. Tam, M. C. Zambon, R. Gopal, C. Drosten, S. van der Werf, N. Escriou, J. C. Manuguerra, K. Stohr, J. S. Peiris, and A. D. Osterhaus. 2003. Newly discovered coronavirus as the primary cause of severe acute respiratory syndrome. Lancet 362:263–270.

30. Locker, J. K., J. K. Rose, M. C. Horzinek, and P. J. Rottier. 1992. Membrane assembly of the triple-spanning coronavirus M protein. Individual transmembrane domains show preferred orientation. J. Biol. Chem. 267:21911–21918.

31. Matthes, N., J. R. Mesters, B. Coutard, B. Canard, E. J. Snijder, R. Moll,and R. Hilgenfeld. 2006. The non-structural protein Nsp10 of mouse hepatitis virus binds zinc ions and nucleic acids. FEBS Lett. 580:4143–4149.

32. McMahon, H. T., and J. L. Gallop. 2005. Membrane curvature and mechanisms of dynamic cell membrane remodelling. Nature 438:590–596.

33. Miller, S., S. Kastner, J. Krijnse-Locker, S. Buhler, and R. Bartenschlager.2007. The non-structural protein 4A of dengue virus is an integral membrane protein inducing membrane alterations in a 2K-regulated manner. J. Biol.Chem. 282:8873–8882.

34. Miller, S., S. Sparacio, and R. Bartenschlager. 2006. Subcellular localization and membrane topology of the Dengue virus type 2 non-structural protein 4B. J. Biol. Chem. 281:8854–8863.

35. Oostra, M., C. A. de Haan, R. J. de Groot, and P. J. Rottier. 2006. Glycosylation of the severe acute respiratory syndrome coronavirus triple-spanning membrane proteins 3a and M. J. Virol. 80:2326–2336.

36. Oostra, M., C. A. de Haan, and P. J. Rottier. 2007. The 29-nucleotide deletion present in human but not in animal severe acute respiratory syndrome coronaviruses disrupts the functional expression of open reading frame 8. J. Virol. 81:13876–13888.

37. Oostra, M., E. G. te Lintelo, M. Deijs, M. H. Verheije, P. J. Rottier, and C. A. de Haan. 2007. Localization and membrane topology of coronavirus nonstructural protein 4: involvement of the early secretory pathway in replication. J. Virol. 81:12323–12336.

38. Paul, A. V., A. Molla, and E. Wimmer. 1994. Studies of a putative amphipathic helix in the N-terminus of poliovirus protein 2C. Virology 199:188–199.

39. Posthuma, C. C., K. W. Pedersen, Z. Lu, R. G. Joosten, N. Roos, J. C. Zevenhoven-Dobbe, and E. J. Snijder. 2008. Formation of the arterivirus replication/transcription complex: a key role for nonstructural protein 3 in the remodeling of intracellular membranes. J. Virol. 82:4480–4491.

40. Prentice, E., W. G. Jerome, T. Yoshimori, N. Mizushima, and M. R. Denison. 2004. Coronavirus replication complex formation utilizes components of cellular autophagy. J. Biol. Chem. 279:10136–10141.

41. Prentice, E., J. McAuliffe, X. Lu, K. Subbarao, and M. R. Denison. 2004. Identification and characterization of severe acute respiratory syndrome coronavirus replicase proteins. J. Virol. 78:9977–9986.

42. Putics, A., W. Filipowicz, J. Hall, A. E. Gorbalenya, and J. Ziebuhr. 2005. ADP-ribose-1'-monophosphatase: a conserved coronavirus enzyme that is dispensable for viral replication in tissue culture. J. Virol. 79:12721–12731.

43. Ricagno, S., M. P. Egloff, R. Ulferts, B. Coutard, D. Nurizzo, V. Campanacci,C. Cambillau, J. Ziebuhr, and B. Canard. 2006. Crystal structure and mechanistic determinants of SARS coronavirus nonstructural protein 15 define an endoribonuclease family. Proc. Natl. Acad. Sci. USA 103:11892–11897.

44. Salonen, A., T. Ahola, and L. Kaariainen. 2005. Viral RNA replication in association with cellular membranes. Curr. Top. Microbiol. Immunol. 285:139–173.

45. Sawicki, S. G., D. L. Sawicki, and S. G. Siddell. 2007. A contemporary view of coronavirus transcription. J. Virol. 81:20–29.

46. Shi, S. T., and M. M. Lai. 2005. Viral and cellular proteins involved in coronavirus replication. Curr. Top. Microbiol. Immunol. 287:95–131.

47. Shi, S. T., J. J. Schiller, A. Kanjanahaluethai, S. C. Baker, J. W. Oh, and M. M. Lai. 1999. Colocalization and membrane association of murine hepatitis virus gene 1 products and de novo-synthesized viral RNA in infected cells. J. Virol. 73:5957–5969.

48. Snijder, E. J., Y. van der Meer, J. Zevenhoven-Dobbe, J. J. Onderwater, J.van der Meulen, H. K. Koerten, and A. M. Mommaas. 2006. Ultrastructure and origin of membrane vesicles associated with the severe acute respiratory syndrome coronavirus replication complex. J. Virol. 80:5927–5940.

49. Snijder, E. J., H. van Tol, N. Roos, and K. W. Pedersen. 2001. Non-structural proteins 2 and 3 interact to modify host cell membranes during the formation of the arterivirus replication complex. J. Gen. Virol. 82:985–994.

50. Sparks, J. S., X. Lu, and M. R. Denison. 2007. Genetic analysis of Murine hepatitis virus nsp4 in virus replication. J. Virol. 81:12554–12563.

51. Sutormin, R. A., and A. A. Mironov. 2006. Membrane probability profile construction based on amino acids sequences multiple alignment. Mol. Biol.[Engl. Transl. Mol. Biol. (Moscow)] 40:541–545.

52. Sutton, G., E. Fry, L. Carter, S. Sainsbury, T. Walter, J. Nettleship, N.Berrow, R. Owens, R. Gilbert, A. Davidson, S. Siddell, L. L. Poon, J. Diprose,D. Alderton, M. Walsh, J. M. Grimes, and D. I. Stuart. 2004. The nsp9 replicase protein of SARS-coronavirus, structure and functional insights. Structure 12:341–353.

53. Taguchi, F., and J. O. Fleming. 1989. Comparison of six different murine coronavirus JHM variants by monoclonal antibodies against the E2 glycoprotein. Virology 169:233–235.

54. Teterina, N. L., A. E. Gorbalenya, D. Egger, K. Bienz, and E. Ehrenfeld. 1997. Poliovirus 2C protein determinants of membrane binding and rearrangements in mammalian cells. J. Virol. 71:8962–8972.

55. Thiel, V., K. A. Ivanov, A. Putics, T. Hertzig, B. Schelle, S. Bayer, B. Weissbrich,E. J. Snijder, H. Rabenau, H. W. Doerr, A. E. Gorbalenya, and J. Ziebuhr. 2003. Mechanisms and enzymes involved in SARS coronavirus genome expression. J. Gen. Virol. 84:2305–2315.

56. Uchil, P. D., and V. Satchidanandam. 2003. Architecture of the flaviviral replication complex. Protease, nuclease, and detergents reveal encasement within double-layered membrane compartments. J. Biol. Chem. 278:24388–24398.

57. van der Meer, Y., E. J. Snijder, J. C. Dobbe, S. Schleich, M. R. Denison, W. J.Spaan, and J. K. Locker. 1999. Localization of mouse hepatitis virus nonstructural proteins and RNA synthesis indicates a role for late endosomes inviral replication. J. Virol. 73:7641–7657.

58. van der Meer, Y., H. van Tol, J. K. Locker, and E. J. Snijder. 1998. ORF1a-encoded replicase subunits are involved in the membrane association of the arterivirus replication complex. J. Virol. 72:6689–6698.

59. Vennema, H., R. Rijnbrand, L. Heijnen, M. C. Horzinek, and W. J. Spaan. 1991. Enhancement of the vaccinia virus/phage T7 RNA polymerase expression system using encephalomyocarditis virus 5'-untranslated region sequences. Gene 108:201–209.

60. Yount, B., K. M. Curtis, and R. S. Baric. 2000. Strategy for systematic assembly of large RNA and DNA genomes: transmissible gastroenteritisvirus model. J. Virol. 74:10600–10611.

61. Yount, B., M. R. Denison, S. R. Weiss, and R. S. Baric. 2002. Systematic assembly of a full-length infectious cDNA of mouse hepatitis virus strain A59. J. Virol. 76:11065–11078.

62. Zhai, Y., F. Sun, X. Li, H. Pang, X. Xu, M. Bartlam, and Z. Rao. 2005. Insights into SARS-CoV transcription and replication from the structure of the nsp7-nsp8 hexadecamer. Nat. Struct. Mol. Biol. 12:980–986.

63. Ziebuhr, J. 2005. The coronavirus replicase. Curr. Top. Microbiol. Immunol. 287:57–94.

64. Ziebuhr, J., E. J. Snijder, and A. E. Gorbalenya. 2000. Virus-encoded proteinases and proteolytic processing in the Nidovirales. J. Gen. Virol. 81:853–879.

65. Zimmerberg, J., and M. M. Kozlov. 2006. How proteins produce cellular membrane curvature. Nat. Rev. Mol. Cell Biol. 7:9–19.

Chapter 3

Dynamics of Coronavirus Replication-Transcription Complexes

Marne C. Hagemeijer[1*], Monique H. Verheije[1*], Mustafa Ulasli[2], Indra A. Shaltiël[1], Lisa A. de Vries[1], Fulvio Reggiori[2], Peter J. M. Rottier[1], and Cornelis A. M. de Haan[1]

Virology Division, Department of Infectious Diseases and Immunology, Faculty of Veterinary Medicine, Utrecht University, Utrecht, the Netherlands[1], and Department of Cell Biology and Institute of Biomembranes, University Medical Centre Utrecht, Utrecht, the Netherlands[2]

Journal of Virology, Feb. 2010, p. 2134–2149 Vol. 84, No. 4

* equal contribution

Supplemental material can be found at http://jvi.asm.org/

ABSTRACT

Coronaviruses induce in infected cells the formation of double-membrane vesicles (DMVs) in which the replication-transcription complexes (RTCs) are anchored. To study the dynamics of these coronavirus replicative structures, we generated recombinant murine hepatitis coronaviruses that express tagged versions of the nonstructural protein nsp2. We demonstrated by using immunofluorescence assays and electron microscopy that this protein is recruited to the DMV-anchored RTCs, for which its C terminus is essential. Live-cell imaging of infected cells demonstrated that small nsp2-positive structures move through the cytoplasm in a microtubule-dependent manner. In contrast, large fluorescent structures are rather immobile. Microtubule-mediated transport of DMVs, however, is not required for efficient replication. Biochemical analyses indicated that the nsp2 protein is associated with the cytoplasmic side of the DMVs. Yet, no recovery of fluorescence was observed when (part of) the nsp2-positive foci were bleached. This result was confirmed by the observation that preexisting RTCs did not exchange fluorescence after fusion of cells expressing either a green or a red fluorescent nsp2. Apparently, nsp2, once recruited to the RTCs, is not exchanged with nsp2 present in the cytoplasm or at other DMVs. Our data show a remarkable resemblance to results obtained recently by others with hepatitis C virus. The observations point to intriguing and as yet unrecognized similarities between the RTC dynamics of different plus-strand RNA viruses.

INTRODUCTION

Viruses have evolved elaborate strategies to manipulate and exploit host cellular components and pathways to facilitate various steps of their replication cycle. One common feature among plus-strand RNA viruses is the assembly of their replication-transcription complexes (RTCs) in association with cytoplasmic membranes [reviewed in references (41, 44, and 54)]. The induction and modification of replicative vesicles seem to be beneficial to the virus (i) in orchestrating the recruitment of all cellular and viral constituents required for viral RNA synthesis and (ii) in providing a protective microenvironment against virus-elicited host defensive (immune) mechanisms.

The enveloped coronaviruses (CoVs) possess impressively large plus-strand RNA genomes, with sizes ranging from ~27 to 32 kb (22). The coronavirus polycistronic genome can roughly be divided into two regions: the first two-thirds of the genome contains the large replicase gene that encodes the proteins collectively responsible for viral RNA replication and transcription while the remaining 3'-terminal part of the genome encodes the structural proteins and some accessory proteins that are expressed from a nested set of subgenomic mRNAs (sgmRNAs) (55).

Almost all of the constituents of the coronavirus RTCs are encoded by the large replicase gene that is comprised of two partly overlapping open reading frames (ORFs), ORF1a and ORF1b. Translation of these ORFs results in two very large polyproteins, pp1a and pp1ab, the latter of which is produced by translational readthrough via a -1 ribosomal frameshift induced by a "slippery" sequence and a pseudoknot structure at the end of ORF1a (46, 69). pp1a and pp1ab are extensively processed into an elaborate set of nonstructural proteins (nsps) via co- and posttranslational cleavages by the viral papain-like proteinase(s) (PLpro) residing in nsp3 and the 3C-like main proteinase (Mpro) in nsp5 (17, 51, 64, 66, 77). The functional domains present in the replicase polyproteins are conserved among all coronaviruses (77). The ORF1a-encoded nsps (nsp1 to nsp11) contain, among others, the viral proteinases (17, 51,64, 66, 77), the membrane-anchoring domains (34, 48, 49), anti-host immune activities (8, 32, 47, 78), and predicted and identified RNA-binding and RNA-modifying activities (20, 27, 31, 43, 67, 76). ORF1b (nsp12 to nsp16) encodes the key enzymes directly involved in RNA replication and transcription, such as the RNA-dependent RNA polymerase (RdRp) and the helicase (2, 7, 11, 18, 29, 30, 33, 45, 60). The nsps collectively form the RTCs; however, the size and complexity of these complexes are unknown.

Coronavirus replicative structures consist of double-membrane vesicles (DMVs) in which the RTCs are anchored (3, 23, 65). Although hardly anything is known about the mechanism by which the DMVs are induced, recent studies by us and others indicate that the DMVs are most likely derived from the endoplasmic reticulum (ER). Electron microscopy (EM) analyses of infected cells showed the partial colocalization of nsps with an ER protein marker while the DMVs were often found in close proximity to the ER and, occasionally, in continuous association with it (35, 65). More recently, the DMVs were reported to be integrated into a reticulovesicular network of modified ER membranes, also referred to as convoluted membranes (CMs) (35). In addition, when expressed in the absence of a coronavirus infection, nsp3, nsp4, and nsp6 were inserted into the ER (26, 34, 48, 49). When expressed in coronavirus-infected cells, nsp4 appeared to exit the ER and to be recruited to the RTCs (49). Furthermore, coronavirus replication was severely affected when the formation of COPI- and COPII-coated vesicles in the early secretory pathway was inhibited by the addition of drugs, by the expression of dominant negative mutants, or by depletion of host proteins using RNA interference (49, 72).

The mechanisms underlying the assembly of membrane-associated replication complexes in cells infected with plus-strand RNA viruses are just beginning to be unraveled. Previous studies have provided valuable information on the formation of the virus-induced replicative structures, resulting, however, in a static view of these processes inherent to the cell biological techniques used. Thus, insight into the dynamics of these structures is largely lacking, certainly in the case of coronaviruses. In the present study, we made the first step to fill this gap by performing live-cell imaging analyses of mouse hepatitis coronavirus (MHV) replicative structures in combination with fluorescent recovery after photobleaching (FRAP) studies. This approach allowed us to monitor the coronavirus DMV-anchored RTCs in real-time and generated new insights into the dynamics of these virus-induced structures, revealing striking similarities between the replicative structures induced by MHV and those generated by the unrelated hepatitis C virus (HCV).

MATERIALS AND METHODS

Cells, viruses, and antibodies. HeLa-CEACAM1a (75), Felis catus whole fetus (FCWF) cells (American Type Culture Collection) and murine LR7 fibroblast cells (36) were maintained as monolayer cultures in Dulbecco's modified Eagle's medium (DMEM-/-; Cambrex BioScience) containing 10% fetal calf serum (FCS; Bodinco BV), 100 IU/ml of penicillin, and 100 μg/ml of streptomycin (both from Life Technologies; this medium is referred to as DMEM+/+).

MHV strain A59, recombinant wild-type MHV (MHV-WT) (13), recombinant MHV-ERLM (12), which expresses the Renilla luciferase (RL) gene, and the recombinant viruses generated in this study, MHV-nsp2GFP (where GFP is green fluorescent protein), MHV-nsp2mCherry, and MHV-nsp2RL, were propagated in LR7 cells.

Antibody directed against double-stranded RNA (dsRNA) (K1) or the GFP was purchased from English and Scientific Consulting Bt. (58) and Immunology Consultants Laboratory, Inc., respectively. The polyclonal anti-p22 antibody, which is directed against MHV nsp8 (39), the monoclonal M_N antibody, recognizing the N-terminal domain of the MHV membrane (M) protein (68), and the polyclonal anti-D3 (nsp2/nsp3) and anti-D11 (nsp4) rabbit antibodies (9) were kindly provided by Mark Denison, John Flemming, and Susan Baker, respectively. The peptide serum recognizing the C-terminal tail (anti-M_C) of the MHV M protein has been described before (38).

Plasmids. The MHV A59 nsp2 gene fragment was generated by reverse transcriptase (RT)-PCR amplification of viral genomic RNA using the primers indicated in Table 1. The obtained PCR product was cloned into the pGEM-T Easy vector (Promega), which resulted in the pGEM-nsp2 plasmid. This plasmid was used as the starting point for the generation of the other nsp2-encoding plasmids that were subsequently used for the generation of recombinant viruses and for expression studies. Gene fragments, encoding C- and/or N-terminal nsp2 deletion mutants, were generated by PCR using the primers indicated in Table 1 and cloned into the pGEM-T Easy vector, generating pGEM-nsp2AB (nsp2 residues 1 to 247), pGEM-nsp2BC (nsp2 residues 122 to 459), and pGEM-nsp2CD (nsp2 residues 247 to 585). The nsp2-encoding gene fragments were subsequently cloned into the pEGFP-N3 vector (Clontech), resulting in pEGFP-nsp2 (where EGFP is enhanced GFP), pEGFP-nsp2AB, pEGFP-nsp2BC, and pEGFP-nsp2CD (Fig. 1B).

Three RNA transcription vectors (pMH54-nsp2EGFP, pMH54-nsp2mCherry, and pMH54-nsp2RL) were generated in order to create

Table 1. Sequence, polarity and position used of primers in this study.

Primer no.	Polarity	Sequence 5' to 3'	Postion in the viral genome (nt)[a]
3327	+	GAATTCGATATCATGGTTAAGCCGATCCTGTTTG	951
3328	-	AGATCTCGCACAGGGAAACCTCCAG	2705
3524	+	GATATCATGGAATTCTGTTATAAAACCAAGC	1314
3525	-	AGATCTACCAACTACTCCTGTATAAG	1691
3527	+	GATATCATGGGTTGTAAGGCAATTGTTC	1689
3528	-	AGATCTAACCTTGAAAAATGCCTTG	2328

[a] nt, nucleotide

recombinant MHVs expressing the gene encoding nsp2 tagged with either EGFP (Clontech), mCherry (Clontech), or *Renilla* luciferase (Invitrogen) at the genomic position of the hemagglutinin esterase (HE) gene. These vectors were constructed similarly as described previously for pMH54-nsp4EGFP (49), with the exception that the nsp2 rather than the nsp4 gene fragment was cloned in frame with either EGFP-, mCherry-, or RL-encoding sequences.

The expression plasmid encoding alpha-tubulin as a yellow fluorescent protein (YFP) fusion construct (pYFP-alpha-tubulin) was obtained from Euroscarf (1). The pER-GFP construct encoding an ER-retained GFP protein was kindly provided by Frank van Kuppeveld. The GFP coding region in this plasmid was replaced by that of firefly luciferase (Fluc) using conventional cloning techniques, resulting in pER-Fluc. All constructs were confirmed by restriction and/or sequence analysis.

Targeted recombination. Incorporation of the nsp2 expression cassettes into the MHV genome by targeted RNA recombination, resulting in recombinant MHV-nsp2GFP, MHV-nsp2mCherry, and MHV-nsp2RL viruses, was carried out as previously described (36). Briefly, donor RNA transcribed from the linearized transcription vectors was electroporated into FCWF cells that had been infected earlier with the interspecies chimeric coronavirus fMHV (an MHV derivative in which the spike ectodomain is of feline coronavirus origin) (36). These cells were plated onto a monolayer of murine LR7 cells. After 24 h of incubation at 37°C, progeny viruses released into the culture medium were harvested and plaque purified twice on LR7 cells before a passage 1 stock was grown. After confirmation of the recombinant genotypes, passage 2 stocks were grown that were subsequently used in the experiments.

Infection and transfection. Subconfluent monolayers of LR7 cells were transfected by overlaying the cells with a mixture of 0.5 ml of OptiMem (Invitrogen), 1 μl of Lipofectamine 2000 (Invitrogen), and 1 μg of each selected construct, followed by incubation at 37°C. Three hours after transfection, the medium was replaced by DMEM+/+. Where indicated, 24 h after transfection the cells were inoculated with (recombinant) MHV A59 at

a multiplicity of infection (MOI) of 1 to 10 for 1 h before the inoculum was replaced by fresh DMEM+/+.

One-step growth curve(s). LR7 cells grown in 0.33-cm^2 tissue culture dishes were infected in parallel using an MOI of 10 for 1 h at 37°C in 5% CO_2. After adsorption, the cells were washed with phosphate-buffered saline (PBS) supplemented with 50 mM Ca^{2+} and 50 mM Mg^{2+} three times, and incubation was continued in DMEM+/+. Viral infectivity in culture medium at different times post infection (p.i.) was determined by a quantal assay on LR7 cells, and the 50% tissue culture infective dose ($TCID_{50}$) values were calculated.

Metabolic labeling and immunoprecipitation. Subconfluent monolayers of LR7 cells in 10-cm^2 tissue culture dishes were infected with the viruses indicated in Fig. 2F for 1 h at an MOI of 10, after which the inoculum was removed; the cells were then washed three times with DMEM+/+, and incubation was continued in DMEM+/+. At 5.5 h p.i., the cells were starved for 30 min in cysteine and methionine-free modified Eagle's medium containing 10 mM HEPES (pH 7.2) and 5% dialyzed FCS. This medium was replaced with 1 ml of a similar medium containing 100 μCi of ^{35}S *in vitro* cell labeling mixture (Amersham), after which the cells were further incubated for 3 h. The cells were washed once with PBS supplemented with 50 mM Ca^{2+} and 50 mM Mg^{2+} and then lysed on ice in 1 ml of lysis buffer (0.5 mM Tris [pH 7.3], 1 mM EDTA, 0.1 M NaCl, 1% Triton X-100). The lysates were cleared by centrifugation for 5 min at 15,000 rpm and 4°C and used in radioimmunoprecipitation studies. Aliquots of the cell lysates were diluted in 1 ml of detergent buffer (50 mM Tris [pH 8.0], 62.5 mM EDTA, 1% NP-40, 0.4% sodium deoxycholate, 0.1% SDS) containing antibodies (4 μl of rabbit anti-nsp2/nsp3). After overnight incubation at 4°C, the immune complexes were adsorbed to Pansorbin cells (Calbiochem) for 60 min at 4°C and subsequently collected by centrifugation. The pellets were washed three times by resuspension and centrifugation with radioimmunoprecipitation assay (RIPA) buffer (10 mM Tris [pH 7.4], 150 mM NaCl, 0.1% SDS, 1% NP-40, 1% sodiumdeoxycholate). The final pellets were suspended in Laemmli sample buffer (LSB) and heated at 95°C for 1 min before analysis by SDS-polyacrylamide gel electrophoresis (PAGE) with 12.5% polyacrylamide gels. The radioactivity in protein bands was quantitated in dried gels using a PhosphorImager (Molecular Dynamics).

Quantitative RT-PCR. Total RNA was isolated from infected cells using TRIzol reagent (Invitrogen), after which it was purified using an RNeasy minikit (Qiagen), both according to the manufacturer's instructions.

Relative gene expression levels of viral (sub)genomic RNA was determined by performing quantitative RT-PCR using Assay-On-Demand reagents (PE Applied Biosystems) as described previously (14, 52). Reactions were performed using an ABI Prism 7000 sequence detection system. The comparative threshold cycle (C_T) method was used to determine the fold change for each individual gene.

Immunofluorescence confocal microscopy. LR7 cells grown on glass coverslips were fixed at the times indicated in the text and figure legends after transfection or infection using a 4% paraformaldehyde (PFA) solution in PBS for 30 min at room temperature. The fixed cells were washed with PBS and permeabilized using either 0.1% Triton X-100 for 10 min at room temperature or 0.5 μg/ml digitonin (diluted in 0.3 M sucrose, 25 mM $MgCl^{2+}$, 0.1 M KCl, 1 mM EDTA, 10 mM PIPES [piperazine-*N,N'*-bis(2-ethanesulfonic acid)], pH 6.8) for 5 min at 4°C. Next, the permeabilized cells were washed with PBS and incubated for 15 min in blocking buffer (PBS–10% normal goat serum), followed by a 60-min incubation with antibodies directed against either nsp4, nsp8, MHV M, EGFP, or dsRNA. After three washes with PBS, the cells were incubated for 45 min with Cy3-conjugated donkey anti-rabbit immunoglobulin G antibodies (Jackson Laboratories), fluorescein isothiocyanate-conjugated goat anti-rabbit immunoglobulin G antibodies (ICN), or Cy3-conjugated donkey anti-mouse immunoglobulin G antibodies (Jackson Laboratories). Where indicated, nuclei of cells were stained with TOPRO 3 iodide (Molecular Probes). After four washes with PBS, the samples were mounted on glass slides in FluorSave (Calbiochem). The samples were examined with a confocal fluorescence microscope (Leica TCS SP), or fluorescence intensities were quantified using a DeltaVision RT microscope and software from Applied Precision, Inc. (API).

Time-lapse live-cell imaging and photobleaching. Subconfluent monolayers of LR7 cells were grown in 0.8-cm^2 Lab-Tek Chambered Coverglasses (ThermoFisher Scientific and Nunc GmbH & Co. KG). The cells were transfected and infected as described above. Where indicated in the text and figure legends, cells were incubated with or without 1 μM nocodazole in DMEM +/+ at 4°C for 1 h, after which the cells were transferred to 37°C, and incubation was continued. Live-cell digital images of cells, placed in an environmental chamber at 37°C, were acquired at x100 magnification by the DeltaVision RT microscope from Applied Precision, Inc. (API). Images were deconvolved and analyzed using SoftWorx software (API). Time-lapse movies in QuickTime format were generated using ImageJ software, version 1.41 (W. S. Rasband, NIH, Bethesda, MD [http://rsb.info.nih.gov/

ij/]). Particle tracking was performed using the MTrackJ plug-in for ImageJ developed by Erik Meijering at the Biomedical Imaging Group Rotterdam (Erasmus Medical Centre, Rotterdam, the Netherlands).

FRAP experiments were performed using the quantifiable laser module (QLM) of the DeltaVision RT microscope at 37°C. For each FRAP experiment, five prebleach images were collected, followed by a 1-s, 488-nm laser pulse with a radius of 0.500 μm to bleach the regions of interest (ROI). In a time frame of 60 s, 52 additional images were captured. Quantitative analysis of the FRAP data was performed using SoftWorx software.

Differential ultracentrifugation and protease protection assay. Subconfluent monolayers of LR7 cells were transfected and/or infected as described above and washed once with PBS before being scraped in homogenization buffer (HB; 50 mM Tris-HCl [pH 7.2] and 10 mM sucrose) and centrifuged for 5 min at 1,200 rpm. Cells were subsequently resuspended in HB, and homogenized cell lysates were prepared by repeated passage through a 21-gauge needle. The differential ultracentrifugation was performed in a Beckman Coulter Optima Max-E ultracentrifuge using a TLA-55 rotor. First, the homogenized cells were centrifuged for 10 min at 3,000 rpm to remove the nuclei and the cellular debris. The resulting supernatant was next centrifuged for 20 min at 23,000 rpm to separate the intracellular membranes (pellet) from the cytosol (supernatant). Where indicated in the text and figure legends, the intracellular membrane fractions were mock treated or treated with 20 μg/ml proteinase K for 10 min at 20°C in the presence or absence of 0.05% TX-100 before proteinase K was inactivated by the addition of 2 mM phenylmethylsulfonyl fluoride (PMSF). *Renilla* and firefly luciferase activity in the different fractions was determined using a Dual-Luciferase Assay Kit (Promega) according to the manufacturer's instructions.

EM procedures. HeLa-CEACAM1a cells infected with recombinant MHV-nsp2GFP were processed for conventional EM and cryo-immuno-EM (IEM) at 8 h p.i. as previously described (63, 72). Cryo-sections were immunolabeled using a polyclonal anti-GFP (Abcam, Cambridge, United Kingdom) antibody, followed by incubation with protein A-gold conjugates prepared following an established protocol (63). Sections were viewed in a JEOL 1010 or a JEOL 1200 electron microscope (JEOL, Tokyo, Japan), and images were recorded on Kodak 4489 sheet films (Kodak, Rochester, NY).

RESULTS

MHV nsp2 is efficiently recruited to the RTCs.

To enable live-cell imaging of coronavirus RTCs in infected cells, we needed to visualize these structures in living cells. Previously, we along with others have shown that (GFP-tagged) nsp2 is efficiently recruited to perinuclear foci in MHV-infected cells (24, 72). To confirm and extend these observations, GFP-tagged nsp2 (nsp2-GFP) was expressed *in trans* in mouse cells that were subsequently infected with MHV or mock infected. Next, the colocalization of nsp2-GFP with nsp8, an established marker for the RTCs (39), was monitored. In the absence of a MHV infection, nsp2-GFP demonstrated a diffuse cytosolic and nuclear fluorescence pattern (Fig. 1A). Upon infection with MHV, nsp2 appeared to be efficiently recruited to the RTCs as this protein was redistributed almost completely to punctuate perinuclear foci, colocalizing with nsp8 (Fig. 1A).

To investigate the recruitment of nsp2 to the RTCs in more detail, we investigated which part of the protein was responsible for this phenotype. To this end, we generated plasmids that encoded nsp2 truncations C-terminally fused with GFP (Fig. 1B). In the absence of a MHV infection, all proteins demonstrated a cytosolic and nuclear expression pattern (Fig. 1C). The different nsp2 truncation mutants displayed very similar expression levels, which were only slightly lower than the level of the full-length nsp2-GFP fusion protein (Fig. 1D).

Next, these plasmids were used in the redistribution assay as described above. Cells expressing the nsp2AB and nsp2BC truncations exhibited a diffuse nuclear and cytoplasmic fluorescence, regardless of whether these cells were mock infected (Fig. 1C) or infected with MHV (Fig. 1E). No colocalization of these proteins with the nsp8 RTC marker protein was observed. In contrast, the nsp2CD truncation localized to perinuclear dots positive for nsp8 in infected cells. Based on these results, we concluded that

Figure 1. Recruitment of MHV nsp2 to the RTCs. (A) LR7 cells transfected with pEGFP-nsp2 were mock infected (–MHV) or infected with MHV A59 (+MHV). Cells were fixed at 6 h p.i. and subsequently processed for immunofluorescence analysis using antibodies against nsp8. (B) Schematic representation of the C- and N-terminal truncations of MHV nsp2. The amino acids remaining are indicated. The EGFP tag at the C-terminal end of nsp2 is not indicated. (C and D) LR7 cells transfected with pEGFP-nsp2, pEGFP-nsp2AB, pEGFP-nsp2BC, or pEGFP-nsp2CD were fixed at 30 h posttransfection and processed for microscopic analysis (C); in addition, the mean arbitrary fluorescent intensities of 25 cells were determined using a DeltaVision RT microscope and software from Applied Precision (D). (E) LR7 cells transfected with pEGFP-nsp2AB, pEGFP-nsp2BC, or pEGFP-nsp2CD were mock infected or infected with MHV-A59. At 6 h p.i. the cells were fixed and processed for immunofluorescence analysis using nsp8 antibodies.

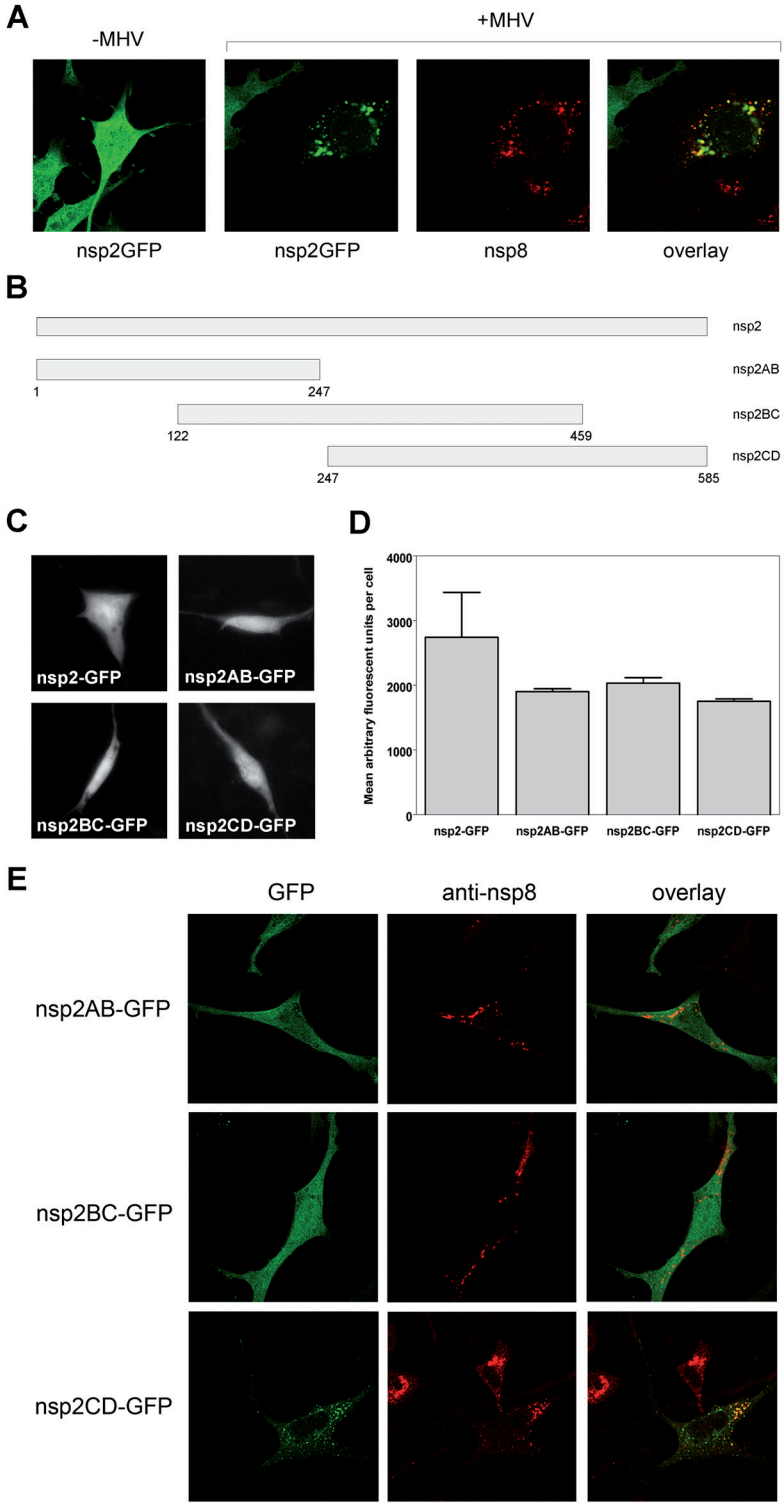
A
-MHV
+MHV
nsp2GFP
nsp2GFP
nsp8
overlay
B
nsp2
nsp2AB
1
247
nsp2BC
122
459
nsp2CD
247
585
C
nsp2-GFP
nsp2AB-GFP
nsp2BC-GFP
nsp2CD-GFP
D
Mean arbitrary fluorescent units per cell
4000
3000
2000
1000
0
nsp2-GFP
nsp2AB-GFP
nsp2BC-GFP
nsp2CD-GFP
E
GFP
anti-nsp8
overlay
nsp2AB-GFP
nsp2BC-GFP
nsp2CD-GFP

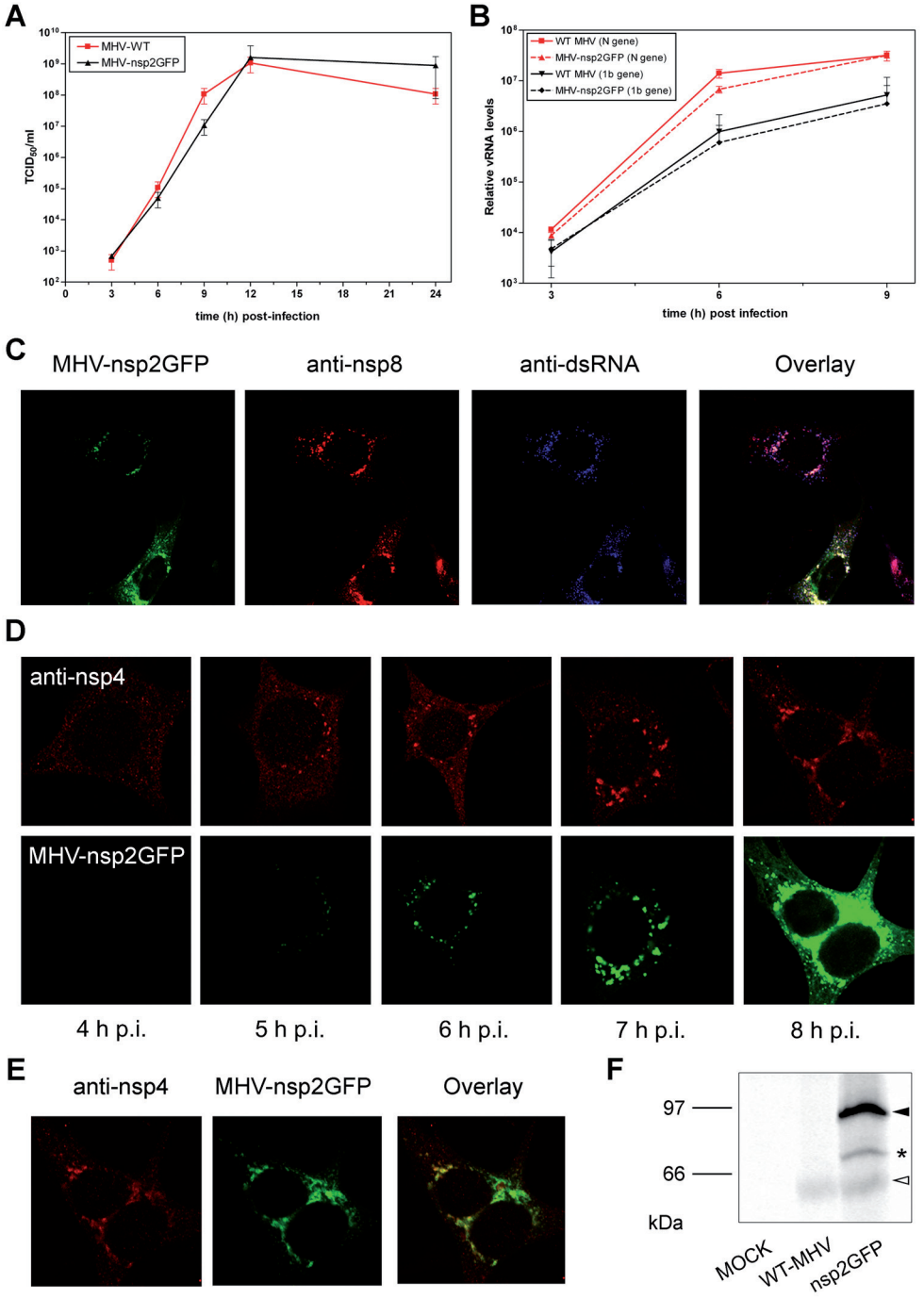
A
MHV-WT
MHV-nsp2GFP
TCID50/ml
time (h) post-infection
B
WT MHV (N gene)
MHV-nsp2GFP (N gene)
WT MHV (1b gene)
MHV-nsp2GFP (1b gene)
Relative vRNA levels
time (h) post infection
C
MHV-nsp2GFP
anti-nsp8
anti-dsRNA
Overlay
D
anti-nsp4
MHV-nsp2GFP
4 h p.i.
5 h p.i.
6 h p.i.
7 h p.i.
8 h p.i.
E
anti-nsp4
MHV-nsp2GFP
Overlay
F
97
66
kDa
MOCK
WT-MHV
nsp2GFP

Figure 2. Characterization of recombinant MHV-nsp2GFP and subcellular localization of nsp2GFP. (A and B) LR7 cells were infected with MHV-nsp2GFP or MHV-WT (MOI of 10). (A) Culture medium was collected at different time points p.i., after which the viral infectivity was determined by a quantal assay on LR7 cells. The $TCID_{50}$ values are indicated. (B) Intracellular viral RNA (vRNA) levels were determined by a quantitative RT-PCR on the 1b and the N genes. The data are presented as relative vRNA levels. (C) LR7 cells infected with recombinant MHV-nsp2GFP were fixed and processed for immunofluorescence analysis using antibodies directed against nsp8 and dsRNA. (D and E) LR7 cells infected with recombinant MHV-nsp2GFP were fixed at the indicated time points and processed for immunofluorescence analysis using antibodies directed against nsp4. Images taken from the cells at the different time points were obtained at identical settings (D) while the settings were adjusted to demonstrate the colocalization between nsp2GFP and nsp4 at the 8-h time point (E). (F) Mock-, MHV-WT-, or MHV-nsp2GFP-infected cells were radiolabeled from 6 till 9 h p.i. Cells were lysed and processed for immunoprecipitation with antibodies directed against the nsp2 protein and analyzed by 12.5% SDS-PAGE. The filled triangle indicates the nsp2-GFP protein, the open triangle indicates the endogenous mature nsp2 protein, and the asterisk indicates an additional unidentified protein species.

the carboxy-terminal part of the nsp2 protein is required and sufficient to target the nsp2-GFP fusion proteins to the replication sites.

Recombinant MHVs expressing nsp2 fusion proteins.

To facilitate the live-cell imaging of coronavirus RTCs during coronavirus infection, we next generated recombinant MHVs expressing nsp2 tagged either with GFP (MHV-nsp2GFP) or with a red fluorescent protein (MHV-nsp2mCherry). In these viruses, the gene encoding the nsp2 fusion protein was incorporated into the viral genome as an additional expression cassette, using a previously described targeted RNA recombination system (36). The nsp2-GFP or the nsp2-mCherry gene, each one preceded by a transcription-regulatory sequence, replaced the nonfunctional HE gene.

The generated recombinant viruses were evaluated for their growth kinetics and viral RNA synthesis. As a control, we used a recombinant wild-type MHV A59 (MHV-WT). MHV-nsp2GFP replicated efficiently in cell culture with titers that were only slightly lower than those of MHV-WT in a one-step growth curve (Fig. 2A). In agreement with these results, viral RNA synthesis, as determined by quantitative RT-PCR on the 1b and the N gene, was only slightly affected by the insertion of the nsp2-GFP expression cassette into the viral genome (Fig. 2B). MHV-nsp2mCherry replicated to the same extent as MHV-nsp2GFP (data not shown).

Next, we studied the subcellular localization of the nsp2 fusion proteins by immunofluorescence. Only the results for MHV-nsp2GFP are shown since essentially identical results were obtained for MHV-nsp2mCherry. As shown in Fig. 2C, cells infected with MHV-nsp2GFP revealed at 6 h p.i. a GFP fluorescence distribution pattern identical to the one observed when nsp2-

GFP was expressed from a plasmid in MHV-infected cells (compare Fig. 1A and 2C). Importantly, nsp2-GFP localized to perinuclear foci positive not only for nsp8 but also for dsRNA, with the latter probably corresponding to replicative intermediates produced during viral replication (49, 55).

Since the tagged nsp2 was expressed from an additional subgenomic RNA (sgRNA) rather than from the genomic RNA as part of pp1a and pp1ab, we analyzed the expression level of the nsp2-GFP fusion protein. To this end, LR7 cells were infected with either MHV-nsp2GFP or MHV-WT at an MOI of 10 and labeled for 3 h with ^{35}S-labeled methionine, starting at 6 h p.i. Cell lysates were processed for immunoprecipitation, followed by SDS-PAGE analysis. The results are shown in Fig. 2F. Antibodies directed against the nsp2 protein precipitated proteins with the expected molecular masses (endogenous mature nsp2, 65 kDa; nsp2-GFP fusion protein, 95kDa). In addition, a protein with an intermediated molecular mass (71 kDa) was detected, which, like the nsp2-GFP fusion protein, could also be precipitated with antibodies against the GFP tag. The nature of this protein species is unknown, but it was also observed when the nsp2-GFP protein was expressed from a plasmid (data not shown). The radioactivity precipitated was quantified by using Phosphor Imager scanning and corrected for the amount of methionines present in the proteins. The results demonstrate that the nsp2-GFP fusion protein was approximately 10-fold more abundant than the endogenous mature nsp2.

Next, we analyzed whether overexpression of the tagged nsp2 affected its localization to the RTCs throughout the infection. To this end, we performed a time-lapse experiment in which MHV-nsp2GFP-infected cells were fixed at different time points p.i. and subsequently processed for immunofluorescence analysis. In this experiment, antibodies directed against nsp4 were used to identify the RTCs (49). The results are shown in Fig. 2D and E. Expression of nsp4, present in distinct foci, could be detected from 4 h p.i. onwards. The maximum level of nsp4 staining was observed at 7 h p.i. Expression of nsp2-GFP could be detected from 5 h p.i., after which the expression level increased until 8 h p.i. Although the cytoplasmic GFP fluorescence at this late time point was higher than at the earlier time points, possibly indicating a saturation of RTCs with nsp2-GFP, the majority of nsp2-GFP was still present in distinct cytoplasmic foci which colocalize with nsp4 (Fig. 2E). In summary, nsp2-GFP or nsp2-mCherry fusion proteins expressed from recombinant MHVs localized to the RTCs, as demonstrated by their colocalization with dsRNA, nsp8, and nsp4 throughout the infection (at least from the time point these fusion proteins become detectable). Importantly, this localization corresponds with the previously reported distribution of nsp2 (5, 21, 24, 62).

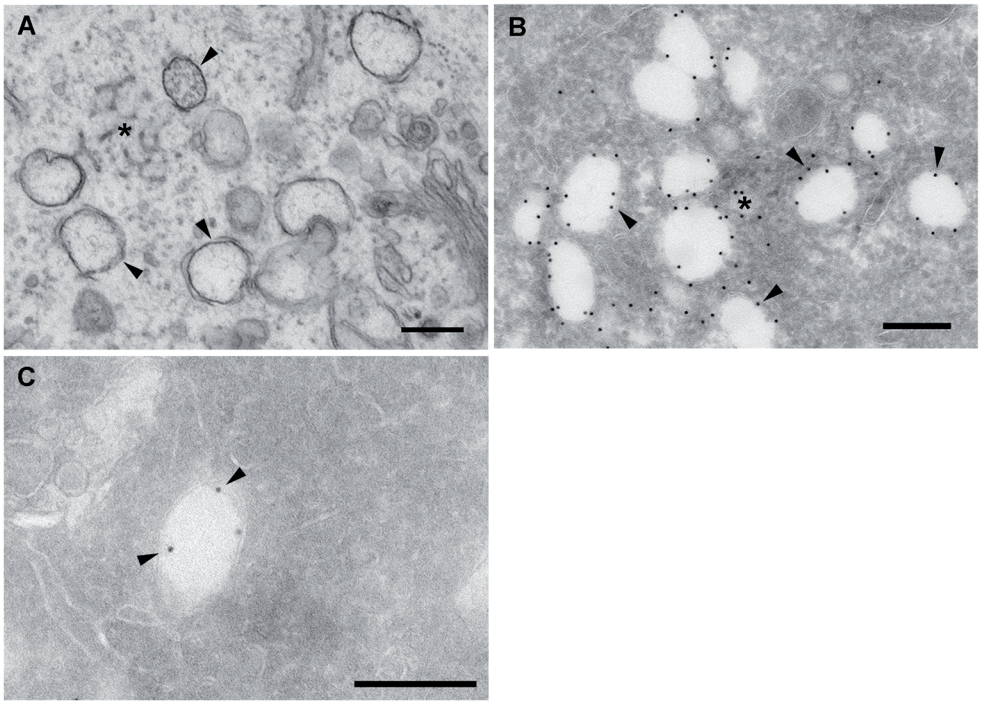

Figure 3. nsp2-GFP localizes to DMVs and CMs. HeLa-CEACAM1a cells, infected with recombinant MHV-nsp2GFP, were fixed at 8 h p.i. and processed for ultrastructural analysis by chemical fixation and epon embedding (A). Alternatively, cryosections were prepared that were incubated with antibodies directed against the GFP tag, followed by immunogold labeling (B and C). Convoluted membranes are indicated by the asterisks. nsp2 labeling is indicated by the arrowheads. Scale bar, 200 nm.

Nsp2-GFP localizes to DMVs and CMs.

To confirm the targeting of nsp2-GFP to the DMV-anchored RTCs, we performed electron microscopy (EM) on infected cells to localize the protein at the ultrastructural level. First, conventional EM was used to demonstrate the appearance of the DMVs. Their morphology and dimensions (approximately 160 nm in diameter) nicely resembled the structures described previously (23, 61, 65, 72) (Fig. 3A, indicated by the arrowheads). The DMVs often appeared clustered together in the perinuclear region of the cell (data not shown). In between these DMV clusters, reticular inclusions, probably corresponding to the recently described CMs (35), were also observed (Fig. 3A, indicated by the asterisk).

Subsequently, immuno-EM was performed on ultrathin cryo-preparations of MHV-nsp2GFP-infected cells with immunogold labeling specifically directed against the GFP tag. Although the general cellular architecture was

preserved, DMVs appeared as empty vesicles in the cryo-sections compared to the ones observed by conventional EM. This dissimilarity is likely due to differences in the fixation methods (35, 65). Mock-infected cells revealed no labeling and no DMVs (data not shown), whereas in MHV-nsp2GFP-infected cells the specific immunogold labeling of nsp2-GFP was observed on both clustered and individual DMVs (Fig. 3B and C, respectively). In addition, nsp2-GFP also decorated CMs (Fig. 3B, asterisk) in between the DMV clusters. These results demonstrate that the nsp2-GFP fusion protein localizes to the MHV-induced DMVs and CMs, confirming the immunofluorescence data, which showed the recruitment of the fusion protein to the RTCs.

Localization of nsp2 on the cytosolic face of the DMVs.

The nsp2 protein may either be associated to the cytoplasmic side of the DMVs or, alternatively, be incorporated into the virus-induced vesicles, thereby being shielded from the cytoplasm. Discriminating between these two possibilities was of interest by itself and also because the intended FRAP experiments would only make sense when the nsp2 fusion proteins are not being shielded. In order to facilitate our biochemical analyses of the membrane association of nsp2, we generated another recombinant virus (MHV-nsp2RL) expressing nsp2 fused to *Renilla* luciferase (nsp2-RL). MHV-ERLM (12), which expresses the *Renilla* luciferase (RL) *per se* was used as a control for our experiments.

First, we verified the membrane recruitment of the nsp2 fusion protein in infected cells. To this end, cells infected with either MHV-ERLM or MHV-nsp2RL were homogenized and subsequently subjected to differential ultracentrifugation such that the cellular membranes were pelleted and separated from the cytosolic fraction. The luciferase expression levels in the different fractions were determined as described in the Materials and Methods section (Fig. 4A). As expected, the majority of the RL protein activity (~90%) was present in the cytosolic fraction of MHV-ERLM-infected cells. In contrast, the large majority of the nsp2-RL fusion protein (~80%) was found in the membrane fraction, in agreement with the idea that nsp2 is recruited to DMVs and CMs.

Next, we performed a protease protection assay on the membrane pellets obtained from the MHV-nsp2RL-infected cells to determine whether the fusion protein was present on the cytosolic face of the DMVs/CMs (i.e., sensitive to protease treatment) or in the interior of these vesicles (i.e., not sensitive to protease treatment). As an internal control, prior to infection cells were transfected with a plasmid expressing a firefly luciferase protein carrying

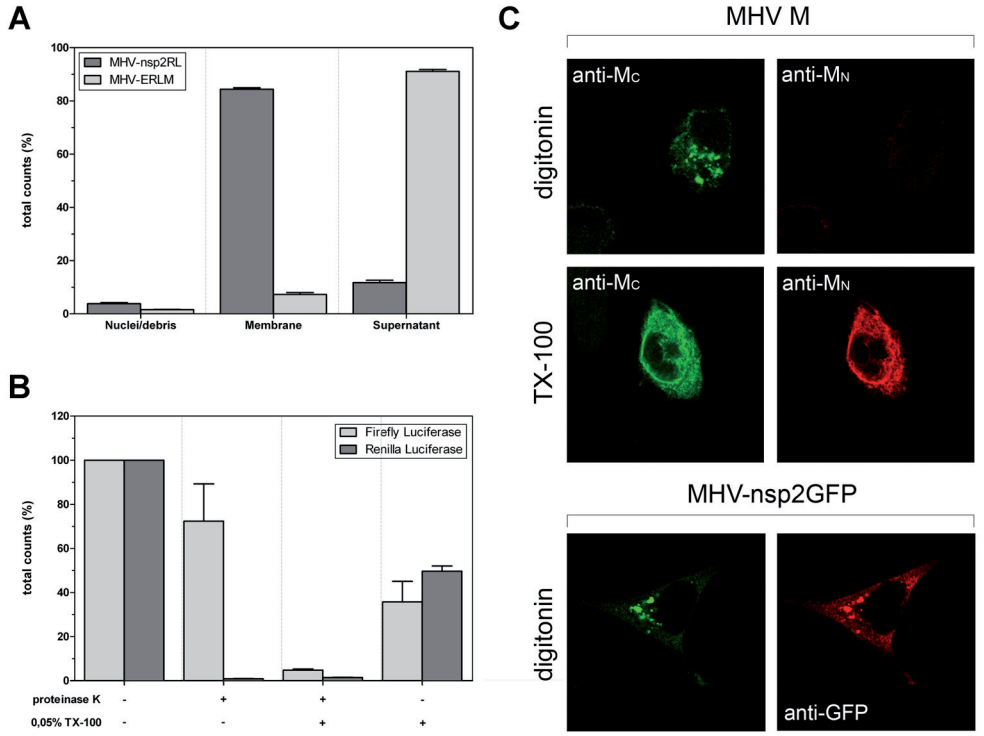

Figure 4. nsp2 associates to the cytoplasmic face of the DMVs and CMs. (A) LR7 cells infected with MHV-nsp2RL or MHV-ERLM were processed for ultracentrifugation as described in the Materials and Methods section. The luciferase activity in the indicated fractions was determined, corrected for the volume of the fraction, and plotted as the percentage of the total amount of luciferase activity. (B) LR7 cells transfected with pER-Fluc were infected with MHV-nsp2RL. Membrane fractions, prepared as described in the Materials and Methods section, were mock treated with 20 μg/ml proteinase K in the presence or absence of 0.05% TX-100. *Renilla* and firefly luciferase activities in the differently treated samples were measured and are depicted relative to the mock-treated samples, which are set at 100%. (C) MHV-nsp2GFP-infected LR7 cells were fixed at 6 h p.i. and permeabilized with buffers containing either 0.5 μg/ml digitonin or 0.1% TX-100. Immunofluorescence was performed using antibodies directed against the N terminus (anti-M_N) or the C terminus (anti-M_C) of the MHV M protein or against the GFP tag (anti-GFP).

a signal peptide and a KDEL retention signal at its amino and carboxy termini, respectively, which direct the protein to the ER lumen. The membrane pellets were treated with the serine endopeptidase proteinase K, either in the presence or in the absence of 0.05% Triton X-100, before the protein expression levels of both the firefly and *Renilla* luciferase were assessed. The luciferase levels in the various samples are depicted in Fig. 4B relative to the mock-treated samples. As expected, the ER-localized firefly luciferase protein present in the membrane pellet was almost completely resistant to the proteinase K treatment in the absence, but not in the presence, of Triton X-100, consistent

with its localization in the ER lumen. In contrast, regardless of the absence or presence of detergent, nsp2-RL was very sensitive to proteinase K and degraded almost completely. Overall, these results demonstrate that at least the large majority of the nsp2-RL protein is exposed at the exterior of the DMVs/CMs.

To further confirm the localization of nsp2 on the cytoplasmic face of the DMVs/CMs by a different approach, cells were infected wth MHV-nsp2GFP and subsequently subjected to selective permeabilization of the plasma membrane using digitonin before the availability of the GFP tag to specific antibodies was assayed. Triton X-100 was used as a control to permeabilize all cellular membranes. The assay was validated with the MHV membrane (M) protein, the amino and carboxy termini of which are known to reside in the lumen of the secretory pathway and in the cytoplasm, respectively (i.e., N terminus in lumen/C terminus in cytoplasm [N_{exo}/C_{endo}] topology) (53). As shown in Fig. 4C, the MHV M protein could be detected with antibodies directed against its N terminus (anti-M_N) after permeabilization of all cellular membranes with Triton X-100 but not after the selective dissolution of the plasma membrane with digitonin. In contrast, antibodies directed against the carboxy-terminal part of the M protein (anti-M_C) were able to bind the protein after permeabilization with both Triton X-100 and digitonin. As these observations were in perfect agreement with the known topology of the type III M protein, the approach was subsequently applied to cells infected with MHV-nsp2GFP. As shown in Fig. 4C, antibodies directed against the GFP tag were able to readily recognize the fusion protein after permeabilization of cells with digitonin, which is in agreement with the results of the protease protection assay, confirming that the nsp2 protein is exposed on the cytoplasmic face of the DMVs and CMs.

Trafficking of replicative structures.

Having established that the nsp2 fusion proteins are recruited to the DMV-anchored RTCs and are suitable for live-cell imaging studies and FRAP analyses, we investigated the real-time dynamics of the nsp2-positive structures. To this end, cells were infected with recombinant MHV expressing either nsp2-GFP or nsp2-mCherry, after which time-lapse recordings were generated over a period of 2 to 2.5 min, with image acquisition every 200 to 300 ms. First, we explored whether the nsp2-positive structures were static or able to move through the cell.

Live-cell imaging of cells infected with MHV-nsp2GFP essentially revealed the presence of two classes of nsp2-GFP positive structures. One

class consisted of relatively large, immobile fluorescent foci (indicated by arrowheads in Fig. 5A). Their only movement appeared to correlate with movementsof the cell(s) itself. The other class consisted of small cytoplasmic fluorescent foci, a considerable fraction of which demonstrated a relatively high mobility. In view of the ultrastructural data, we think that the small and large fluorescent foci likely correspond to single DMVs and clusters of DMVs and CMs, respectively.

Two types of movement could be observed for the small fluorescent structures: nsp2-positive foci either (i) demonstrated confined movement (42.3% out of 200 foci tracked) or (ii) moved in a stop-and-go fashion on what appeared to be specific cellular tracks (saltatory movement, 15.0%). The movements of several of the small nsp2-GFP-positive foci were tracked, as indicated by the white lines in Fig. 5A. The complete recording of this

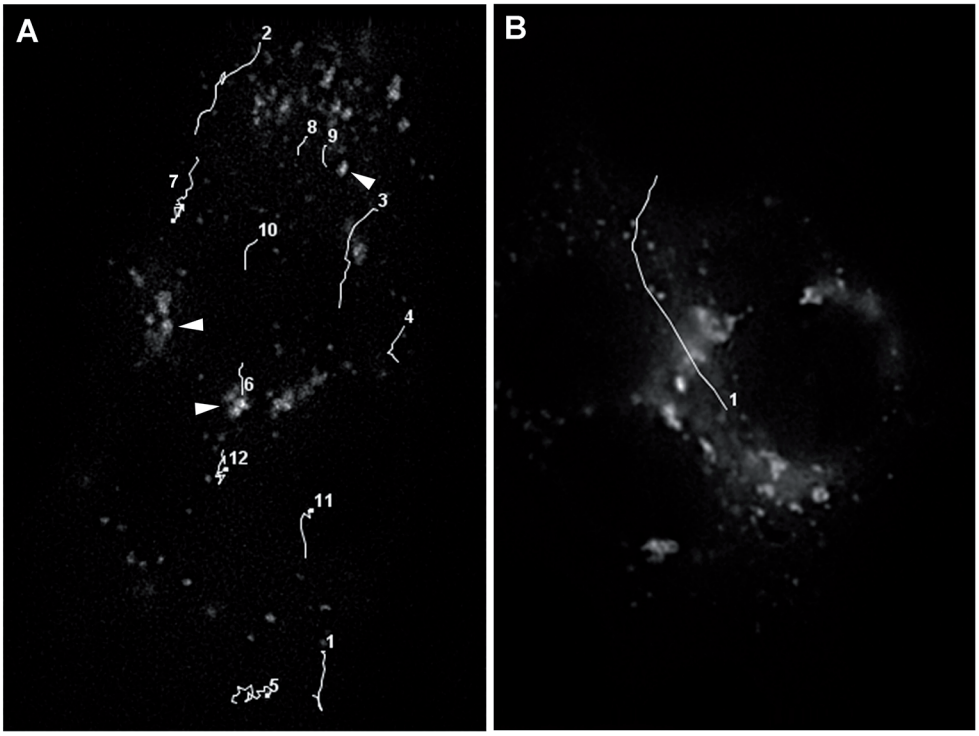

Figure 5. Trafficking of MHV replicative structures. Time-lapse recordings of MHV-nsp2GFP-infected LR7 cells were obtained using DeltaVision Core (API). Trafficking of selected nsp2-positive structures was determined. Tracks are indicated by white lines and numbered. (A) Tracks 1 to 4, 6, and 8 to 10 represent saltatory movements while tracks 5, 7, and 12 represent confined movements of small nsp2-GFP-positive structures. Track 11 represents confined movement followed by saltatory trafficking. Large, immobile nsp2-positive structures are indicated by the arrowheads. (B) The very long track taken by a small RTC demonstrating saltatory movement is shown. See also Videos S1 and S2 in the supplemental material.

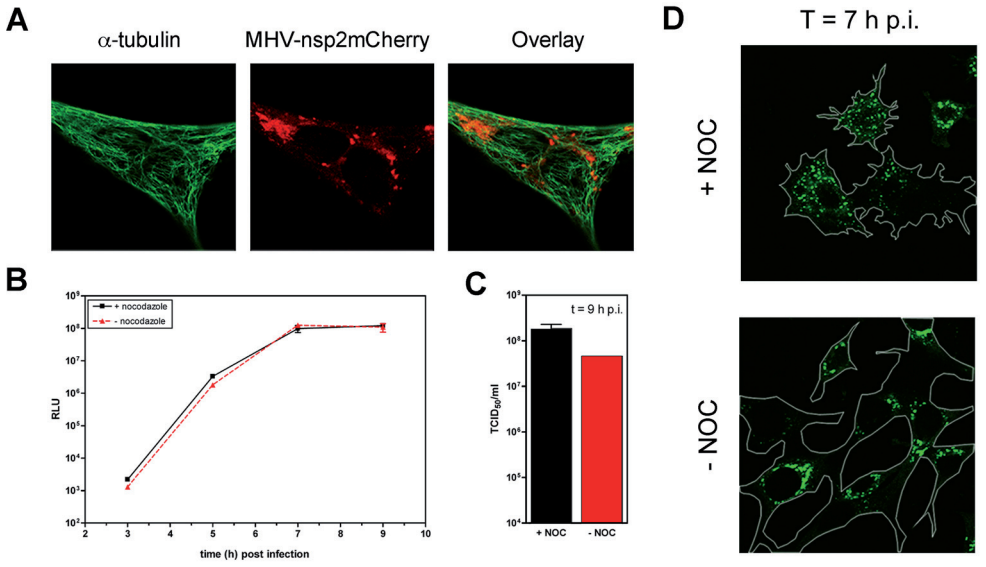

Figure 6. The role of microtubules in transport. (A) Cells infected with MHV-nsp2mCherry were fixed at 6 h p.i. and processed for immunofluorescence analysis using the α-tubulin antibody to visualize microtubules. (B to D) LR7 cells were infected with MHV-nsp2RL or MHV-nsp2GFP either in the presence (+NOC) or absence (–NOC) of 1 μM nocodazole. Cells were lysed or fixed at the indicated time point, followed by determination of the luciferase expression levels (B); the $TCID_{50}$ value of the culture medium was determined (C), or cells were processed for microscopical analysis (D). The white lines in panel D indicate the contours of the cell. T, time.

movie is shown in Video S1 in the supplemental material. The nsp2-GFP-positive structures numbered 5, 7, and 12 in Fig. 5A displayed confined movements while the others are examples of structures that exhibited saltatory movements. The mean velocity of these latter movements was calculated at 1.3 ± 0.7 μm/s, with a peak velocity of 4.1 μm/s. Occasionally, fluorescent puncta were observed that traveled particularly large distances, clearly revealing the saltatory movement. An example is shown in Fig. 5B (track 1) and in Video S2 in the supplemental material. The peak velocity of this specific displacement was 3.7 μm/s, with a mean velocity of 1.7 μm/s.

The characteristics of the movements of the small nsp2-GFP-positive foci (velocity and cellular tracks taken) are suggestive of microtubule-dependent transport (40). Therefore, we investigated whether these structures were associated to microtubules in infected cells. Staining for α-tubulin (Fig. 6A) suggested that the small nsp2-positive foci were associated with or in close proximity to the microtubules. Given the extensive network of microtubules present in the cells, we next performed live-cell imaging experiments to confirm that the mobility of these small structures was indeed dependent

on microtubules. In MHV-nsp2mCherry-infected cells, microtubules were visualized by prior transfection with the plasmid expressing a YFP-alpha-tubulin fusion protein, followed by live-cell imaging. As can be seen in Video S3 in the supplemental material, the small fluorescent foci were in close proximity to the microtubules and appeared to move along these cellular tracks. Furthermore, live-cell imaging was performed in the absence of a functional microtubular network. To this end, cells were treated with 1 μM nocodazole, a drug that interferes with the polymerization of microtubules. Treatment of cells with this drug resulted in a complete disruption of the microtubules (data not shown). Importantly, no movement of the fluorescent puncta could be observed under these conditions, as demonstrated in Video S4 in the supplemental material.

Next, we studied whether breakdown of the microtubules affected MHV RNA replication and production of infectious virus particles. To this end, cells treated with nocodazole or mock treated were infected with a luciferase-expressing recombinant MHV. At different time points p.i., luciferase expression, which is directly correlated to RNA replication (15), and virus production were measured. The nocodazole was kept present throughout the experiment. As shown in Fig. 6B, luciferase expression was not affected by the disruption of microtubules by nocodazole. Moreover, nocodazole treatment also did not affect virus production (Fig. 6C). In agreement with these results, RTCs were still formed in the presence of nocodazole, as demonstrated by the appearance of nsp2-GFP positive foci at 7 h p.i. (Fig. 6D). However, while in the mock treated cells the RTCs appeared to be concentrated in the perinuclear region of the cell, in the nocodazole-treated cells, the nsp2-positive foci were scattered throughout the cells. In summary, the results show that the small, but not the large, fluorescent foci were able to move through the cell in a microtubule-dependent fashion. This movement was not, however, essential for MHV RNA replication and the production of infectious virus.

Replicative structures are static entities.

Essentially, nothing is known about the dynamics of the coronavirus nsps present at the DMV-anchored RTCs. The RTCs might be relatively static entities, which allow little exchange of proteins with other RTCs, even when these RTCs are anchored to the same DMV; the nsps might be able to move around on a DMV; or the RTCs might even display a continuous exchange of proteins with their cellular environment. We took advantage of our recombinant viruses expressing the fluorescent nsp2 fusion proteins to investigate the dynamics of the replicative structures by means of FRAP

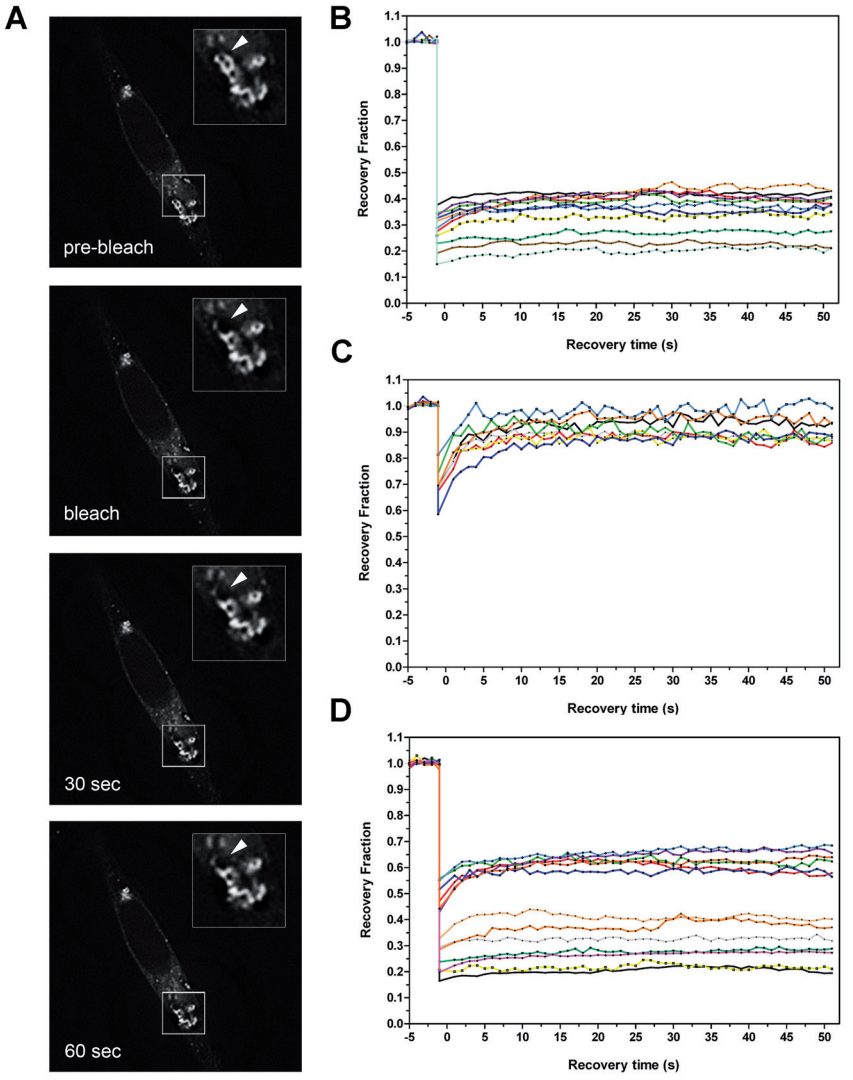
A
pre-bleach
bleach
30 sec
60 sec
B
Recovery Fraction
Recovery time (s)
C
Recovery Fraction
Recovery time (s)
D
Recovery Fraction
Recovery time (s)
E
MHV-nsp2GFP
MHV-nsp2mCherry
Topro
Overlay
-CHX
+CHX

Figure 7. Coronavirus RTCs are static entities. (A) FRAP was performed on MHV-nsp2GFP-infected cells at 7 h p.i. using the quantifiable laser module of the DeltaVision Core (API). A representative FRAP experiment is depicted, with the bleached area indicated by the white arrowheads in the magnification in the top right corners. (B to D) Fluorescence recovery graphs were generated of bleached ROI either in MHV-nsp2GFP-infected cells (B) or in cells transfected with nsp2-GFP which were subsequently mock infected with MHV-A59 (C) or infected with MHV-A59 (D). (E) Two LR7 cell cultures were infected with either MHV-nsp2GFP or MHV-nsp2mCherry, followed by incubation in the presence of HR2 peptide. At 6 h p.i., the HR2 peptide was removed; cells were trypsinized, mixed, and subsequently plated in the presence (+) or absence (–) of CHX. At 9 h p.i. the cells were processed for immunofluorescence analysis. Nuclear staining was obtained by TOPRO 3 iodide.

analysis. This technique allows measuring the recovery rates of proteins in specific regions of interest (ROI), after irreversible photobleaching, by non-bleached counterparts [reviewed in reference (37)]. With this assay we are able to determine whether nsp2 recruited to the RTCs is exchanged with nsp2 located outside of the ROI, in the cytoplasm, or at other DMVs. In our experimental set up, ROI were photobleached for 1 s, followed by signal acquisition every second during a period of 60 s. The FRAP assay was first performed on cells infected with MHV-nsp2GFP. Representative images of such an experiment are shown in Fig. 7A. The corresponding fluorescence recovery graphs are depicted in Fig. 7B to D. Photobleached nsp2-GFP-positive structures (n = 11) in infected cells (Fig. 7B) demonstrated a reduction of about 60 to 80% of the prebleached fluorescent signal. Essentially no recovery of the fluorescent signal in the ROI was observed over time. Identical results were obtained when only part of a larger fluorescent structure was bleached (data not shown).

As a control, cells were transfected with a plasmid encoding the nsp2-GFP fusion protein and subsequently infected with MHV A59 or mock infected. Next, FRAP experiments were performed as described above. In the absence of an infection, the nsp2-GFP protein revealed a diffuse cytoplasmic localization, which is in agreement with previous observations (Fig. 1). The photobleached ROI (n = 8) in these cells demonstrated a fast recovery of fluorescence within 10 s (Fig. 7C). Moreover, we were unable to bleach the fluorescent signal below ~75% intensity of the prebleach intensity, probably because of the high mobility of the cytoplasmic nsp2-GFP. In contrast, upon infection of the transfected cells with MHV, nsp2-GFP localized to distinct fluorescent foci in the perinuclear region of the cell. When these fluorescent foci were photobleached, no recovery of fluorescence in the ROI (n = 13) was observed (Fig. 7D). Apparently, nsp2, once recruited to the RTCs, is not exchanged with nsp2 present in the cytoplasm or in other DMVs.

To verify the lack of exchangeability of nsp2 once recruited to the RTCs,

another experiment was performed in which we studied the exchange of fluorescence between preexisting RTCs after fusion of cells expressing either a green or a red fluorescent nsp2. To this end, two LR7 cell cultures were infected, one with MHV-nsp2GFP and the other with MHV-nsp2mCherry, both in the presence of a heptad repeat 2 (HR2) fusion-inhibitory peptide (4). The HR2 peptide was removed at 6 h p.i., after which cells were trypsinized, mixed, and subsequently plated in the presence or absence of cycloheximide (CHX), an inhibitor of protein synthesis. The HR2 peptide was omitted from these cultures to enable cell-cell fusion. The cells were then fixed and processed for microscopy at 9 h p.i. Both in the presence and in the absence of CHX, the formation of syncytia could be observed, as was obvious by the appearance of multinucleated cells. In the absence of CHX, many multinucleated cells were observed that exhibited both green (nsp2-GFP) and red (nsp2-mCherry) fluorescent foci (Fig. 7E, top row). The large majority of these nsp2-GFP- and nsp2-mCherry-positive fluorescent foci were found to colocalize. In contrast, in the presence of CHX, when viral protein synthesis and formation of new RTCs was inhibited (49, 56, 70), no colocalizaton between nsp2-GFP- and nsp2-mCherry-positive structures was observed in multinucleated cells that were positive for both fusion proteins (Fig. 7E, bottom row). Apparently, while newly synthesized RTCs are able to recruit both fusion proteins, already existing RTCs are not able to exchange or to recruit fluorescent nsp2 fusion proteins. These results are consistent with the lack of fluorescence recovery after photobleaching of nsp2-positive structures and demonstrate that once formed, the replicative structures are static entities.

DISCUSSION

In this study, the dynamics of the coronavirus replicative structures was analyzed for the first time by performing live-cell imaging of coronavirus-infected cells in combination with FRAP analyses. Ideally, one may prefer to visualize these structures by using recombinant viruses expressing tagged versions of an nsp in the context of the replicase precursor proteins; however, such recombinants are currently not available. Therefore, we applied an alternative approach in which the replicative structures were visualized by the expression of fluorescently marked nsp2 proteins *in trans* in MHV-infected cells. Although this protein is dispensable in virus replication and the formation of the viral RTCs (24), this protein was more efficiently recruited to the RTCs than other nsps, at least when expressed *in trans* (data no shown). The tagged nsp2 proteins were found by immunofluorescence analyses to

colocalize with several RTC markers, such as nsp8, nsp4, and dsRNA. nsp8 was recently shown to contain RdRp activity and has been proposed to function as a primase (27) while nsp4 has a critical role in directing coronavirus RTC/DMV assembly (9). dsRNA molecules, which are readily detected in coronavirus-infected cells (49), are likely to represent replicative intermediates. Consistently, nsp2-GFP was shown by immuno-EM analysis to be efficiently recruited to the virus-induced DMVs and CMs in MHV-nsp2GFP-infected cells. Previously, newly synthesized viral RNA as well as (viral) dsRNA had been found to be associated with the DMVs (23, 35, 65) while all nsps studied to date have been localized to the DMVs and CMs (16, 24, 49, 51, 61). Taking all these observations together, we conclude that the expressed nsp2 fusion proteins are recruited to the coronavirus RTCs, which are anchored to DMVs. Importantly, this localization corresponds with the previously reported distribution of nsp2 (5, 21, 24, 62).

The nsp2 fusion proteins were associated with the cytoplasmic face of the DMVs/CMs. After selective permeabilization of the plasma membrane, antibodies directed against the GFP tag were able to detect the nsp2 fusion protein. Furthermore, the large majority of the membrane-associated nsp2 was sensitive to protease treatment in the absence of detergents. Apparently, no appreciable fraction of nsp2 was protected by the membranes, which indicates that this protein is not targeted into the lumen of the DMVs. In agreement with the association of nsp2 to the DMV external surface, nsp2-GFP could also be detected in the sections prepared for immuno-EM, in which the DMVs appeared as empty vesicles that lacked the inner membrane. Recently, van Hemert and coworkers (70) demonstrated that dsRNA, nsp5, and nsp8 present in partially purified severe acute respiratory syndrome (SARS)-CoV RTC preparations were protected by membranes from nuclease or protease treatment. Interestingly, however, this was not the case for the very large nsp3. Thus, it appears that some nsps (e.g., nsp5 and nsp8) are protected by membranes, e.g., by their localization inside the DMVs, while others are not (e.g., nsp2 and nsp3). This raises intriguing questions about the overall structure of the coronavirus RTCs and their association with cellular membranes.

As nsp2-GFP was recruited both to single DMVs and to DMV/CM assemblies but not to any other cytoplasmic structure, we conclude that the small, mobile nsp2-positive structures are likely to correspond to single DMVs while the large immobile nsp2-positive structures probably represent the DMV/CM assemblies. Correlative light-electron microscopy, in which live-cell imaging of fluorescently tagged proteins together with immunogold

labeling of ultrathin cryosections of the same cells is combined (71), will be required to unequivocally prove this point. As our results indicate that single DMVs are mobile but that the DMV/CM assemblies are not, one might speculate that newly formed DMVs are able to freely move around until they are "captured" by the DMV/CM assemblies.

The small nsp2-positive foci, supposedly corresponding to single DMVs, traffic through the cell in a microtubule-dependent fashion. Several lines of evidence support this conclusion. The fluorescent structures appeared to traffic on specific cellular tracks, displaying velocities and saltatory movements typical for microtubule-mediated transport (40), while such movements were not observed in the presence of nocodazole. Furthermore, when cells lacking a microtubular network were infected with MHV, the nsp2-positive structures did not accumulate in the perinuclear region of the cell but, rather, were scattered throughout the cytoplasm. Disruption of microtubule-mediated transport of DMVs, however, had no significant impact on coronavirus RNA replication. Trafficking of viral replication complexes along microtubule tracks has previously also been observed for other plus-strand RNA viruses, e.g., HCV (74), poliovirus (10, 19), and the double-stranded DNA vaccinia virus (57). Strikingly, also for these viruses replication was not affected or only modestly affected by the disruption of microtubules (6, 19, 59).

While the trafficking of viral replication complexes along microtubule tracks has been documented for several viruses, the dynamics of these structures has so far been reported in detail only for HCV (74) and vaccinia virus (59). Live-cell imaging of vaccinia virus RTCs demonstrated that only the small (early), and not the large (late), replication sites displayed microtubule motor-mediated motility (59). In the case of HCV, Wölk and coworkers used replicons harboring a GFP insertion in NS5A. Again, two distinct patterns of NS5A-GFP fluorescence were reported: (i) large structures which showed restricted motility and (ii) small structures which showed fast, saltatory movements over large distances. Interestingly, the NS5A-GFP-positive structures displayed a static internal architecture without detectable exchange of NS5A within or in between these structures, as determined by FRAP analyses. Although the experimental approach of this study differs from ours (i.e., the HCV NS5A is an essential replicase protein and was expressed in the context of the viral polyprotein), the dynamics of the HCV replicative structures show several remarkable similarities with those of MHV.

The large MHV DMV/CM assemblies very likely correspond to the recently reported reticulovesicular network of modified ER membranes that is connected to clusters of interconnected DMVs found in SARS-CoV-infected

cells (35). From this perspective, it is not surprising that these large assemblies of interconnected ER and DMVs are not able to traffic on microtubule tracks. Interestingly and similar to our observations, movement in HCV and vaccinia virus was observed for only the small RTC assemblies and not the large ones (59, 74). The fast saltatory movements of the small HCV fluorescent foci were shown to occur independently of ER dynamics (74). Whether this also holds true for MHV remains to be established. Despite the movement of the small nsp2-positive foci, the coronavirus replicative structures turn out to be inherently static entities. No recovery of fluorescence was observed when (part of) the nsp2-positive structures were photobleached. Apparently, the nsp2 protein, once recruited to the RTCs, is not exchanged by nsp2 protein occurring in the cytoplasm or at other DMVs. This result was confirmed by the observation that preexisting RTCs did not exchange fluorescence after fusion of cells expressing either a green or a red fluorescent nsp2. Our data thus indicate that recruitment of nsp2 occurs only during RTC assembly. Again, similar results were obtained for the HCV RTCs, which also displayed a lack of fluorescence recovery after photobleaching (74). We hypothesize that during RTC assembly, the coronavirus nsp2 is captured within an elaborate network of protein-protein interactions. Indeed, for the nsp2 of SARS-CoV, a large number of viral protein interaction partners have been identified including nsp2, nsp3, nsp6, nsp8, and nsp11 (50, 73). Other coronavirus nsps also appear to be contained in rigid protein-protein interaction networks (28, 50, 73; also unpublished results).

Our findings have important consequences for our understanding of RTC assembly and functioning. The lack of exchange of nsps present in different RTCs fits well with the model of RTC maturation/aging, as has been proposed for coronaviruses (56). In this model, the RNA synthesizing activity of the RTC changes in time, possibly by proteolytic turnover of the replicase polyprotein. Moreover, were nsps generally contained within static networks, complementation between different (e.g., temperature sensitive) viruses carrying a mutation in one of these nsps would have to occur during the formation of these networks at the time of RTC/DMV assembly and would not be possible once these replicative structures had been assembled.

So far, live-cell imaging of viral infections has been limited mainly to the processes of entry and release of viral particles (25, 42). Trafficking and the dynamics of viral replicative structures have received much less attention and for plus-strand RNA viruses have, so far, essentially been reported only for HCV (74) and MHV (this study). Considering that these viruses belong to different virus families (the *Coronaviridae* and the *Flaviviridae*, respectively),

the similarities observed between the two viruses are, at least in our opinion, quite remarkable. One feature is the occurrence of differently sized replicative structures, and we have now shown that the small but not the large ones traffic along microtubule tracks. Another, perhaps even more intriguing, feature is that in both cases structures appear to function as rigid entities. In view of the parallels observed between MHV and HCV, it is tempting to hypothesize that our findings reflect general features of the replication of plus-strand RNA viruses.

ACKNOWLEDGEMENTS

We thank Corlinda ten Brink from the Cell Microscopy Center, University Medical Centre Utrecht, for technical support and Matthijs Raaben and Mijke Vogels for stimulating discussions. We thank John Flemming, Susan Baker, and Mark Denison for kindly providing antibodies. This work was supported by grants from the Netherlands Organization for Scientific Research (NWO-VIDI and NWO-ALW) and the Utrecht University (High Potential) to C. A. M. de Haan and F. R. Reggiori. The funding source had no role in the study design, data collection, analysis, interpretation or writing of this article.

REFERENCES

1. Beaudouin, J., D. Gerlich, N. Daigle, R. Eils, and J. Ellenberg. 2002. Nuclear envelope breakdown proceeds by microtubule-induced tearing of the lamina. Cell 108:83-96.

2. Bhardwaj, K., L. Guarino, and C. C. Kao. 2004. The severe acute respiratory syndrome coronavirus Nsp15 protein is an endoribonuclease that prefers manganese as a cofactor. J. Virol. 78:12218-12224.

3. Bi, W., J. D. Pinon, S. Hughes, P. J. Bonilla, K. V. Holmes, S. R. Weiss, and J. L. Leibowitz. 1998. Localization of mouse hepatitis virus open reading frame 1A derived proteins. J. Neurovirol. 4:594-605.

4. Bosch, B. J., R. van der Zee, C. A. de Haan, and P. J. Rottier. 2003. The coronavirus spike protein is a class I virus fusion protein: structural and functional characterization of the fusion core complex. J. Virol. 77:8801-8811.

5. Bost, A. G., E. Prentice, and M. R. Denison. 2001. Mouse hepatitis virus replicase protein complexes are translocated to sites of M protein accumulation in the ERGIC at late times of infection. Virology 285:21-29.

6. Bost, A. G., D. Venable, L. Liu, and B. A. Heinz. 2003. Cytoskeletal requirements for hepatitis C virus (HCV) RNA synthesis in the HCV replicon cell culture system. J. Virol. 77:4401-4408.

7. Brockway, S. M., C. T. Clay, X. T. Lu, and M. R. Denison. 2003. Characterization of the expression, intracellular localization, and replication complex association of the putative mouse hepatitis virus RNA-dependent RNA polymerase. J. Virol. 77:10515-10527.

8. Brockway, S. M., and M. R. Denison. 2005. Mutagenesis of the murine hepatitis virus nsp1-coding region identifies residues important for protein processing, viral RNA synthesis, and viral replication. Virology 340:209-223.

9. Clementz, M. A., A. Kanjanahaluethai, T. E. O'Brien, and S. C. Baker. 2008. Mutation in murine coronavirus replication protein nsp4 alters assembly of double membrane vesicles. Virology 375:118-129.

10. Cui, Z. Q., Z. P. Zhang, X. E. Zhang, J. K. Wen, Y. F. Zhou, and W. H. Xie. 2005. Visualizing the dynamic behavior of poliovirus plus-strand RNA in living host cells. Nucleic Acids Res. 33:3245-3252.

11. Decroly, E., I. Imbert, B. Coutard, M. Bouvet, B. Selisko, K. Alvarez, A. E. Gorbalenya, E. J. Snijder, and B. Canard. 2008. Coronavirus nonstructural protein 16 is a cap-0 binding enzyme possessing (nucleoside-2'O)-methyltransferase activity. J. Virol. 82:8071-8084.

12. de Haan, C. A., B. J. Haijema, D. Boss, F. W. Heuts, and P. J. Rottier. 2005. Coronaviruses as vectors: stability of foreign gene expression. J. Virol. 79:12742-12751.

13. de Haan, C. A., P. S. Masters, X. Shen, S. Weiss, and P. J. Rottier. 2002. The group-specific murine coronavirus genes are not essential, but their deletion, by reverse genetics, is attenuating in the natural host. Virology 296:177-189.

14. de Haan, C. A., K. Stadler, G. J. Godeke, B. J. Bosch, and P. J. Rottier. 2004. Cleavage inhibition of the murine coronavirus spike protein by a furin-like enzyme affects cell-cell but not virus-cell fusion. J. Virol. 78:6048-6054.

15. de Haan, C. A., L. van Genne, J. N. Stoop, H. Volders, and P. J. Rottier. 2003. Coronaviruses as vectors: position dependence of foreign gene expression. J. Virol. 77:11312-11323.

16. Deming, D. J., R. L. Graham, M. R. Denison, and R. S. Baric. 2007. Processing of open reading frame 1a replicase proteins nsp7 to nsp10 in murine hepatitis virus strain A59 replication. J. Virol. 81:10280-10291.

17. Denison, M. R., P. W. Zoltick, S. A. Hughes, B. Giangreco, A. L. Olson, S. Perlman, J. L. Leibowitz, and S. R. Weiss. 1992. Intracellular processing of the N-terminal ORF 1a proteins of the coronavirus MHV-A59 requires multiple proteolytic events. Virology 189:274-284.

18. Eckerle, L. D., X. Lu, S. M. Sperry, L. Choi, and M. R. Denison. 2007. High fidelity of murine hepatitis virus replication is decreased in nsp14 exoribonuclease mutants. J. Virol. 81:12135-12144.

19. Egger, D., and K. Bienz. 2005. Intracellular location and translocation of silent and active poliovirus replication complexes. J. Gen. Virol. 86:707-718.

20. Egloff, M. P., F. Ferron, V. Campanacci, S. Longhi, C. Rancurel, H. Dutartre, E. J. Snijder, A. E. Gorbalenya, C. Cambillau, and B. Canard. 2004. The severe acute respiratory syndrome-coronavirus replicative protein nsp9 is a single-stranded RNA-binding subunit unique in the RNA virus world. Proc. Natl. Acad. Sci. U. S. A. 101:3792-3796.

21. Gadlage, M. J., R. L. Graham, and M. R. Denison. 2008. Murine coronaviruses encoding nsp2 at different genomic loci have altered replication, protein expression, and localization. J. Virol. 82:11964-11969.

22. Gorbalenya, A. E., L. Enjuanes, J. Ziebuhr, and E. J. Snijder. 2006. Nidovirales: evolving the largest RNA virus genome. Virus Res. 117:17-37.

23. Gosert, R., A. Kanjanahaluethai, D. Egger, K. Bienz, and S. C. Baker. 2002. RNA replication of mouse hepatitis virus takes place at double-membrane vesicles. J. Virol. 76:3697-3708.

24. Graham, R. L., A. C. Sims, S. M. Brockway, R. S. Baric, and M. R. Denison. 2005. The nsp2 replicase proteins of murine hepatitis virus and severe acute respiratory syndrome coronavirus are dispensable for viral replication. J. Virol. 79:13399-13411.

25. Greber, U. F., and M. Way. 2006. A superhighway to virus infection. Cell 124:741-754.

26. Harcourt, B. H., D. Jukneliene, A. Kanjanahaluethai, J. Bechill, K. M. Severson, C. M. Smith, P. A. Rota, and S. C. Baker. 2004. Identification of severe acute respiratory syndrome coronavirus replicase products and characterization of papain-like protease activity. J. Virol. 78:13600-13612.

27. Imbert, I., J. C. Guillemot, J. M. Bourhis, C. Bussetta, B. Coutard, M. P. Egloff, F. Ferron, A. E. Gorbalenya, and B. Canard. 2006. A second, non-canonical RNA-dependent RNA polymerase in SARS coronavirus. EMBO J. 25:4933-4942.

28. Imbert, I., E. J. Snijder, M. Dimitrova, J. C. Guillemot, P. Lecine, and B. Canard. 2008. The SARS-coronavirus PLnc domain of nsp3 as a replication/transcription scaffolding protein. Virus Res. 133:136-148.

29. Ivanov, K. A., T. Hertzig, M. Rozanov, S. Bayer, V. Thiel, A. E. Gorbalenya, and J. Ziebuhr. 2004. Major genetic marker of nidoviruses encodes a replicative endoribonuclease. Proc. Natl. Acad. Sci. U. S. A. 101:12694-12699.

30. Ivanov, K. A., V. Thiel, J. C. Dobbe, Y. van der Meer, E. J. Snijder, and J. Ziebuhr. 2004. Multiple enzymatic activities associated with severe acute respiratory syndrome coronavirus helicase. J. Virol. 78:5619-5632.

31. Joseph, J. S., K. S. Saikatendu, V. Subramanian, B. W. Neuman, A. Brooun, M. Griffith, K. Moy, M. K. Yadav, J. Velasquez, M. J. Buchmeier, R. C. Stevens, and P. Kuhn. 2006. Crystal structure of nonstructural protein 10 from the severe acute respiratory syndrome coronavirus reveals a novel fold with two zinc-binding motifs. J. Virol. 80:7894-7901.

32. Kamitani, W., K. Narayanan, C. Huang, K. Lokugamage, T. Ikegami, N. Ito, H. Kubo, and S. Makino. 2006. Severe acute respiratory syndrome coronavirus nsp1 protein suppresses host gene expression by promoting host mRNA degradation. Proc. Natl. Acad. Sci. U. S. A. 103:12885-12890.

33. Kang, H., K. Bhardwaj, Y. Li, S. Palaninathan, J. Sacchettini, L. Guarino, J. L. Leibowitz, and C. C. Kao. 2007. Biochemical and genetic analyses of murine hepatitis virus Nsp15 endoribonuclease. J. Virol. 81:13587-13597.

34. Kanjanahaluethai, A., Z. Chen, D. Jukneliene, and S. C. Baker. 2007. Membrane topology of murine coronavirus replicase nonstructural protein 3. Virology 361:391-401.

35. Knoops, K., M. Kikkert, S. H. Worm, J. C. Zevenhoven-Dobbe, Y. van der Meer, A. J. Koster, A. M. Mommaas, and E. J. Snijder. 2008. SARS-coronavirus replication is supported by a reticulovesicular network of modified endoplasmic reticulum. PLoS Biol. 6:e226.

36. Kuo, L., G. J. Godeke, M. J. Raamsman, P. S. Masters, and P. J. Rottier. 2000. Retargeting of coronavirus by substitution of the spike glycoprotein ectodomain: crossing the host cell species barrier. J. Virol. 74:1393-1406.

37. Lippincott-Schwartz, J., E. Snapp, and A. Kenworthy. 2001. Studying protein dynamics in living cells. Nat. Rev. Mol. Cell Biol. 2:444-456.

38. Locker, J. K., J. K. Rose, M. C. Horzinek, and P. J. Rottier. 1992. Membrane assembly of the triple-spanning coronavirus M protein. Individual transmembrane domains show preferred orientation. J. Biol. Chem. 267:21911-21918.

39. Lu, X. T., A. C. Sims, and M. R. Denison. 1998. Mouse hepatitis virus 3C-like protease cleaves a 22-kilodalton protein from the open reading frame 1a polyprotein in virus-infected cells and in vitro. J. Virol. 72:2265-2271.

40. Ma, S., and R. L. Chisholm. 2002. Cytoplasmic dynein-associated structures move bidirectionally in vivo. J. Cell Sci. 115:1453-1460.

41. Mackenzie, J. 2005. Wrapping things up about virus RNA replication. Traffic 6:967-977.

42. Marsh, M., and A. Helenius. 2006. Virus entry: open sesame. Cell 124:729-740.

43. Matthes, N., J. R. Mesters, B. Coutard, B. Canard, E. J. Snijder, R. Moll, and R. Hilgenfeld. 2006. The non-structural protein Nsp10 of mouse hepatitis virus binds zinc ions and nucleic acids. FEBS Lett. 580:4143-4149.

44. Miller, S., and J. Krijnse-Locker. 2008. Modification of intracellular membrane structures for virus replication. Nat. Rev. Microbiol. 6:363-374.

45. Minskaia, E., T. Hertzig, A. E. Gorbalenya, V. Campanacci, C. Cambillau, B. Canard, and J. Ziebuhr. 2006. Discovery of an RNA virus 3'→5' exoribonuclease that is critically involved in coronavirus RNA synthesis. Proc. Natl. Acad. Sci. U. S. A. 103:5108-5113.

46. Namy, O., S. J. Moran, D. I. Stuart, R. J. Gilbert, and I. Brierley. 2006. A mechanical explanation of RNA pseudoknot function in programmed ribosomal frameshifting. Nature 441:244-247.

47. Narayanan, K., C. Huang, K. Lokugamage, W. Kamitani, T. Ikegami, C. T. Tseng, and S. Makino. 2008. Severe acute respiratory syndrome coronavirus nsp1 suppresses host gene expression, including that of type I interferon, in infected cells. J. Virol. 82:4471-4479.

48. Oostra, M., M. C. Hagemeijer, M. van Gent, C. P. Bekker, E. G. te Lintelo, P. J. Rottier, and C. A. de Haan. 2008. Topology and membrane anchoring of the coronavirus replication complex: not all hydrophobic domains of nsp3 and nsp6 are membrane spanning. J. Virol. 82:12392-12405.

49. Oostra, M., E. G. te Lintelo, M. Deijs, M. H. Verheije, P. J. Rottier, and C. A. de Haan. 2007. Localization and membrane topology of coronavirus nonstructural protein 4: involvement of the early secretory pathway in replication. J. Virol. 81:12323-12336.

50. Pan, J., X. Peng, Y. Gao, Z. Li, X. Lu, Y. Chen, M. Ishaq, D. Liu, M. L. Dediego, L. Enjuanes, and D. Guo. 2008. Genome-wide analysis of protein-protein interactions and involvement of viral proteins in SARS-CoV replication. PLoS One 3:e3299.

51. Prentice, E., J. McAuliffe, X. Lu, K. Subbarao, and M. R. Denison. 2004. Identification and characterization of severe acute respiratory syndrome coronavirus replicase proteins. J. Virol. 78:9977-9986.

52. Raaben, M., A. W. Einerhand, L. J. Taminiau, M. van Houdt, J. Bouma, R. H. Raatgeep, H. A. Buller, C. A. de Haan, and J. W. Rossen. 2007. Cyclooxygenase activity is important for efficient replication of mouse hepatitis virus at an early stage of infection. Virol. J. 4:55.

53. Rottier, P. J., G. W. Welling, S. Welling-Wester, H. G. Niesters, J. A. Lenstra, and B. A. Van der Zeijst. 1986. Predicted membrane topology of the coronavirus protein E1. Biochemistry 25:1335-1339.

54. Salonen, A., T. Ahola, and L. Kaariainen. 2005. Viral RNA replication in association with cellular membranes. Curr. Top. Microbiol. Immunol. 285:139-173.

55. Sawicki, S. G., D. L. Sawicki, and S. G. Siddell. 2007. A contemporary view of coronavirus transcription. J. Virol. 81:20-29.

56. Sawicki, S. G., D. L. Sawicki, D. Younker, Y. Meyer, V. Thiel, H. Stokes, and S. G. Siddell. 2005. Functional and genetic analysis of coronavirus replicase-transcriptase proteins. PLoS Pathog. 1:e39.

57. Schepis, A., B. Schramm, C. A. de Haan, and J. K. Locker. 2006. Vaccinia virus-induced microtubule-dependent cellular rearrangements. Traffic 7:308-323.

58. Schonborn, J., J. Oberstrass, E. Breyel, J. Tittgen, J. Schumacher, and N. Lukacs. 1991. Monoclonal antibodies to double-stranded RNA as probes of RNA structure in crude nucleic acid extracts. Nucleic Acids Res. 19:2993-3000.

59. Schramm, B., C. A. de Haan, J. Young, L. Doglio, S. Schleich, C. Reese, A. V. Popov, W. Steffen, T. Schroer, and J. K. Locker. 2006. Vaccinia-virus-induced cellular contractility facilitates the subcellular localization of the viral replication sites. Traffic 7:1352-1367.

60. Seybert, A., C. C. Posthuma, L. C. van Dinten, E. J. Snijder, A. E. Gorbalenya, and J. Ziebuhr. 2005. A complex zinc finger controls the enzymatic activities of nidovirus helicases. J. Virol. 79:696-704.

61. Shi, S. T., J. J. Schiller, A. Kanjanahaluethai, S. C. Baker, J. W. Oh, and M. M. Lai. 1999. Colocalization and membrane association of murine hepatitis virus gene 1 products and De novo-synthesized viral RNA in infected cells. J. Virol. 73:5957-5969.

62. Sims, A. C., J. Ostermann, and M. R. Denison. 2000. Mouse hepatitis virus replicase proteins associate with two distinct populations of intracellular membranes. J. Virol. 74:5647-5654.

63. Slot, J. W., and H. J. Geuze. 2007. Cryosectioning and immunolabeling. Nat. Protoc. 2:2480-2491.

64. Snijder, E. J., P. J. Bredenbeek, J. C. Dobbe, V. Thiel, J. Ziebuhr, L. L. Poon, Y. Guan, M. Rozanov, W. J. Spaan, and A. E. Gorbalenya. 2003. Unique and conserved features of genome and proteome of SARS-coronavirus, an early split-off from the coronavirus group 2 lineage. J. Mol. Biol. 331:991-1004.

65. Snijder, E. J., Y. van der Meer, J. Zevenhoven-Dobbe, J. J. Onderwater, J. van der Meulen, H. K. Koerten, and A. M. Mommaas. 2006. Ultrastructure and origin of membrane vesicles associated with the severe acute respiratory syndrome coronavirus replication complex. J. Virol. 80:5927-5940.

66. Sparks, J. S., E. F. Donaldson, X. Lu, R. S. Baric, and M. R. Denison. 2008. A novel mutation in murine hepatitis virus nsp5, the viral 3C-like proteinase, causes temperature-sensitive defects in viral growth and protein processing. J. Virol. 82:5999-6008.

67. Sutton, G., E. Fry, L. Carter, S. Sainsbury, T. Walter, J. Nettleship, N. Berrow, R. Owens, R. Gilbert, A. Davidson, S. Siddell, L. L. Poon, J. Diprose, D. Alderton, M. Walsh, J. M. Grimes, and D. I. Stuart. 2004. The nsp9 replicase protein of SARS-coronavirus, structure and functional insights. Structure 12:341-353.

68. Taguchi, F., and J. O. Fleming. 1989. Comparison of six different murine coronavirus JHM variants by monoclonal antibodies against the E2 glycoprotein. Virology 169:233-235.

69. Thiel, V., K. A. Ivanov, A. Putics, T. Hertzig, B. Schelle, S. Bayer, B. Weissbrich, E. J. Snijder, H. Rabenau, H. W. Doerr, A. E. Gorbalenya, and J. Ziebuhr. 2003. Mechanisms and enzymes involved in SARS coronavirus genome expression. J. Gen. Virol. 84:2305-2315.

70. van Hemert, M. J., S. H. van den Worm, K. Knoops, A. M. Mommaas, A. E. Gorbalenya, and E. J. Snijder. 2008. SARS-coronavirus replication/transcription complexes are membrane-protected and need a host factor for activity in vitro. PLoS Pathog. 4:e1000054.

71. van Rijnsoever, C., V. Oorschot, and J. Klumperman. 2008. Correlative light-electron microscopy (CLEM) combining live-cell imaging and immunolabeling of ultrathin cryosections. Nat. Methods 5:973-980.

72. Verheije, M. H., M. Raaben, M. Mari, E. G. Te Lintelo, F. Reggiori, F. J. van Kuppeveld, P. J. Rottier, and C. A. de Haan. 2008. Mouse hepatitis coronavirus RNA replication depends on GBF1-mediated ARF1 activation. PLoS Pathog. 4:e1000088.

73. von Brunn, A., C. Teepe, J. C. Simpson, R. Pepperkok, C. C. Friedel, R. Zimmer, R. Roberts, R. Baric, and J. Haas. 2007. Analysis of intraviral protein-protein interactions of the SARS coronavirus ORFeome. PLoS One 2:e459.

74. Wolk, B., B. Buchele, D. Moradpour, and C. M. Rice. 2008. A dynamic view of hepatitis C virus replication complexes. J. Virol. 82:10519-10531.

75. Wurdinger, T., M. H. Verheije, M. Raaben, B. J. Bosch, C. A. de Haan, V. W. van Beusechem, P. J. Rottier, and W. R. Gerritsen. 2005. Targeting non-human coronaviruses to human cancer cells using a bispecific single-chain antibody. Gene Ther. 12:1394-1404.

76. Zhai, Y., F. Sun, X. Li, H. Pang, X. Xu, M. Bartlam, and Z. Rao. 2005. Insights into SARS-CoV transcription and replication from the structure of the nsp7-nsp8 hexadecamer. Nat. Struct. Mol. Biol. 12:980-986.

77. Ziebuhr, J., E. J. Snijder, and A. E. Gorbalenya. 2000. Virus-encoded proteinases and proteolytic processing in the Nidovirales. J. Gen. Virol. 81:853-879.

78. Zust, R., L. Cervantes-Barragan, T. Kuri, G. Blakqori, F. Weber, B. Ludewig, and V. Thiel. 2007. Coronavirus non-structural protein 1 is a major pathogenicity factor: implications for the rational design of coronavirus vaccines. PLoS Pathog. 3:e109.

Chapter 4

The Coronavirus Nucleocapsid Protein Is Dynamically Associated with the Replication-Transcription Complexes

Monique H. Verheije[1*], **Marne C. Hagemeijer**[1*], Mustafa Ulasli[2], Fulvio Reggiori[2], Peter J. M. Rottier[1], Paul S. Masters[3], and Cornelis A. M. de Haan[1]

Virology Division, Department of Infectious Diseases and Immunology, Faculty of Veterinary Medicine, Utrecht University, Utrecht, the Netherlands[1], Department of Cell Biology and Institute of Biomembranes, University Medical Centre Utrecht, Utrecht, the Netherlands[2], and David Axelrod Institute, Wadsworth Center, New York State Department of Health, Albanay, New York[3]

Journal of Virology, Nov. 2010, p. 11575–11579 Vol. 84, No. 21

* equal contribution

Supplemental material can be found at http://jvi.asm.org/

ABSTRACT

The coronavirus nucleocapsid (N) protein is a virion structural protein. It also functions, however, in an unknown way in viral replication and localizes to the viral replication-transcription complexes (RTCs). Here we investigated, using recombinant murine coronaviruses expressing green fluorescent protein (GFP)-tagged versions of the N protein, the dynamics of its interactions with the RTCs and the domain(s) involved. Using fluorescent recovery after photobleaching, we showed that the N protein, unlike the nonstructural protein 2, is dynamically associated with the RTCs. Recruitment of the N protein to the RTCs requires the C-terminal N2b domain, which interacts with other N proteins in an RNA-independent manner.

All positive-strand RNA viruses assemble their replication complexes in association with intracellular membranes. Coronaviruses, enveloped plus-strand RNA viruses, induce in infected cells the formation of double-membrane vesicles (DMVs) and convoluted membranes (CMs). These structures harbor the nonstructural proteins (nsps) (9, 14, 25, 26, 28) and are associated with viral RNA synthesis (1, 9, 20, 22). The nsps, which jointly form the replication-transcription complexes (RTCs), presumably mediate the formation of these membranous structures by modifying endoplasmic reticulum-derived membranes and by recruiting cellular components to their need.

In addition to the nsps, coronaviruses express several structural proteins, including at least the spike (S), envelope (E), membrane (M), and nucleocapsid (N) proteins (6). The N protein packages the viral genomic RNA to form the helical nucleocapsid that is incorporated into the budding particle but also fulfills additional roles during the viral infection. It has been shown to function as an RNA chaperone (33) and to facilitate viral RNA synthesis (2, 5, 16). Not surprisingly, the N protein localizes to DMVs and CMs, the sites where the RTCs are concentrated, in addition to the virion assembly sites (3, 7, 23, 28, 29). Furthermore, the nucleocapsid protein contributes to the perturbation of several host cellular processes [reviewed in reference (27)].

Recently, we demonstrated that nsp2, once recruited to the RTCs, is not exchanged for nsp2 molecules present in the cytoplasm and in other DMVs/CMs. That is, no recovery of fluorescence was observed when (part of) the nsp2-positive foci were photobleached (10). Whether the other nsps or the N protein pool associated with the RTCs also lacks mobility at these sites remains unknown. Of particular interest are the dynamics of the N protein, as it is involved in different, spatially and temporally separated steps of the viral life cycle. We hypothesized that the N protein is not permanently bound to the RTCs but rather possesses a manifest intracellular mobility, as it is probably not involved only in viral RNA synthesis but also in its transport from the site of synthesis to the virion assembly sites, where it participates in virion assembly.

To test our hypothesis, we studied the dynamics of the N protein localized at the RTCs by live-cell imaging. To this end, we generated a recombinant mouse hepatitis coronavirus (MHV) expressing an additional copy of the N protein C terminally fused to green fluorescent protein (N-GFP). The coding sequence for N-GFP was introduced into the viral genome as an additional

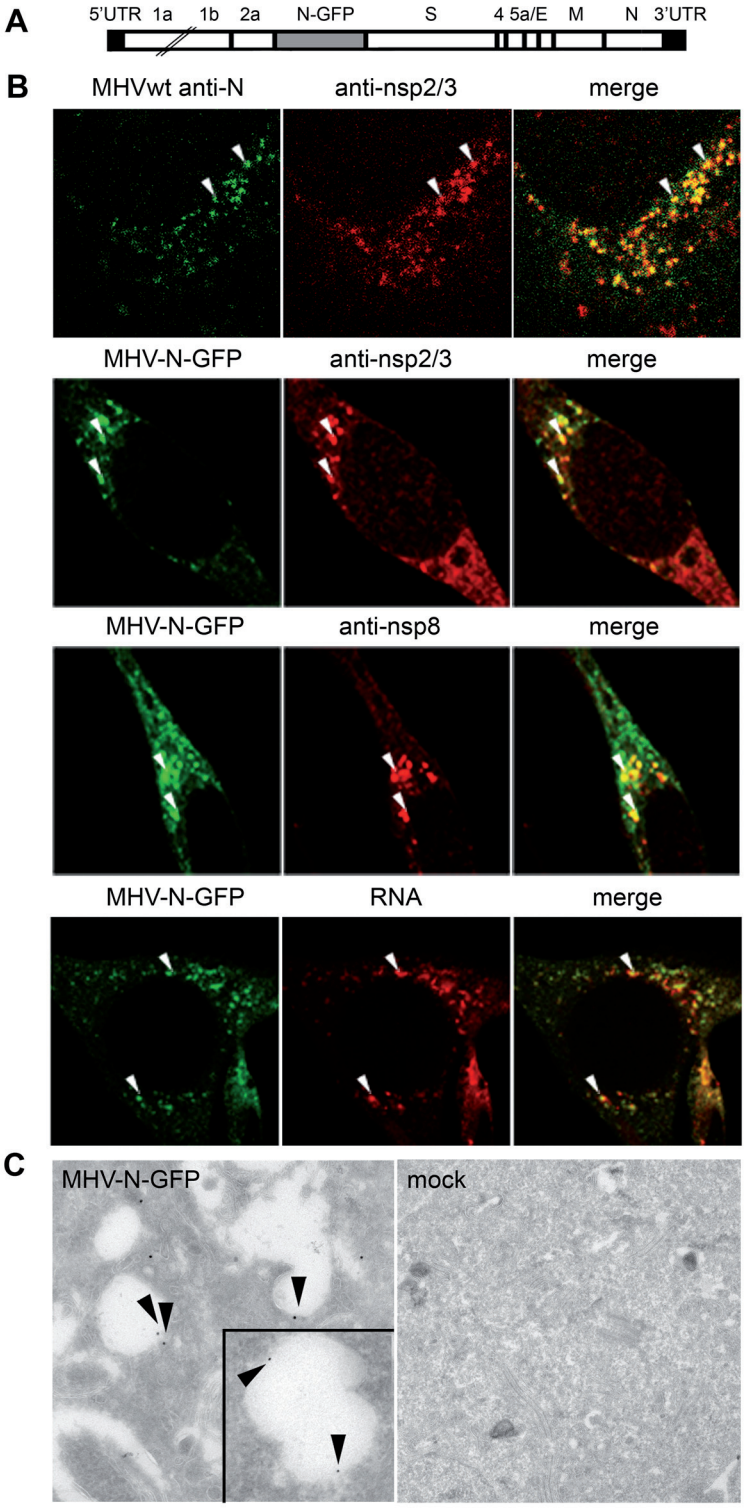
A
5'UTR 1a 1b 2a N-GFP S 4 5a/E M N 3'UTR
B
MHVwt anti-N
anti-nsp2/3
merge
MHV-N-GFP
anti-nsp2/3
merge
MHV-N-GFP
anti-nsp8
merge
MHV-N-GFP
RNA
merge
C
MHV-N-GFP
mock

Figure 1. Recruitment and localization of the N protein to the RTCs and DMVs. (A) Schematic outline of the MHV-N-GFP recombinant virus (not drawn to scale). UTR, untranslated region. (B) LR7 cells inoculated with MHV or MHV-N-GFP were fixed at 6 h p.i. and stained with antibodies directed against nsp2/3 (D4 [24]; kind gift of S. Baker) or nsp8 (anti-p22 antibody [15]; kind gift of M. Denison). Production of newly synthesized viral RNA was visualized by using Click-It detection of RNA. To this end, infected cells were fed with 5-ethynyl uridine from 5.5 to 6.5 h p.i., after which the cells were fixed. (C) HeLa-CEACAM1a cells infected with MHV-N-GFP and control cells (mock) were fixed at 6 h p.i. and processed for immunoelectron microscopy using antibodies against GFP. Arrowheads indicate colocalization sites between N-GFP and either RTC protein markers (B) or DMVs (C).

expression cassette between genes 2a and S by targeted RNA recombination as previously described (18), thereby replacing the nonfunctional hemagglutinin-esterase gene (Fig. 1A). The resulting recombinant virus, MHV–N-GFP, was viable; however, it was rapidly outcompeted by viruses that had lost expression of the N fusion protein. As we were unable to demonstrate incorporation of N-GFP into progeny virions, we speculated that the fusion protein acts as a dominant negative during virion assembly. Of passage 2, approximately 10 to 20% of the virus population expressed detectable levels of N-GFP (data not shown), which was sufficient for our experimental goal.

To determine whether the N-GFP fusion protein, when expressed from the viral genome, was recruited to the RTCs, LR7 cells were inoculated with MHV–N-GFP, fixed at 6 h post infection (p.i.), and subsequently processed for immunofluorescence analysis. The results show that the N-GFP was present throughout the cytoplasm at a low level and was concentrated in cytoplasmic foci that were colocalizing with the RTC protein markers nsp2/3 (antibody D4) and nsp8 (anti-p22 antibody). Similar colocalization of the N protein with nsp2/3 was observed in cells infected with wild-type MHV (Fig. 1B). To confirm the recruitment of N-GFP to the sites of viral RNA synthesis, we also studied the colocalization of N-GFP with newly synthesized viral RNA, using the Click-iT RNA detection assay (Invitrogen). Essentially all N-GFP-positive foci were also positive for newly synthesized viral RNA. Subsequently, immunoelectron microscopy was performed on MHV–N-GFP-infected cells, with the GFP tag labeled as described before (10). Although only few gold particles per cell could be detected, the profiles clearly show that N-GFP localized to the DMVs (Fig. 1C), which appeared here as empty vesicles as observed before when using the same immunoelectron microscopy procedure (10, 28), as well as to the CMs (data not shown). All together, these results show that the N-GFP fusion proteins, when expressed from the viral genome, are recruited to the coronavirus replicative structures, which are corresponding with the active RTCs, similarly to the nontagged N protein (28).

To study the dynamics of the N protein association with the RTCs, we performed fluorescence recovery after photobleaching (FRAP) analysis of MHV–N-GFP-infected LR7 cells. At 6 h p.i., specific regions of interest (ROI) that contained one N-GFP-positive structure were irreversibly photobleached and recovery rates were determined as previously described (10). The photobleached N-GFP-positive structures had a reduction in signals to about 35% of that of the prebleached structures (Fig. 2A and D; see also Movie S1A in the supplemental material). Within 60 s, the signal at the ROI recovered to 60% of the original signal intensity, indicating an exchange of N-GFP with its surrounding environment. Recovery after photobleaching was also observed when N-GFP was expressed from a plasmid transfected into cells prior to infection with wild-type MHV (Fig. 2B and D; see also Movie S1B in the supplemental material). However, the mobility fraction (Mf) of N-GFP-positive foci in these cells was higher (Mf = 63%) than

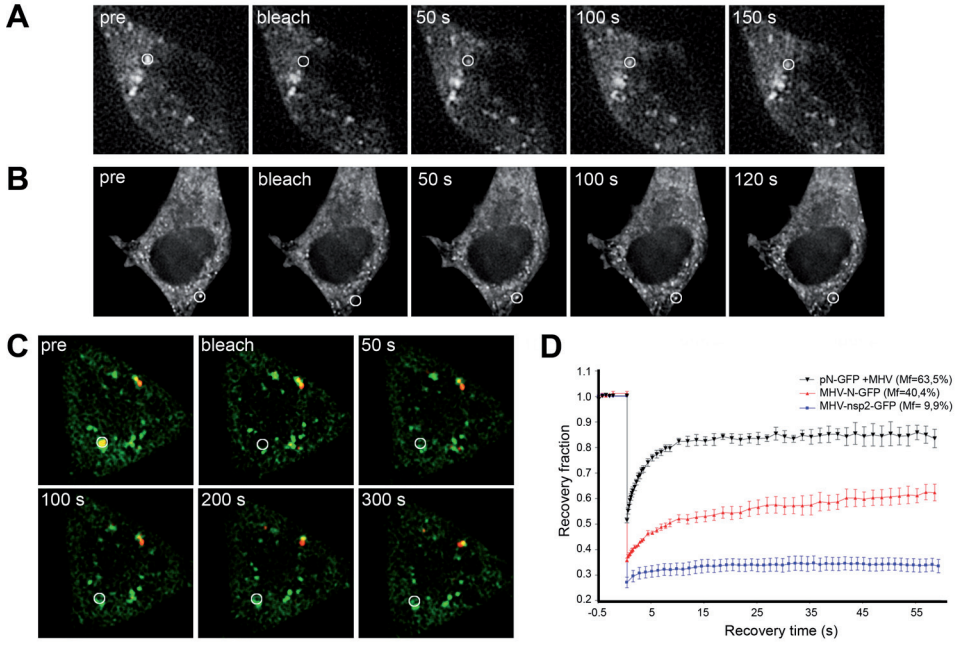

Figure 2. Recovery of nucleocapsid protein N on DMVs after photobleaching. (A to C) FRAP was performed using the quantifiable laser module of the DeltaVision Core (API) at 6 h p.i. on LR7 cells infected with MHV-N-GFP (A), transfected with the N-GFP plasmid and subsequently infected with MHV-A59 (B), or cotransfected with pN-GFP (green) and pnsp2-mCherry (red) expression vectors and subsequently infected with MHV-A59 (C). Representative-experiment snapshots with the ROI indicated by white circles are depicted. (D) Fluorescence recovery graphs for photobleached ROIs from panels A (n = 5) and B (n = 4) are shown and compared with identically generated graphs for MHV-nsp2-GFP (n = 10) from a different study (10). Mf, mobile fraction, defined as the percentage of fluorescence recovery at the bleached site.

that of N-GFP in MHV–N-GFP-infected cells (Mf = 40%) (Fig. 2D). This might be attributed to the higher N-GFP expression levels in the transfected cells (compare Fig. 2A and B) (also data not shown). Although we previously did not observe any recovery of the nsp2-GFP signal in FRAP experiments (10) (Fig. 2D), we decided to simultaneously compare the recovery rates of N with those of nsp2 in the same cell. To this end, we cotransfected cells with plasmids expressing N-GFP and nsp2-mCherry (10) before infecting them with MHV. After subsequent infection with MHV, the N-GFP and nsp2-mCherry localized to partly overlapping cytoplasmic foci. Again, recovery of the N protein signal, but not that of nsp2, was detected after photobleaching (Fig. 2C; see also Movie S1C in the supplemental material), although the recovery of the N protein appeared to be less efficient than that in nsp2-mCherry-negative cells (Fig. 2B). This difference might be caused by differences in expression level. Alternatively, overexpression of nsp2 might affect the recovery of N-GFP, for instance, by yet-unrevealed protein-protein interactions. In conclusion, at 6 to 7 h p.i., the nsp2 and N protein present at the RTCs display different motilities, with the nsp2 being much less mobile in the cell than the N protein. It will be interesting to analyze the motility of the N protein at other time points of the infection cycle as well.

Next, we elucidated which part of the N protein is required for its dynamic recruitment to the RTCs. We made use of the recently described set of recombinant MHVs (12), each expressing, in addition to the full-length N protein, one of the following N-terminally GFP-tagged N segments: N1a (amino terminus), N1b (corresponding to the previously designated N-terminal domain [NTD]), N2a (region linking N1b and N2b), N2b (corresponding to the previously designated C terminal domain [CTD]), and NBd3 (carboxyl terminus) (Fig.3A) [see references in reference (12)]. We infected cells with these recombinant MHVs and analyzed at 6 h p.i. the recruitment of GFP-N domains to the RTCs after immunostaining them with antibodies directed against nsp8 (Fig. 3B). None of the N protein segments, with the exception of GFP-N2b (Fig. 3B), was efficiently recruited to the RTCs. As a result, the N2b domain probably contains the information required for recruitment of the N protein to the RTCs, at least in the presence of a full-length N protein. To a minor extent, some colocalization of GFP-N2a with nsp8 was also observed, which is in agreement with this domain interacting with nsp3 (12a). Importantly, the FRAP experiments showed that the dynamic association/dissociation of GFP-N2b with the RTCs was similar to that of the full-length N-GFP (data not shown). Interestingly, all of the N protein segments except N2b also localized to the nucleus. Also, the full-length

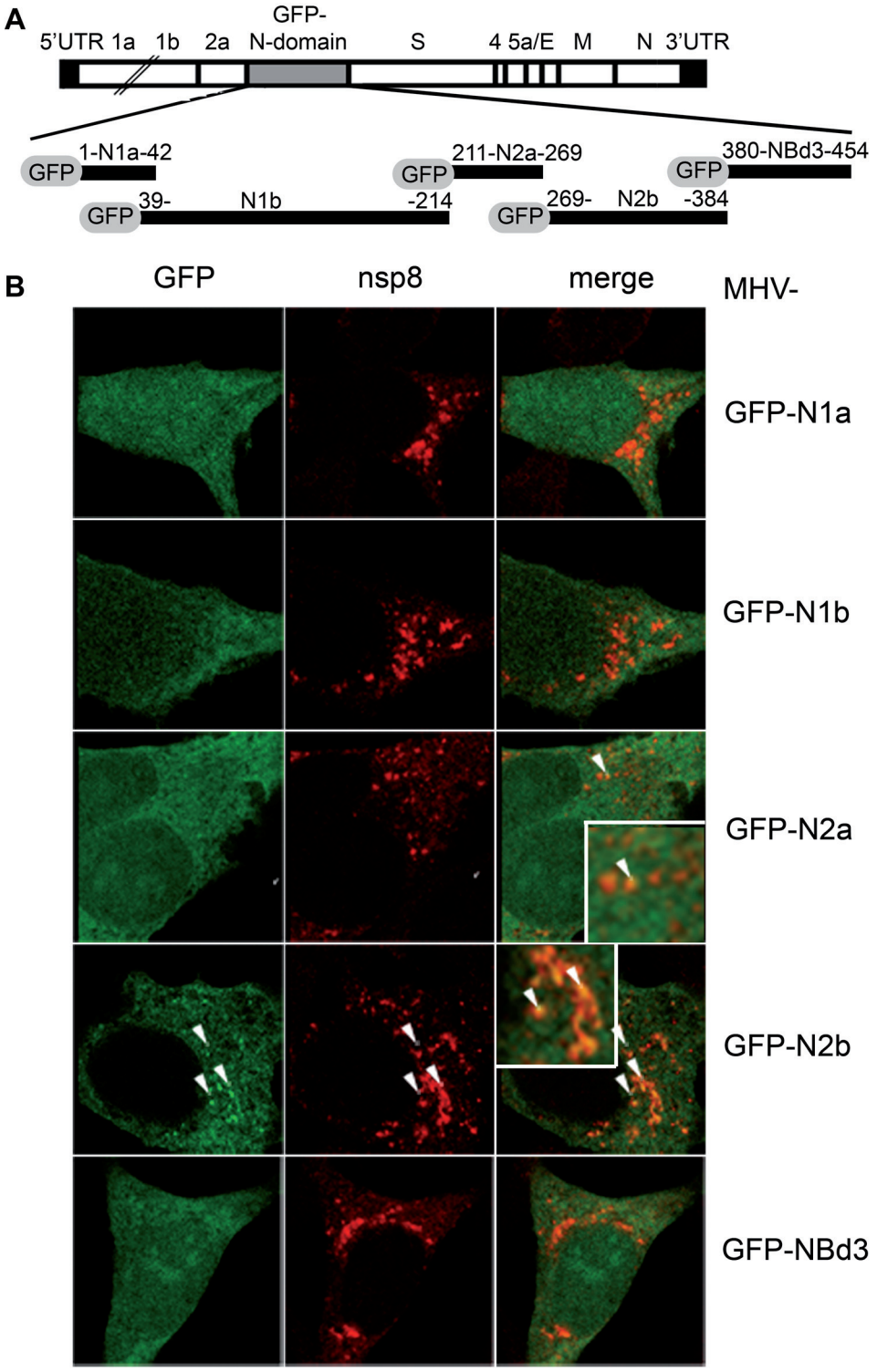
A
GFP-
5'UTR 1a 1b 2a N-domain S 4 5a/E M N 3'UTR
GFP 1-N1a-42
GFP 211-N2a-269
GFP 380-NBd3-454
GFP 39- N1b -214
GFP 269- N2b -384
B
GFP
nsp8
merge
MHV-
GFP-N1a
GFP-N1b
GFP-N2a
GFP-N2b
GFP-NBd3

Figure 3. Role of N domains in RTC recruitment. (A) Schematic outline of the MHV-GFP-N domain recombinant viruses (not drawn to scale). (B) LR7 cells infected with MHV-GFP-N domain viruses were fixed and processed for immunofluorescence at 6 h p.i. using the RTC protein marker nsp8. Examples of GFP-N2a and -N2b-positive foci colocalizing with nsp8 are indicated by arrowheads.

protein hardly localized to the nucleus (Fig. 1B). The biological significance of these observations is not clear at present.

The N2b segment has been demonstrated to be involved in both N protein self-interaction and binding to the RNA [see references in reference (12)]. To determine which of these two interactions is essential for the recruitment of the N2b fragment to the RTCs, we performed coimmunoprecipitation experiments. To this end, cells infected with the different recombinant MHVs were metabolically labeled as previously described (10) from 5 h to 7 h p.i. Subsequently, cell lysates were prepared and immunoprecipitations were performed essentially as described previously (31) either in the presence or absence of the anti-GFP antibody (Fig. 4A). When immuno-precipitations were performed in the absence of the anti-GFP antibody, very low levels of full-length N protein were detected, likely due to the nonspecific binding to protein A Sepharose. In the presence of anti-GFP antibody, protein bands corresponding to the different fusion proteins were observed. Importantly, wild-type, nontagged N protein was efficiently coimmunoprecipitated in cells infected with viruses expressing N-GFP, GFP-N1b, or GFP-N2b (Fig. 4A). Since GFP-N2b, but not GFP-N1b, was recruited to the RTCs (Fig. 3B), we subsequently investigated whether these interactions were dependent on the presence of viral RNA. To this end, the immunoprecipitates were treated with RNase A (17). As expected, the interaction between wild-type N protein and full-length N-GFP protein was lost after RNase A treatment (Fig. 4B) (17). The same result was obtained for the GFP-N1b protein, whereas for the GFP-N2b protein, the interaction with N was maintained after RNase A incubation (Fig. 4B).

In this study, we show that the N protein, in contrast to nsp2 (10), is dynamically associated with the RTCs. The dynamics of other proteins present at the RTCs have not yet been evaluated. Whereas nsp2 may be immobilized within an elaborate network of protein-protein interactions (10, 19, 30), this is apparently not the case for the N protein. We hypothesize that the difference in mobility between nsp2 and N likely reflects their different functions in the viral life cycle. Although the function of nsp2 at the RTC is not known, the N protein is a multifunctional protein that facilitates RNA synthesis but also plays an essential role in virus assembly and is presumably involved in facilitating the transport of the viral genome from its location of

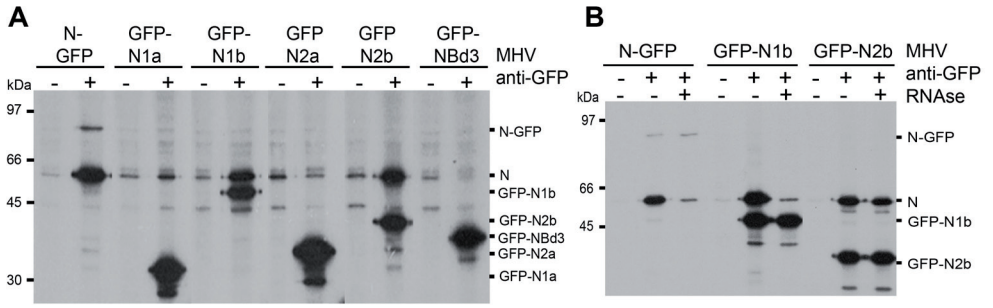

Figure 4. Intracellular N-N interactions and their RNA dependency. LR7 cells were infected with MHV-GFP-N domain viruses and radioactively labeled from 5 h to 7 h p.i. before cell lysates were prepared. (A and B) Immunoprecipitations were performed in the absence (–) or presence (+) of GFP antibody (Immunology Consultants Laboratory, Inc.). Where indicated in panel B, the immunoprecipitates were treated with protease-free RNase A (Fermentas GmbH, St. Leon-Rot, Germany) and extensively washed prior to SDS-PAGE analysis. Of note, in the second lane in panels A and B, the small amount of coprecipitated N-GFP compared to that of nontagged N protein is likely due to only 10 to 20% of the MHV-N-GFP stock expressing N-GFP.

synthesis to the virion assembly sites. The dynamic nature of the N protein at the RTCs may be a prerequisite for the N protein to exert and coordinate its diverse functions.

The N2b domain appeared to be required for N protein recruitment to the RTCs and was furthermore engaged in RNA-independent N-N interactions. The latter observation is consistent with previous studies that showed the importance of the CTD domain in N protein self-interactions (4, 8, 11, 13, 21, 32). Conceivably, GFP-N2b is recruited to the RTCs by binding a wild-type N protein molecule. We can, however, not rule out that its association with the DMVs is mediated by another RTC component. Strikingly, in contrast to N1b and NBd3, the N2b domain hardly appeared to be incorporated into progeny virions (12). This was ascribed to its presumed inability to compete with full-length N monomers as the nucleocapsid condenses to be incorporated into the budding virion. Another explanation might be that RNA binding is an essential requirement for incorporation of N into virions, a feature the N2b did not seem to possess (12). Apparently, different N protein requirements exist with respect to its recruitment to the RTCs (this study) and its incorporation into virus particles (12). Differences in protein behavior are also observed between GFP-N2b and N-GFP. While the full-length N-GFP protein was efficiently recruited to the RTCs, more so than with GFP-N2b (compare Fig. 1B and 3B), its interaction with wild-type N protein was largely sensitive to RNase A treatment in the same manner as was GFP-N1b, which was not recruited to the RTCs. We speculate that while protein-protein interactions

between N molecules are required for RTC recruitment, these interactions are somehow additionally influenced or converted by the presence of other N protein domains, for example, via N-RNA interactions.

ACKNOWLEDGEMENTS

We thank Corlinda ten Brink (Department of Cell Biology and the Cell Microscopy Center, University Medical Centre Utrecht) and Colleen O'Hare (Applied Precision, Inc.) for technical support. We thank Susan Baker and Mark Denison for providing antibodies. This work was supported by grants from the Netherlands Organization for Scientific Research (NWO-VIDI) and the Utrecht University (High Potential) to C. A. M. de Haan and F. Reggiori.

REFERENCES

1. Ahlquist, P., A. O. Noueiry, W. M. Lee, D. B. Kushner, and B. T. Dye. 2003. Host factors in positive-strand RNA virus genome replication. J. Virol. 77:8181-8186.

2. Baric, R. S., G. W. Nelson, J. O. Fleming, R. J. Deans, J. G. Keck, N. Casteel, and S. A. Stohlman. 1988. Interactions between coronavirus nucleocapsid protein and viral RNAs: implications for viral transcription. J. Virol. 62:4280-4287.

3. Bost, A. G., R. H. Carnahan, X. T. Lu, and M. R. Denison. 2000. Four proteins processed from the replicase gene polyprotein of mouse hepatitis virus colocalize in the cell periphery and adjacent to sites of virion assembly. J. Virol. 74:3379-3387.

4. Chang, C. K., S. C. Sue, T. H. Yu, C. M. Hsieh, C. K. Tsai, Y. C. Chiang, S. J. Lee, H. H. Hsiao, W. J. Wu, W. L. Chang, C. H. Lin, and T. H. Huang. 2006. Modular organization of SARS coronavirus nucleocapsid protein. J. Biomed. Sci. 13:59-72.

5. Compton, S. R., D. B. Rogers, K. V. Holmes, D. Fertsch, J. Remenick, and J. J. McGowan. 1987. In vitro replication of mouse hepatitis virus strain A59. J. Virol. 61:1814-1820.

6. de Haan, C. A., and P. J. Rottier. 2005. Molecular interactions in the assembly of coronaviruses. Adv. Virus Res. 64:165-230.

7. Denison, M. R., W. J. Spaan, Y. van der Meer, C. A. Gibson, A. C. Sims, E. Prentice, and X. T. Lu. 1999. The putative helicase of the coronavirus mouse hepatitis virus is processed from the replicase gene polyprotein and localizes in complexes that are active in viral RNA synthesis. J. Virol. 73:6862-6871.

8. Fan, H., A. Ooi, Y. W. Tan, S. Wang, S. Fang, D. X. Liu, and J. Lescar. 2005. The nucleocapsid protein of coronavirus infectious bronchitis virus: crystal structure of its N-terminal domain and multimerization properties. Structure 13:1859-1868.

9. Gosert, R., A. Kanjanahaluethai, D. Egger, K. Bienz, and S. C. Baker. 2002. RNA replication of mouse hepatitis virus takes place at double-membrane vesicles. J. Virol. 76:3697-3708.

10. Hagemeijer, M. C., M. H. Verheije, M. Ulasli, I. A. Shaltiel, L. A. de Vries, F. Reggiori, P. J. Rottier, and C. A. M. de Haan. 2010. Dynamics of coronavirus replication-transcription complexes. J. Virol. 84:2134-2149.

11. Huang, C. Y., Y. L. Hsu, W. L. Chiang, and M. H. Hou. 2009. Elucidation of the stability and functional regions of the human coronavirus OC43 nucleocapsid protein. Protein Sci. 18:2209-2218.

12. Hurst, K. R., C. A. Koetzner, and P. S. Masters. 2009. Identification of in vivo-interacting domains of the murine coronavirus nucleocapsid protein. J. Virol. 83:7221-7234.

12a Hurst, K. R., R. Ye, S. F. Goebel, P. Jayaraman, and P. S. Masters. 2010. An interaction between the nucleocapsid protein and a component of the replicase-transcriptase complex is crucial for the infectivity of coronavirus genomic RNA. J. Virol. 84:10276-10288.

13. Jayaram, H., H. Fan, B. R. Bowman, A. Ooi, J. Jayaram, E. W. Collisson, J. Lescar, and B. V. Prasad. 2006. X-ray structures of the N- and C-terminal domains of a coronavirus nucleocapsid protein: implications for nucleocapsid formation. J. Virol. 80:6612-6620.

14. Knoops, K., M. Kikkert, S. H. Worm, J. C. Zevenhoven-Dobbe, Y. van der Meer, A. J. Koster, A. M. Mommaas, and E. J. Snijder. 2008. SARS-coronavirus replication is supported by a reticulovesicular network of modified endoplasmic reticulum. PLoS Biol. 6:e226.

15. Lu, X. T., A. C. Sims, and M. R. Denison. 1998. Mouse hepatitis virus 3C-like protease cleaves a 22-kilodalton protein from the open reading frame 1a polyprotein in virus-infected cells and in vitro. J. Virol. 72:2265-2271.

16. Mizutani, T., A. Maeda, M. Hayashi, H. Isogai, and S. Namioka. 1994. Both antisense and sense RNAs against the nucleocapsid protein gene inhibit the multiplication of mouse hepatitis virus. J. Vet. Med. Sci. 56:211-215.

17. Narayanan, K., K. H. Kim, and S. Makino. 2003. Characterization of N protein self-association in coronavirus ribonucleoprotein complexes. Virus Res. 98:131-140.

18. Oostra, M., E. G. te Lintelo, M. Deijs, M. H. Verheije, P. J. M. Rottier, and C. A. M. de Haan. 2007. Localization and membrane topology of the coronavirus nonstructural protein 4: involvement of the early secretory pathway in replication. J. Virol. 81:12323-12336.

19. Pan, J., X. Peng, Y. Gao, Z. Li, X. Lu, Y. Chen, M. Ishaq, D. Liu, M. L. Dediego, L. Enjuanes, and D. Guo. 2008. Genome-wide analysis of protein-protein interactions and involvement of viral proteins in SARS-CoV replication. PLoS One 3:e3299.

20. Prentice, E., W. G. Jerome, T. Yoshimori, N. Mizushima, and M. R. Denison. 2004. Coronavirus replication complex formation utilizes components of cellular autophagy. J. Biol. Chem. 279:10136-10141.

21. Saikatendu, K. S., J. S. Joseph, V. Subramanian, B. W. Neuman, M. J. Buchmeier, R. C. Stevens, and P. Kuhn. 2007. Ribonucleocapsid formation of severe acute respiratory syndrome coronavirus through molecular action of the N-terminal domain of N protein. J. Virol. 81:3913-3921.

22. Sawicki, S. G., D. L. Sawicki, and S. G. Siddell. 2007. A contemporary view of coronavirus transcription. J. Virol. 81:20-29.

23. Shi, S. T., and M. M. Lai. 2005. Viral and cellular proteins involved in coronavirus replication. Curr. Top. Microbiol. Immunol. 287:95-131.

24. Shi, S. T., J. J. Schiller, A. Kanjanahaluethai, S. C. Baker, J. W. Oh, and M. M. Lai. 1999. Colocalization and membrane association of murine hepatitis virus gene 1 products and de novo-synthesized viral RNA in infected cells. J. Virol. 73:5957-5969.

25. Snijder, E. J., Y. van der Meer, J. Zevenhoven-Dobbe, J. J. Onderwater, J. van der Meulen, H. K. Koerten, and A. M. Mommaas. 2006. Ultrastructure and origin of membrane vesicles associated with the severe acute respiratory syndrome coronavirus replication complex. J. Virol. 80:5927-5940.

26. Stertz, S., M. Reichelt, M. Spiegel, T. Kuri, L. Martinez-Sobrido, A. Garcia-Sastre, F. Weber, and G. Kochs. 2007. The intracellular sites of early replication and budding of SARS-coronavirus. Virology 361:304-315.

27. Surjit, M., and S. K. Lal. 2008. The SARS-CoV nucleocapsid protein: a protein with multifarious activities. Infect. Genet. Evol. 8:397-405.

28. Ulasli, M., M. H. Verheije, C. A. de Haan, and F. Reggiori. 2010. Qualitative and quantitative ultrastructural analysis of the membrane rearrangements induced by coronavirus. Cell Microbiol. 12:844-861.

29. Verheije, M. H., M. Raaben, M. Mari, E. G. Te Lintelo, F. Reggiori, F. J. van Kuppeveld, P. J. Rottier, and C. A. de Haan. 2008. Mouse hepatitis coronavirus RNA replication depends on GBF1-mediated ARF1 activation. PLoS Pathog. 4:e1000088.

30. von Brunn, A., C. Teepe, J. C. Simpson, R. Pepperkok, C. C. Friedel, R. Zimmer, R. Roberts, R. Baric, and J. Haas. 2007. Analysis of intraviral protein-protein interactions of the SARS coronavirus ORFeome. PLoS One 2:e459.

31. Wessels, E., D. Duijsings, R. A. Notebaart, W. J. Melchers, and F. J. van Kuppeveld. 2005. A proline-rich region in the coxsackievirus 3A protein is required for the protein to inhibit endoplasmic reticulum-to-Golgi transport. J. Virol. 79:5163-5173.

32. Yu, I. M., M. L. Oldham, J. Zhang, and J. Chen. 2006. Crystal structure of the severe acute respiratory syndrome (SARS) coronavirus nucleocapsid protein dimerization domain reveals evolutionary linkage between Corona- and Arteriviridae. J. Biol. Chem. 281:17134-17139.

33. Zuniga, S., I. Sola, J. L. Moreno, P. Sabella, J. Plana-Duran, and L. Enjuanes. 2007. Coronavirus nucleocapsid protein is an RNA chaperone. Virology 357:215-227.

Chapter 5

Mobility and Interactions of Coronavirus Nonstructural Protein 4

Marne C. Hagemeijer[1], Mustafa Ulasli[2], Annelotte M. Vonk[1], Fulvio Reggiori[2], Peter J. M. Rottier[1], and Cornelis A. M. de Haan[1]

Virology Division, Department of Infectious Diseases and Immunology, Faculty of Veterinary Medicine, Utrecht University, Utrecht, the Netherlands[1], and Department of Cell Biology and Institute of Biomembranes, University Medical Centre Utrecht, Utrecht, the Netherlands[2]

Journal of Virology, May 2011, p. 4572–4577 Vol. 85, No. 9

Supplemental material can be found at http://jvi.asm.org/

ABSTRACT

Green fluorescent protein (GFP)-tagged mouse hepatitis coronavirus nonstructural protein 4 (nsp4) was shown to localize to the endoplasmic reticulum (ER) and to be recruited to the coronavirus replicative structures. Fluorescence loss in photobleaching and fluorescence recovery after photobleaching experiments demonstrated that while the membranes of the ER are continuous with those harboring the replicative structures, the mobility of nsp4 at the latter structures is relatively restricted. In agreement with that observation, nsp4 was shown to be engaged in homotypic and heterotypic interactions, the latter with nsp3 and nsp6. In addition, the coexpression of nsp4 with nsp3 affected the subcellular localization of the two proteins.

All positive-strand RNA viruses induce modified cellular membranes in infected cells, onto which their replication complexes are anchored [reviewed in references (23) and (30)]. Coronaviruses induce the formation of double-membrane vesicles (DMVs) and convoluted membranes (CMs) (14, 18, 24, 29, 32, 34), which form a large reticulovesicular network with which viral replication and transcription are associated (14, 18, 37). The nonstructural proteins (nsps) localize to the CMs and the DMVs (16, 18, 34, 37), while double-stranded RNA (dsRNA), probably corresponding to replicative intermediates, has been detected at the DMV interior (18, 34). Not much is known about the mechanism by which the coronavirus replicative structures (DMVs and CMs) are formed (4, 26), let alone about the functioning of the different structures in viral RNA synthesis (18, 37).

The coronavirus nsps 3, 4, and 6 are integral membrane proteins. These proteins, the membrane topology of which was recently established (1, 17, 24, 25), are supposed to drive the induction of the membrane rearrangements and to provide the scaffold onto which the replication complexes are assembled. Key roles have been attributed in particular to nsp3 and nsp4 in the induction of the typical membrane structures, as ectopic coexpression of the arterivirus nsp3 and nsp4 counterparts results in the appearance of the corresponding structures (35). The importance of coronavirus nsp4 in DMV biogenesis is indicated by several other observations. nsp4 was shown to be an essential protein (36), while mutation of residue 258 resulted in a temperature-sensitive phenotype, with reduced numbers of DMVs and nsp4 localizing to the mitochondria at the restrictive temperature (3). Abrogation of the nsp4 glycosylation sites led to an impairment of viral RNA synthesis accompanied by the appearance of aberrant DMVs and increased numbers of CMs (13).

In view of the essential role of nsp4 in replication and the assembly of the replicative structures, we analyzed its dynamics using fluorescence loss in photobleaching (FLIP) and fluorescence recovery after photobleaching (FRAP) approaches. As we have been unable to generate recombinant viruses expressing green fluorescent protein (GFP)-tagged nsp4 in the context of the replicase precursor proteins, we used a recombinant mouse hepatitis virus (MHV) in which a GFP-tagged version of nsp4 was expressed as an additional expression cassette (MHV-nsp4GFP) (25).

MHV-nsp4GFP replication kinetics and peak titers in LR7 cells were similar to those of recombinant wild-type MHV (MHV-WT) (5) (Fig. 1A). Apparently, expression of nsp4-GFP, which was expressed approximately

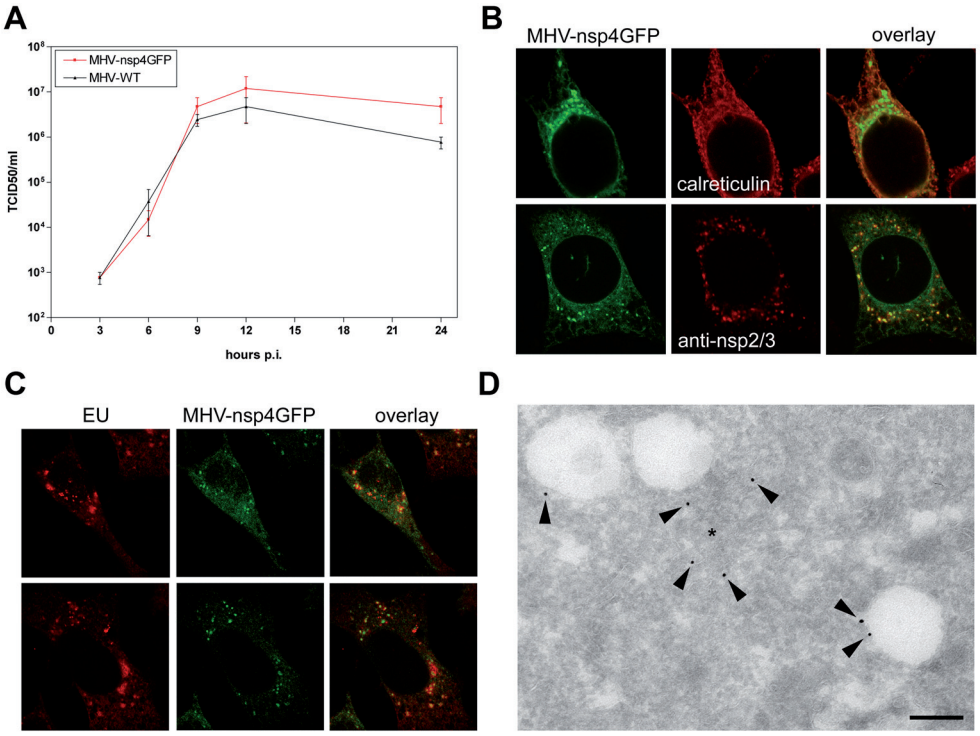

Figure 1. Characterization of recombinant MHV-nsp4GFP virus. (A) LR7 cells were infected with either MHV-nsp4GFP or recombinant wild-type MHV (MHV-WT; [5]) at a multiplicity of infection (MOI) of 10. Culture media were collected at the indicated time points post infection (p.i.), and viral infectivity was determined by performing quantal assays with LR7 cells. $TCID_{50}$, 50% tissue culture infective dose. (B) LR7 cells were infected with MHV-nsp4GFP, fixed, and subjected to immunofluorescence analysis using antibodies directed against calreticulin (Sigma) and nsp2/3 (31). (C) The sites of viral RNA synthesis in MHV-nsp4GFP-infected cells were visualized by EU labeling at 6 h p.i., followed by fixation and coupling of an Alexa 594 fluorophore to the incorporated EU using click chemistry (Click-iT; Invitrogen). (D) Cryosections of MHV-nsp4GFP-infected cells were prepared and incubated with antibodies directed against the GFP tag (Abcam), followed by immunogold labeling (indicated by the arrowheads) (33). The asterisk indicates the ER and/or the convoluted membrane assemblies. Bar, 200 nm.

12-fold more abundantly than the endogenous mature nsp4 protein (data not shown), did not interfere with virus replication. Consistent with our earlier observations (25), the protein displayed a reticular staining pattern that coincided with the endoplasmic reticulum (ER) marker calreticulin (Fig. 1B). In addition, nsp4-GFP was also present in puncta that colocalized not with calreticulin but with markers for the coronavirus replicative structures, such as nsp8 and nsp2/3 (Fig. 1B) (25). Most nsp4-GFP-positive foci colocalized with or were found adjacent to newly synthesized viral RNA (Fig. 1C), which was detected by feeding cells with an alkyne-modified nucleoside, 5-ethynyl

uridine (EU), as described previously (39), indicating that nsp4-GFP is recruited to sites of active RNA synthesis. Finally, we studied the localization of nsp4-GFP by analyzing MHV-nsp4GFP-infected cells by immunoelectron microscopy (IEM) using anti-GFP antibodies as described previously (16, 33, 37, 38). Although the labeling was weak, it was specific and showed nsp4-GFP localization on the surface of the DMVs, which appeared as empty holes inherent to the method used (Fig. 1D) (16, 37, 39). Some additional staining could be observed on membranes that probably correspond to either the CMs or the ER. No labeling of noninfected cells was observed (data not shown).

The presence of nsp4-GFP in ER membranes and its recruitment to the viral replicative structures allowed us to assess whether the membranes of the DMVs/CMs and the ER are interconnected in MHV-infected cells. We applied FLIP to MHV-nsp4GFP-infected cells to verify whether this continuity existed. With this technique, a specific area of the cell is repeatedly photobleached, and loss of fluorescence outside the bleached area is monitored [for more details, see references (19) and (20)]. After a specific area has been photobleached, fluorescence is recovered by diffusion. When the same area gets repeatedly bleached, the fluorescence of the whole organelle will be lost. Thus, while loss of fluorescence outside the photobleached area is indicative of membrane continuity, a persisting signal indicates the lack of connectivity between membrane systems. At 6 h p.i., a defined region targeting the ER in MHV-nsp4GFP-infected cells was repeatedly photobleached, each time followed by the acquisition of postbleaching images at different locations in the cell. No fluorescence loss was observed for neighboring cells. Repeated photobleaching of infected cells resulted in fluorescence loss of the nsp4-GFP present in the ER as well as in the replicative structures (Fig. 2A and B) (see Video S1 in the supplemental material). However, significantly less fluorescence was lost after repeated photobleaching over a period of 30 min in the replicative structures than that lost in the ER (60% versus 80%). Furthermore, nsp4-GFP fluorescence decreased significantly faster in the ER than in the replicative structures ($P = 0.011$).

These results revealed continuity between the ER and the replicative structures. Although we cannot exclude the possibility that this continuity results from (rapid) vesicular transport between these structures, direct continuity between the membranes of the ER and of the replicative structures appears a more likely explanation in view of an electron tomography study of severe acute respiratory syndrome coronavirus (SARS-CoV)-infected cells (18). For MHV-A59, electron tomography may be required to demonstrate this kind of continuity, as it was previously not observed for MHV-infected

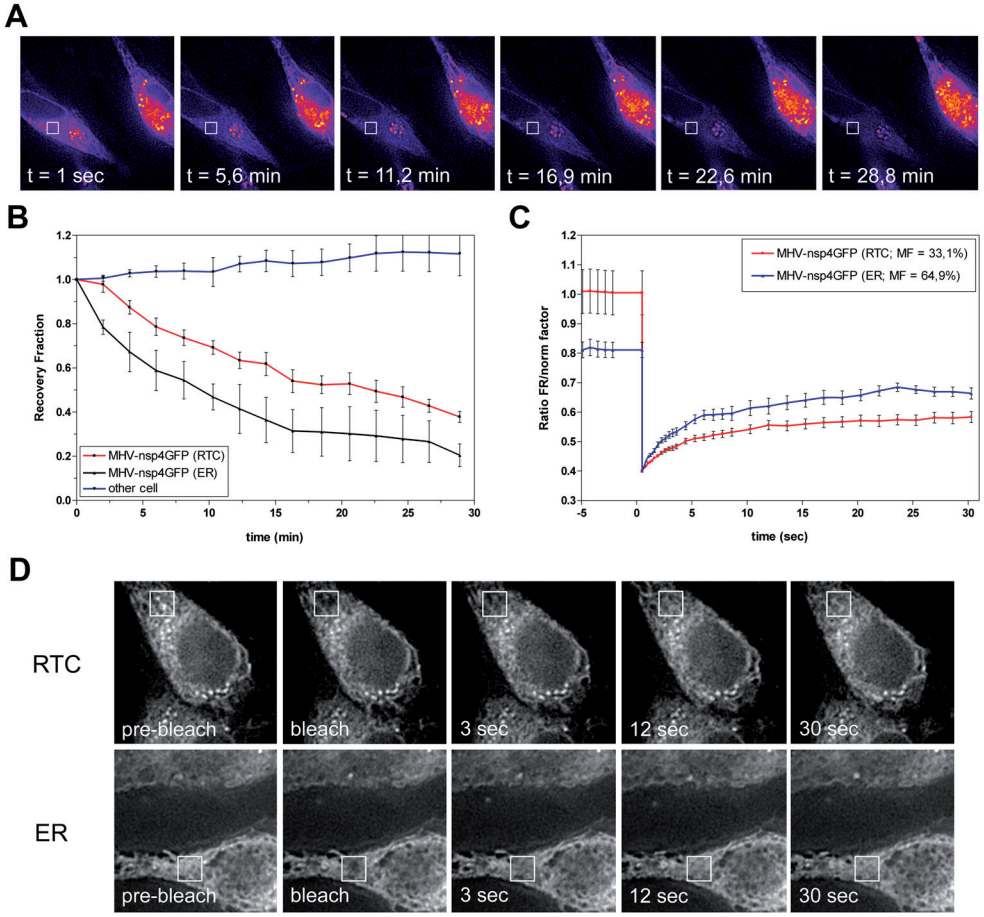

Figure 2. FLIP and FRAP analyses of MHV-nsp4GFP-infected cells. (A) In the FLIP experiments, the ER of MHV-nsp4GFP-infected cells was repeatedly photobleached, 25 times for 1 s every 60 s, and fluorescence loss was monitored at the nsp4GFP-positive replicative structures (dots) or at sites that contain reticular nsp4-GFP fluorescence. Representative images of such an experiment are depicted and were enhanced using the "hot" look-up table of ImageJ (28), in which the observed fluorescence is represented as colors corresponding to the strength of the fluorescence intensities, ranging from white/yellow (high intensities) to purple/black (low intensities). The bleached area is indicated by the white box. t, time. (B) The recovery fractions of the FLIP experiments were obtained by background correction of the measured fluorescence intensities and by normalizing these to the prebleach fluorescence intensities at the indicated cellular locations. The mean results from five experiments are shown. The error bars indicate the standard errors of the means. (C) FRAP was performed as previously described (16), using MHV-nsp4GFP-infected cells, thereby targeting nsp4-GFP-positive dots or sites containing reticular nsp4-GFP fluorescence only. The corresponding fluorescence recovery graphs, after background correction and normalization of the measured fluorescence intensities, are depicted, and calculated mobile fractions (MF) are indicated. The mean results from six and nine experiments are shown for nsp4-GFP-positive dots and reticular nsp4-GFP, respectively. The error bars indicate the standard errors of the means. FR, fluorescence recovery; norm factor, normalization factor. (D) Representative images of such FRAP experiments are depicted, with the bleached area indicated by the white box. For all live-cell imaging experiments, the spike protein heptad repeat 2 (HR2) peptide (2) was added to inhibit cell-cell fusion.

cells by conventional electron microscopy (37). The electron tomography study of SARS-CoV-infected cells also showed that the inner membranes of the DMVs are sealed and do not display continuity with the other membranes. The absence of any "pockets" of fluorescence, i.e., regions of restricted mobility, in our FLIP experiments indicates either that nsp4 is present at minimal levels in the inner lipid bilayer of the DMVs or that continuity between the inner and the outer membranes exists.

The FLIP experiments indicated that the nsp4-GFP proteins display different diffusion properties depending on their subcellular localization. To confirm this observation, we investigated the mobility of nsp4-GFP in more detail by performing FRAP experiments, as previously described [for details, see references (16, 20, 21, and 39)], targeting the nsp4-GFP fluorescence in MHV-nsp4GFP-infected cells either at the ER (reticular staining) or at the replicative structures (dots); representative images and corresponding fluorescence recovery graphs are depicted in Fig. 2C and D. Bleaching of reticular nsp4-GFP resulted in a reduction of ~50% of the prebleaching fluorescent signal. Within 30 s, ~35% of the nsp4-GFP fluorescent signal was recovered, with a calculated mobile fraction (Mf) of 64.9%. These results indicate that nsp4-GFP is able to laterally diffuse through the lipid bilayers of the ER, in agreement with our FLIP experiments. Photobleaching of nsp4-GFP-positive dots resulted in a reduction of ~60% of the prebleached signal. Much less recovery of the fluorescent signal was observed at these structures (Mf of 33.1%). Furthermore, it appeared that the measured recovery resulted largely from mobility of nsp4-GFP in ER membranes, which are also present in the bleached areas, rather than from recovery in the replicative structures.

The FRAP experiments are consistent with the FLIP data and show that while the nsp4-GFP protein pool present at the replicative structures is mobile, its mobility is clearly less than that of the nsp4-GFP present in ER membranes. Apparently, the protein experiences some kind of diffusion barrier when present at the replicative structures. Until now, we have analyzed the mobility of two other proteins at the replicative structures: nsp2 (16) and the nucleocapsid protein N (39). While nsp2, once recruited to the replication-transcription complexes (RTCs), was immobilized (16), the N protein was dynamically associated to the RTCs (39). Although the recovery of nsp4 and nsp2 to the bleached replicative structures cannot be compared directly, as nsp2 is a cytosolic protein and nsp4 is an integral membrane protein, it appears that nsp2 is constrained at the replicative structures to a much greater extent than is nsp4.

As all nsps studied to date are located at the replicative structures (8, 15, 25, 27, 31, 34), the local interaction of nsp4-GFP with other nsps may very well account for the observed differences in diffusion. Therefore, we investigated whether nsp4 binds to other nsps. We decided to focus on the coronavirus integral membrane nsps (nsp3, nsp4, and nsp6), as the equine arterivirus (EAV) counterparts of the coronavirus nsp3 and nsp4 have previously been shown to interact with each other (35). The proteins were expressed in OST7-1 cells using the recombinant vaccinia virus encoding the bacteriophage T7 RNA polymerase (vTF7-3) expression system (11, 12), after which cells were labeled with ^{35}S-labeled amino acids and coimmunoprecipitation (coIP) experiments were performed as described previously (6, 7). The gene fragments encoding the nsps were fused to either GFP- or hemagglutinin (HA)-encoding sequences and cloned under the control of a T7 promoter (24, 25). For nsp3, only the fragment encoding the C-terminal domain (nsp3$_C$), which contains all transmembrane domains, was cloned (24), as the gene encoding the full-length protein appeared to be too toxic to clone and express. Interaction between the coexpressed proteins is monitored by the coprecipitation of HA-tagged proteins using anti-GFP antibodies and *vice versa*. As a control for the specificity of the detected interactions, lysates of cells singly expressing the nsps were pooled and subsequently processed similarly for IP, as described previously (6). As an additional control, the coIP assay was also applied after coexpression of nsp4 with the MHV triple-spanning membrane (M) protein. Antibodies directed against the GFP or HA tag of nsp4 did not coprecipitate the MHV M protein, and M protein-specific antibodies did not coprecipitate the nsp4 fusion proteins (data not shown). We first investigated whether nsp4 is engaged in homotypic interactions (Fig. 3A). The pooled lysates of separately expressed nsp4 proteins did not demonstrate coIP of nsp4, demonstrating the specificity of the assay and of the anti-GFP and anti-HA antibodies. When coexpressed, however, nsp4-GFP was coprecipitated with nsp4-HA and *vice versa*. Similar results were obtained when nsp4 fusion proteins were coexpressed with nsp3$_C$ or nsp6 fusion proteins (Fig. 3B and C).

As a second independent assay to detect these interactions, we made use of the yellow fluorescent Venus protein-based protein complementation assay (PCA) (22). In this assay, two complementary Venus reporter fragments, V1 and V2, are fused to the protein(s) of interest. Upon interaction of the fusion proteins, the Venus fluorescent reporter activity is reconstituted. C-terminal V1 and V2 reporter fusion constructs of nsp3$_C$, nsp4, and nsp6 were generated and coexpressed in different combinations using the vTF7-3 expression system, after which the cells were processed for (quantitative) fluorescence

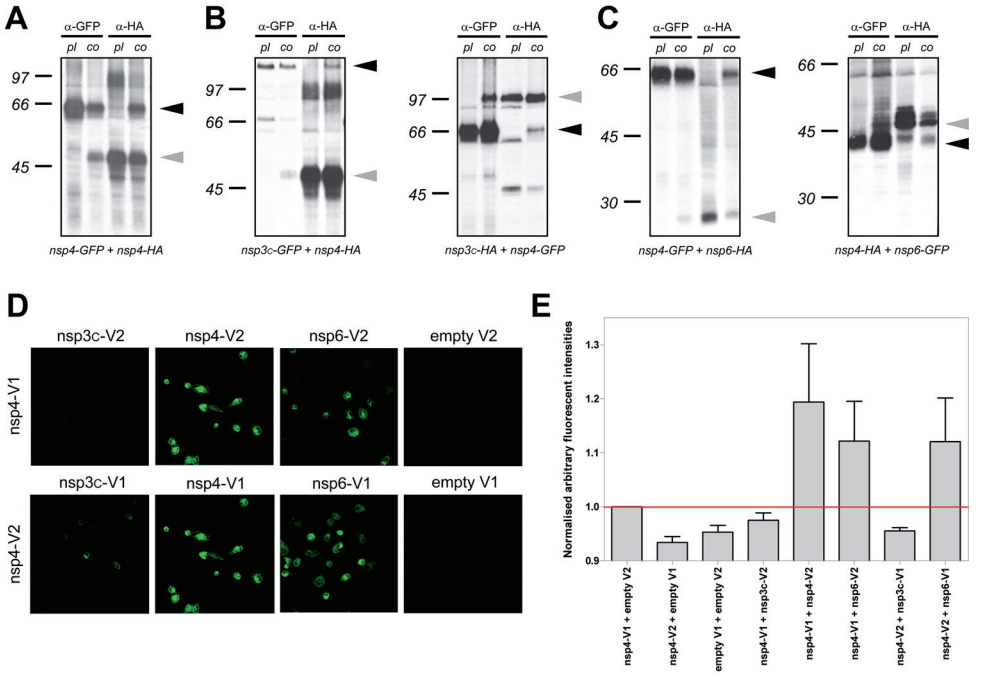

Figure 3. CoIP and PCA analysis of homo- and heterotypic interactions of nsp4. GFP- and HA-tagged nsp constructs were expressed in OST7-1 cells, either alone or in the following combinations: (A) nsp4-GFP with nsp4-HA, (B) $nsp3_C$-GFP with nsp4-HA and $nsp3_C$-HA with nsp4-GFP, and (C) nsp4-GFP with nsp6-HA and nsp4-HA with nsp6-GFP. Cells were radiolabeled for 1 h. Cell lysates were prepared and subjected to IP with either anti-GFP (α-GFP) or anti-HA (α-HA) antibodies (Immunology Consultants Laboratory, Inc.). Precipitates were analyzed using SDS-PAGE. As a control for the coexpression (co), lysates of singly expressed proteins were pooled (pl) and processed similarly for IP. The black and gray arrowheads indicate the positions in the gel of GFP- and HA-tagged proteins, respectively. (D) vTF7-3-infected OST7-1 cells were transfected with the indicated combinations of the split-Venus PCA fragments, after which the cells were fixed at 6 h p.i. and processed for immunofluorescence microscopy. Representative images are shown. (E) The mean arbitrary fluorescence intensities of 10 randomly chosen cells per cotransfection in the PCA experiments were determined using a Deltavision RT microscope and the Volocity software package from Improvision. V1 and V2 indicate Venus fragments 1 and 2.

analysis. Cotransfection of the empty V1 or empty V2 plasmid with the nsp4-V2 or nsp4-V1 construct did not result in reconstitution of the Venus fluorescence and served as a negative control (Fig. 3D and E), in agreement with the inability of the Venus reporter fragments to spontaneously refold in their native structure in the absence of interacting partners being fused to them (22). With this assay, we were able to confirm the interaction of nsp4 with itself and with nsp6, as a reticular fluorescence signal was observed when these gene fragments were coexpressed (Fig. 3D and E). However, we were not able to demonstrate interaction between nsp4-V1 and $nsp3_C$-V2,

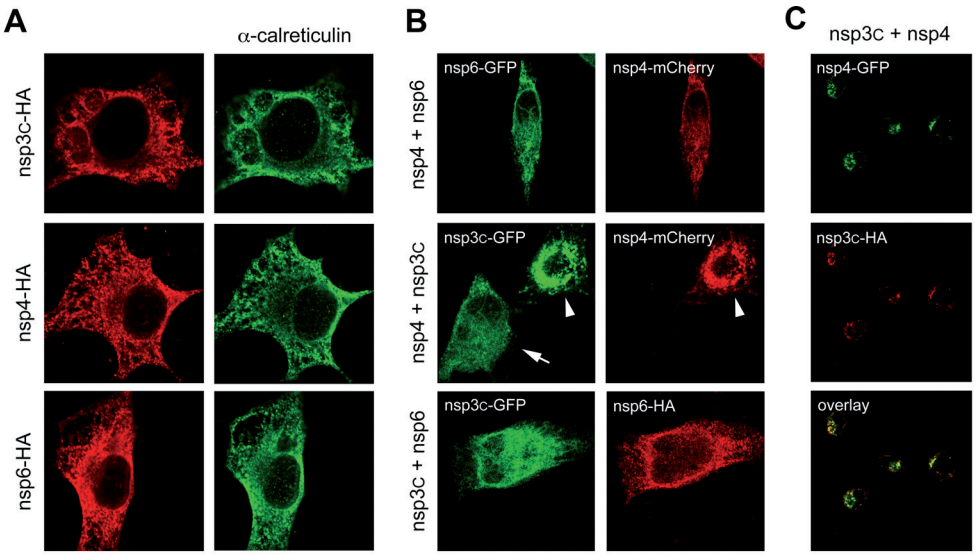

Figure 4. Coexpression of nsp4 and nsp3$_C$ results in altered subcellular localization of these proteins. vTF7-3-infected OST7-1 cells were (co)transfected with plasmids encoding, nsp3$_C$-HA, nsp4-HA, nsp6-HA, nsp3$_C$-GFP, nsp4-mCherry, nsp4-GFP, or nsp6-GFP as indicated in the figure. Six hours p.i., cells were fixed and processed for confocal microscopy. (A) Single expression. Cells were subjected to immunofluorescence analysis using antibodies directed against the HA tag and calreticulin. α, anti. (B) Coexpression experiments with nsp3$_C$, nsp4, and nsp6. The arrowhead points to a cell demonstrating perinuclear fluorescent foci as observed in nsp3$_C$- and nsp4-cotransfected cells, whereas the arrow points to a single transfected cell expressing only reticular nsp3$_C$-GFP, for which these dots are not observed. (C) Coexpression of nsp3$_C$-HA and nsp4-GFP also results in the appearance of perinuclear fluorescent foci. The panel shows multiple cells in a field.

and only occasionally was a weakly positive cell found for the nsp4-V2 and nsp3$_C$-V1 combination. The absence of fluorescence was not due to the nsp3$_C$ constructs themselves, as coexpression of nsp3$_C$-V1 and nsp3$_C$-V2 clearly resulted in reconstitution of fluorescence, indicative of nsp3 homotypic interactions (data not shown). The fact that the interaction between nsp4 and nsp3$_C$ was not observed with PCA may be caused by the C termini of the two proteins not being oriented in a configuration allowing the reconstitution of the fluorescence activity. In agreement with the coIP results, interaction between nsp4 and nsp3 was observed using yeast two-hybrid assays (data not shown). These results show that nsp4 is contained within a network of protein-protein interactions and probably explain the recruitment of nsp4 to the RTCs when expressed *in trans* [reference (25) and this study]. Moreover, nsp4 is likely to play a central role within this network, as the infection of cells with a temperature-sensitive MHV, carrying a mutation in nsp4, resulted in a partial localization not only of nsp4 but also of nsp3 and possibly other nsps

to mitochondria at the restrictive temperature (3).

Finally, we analyzed whether coexpression of nsp4 with $nsp3_C$ or nsp6 would affect the localization of the proteins, similarly to what has been described for EAV nsp2 and nsp3 (35). First, we studied the subcellular localization of the C-terminally tagged membrane proteins using the vTF7-3 expression system. As shown in Fig. 4A and in agreement with previous reports (1, 17, 24, 25), individually expressed $nsp3_C$, nsp4, and nsp6 exhibited a reticular pattern and colocalized with the ER marker calreticulin regardless of the identity of the C-terminal tag (data not shown). Next, we coexpressed $nsp3_C$, nsp4, and nsp6 in various combinations. While the reticular staining pattern of these proteins by coexpression of nsp6 with either nsp4 or $nsp3_C$ was not affected, coexpression of nsp4 with $nsp3_C$ resulted in the formation of perinuclear fluorescent foci in which these proteins appeared to be concentrated (Fig. 4B). Similar results were obtained when nsp4 or $nsp3_C$ carried different tags (Fig. 4C). We hypothesize that the coexpression of $nsp3_C$ and nsp4 results in a rearrangement of host cell membranes. We are currently studying to what extent these rearrangements resemble the membrane modifications in MHV-infected cells (37). For several other plus-strand RNA viruses, the viral proteins responsible for the membrane rearrangements, with which viral RNA synthesis is associated, have been identified [reviewed in references (9, 10)]. These key organizers of plus-strand RNA virus replication complexes appear to have in common the characteristic of exerting their function as oligomeric complexes. In this respect, this study shows that the coronavirus transmembrane-containing nsps are no exception.

ACKNOWLEDGEMENTS

We thank Corlinda ten Brink from the Cell Microscopy Center, University Medical Centre Utrecht, Richard Wubbolts from the Center for Cell Imaging (CCI) of the Faculty of Veterinary Medicine, University Utrecht, and Boaz van Driel and Eddie te Lintelo for technical assistance. We thank Susan Baker and Stephen Michnick for kindly providing antibodies and plasmids. This work was supported by grants from the Netherlands Organization for Scientific Research (NWO-VIDI and NWO-ALW) and the Utrecht University (High Potential) to C. A. M. de Haan and F. Reggiori.

REFERENCES

1. Baliji, S., S. A. Cammer, B. Sobral, and S. C. Baker. 2009. Detection of nonstructural protein 6 in murine coronavirus-infected cells and analysis of the transmembrane topology by using bioinformatics and molecular approaches. J. Virol. 83:6957–6962.

2. Bosch, B. J., R. van der Zee, C. A. de Haan, and P. J. Rottier. 2003. The coronavirus spike protein is a class I virus fusion protein: structural and functional characterization of the fusion core complex. J. Virol. 77:8801–8811.

3. Clementz, M. A., A. Kanjanahaluethai, T. E. O'Brien, and S. C. Baker. 2008. Mutation in murine coronavirus replication protein nsp4 alters assembly of double membrane vesicles. Virology 375:118–129.

4. de Haan, C. A. M., F. Reggiori, and M. Molinari. 2010. Autophagy-independent LC3 function in vesicular traffic. Autophagy 6:994.

5. de Haan, C. A. M., P. S. Masters, X. Shen, S. Weiss, and P. J. M. Rottier. 2002. The group-specific murine coronavirus genes are not essential, but their deletion, by reverse genetics, is attenuating in the natural host. Virology 296:177–189.

6. de Haan, C. A. M., M. Smeets, F. Vernooij, H. Vennema, and P. J. M. Rottier. 1999. Mapping of the coronavirus membrane protein domains involved in interaction with the spike protein. J. Virol. 73:7441–7452.

7. de Haan, C. A. M., H. Vennema, and P. J. M. Rottier. 2000. Assembly of the coronavirus envelope: homotypic interactions between the M proteins. J. Virol. 74:4967–4978.

8. Deming, D. J., R. L. Graham, M. R. Denison, and R. S. Baric. 2007. Processing of open reading frame 1a replicase proteins nsp7 to nsp10 in murine hepatitis virus strain A59 replication. J. Virol. 81:10280–10291.

9. den Boon, J. A., and P. Ahlquist. 2010. Organelle-like membrane compartmentalization of positive-strand RNA virus replication factories. Annu. Rev. Microbiol. 64:241–256.

10. den Boon, J. A., A. Diaz, and P. Ahlquist. 2010. Cytoplasmic viral replication complexes. Cell. Host Microbe 8:77–85.

11. Elroy-Stein, O., and B. Moss. 1990. Cytoplasmic expression system based on constitutive synthesis of bacteriophage T7 RNA polymerase in mammalian cells. Proc. Natl. Acad. Sci. U. S. A. 87:6743–6747.

12. Fuerst, T. R., E. G. Niles, F. W. Studier, and B. Moss. 1986. Eukaryotic transient-expression system based on recombinant vaccinia virus that synthesizes bacteriophage T7 RNA polymerase. Proc. Natl. Acad. Sci. U. S. A. 83:8122–8126.

13. Gadlage, M. J., et al. 2010. Murine hepatitis virus nonstructural protein 4 regulates virus-induced membrane modifications and replication complex function. J. Virol. 84:280–290.

14. Gosert, R., A. Kanjanahaluethai, D. Egger, K. Bienz, and S. C. Baker. 2002. RNA replication of mouse hepatitis virus takes place at double-membrane vesicles. J. Virol. 76:3697–3708.

15. Graham, R. L., A. C. Sims, S. M. Brockway, R. S. Baric, and M. R. Denison. 2005. The nsp2 replicase proteins of murine hepatitis virus and severe acute respiratory syndrome coronavirus are dispensable for viral replication. J. Virol. 79:13399–13411.

16. Hagemeijer, M. C., et al. 2010. Dynamics of coronavirus replication-transcription complexes. J. Virol. 84:2134–2149.

17. Kanjanahaluethai, A., Z. Chen, D. Jukneliene, and S. C. Baker. 2007. Membrane topology of murine coronavirus replicase nonstructural protein 3. Virology 361:391–401.

18. Knoops, K., et al. 2008. SARS-coronavirus replication is supported by a reticulovesicular network of modified endoplasmic reticulum. PLoS Biol. 6:e226.

19. Lippincott-Schwartz, J., N. Altan-Bonnet, and G. H. Patterson. 2003. Photobleaching and photoactivation: following protein dynamics in living cells. Nat. Cell Biol. 2003(Suppl.):S7–S14.

20. Lippincott-Schwartz, J., and G. H. Patterson. 2003. Development and use of fluorescent protein markers in living cells. Science 300:87–91.

21. Lippincott-Schwartz, J., E. Snapp, and A. Kenworthy. 2001. Studying protein dynamics in living cells. Nat. Rev. Mol. Cell Biol. 2:444–456.

22. MacDonald, M. L., et al. 2006. Identifying off-target effects and hidden phenotypes of drugs in human cells. Nat. Chem. Biol. 2:329–337.

23. Miller, S., and J. Krijnse-Locker. 2008. Modification of intracellular membrane structures for virus replication. Nat. Rev. Microbiol. 6:363–374.

24. Oostra, M., et al. 2008. Topology and membrane anchoring of the coronavirus replication complex: not all hydrophobic domains of nsp3 and nsp6 are membrane spanning. J. Virol. 82:12392–12405.

25. Oostra, M., et al. 2007. Localization and membrane topology of coronavirus nonstructural protein 4: involvement of the early secretory pathway in replication. J. Virol. 81:12323–12336.

26. Perlman, S., and J. Netland. 2009. Coronaviruses post-SARS: update on replication and pathogenesis. Nat. Rev. Microbiol. 7:439–450.

27. Prentice, E., J. McAuliffe, X. Lu, K. Subbarao, and M. R. Denison. 2004. Identification and characterization of severe acute respiratory syndrome coronavirus replicase proteins. J. Virol. 78:9977–9986.

28. Rasband, W. S. 1997–2008. ImageJ. National Institutes of Health, Bethesda, MD. http://rsbweb.nih.gov/ij/.

29. Reggiori, F., et al. 2010. Coronaviruses hijack the LC3-I-positive EDEMosomes, ER-derived vesicles exporting short-lived ERAD regulators, for replication. Cell Host Microbe 7:500–508.

30. Salonen, A., T. Ahola, and L. Kaariainen. 2005. Viral RNA replication in association with cellular membranes. Curr. Top. Microbiol. Immunol. 285:139–173.

31. Shi, S. T., et al. 1999. Colocalization and membrane association of murine hepatitis virus gene 1 products and de novo-synthesized viral RNA in infected cells. J. Virol. 73:5957–5969.

32. Sims, A. C., J. Ostermann, and M. R. Denison. 2000. Mouse hepatitis virus replicase proteins associate with two distinct populations of intracellular membranes. J. Virol. 74:5647–5654.

33. Slot, J. W., and H. J. Geuze. 2007. Cryosectioning and immunolabeling. Nat. Protoc. 2:2480–2491.

34. Snijder, E. J., et al. 2006. Ultrastructure and origin of membrane vesicles associated with the severe acute respiratory syndrome coronavirus replication complex. J. Virol. 80:5927–5940.

35. Snijder, E. J., H. van Tol, N. Roos, and K. W. Pedersen. 2001. Non-structural proteins 2 and 3 interact to modify host cell membranes during the formation of the arterivirus replication complex. J. Gen. Virol. 82:985–994.

36. Sparks, J. S., X. Lu, and M. R. Denison. 2007. Genetic analysis of murine hepatitis virus nsp4 in virus replication. J. Virol. 81:12554–12563.

37. Ulasli, M., M. H. Verheije, C. A. de Haan, and F. Reggiori. 2010. Qualitative and quantitative ultrastructural analysis of the membrane rearrangements induced by coronavirus. Cell. Microbiol. 12:844–861.

38. Verheije, M. H., et al. 2008. Mouse hepatitis coronavirus RNA replication depends on GBF1-mediated ARF1 activation. PLoS Pathog. 4:e1000088.

39. Verheije, M. H., et al. 2010. The coronavirus nucleocapsid protein is dynamically associated with the replication-transcription complexes. J. Virol. 84:11575–11579.

Chapter 6

Temporal Modulation of Coronavirus RNA Synthesis Visualized by Click Chemistry

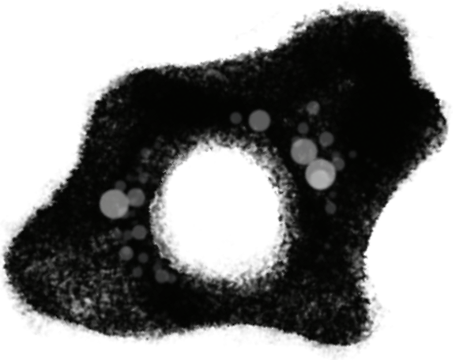

Marne C. Hagemeijer, Annelotte M. Vonk, Iryna Monastyrska, Peter J. M. Rottier, and Cornelis A. M. de Haan

Virology Division, Department of Infectious Diseases and Immunology, Faculty of Veterinary Medicine, Utrecht University, Utrecht, the Netherlands

Submitted for publication

ABSTRACT

Like all other plus-strand RNA viruses, coronaviruses induce in infected cells the formation of membranous structures that are associated with RNA synthesis. The coronavirus replicative structures consist of a network of double-membrane vesicles (DMVs) and convoluted membranes (CMs), to which the nonstructural proteins (nsps) localize. Double-stranded (ds) RNA replicative intermediates, which are a hallmark for plus-strand RNA virus genome replication, are localized to the DMV interior. However, as pores connecting the DMV interior with the cytoplasm have not been detected, it is unclear whether coronaviral RNA synthesis occurs at the same sites where the presumed dsRNA intermediates accumulate. Here, we studied coronavirus RNA synthesis with a new approach in which cells are fed with a uridine analogue, after which nascent viral RNAs are detected using click chemistry. The observations, while illustrating the potential of the click chemistry technology for detection of nascent viral RNA, indicate that early in infection nascent viral RNA and nsps colocalized with or occurred adjacent to dsRNA dots. Late in infection the correlation between dsRNA dots, then found dispersed throughout the cytoplasm, and nsps and nascent RNAs was less obvious, suggestive of maturation of the replicative structures. However, foci of nascent RNAs were always found to colocalize with the nsp12-encoded RNA-dependent RNA polymerase. These results demonstrate the feasibility of detecting viral RNA synthesis by using click chemistry and indicate that dsRNA dots not necessarily correspond with sites of active viral RNA synthesis. Rather, the DMVs may harbor dsRNA molecules that are not (longer) functioning as intermediates in RNA synthesis.

INTRODUCTION

Plus-strand RNA viruses induce dramatic membrane rearrangements in infected cells, thereby generating a subcellular microenvironment that facilitates RNA replication. A general feature of the membrane rearrangements is the induction of invaginations, giving rise to the formation of vesicles which are tethered to a cellular membrane. These spherules probably shield the viral double-stranded RNA (dsRNA) replication intermediates from immune surveillance, while at the same time providing access of cytoplasmic constituents to the replication machinery and means of exit for the newly synthesized RNA to enter the cytoplasm (8, 9).

Mouse hepatitis virus (MHV) belongs to the *Coronaviridae*, which is a family of enveloped, plus-strand RNA viruses that infect a wide variety of animals. MHV strain A59 is the prototype coronavirus (CoV) and serves as a model for the illustrious severe acute respiratory syndrome (SARS)-CoV. CoVs have a very large genome (~27 to 32 kb), the first two-thirds of which encode the replicase nonstructural proteins (nsps) that collectively form the replication-transcription complexes (RTCs). The nsps contain enzymatic activities required for RNA synthesis, including the RNA-dependent RNA polymerase [RdRp; residing in nsp12 (5)], but also transmembrane domains [residing in nsp3, 4 and 6 (1, 15, 22, 23)] that anchor the RTCs to the modified cellular membranes. The remaining part of the genome encodes the structural and accessory proteins, including the nucleocapsid protein (N), which is also found in association with the RTCs (4, 10, 38, 40, 41).

The CoV RTCs synthesize both full-length genomic RNA (gRNA; *replication*) and subgenomic RNAs (sgRNAs; *transcription*) [reviewed in (31)]. While a negative-sense full-length RNA strand functions as a template for new (positive-sense) gRNA, the 3' coterminal nested set of sgRNAs are synthesized via a discontinuous transcription mechanism during subgenome-length minus strand synthesis (30); as a consequence, all sgRNAs contain a short 5'-leader sequence corresponding to the 5'-end of the genome. The plus-strand RNAs are synthesized more abundantly than their negative-sense counterparts, approximately in a 100-fold excess (28). During CoV replication and transcription various complete and partially double-stranded RNA (dsRNA) intermediates are produced, which are either active in transcription (termed transcriptive intermediates and forms) or active in replication [termed replicative intermediates and forms; (28, 31)]. These dsRNA intermediates are generally considered to be a good marker for the location of the sites of active viral RNA synthesis in infected cells (31).

The replicative structures induced by CoVs in infected cells consist of a network of double-membrane vesicles (DMVs) and convoluted membranes (CMs), to which the nsps localize (12, 13, 18, 23, 27, 35, 36, 38). dsRNA, which is considered a hallmark for plus-strand RNA virus genome replication, is localized to the DMV interior (18). Strikingly, while tomography studies for flock house virus, dengue virus and Kunjin virus reveal the presence of a neck between the virus-induced vesicles and host membranes (11, 19, 44), the inner vesicles of the coronavirus-induced DMVs appear to be closed structures (18).

Studies with other viruses show that viral genome replication occurs at the same sites where dsRNA is accumulated [reviewed in (8, 9)]. However, as no pores have been observed that connect the interior of the inner vesicles of the coronaviral DMVs with the cytoplasm, the role of the dsRNA-containing DMVs in coronavirus RNA synthesis remains obscure. Therefore, we explored the feasibility of studying coronavirus RNA synthesis using a recently developed chemical method. This method is based on the biosynthetic incorporation of the alkyne-modified uridine analog 5-ethynyl uridine (EU) into newly transcribed RNA. EU-labeled RNA is subsequently detected by using a copper (I)-catalyzed cycloaddition reaction (referred to as click chemistry) with azide-derivatized fluorophores, followed by microscopic imaging (14). By performing a time course analysis we were able to visualize newly synthesized viral RNAs early in infection to localize at or adjacent to concentrated patches of dsRNA foci and nsps, including the CoV RdRp. At later time points post infection (p.i.) the dsRNA dots have become dispersed throughout the cytoplasm and colocalization between foci of newly synthesized RNA and dsRNA is less apparent. Many dsRNA dots are then no longer associated with newly synthesized RNA, indicating that they are not transcriptionally active. Moreover, at these later times not all foci of newly synthesized RNA are observed at the same sites where dsRNA dots reside. However, at all times the foci of newly synthesized RNA had the nsp12-encoding RdRp associated with them indicating that these foci correspond with the active RTCs.

MATERIALS AND METHODS

Cells and viruses. Murine LR7 fibroblast cells (20) were maintained as monolayer cultures in Dulbecco's modified Eagle's medium (DMEM–/–; Cambrex BioScience) containing 10% fetal calf serum (FCS; Bodinco BV), 100 IU/ml of penicillin, and 100 μg/ml of streptomycin (both from Life Technologies; this medium is referred to as DMEM+/+). MHV strain A59,

recombinant MHV-EFLM (7) and MHV-nsp2GFP (13), which express the firefly luciferase (FL) gene and the nsp2 coding sequence fused to that of green fluorescent protein (GFP) from an additional expression cassette, were propagated in LR7 cells.

Antibodies and plasmids. Antibodies directed against double-stranded RNA [dsRNA; K1; (33)] or α-tubulin were purchased from English and Scientific Consulting Bt. and Sigma, respectively. The polyclonal antibodies VU145 [α-pol; (5)] and anti-D3 (34), which are directed against MHV nsp12 or nsp2/3, respectively, were kindly provided by Mark Denison and Susan Baker, respectively. The monoclonal antibody M_N, recognizing the N-terminal domain of the MHV membrane (M) protein (37), was kindly provided by John Flemming. The expression plasmid encoding *Gaussia* luciferase under the control of a CMV promoter was obtained from New England Biolabs, while the vector encoding the stress granule marker RasGAP-associated endoribonuclease fused to GFP (G3BP-GFP), which was kindly provided by Paul Anderson, has been described before (17).

5-ethynyl uridine (EU) labeling. LR7 cells grown on glass coverslips were fed with different concentrations of EU (Invitrogen) in DMEM+/+ at the times and for the time periods indicated in the text and figure legends, after which they were fixed using a 4% paraformaldehyde (PFA) solution in PBS. Where indicated in the text, cells were transfected with the G3BP-GFP expression plasmid as previously described (13). The fixed cells were washed with PBS and permeabilized using 0.1% Triton X-100 for 10 min at room temperature. EU labeling of cells was visualized according to the manufacturer's instructions (Invitrogen; Click-iT RNA Imaging Kits). Briefly, the samples were incubated with a 1X working solution of Click-iT reaction cocktail, containing among others the Alexa Fluor 594 azide and $CuSO_4$, for 30 min at room temperature. After removal of the reaction cocktail, cells were washed once with Click-iT reaction rinse buffer. After this step, samples were washed with PBS and mounted on glass slides in FluorSave (Calbiochem), or samples were processed further for antibody staining as described below.

Antibody staining and fluorescence confocal microscopy. Permeabilized cells were washed with PBS and incubated for 15 min in blocking buffer (PBS-10% normal goat serum), followed by a 60 min incubation with antibodies directed against either nsp2/3 or dsRNA. RNasin (0,125 U/μl) was added to all incubation and washing steps. After washing the cells three times with PBS-containing 0,05% Tween-20, they were incubated for 60 min with Cy3-conjugated donkey anti-rabbit immunoglobulin G antibodies (Jackson Laboratories), fluorescein isothiocyanate-conjugated goat anti-rabbit

immunoglobulin G antibodies (ICN), or Cy3-conjugated donkey anti-mouse immunoglobulin G antibodies (Jackson Laboratories). After four washes with PBS, the samples were mounted on glass slides in FluorSave (Calbiochem). The samples were examined using a confocal fluorescence microscope (Leica TCS SP). Pearson's correlation coefficients of the different fluorescent signals were determined using the JACoP plugin (2) for the ImageJ processing and analyses software, version 1.41 (26).

Analysis of luciferase expression levels. Virus replication was quantified by determining the virus-driven firefly luciferase expression levels. To this end, LR7 cells were infected with MHV-EFLM. At the indicated time points, the luciferase expression levels in the cells was determined using the firefly luciferase assay system (Promega) according to manufacturer's instructions and using a Berthold Centro LB 960 plate luminometer.

RESULTS

EU labeling of nascent viral RNA in CoV-infected cells

We started our experiments by analyzing the feasibility of labeling and detecting newly synthesized viral RNAs by metabolic labeling of cells with the uridine analog EU. To this end, cells were either infected with MHV or mock-infected, after which they were (mock-) treated with the inhibitor of (cellular) DNA-dependent RNA transcription actinomycin D. Replication of MHV is not inhibited by this drug (21). At 5 h p.i. cells were fed with 1mM EU for 1 h, after which they were fixed and prepared for detection of the incorporated alkyne-modified uridine analog by using click chemistry with azide-derivatized Alexa 594 fluorophores. As shown in Fig. 1A, in mock-infected cells EU was incorporated into RNA in the nuclei, which was inhibited by the presence of actinomycin D. In infected cells, EU was incorporated into perinuclear cytoplasmic foci, besides the nuclei, while in the presence of actinomycin D, only the cytoplasmic foci were labeled. Apparently, this cytoplasmic staining corresponds to newly synthesized viral RNA. Next, we determined the minimal time of EU labeling needed to visualize these newly synthesized RNAs. As shown in Fig. 1B, hardly any labeling of viral RNAs could be detected when cells were fed the uridine analog for 15 or 30 min. However, viral RNAs could readily be detected after 45 min of labeling, which resulted in a staining pattern that was still very similar to the one obtained after a 60 min labeling. Subsequently, we studied whether labeling of newly synthesized viral RNAs could be inhibited by cycloheximide (CHX), an inhibitor of protein synthesis, shown earlier to

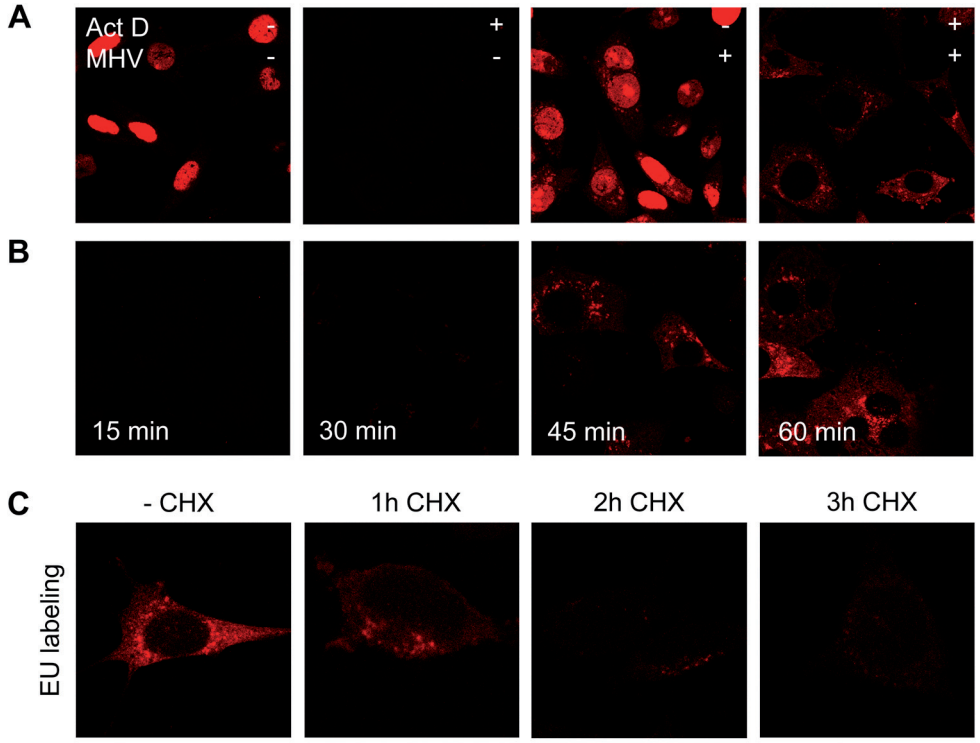

Figure 1. EU labeling of nascent viral RNA. MHV- or mock-infected LR7 cells were fed with 1 mM of EU for 1 h (or for the indicated time period). Fixation of the cells was followed by detection of incorporated alkyne-modified EU with azide-derivatized Alexa 594 fluophores by using click chemistry. (A) When indicated in the figure, 20 μM actinomycin D (Act D) was added to the infected cells at t = 1 h p.i. to inhibit cellular DNA-dependent RNA transcription. Cells were fed with EU at 5 h p.i. (B) Representative images of a time-course analysis of EU labeling in the presence of actinomycin D in infected cells are shown, performed as described above, with the EU labeling times indicated (C) 35 μM of cycloheximide (CHX) was added to the infected cells at 5 h p.i. to inhibit protein synthesis. Cells were fed with 1mM EU at 5 h (1 h CHX), 6 h (2 h CHX) or 7 h (3 h CHX) p.i. Cells were also fed with EU in the absence of cycloheximide at 5 h p.i. (-CHX). At the end of the EU labeling period cells were fixed.

affect MHV RNA synthesis (29). In agreement with the previous results, the addition of CHX inhibited the labeling of viral RNAs (Fig. 1C) in a time-dependent manner. Our results indicate that in the presence of an inhibitor of cellular transcription, labeling of cells with EU can be used to specifically detect viral RNA synthesis.

Next, we wanted to analyze whether addition of EU to infected cells would affect replication of MHV. Therefore, cells infected with a recombinant MHV expressing the luciferase reporter gene (MHV-EFLM) were treated with various concentrations of EU (0 to 4 mM) from 2 till 7 h p.i. The results (Fig. 2A) show that replication of MHV, as determined by the luciferase

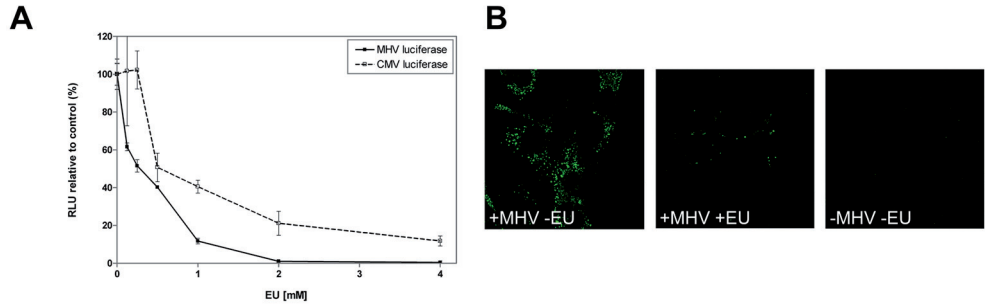

Figure 2. MHV replication is inhibited by prolonged labeling of cells with EU. (A) LR7 cells were either infected with MHV-EFLM at a MOI of 10 or transfected with a plasmid expressing *Gaussia* luciferase, followed by treatment with different concentrations of EU from 2 till 7 h p.i. After lysis, the luciferase activity was determined and plotted as a percentage normalized to the control. The error bars indicate the standard error of the mean. (B) Immunofluorescence analysis of dsRNA synthesis in MHV-infected LR7 cells after EU labeling from 2-6 h p.i. in the presence of actinomycin D. A negative control is also shown.

expression levels, was inhibited by EU in a concentration dependent manner. Similarly, expression of a *Gaussia* luciferase reporter enzyme under the control of a CMV promoter was also affected by addition of EU to the cells. To confirm these results, we also analyzed the inhibition of MHV replication by EU by performing immunofluorescence analysis using dsRNA specific antibodies. As shown in Fig. 2B, dsRNA was detected in cells infected with MHV, but not in mock-infected cells. When EU had been present from 2 to 6 h p.i., clearly much less dsRNA was present in the infected cells, consistent with the reduced luciferase expression levels. These results indicate that MHV RNA synthesis and/or translation is affected by feeding cells with EU. However, this inhibition is not specific for the viral RNAs as also the synthesis of a reporter enzyme expressed under the control of a CMV promotor was affected.

Newly synthesized viral RNA localizes to RTCs but not to stress granules

Copper (I)-catalyzed click chemistry has been reported to affect the detection of GFP fluorescence (Invitrogen). To study whether detection of EU labeling and of GFP fluorescence was compatible in our experiments, we analyzed the expression of newly synthesized RNAs by EU labeling in cells infected with a recombinant MHV, which expresses an additional expression cassette encoding GFP-tagged nsp2 (MHV-nsp2GFP). Nsp2-GFP was previously shown by electron microscopy to localize to the replicative structures (DMVs and CMs) induced by MHV in infected cells (13). As can be seen in Fig. 3A, perinuclear nsp2-GFP fluorescence was evident in combination with newly synthesized viral RNA using copper (I)-dependent click chemistry,

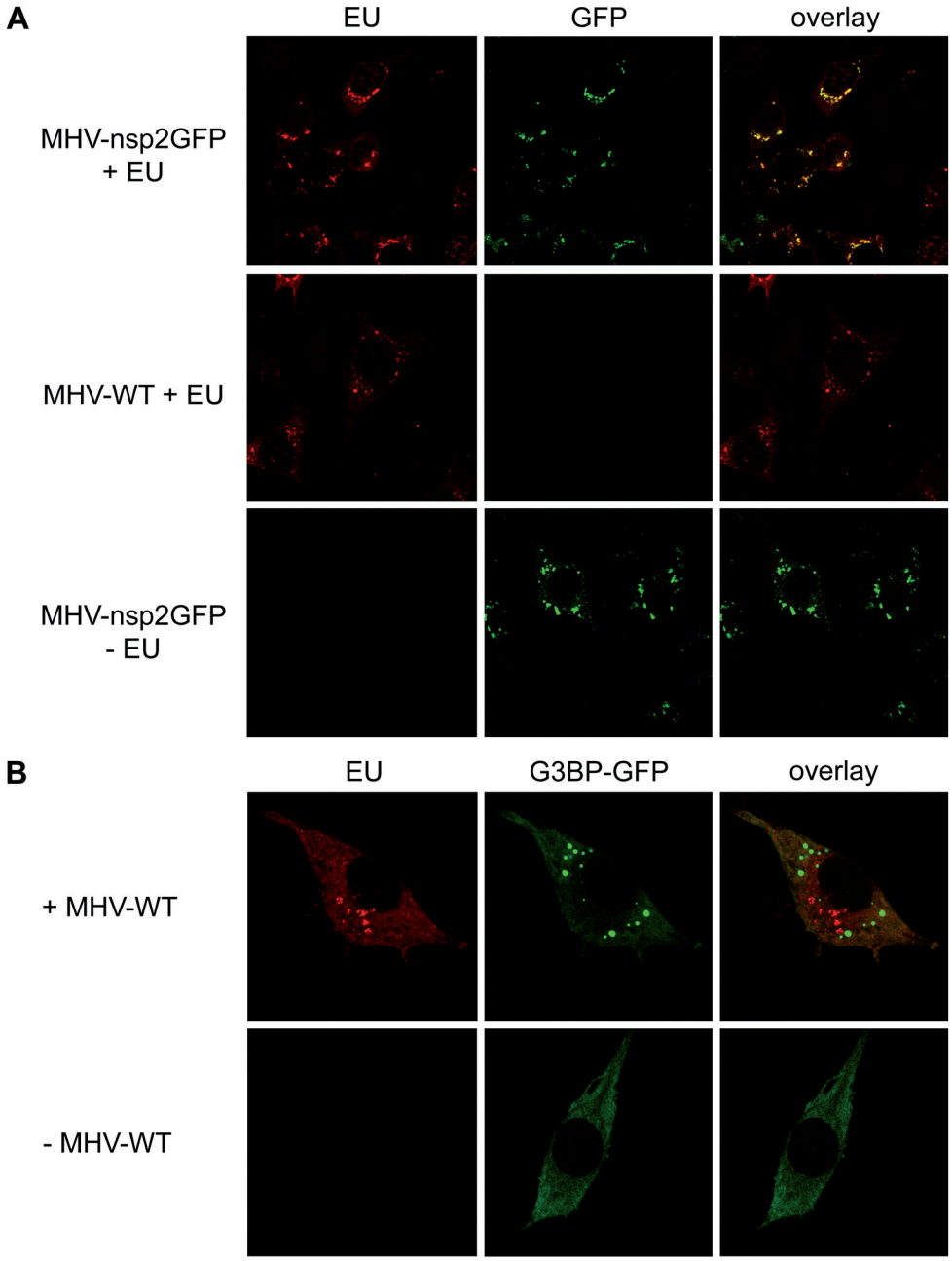

Figure 3. Nascent viral RNA localizes to nsp2GFP-positive foci but is excluded from stress granules. (A) LR7 cells were infected with either MHV-nsp2GFP or MHV-WT at a MOI of 10. At 7 h p.i., cells were labeled for 45 min with EU, fixed and subsequently processed for immunofluorescence analysis. (B) Prior to infection with MHV-WT, cells were transfected with a plasmid expressing the stress granule marker G3BP-GFP, labeled for 45 min at t = 7 h p.i., fixed and subsequently processed for immunofluorescence analysis.

although the fluorescent signal was somewhat lower than in non-treated cells (compare the top row with the bottom row of Fig. 3A). The newly synthesized RNA colocalized with the nsp2-GFP fluorescent foci, confirming that this fusion protein when expressed *in trans* localized to the structures involved in viral RNA synthesis (13).

The compatibility of fluorescence detection of GFP and viral RNAs allowed us to study to what extent the viral RNAs were localizing to stress granules in infected cells. Stress granules are cytoplasmic foci containing mRNAs stalled in translation (17). MHV is known to induce these cytoplasmic structures in infected cells (24). As is shown in Fig. 3B, the stress granule marker G3BP-GFP was distributed throughout the cytoplasm in non-infected cells, indicating the absence of stress granules. In infected cells, the protein concentrated in cytoplasmic foci corresponding to stress granules. Clearly, the newly synthesized RNA was not localizing to these foci indicating that EU-positive foci do not correspond to stress granules and that it is not nascent viral RNAs that accumulate in stress granules.

Colocalization of nascent viral RNA with dsRNA and nsp2/3

As a next step, we evaluated the possibility of combining the EU-mediated detection of nascent viral RNAs with immunocytochemistry using antibodies directed to viral components. Strikingly, the EU labeling was readily detected without, but not with additional immunofluorescence staining of dsRNA in MHV-infected cells (Fig. 4). However, when we added an inhibitor of RNase-A like enzymes (RNasin), the EU signal was preserved after immunofluorescence analysis of viral proteins and/or dsRNA. We hypothesize that the EU-containing viral RNAs are sensitive to RNases present in one of the components used in the immunocytochemical assay, presumably the FCS. Interestingly, we never observed a similar sensitivity when detecting dsRNA by immunofluorescence analysis. From these results we conclude that EU is mainly incorporated into RNase-sensitive, single-stranded RNA and not to detectable levels into dsRNA.

When performing the analyses described above, we noticed that the dsRNA foci were distributed in the infected cells in one of two distinct patterns, as exemplified in Fig. 5A. When cells were fixed at 6 h p.i., dsRNA foci were either spread throughout the cytoplasm or appeared to be more concentrated in perinuclear foci. Interestingly, the newly synthesized RNAs appeared to colocalize to a larger extent with the dsRNA foci when present in the concentrated patches. To extend these observations, we performed a timecourse experiment in which cells were EU-labeled for 45 min at different

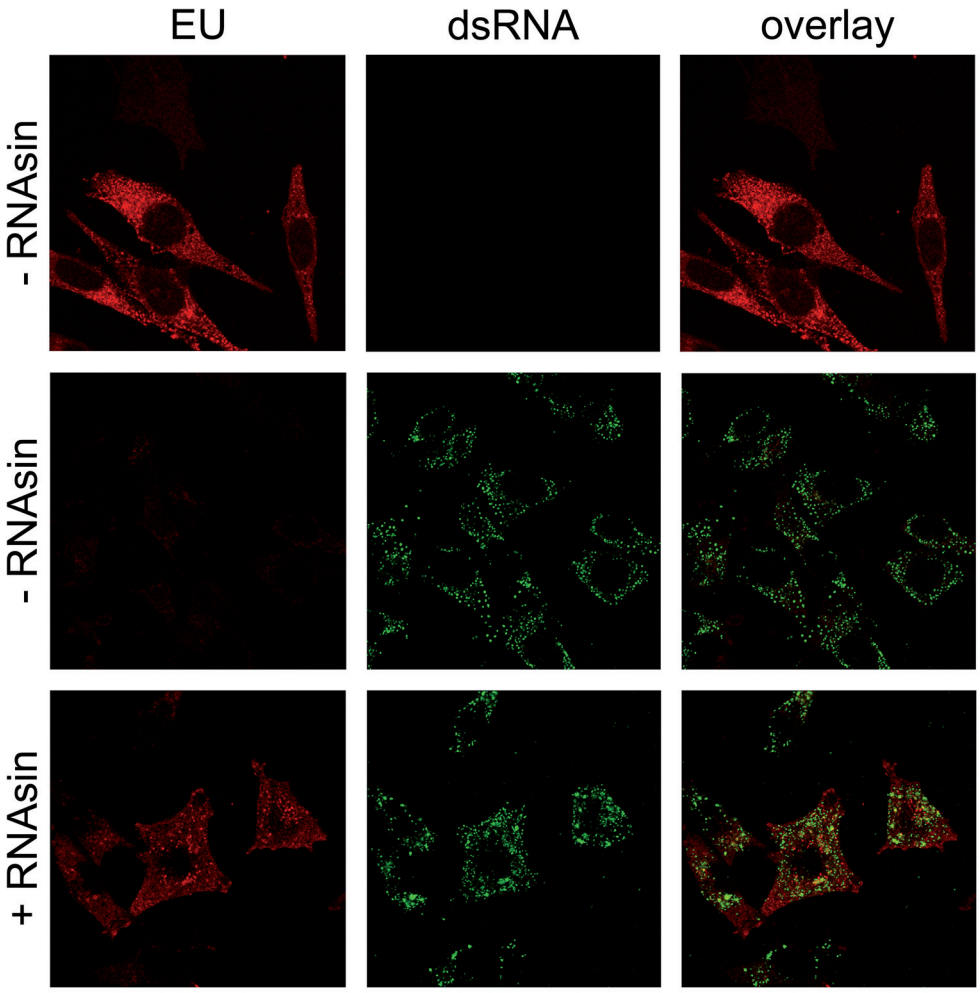

Figure 4. EU-labeled viral RNAs are more sensitive to RNAse than dsRNA. LR7 cells were infected with MHV-WT at a MOI of 10, followed by EU labeling for 45 min at 6 h p.i., fixed and processed for immunofluorescence analysis using antibodies directed against dsRNA, either in the presence or in the absence of RNase inhibitors (RNasin).

times p.i., after which the cells were fixed and processed for EU visualization and for immunofluorescence detection of dsRNA (see Fig. 5B). At early time points p.i. (4.15-5 h p.i.) the concentrated patches of dsRNA were observed, while at later time points (8.15-9 h p.i.), when RNA synthesis has started to decline, mainly the dispersed pattern of dsRNA foci was detected. Colocalization of newly synthesized RNA with dsRNA was more apparent at early than at later infection times. Close inspection of magnifications of cells at early times (for an example see Fig. 6A) revealed that the EU labeling and dsRNA foci were present at closely adjacent locations rather than at identical

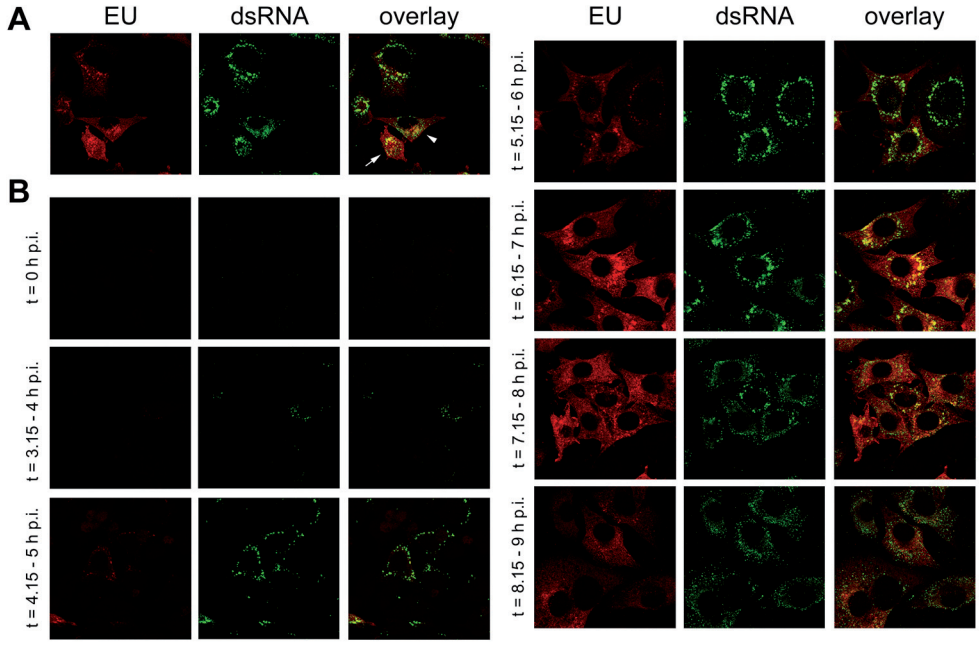

Figure 5. Time-course analysis of dsRNA and nascent viral RNA in MHV-infected cells. (A and B) LR7 cells were infected with MHV-WT at a MOI of 10, EU-labeled at the indicated times p.i. for 45 min, fixed and processed for immunofluorescence detection of EU and dsRNA. The arrowhead and the arrow in the cells indicate dispersed foci and concentrated perinuclear foci, respectively.

sites. At the later times, the EU labeling did not appear to correlate to the same extent with the dsRNA foci now spread throughout the cell. Many dsRNA foci were not located adjacent to newly synthesized RNA, indicating that they were transcriptionally silent. In addition, the EU labeling was more spread throughout the cell, while foci containing concentrated EU labeling were located at areas in the cell that were devoid of bright dsRNA dots. This observation was confirmed by determining the Pearson's correlation coefficients of the two fluorescent signals at early and late time points of infection (Fig. 6B). The Pearson's correlation coefficient is one of the standard parameters used in pattern recognition to describe the degree of overlap between two patterns. A relatively high correlation was found at the early time point p.i. (~ 0,60), while this correlation dropped significantly (P = 0.004) at the later time point (~ 0,33).

To further extend these observations, we performed a triple fluorescent labeling experiment in which, in addition to the EU labeling and dsRNA detection, also the nsp2/3 proteins were visualized (Fig. 7A). Antibodies to these nsps label the coronavirus replicative structures (DMVs and CMs) as has been demonstrated by immunoelectron microscopy (38). While at the

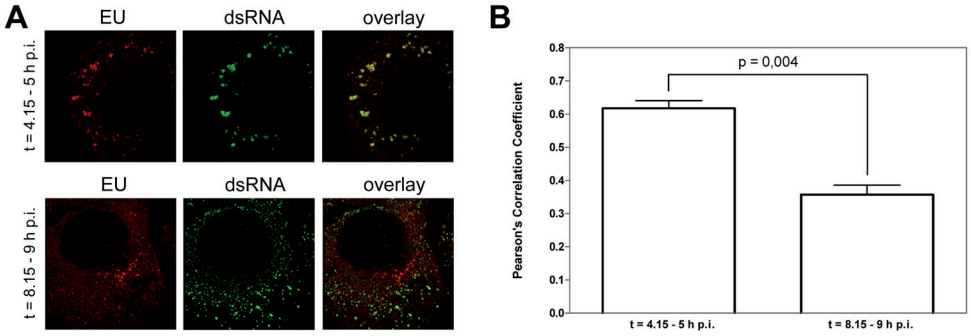

Figure 6. Distinct dsRNA patterns at early and late times of infection. (A) Magnification of individual infected cells that were fed with EU either at the early time points (4 or 5 h p.i.) or at the later time points (8 or 9 h p.i.). EU-labeling and dsRNA staining is shown (see also the legend of Fig. 5.). (B) Quantification of the colocalization by determining the Pearson's correlation coefficients of EU and dsRNA at both the early and the late times (n = 4). Error bars indicate the standard error of the mean.

early time point, the signals for EU, dsRNA and nsp2/3 labeling colocalized or were closely juxtaposted, this picture was much less apparent at the later times. The observation was again confirmed by determining the Pearson's correlation coefficients between the different staining patterns, which were all significantly lower at the later time points (see Fig. 7B).

Dispersal of dsRNA does not depend on a functional microtubular or actin network

Previously, we demonstrated that nsp2-GFP positive foci are mobile and move through MHV-infected cell using microtubular tracks (13). Hence, we hypothesized that the dispersal of the dsRNA foci might be dependent on an intact microtubular network as well. Therefore the (co)localization of the EU labeling and the dsRNA foci was analyzed when cells were (mock)-treated with 1 μM nocodazole, a microtubule disturbing agent. Disruption of the microtubular network by the drug was confirmed by immunofluorescence analysis of α-tubulin (data not shown). As a control, we also stained for the nsp2/3 proteins and found, consistent with our previous results (13), the nsp2/3 positive foci to be concentrated in the perinuclear region in the absence, but much less so in the presence of nocodazole, as illustrated in Fig. 8A. However, the dispersal of the dsRNA foci was not affected by nocodazole. From these results we conclude that dispersal of the dsRNA foci is not dependent on an intact microtubular network. Subsequently, we investigated whether intact actin filaments were required for the dispersal of the dsRNA foci. To this end, we (mock)-treated cells with 20 μM of cytochalasin B or with 1 μM of

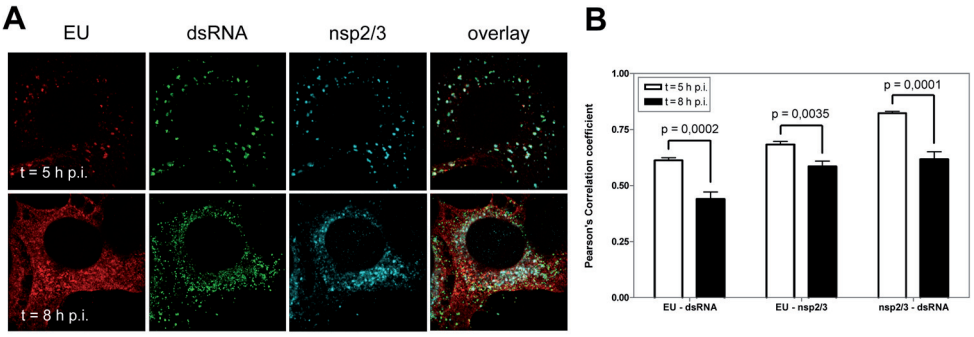

Figure 7. Temporal analysis of colocalization of EU with dsRNA and nsp2/3. LR7 cells were infected with MHV-WT at a MOI of 10 and labeled with EU for 45 min starting at 5 or 8 h p.i., fixed and processed for EU visualization and immunofluorescence using antibodies against dsRNA or nsp2/3 (A). Quantification of the colocalization of EU–dsRNA, EU–nsp2/3 and nsp2/3–dsRNA was performed by calculation of the Pearson's correlation coefficients for both the early and the late times p.i. (n = 6). Error bars indicate the standard error of the mean.

jasplakinolide to disrupt the actin network in MHV-infected cells. Complete disruption of the actin filaments was observed in these cells (data not shown). In mock-treated cells, the localization of nsp2/3 and dsRNA was similar to the previous observations in the earlier experiments (Fig. 8B). Treatment of infected cells with jasplakinolide or cytochalasin B did not inhibit the dispersal of the dsRNA foci at the late infection times (Fig. 8B). Furthermore, disruption of the actin filaments also resulted in the dispersal of the nsp2/3-positive fluorescent foci, also at early times. In conclusion, dispersal of the dsRNA foci is not dependent on a functional microtubular or actin network whereas both networks appear to be required for the efficient perinuclear accumulation of the nsp2/3-positive foci.

Identifying the active sites of viral RNA replication

Our results indicated that not all DMVs, despite them being the structures that harbor the dsRNAs, are actively involved in RNA synthesis. On the other hand, while, the EU-positive foci may very well correspond with active RTCs, the EU-labeled nascent RNAs might as well be transported away from their original sites of synthesis. As several foci containing the EU labeling at the later time points did not display apparent colocalization with the dsRNA dots, these EU-positive foci might correspond to the virion assembly sites, where newly synthesized genomic RNA is packaged into budding virions. Because the membrane (M) protein is the key player in the assembly of progeny virions (6), we studied the relative localization of the EU label and the M protein. No colocalization between nascent RNA and M proteins was

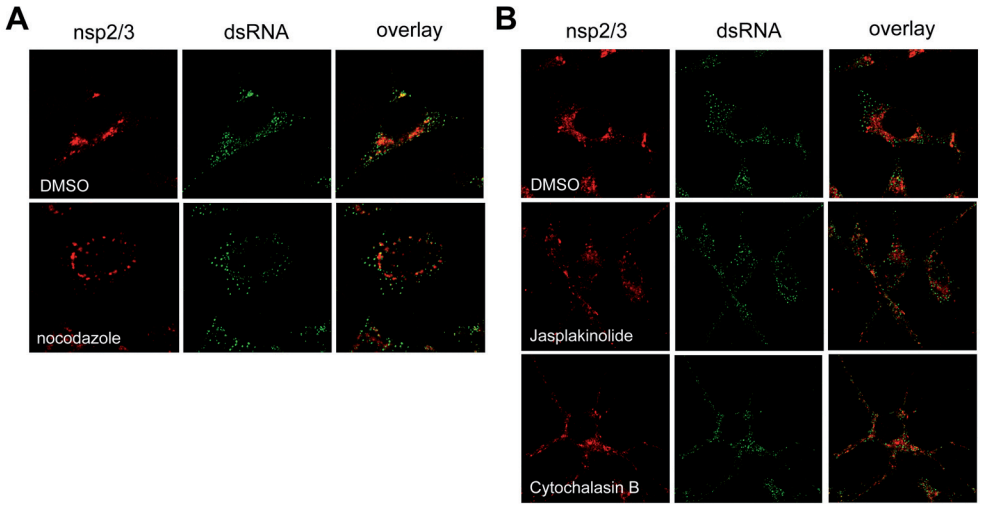

Figure 8. Microtubule- and actin-independent movement of dsRNA foci. LR7 cells were infected with MHV-WT at a MOI of 10 and labeled for 45 min starting at 7 h p.i. either in the presence or in the absence (DMSO) of 1 μM nocodazole (A), 20 μM cytochalasin B, or 1 μM jasplakinolide (B), to disrupt the microtubular or actin network, respectively, followed by fixation and processing for EU visualization and immunofluorescence using antibodies against nsp2/3 or dsRNA. The cytoskeleton-disrupting drugs were added to the culture media from 2 h p.i. onwards.

observed, neither at early nor at late times of infection, thereby excluding this possibility (data not shown).

To confirm that EU positive foci indeed correspond to the active sites of CoV RNA synthesis we investigated whether the CoV RdRp (residing in nsp12) was also present at these sites. As shown in Fig. 9, early in infection nascent RNAs (EU labeling) and dsRNA dots colocalized with each other and with nsp12. At later time points, dsRNA dots were dispersed throughout the cell and RNA synthesis was decreased although foci of EU labeling were readily detectable in many cells, which is in agreement with our previous results. At this later time point, the nsp12 staining appeared less intense and somewhat more dispersed. However, EU-positive foci were still clearly colocalizing with nsp12 at this stage. *Vice versa*, not all nsp12 staining was associated with EU-positive foci, which was most apparent in cells exhibiting only very limited viral RNA synthesis. Taken together, our results indicate that foci of EU-labeled viral RNAs correspond with active RTCs as they colocalize with the RdRp throughout the infection. Furthermore, our results indicate that while at early time points the RdRp is a good marker for sites of active RNA synthesis, this is not the case at late stages, when viral RNA synthesis is decreasing.

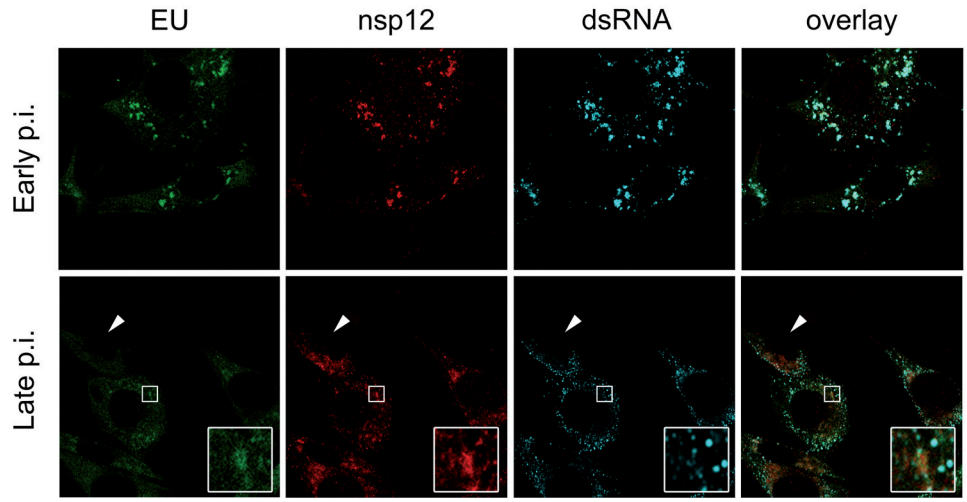

Figure 9. Identifying the active sites of CoV RNA synthesis. LR7 cells were infected with MHV-WT at a MOI of 10, EU-labeled at early and late times p.i. and fixed and processed for immunofluorescence detection of EU, dsRNA and nsp12. Arrowhead indicates a nsp12-postive cell lacking most EU labeling and the white boxes indicate examples of colocalization of EU and nsp12-positive foci at late times of infection.

DISCUSSION

To visualize viral RNA (synthesis) at the (sub)cellular level in infected cells, various methods have been used, like *in situ* hybridization -using fluorescently labeled probes- or dsRNA detection –using antibodies specific for dsRNA- and have been of great value but provide information only on the steady state localization of specific RNA species. For the plus-strand RNA viruses, dsRNAs are thought to function as intermediates in RNA synthesis (23, 31) and have been shown to localize to the membrane-wrapped compartments dedicated to this process (18). Analysis of transcription rates of nascent RNAs, however, requires the labeling of newly synthesized RNAs with tritiated nucleotides or with uridine analogs, such a 5-bromouridine (BrU). BrU is usually delivered to cells as BrUTP. However, as BrUTP is not taken up by cells, labor intensive and cumbersome delivery methods such as microinjection or liposome transfection of BrUTP are needed. In the present study we have employed yet another, novel method suitable for the detection of nascent RNAs, based on the biosynthetic incorporation of an alkyne-modified EU, followed by click chemistry to attach fluorescent azide derivatives to the synthesized RNA. We show that this method is suitable for the specific visualization of newly synthesized coronaviral RNAs in the

presence of actinomycin D. Furthermore, we show that this method can be combined with the detection of viral and host proteins by using GFP-tags or immunohistochemistry. Our results indicate that foci of EU labeling correspond with active sites of coronaviral RNA synthesis throughout the infection. In contrast, at later times of infection many dsRNA-positive foci, the presumed intermediates generated during plus-strand RNA virus replication, as well as foci positive for the RdRP-containing protein nsp12 do not correspond with coronaviral replicative structures actively involved in RNA synthesis.

Upon infection, CoVs induce a network of DMVs, which harbor dsRNA, and CMs. It is not clear, however, which of these structures are actually associated with the biosynthesis of the CoV RNA, even though BrUTP incorporation was detected in the vicinity of the presumed CoV-induced DMVs (12). Although dsRNA molecules function as intermediates of replication or transcription, their presence at certain sites *per se* does not imply (all) these structures to be actively involved in RNA synthesis. Likewise, the location of viral enzymes that are required for RNA synthesis does not need to correlate with active RTCs. Moreover, nascent RNAs are not necessarily located at their site of synthesis as they may diffuse or be transported away to other subcellular locations. Even so, our results indicate that foci of nascent RNAs detected in MHV-infected cells correspond with sites of active coronaviral RNA synthesis. Although the colocalization of EU-labeling with nsp2/3 and dsRNA, which was obvious early in infection (Fig. 6 and 7), appeared to decrease in time, the foci of nascent RNAs colocalized with the RdRp-containing nsp12 throughout the infection (Fig. 9). Furthermore, these foci did not colocalize with a marker for stress granules (Fig. 3), i.e., cytoplasmic structures containing mRNAs halted in their translation (17), which are induced upon infection with MHV (24) or with the M protein, which is the key player in viral assembly (data not shown). As an obvious next step, it will be interesting to further characterize the site(s) of coronaviral RNA synthesis at the ultrastructural level. We are currently initiating such studies.

Simultaneous visualization of dsRNA, which is localized to the DMV interior (18), and EU incorporation revealed that while early in infection nascent RNAs were found colocalizing at or adjacent to patches of dsRNA dots, this correlation was much less apparent at later times when the dsRNA dots had spread throughout the cell. Many dsRNA dots were apparently not transcriptionally active as no EU labeling was associated with them, while many foci of EU labeling did not appear to colocalize with the dsRNA dots. Since dsRNA molecules are known to function as intermediates in replication

and transcription, it is conceivable that at later times, when RNA synthesis has decreased, DMVs (or other structures) actively involved in RNA synthesis contain only little dsRNA resulting in less apparent colocalization of dsRNA and EU labeling. However, the results may also be explained by assuming that the DMVs are not actively involved in RNA synthesis but harbor dsRNAs that are not (longer) functioning as intermediates in RNA synthesis. In other words, dsRNA-containing DMVs may represent non-functional end-stage structures. According to this model, the DMVs might serve the important function of shielding dsRNA molecules from the innate immune system of the cell (16). In agreement herewith is the apparent lack of obvious pores that connect their inside with the cytoplasm. Also consistent are observations that CoVs prevent early induction of interferon synthesis (25, 43) presumably by keeping viral RNA away from host cell sensors (42). If DMVs would not be the active sites of RNA synthesis, the only plausible alternative would be the CMs. These latter structures harbor most nsps studied to date (18, 38) although nsp12 (RdRp) has not been localized at the ultrastructural level yet, and may provide the RTCs with the membrane-protective environment (39). Of note, these different models do not necessarily exclude each other as DMVs may be the initial site of active RNA synthesis, particularly early in infection, while at a later state the membranes become sealed and connections are lost and RNA synthesis shifts to the CM assemblies.

Whatever model is correct, our results show that the CoV replicative structures evolve over time as exemplified by the changing relations between different components (dsRNA, nsps and nascent RNA). Accordingly, others have reported the segregation of MHV replicase proteins and viral RNA into distinct populations of intracellular membranes (35), which became physically separated during the course of infection (3). Maturation of the CoV RTCs, which may involve processing of the replicase polyproteins, has also been suggested by others to be important in regulating the plus- and minus-strand RNA synthesizing capacity of the RTCs (29, 32). One of the most notable changes during infection in our experiments was the dispersal of the dsRNA-containing DMVs. These changes, however, are difficult to reconcile with the previous observation of the DMVs forming an interconnected network via their outer membranes (18). We expect that more extensive electron tomography studies as well as correlative light electron microscopy, ideally combined with labeling of nascent RNAs, will be required to really understand the biogenesis, maturation and function of these remarkable structures.

ACKNOWLEDGEMENTS

We thank Richard Wubbolts and Esther van 't Veld from the Center for Cell Imaging of the Utrecht Faculty of Veterinary Medicine for technical support and Oliver Wicht and Christine Burkard for stimulating discussions. We thank Mark Denison and Susan Baker for kindly providing antibodies. This work was supported by grants from the Netherlands Organization for Scientific Research (NWO-ALW) and the Utrecht University (High Potential) to C. A. M. de Haan and F. R. Reggiori. The funding source had no role in the study design, data collection, analysis, interpretation or writing of this article.

REFERENCES

1. Baliji, S., S. A. Cammer, B. Sobral, and S. C. Baker. 2009. Detection of nonstructural protein 6 in murine coronavirus-infected cells and analysis of the transmembrane topology by using bioinformatics and molecular approaches. J Virol. 83:6957-62.

2. Bolte, S., and F. P. Cordelieres. 2006. A guided tour into subcellular colocalization analysis in light microscopy. J. Microsc. 224:213-232. doi: 10.1111/j.1365-2818.2006.01706.x.

3. Bost, A. G., E. Prentice, and M. R. Denison. 2001. Mouse hepatitis virus replicase protein complexes are translocated to sites of M protein accumulation in the ERGIC at late times of infection. Virology. 285:21-29. doi: 10.1006/viro.2001.0932.

4. Bost, A. G., R. H. Carnahan, X. T. Lu, and M. R. Denison. 2000. Four Proteins Processed from the Replicase Gene Polyprotein of Mouse Hepatitis Virus Colocalize in the Cell Periphery and Adjacent to Sites of Virion Assembly. J. Virol. 74:3379-3387. doi: 10.1128/JVI.74.7.3379-3387.2000.

5. Brockway, S. M., C. T. Clay, X. T. Lu, and M. R. Denison. 2003. Characterization of the expression, intracellular localization, and replication complex association of the putative mouse hepatitis virus RNA-dependent RNA polymerase. J Virol. 77:10515-27.

6. de Haan, C. A., and P. J. Rottier. 2005. Molecular interactions in the assembly of coronaviruses. Adv. Virus Res. 64:165-230. doi: 10.1016/S0065-3527(05)64006-7.

7. de Haan, C. A., L. van Genne, J. N. Stoop, H. Volders, and P. J. Rottier. 2003. Coronaviruses as vectors: position dependence of foreign gene expression. J. Virol. 77:11312-11323.

8. den Boon, J. A., and P. Ahlquist. 2010. Organelle-like membrane compartmentalization of positive-strand RNA virus replication factories. Annu. Rev. Microbiol. 64:241-256. doi: 10.1146/annurev.micro.112408.134012.

9. den Boon, J. A., A. Diaz, and P. Ahlquist. 2010. Cytoplasmic viral replication complexes. Cell. Host Microbe. 8:77-85. doi: 10.1016/j.chom.2010.06.010.

10. Denison, M. R., W. J. Spaan, Y. van der Meer, C. A. Gibson, A. C. Sims, E. Prentice, and X. T. Lu. 1999. The putative helicase of the coronavirus mouse hepatitis virus is processed from the replicase gene polyprotein and localizes in complexes that are active in viral RNA synthesis. J. Virol. 73:6862-6871.

11. Gillespie, L. K., A. Hoenen, G. Morgan, and J. M. Mackenzie. 2010. The endoplasmic reticulum provides the membrane platform for biogenesis of the flavivirus replication complex. J. Virol. 84:10438-10447. doi: 10.1128/JVI.00986-10.

12. Gosert, R., A. Kanjanahaluethai, D. Egger, K. Bienz, and S. C. Baker. 2002. RNA replication of mouse hepatitis virus takes place at double-membrane vesicles. J. Virol. 76:3697-3708.

13. Hagemeijer, M. C., M. H. Verheije, M. Ulasli, I. A. Shaltiel, L. A. de Vries, F. Reggiori, P. J. Rottier, and C. A. de Haan. Dynamics of coronavirus replication-transcription complexes. J Virol. 84:2134-49.

14. Jao, C. Y., and A. Salic. 2008. Exploring RNA transcription and turnover in vivo by using click chemistry. Proc. Natl. Acad. Sci. U. S. A. 105:15779-15784.doi: 10.1073/pnas.0808480105.

15. Kanjanahaluethai, A., Z. Chen, D. Jukneliene, and S. C. Baker. 2007. Membrane topology of murine coronavirus replicase nonstructural protein 3. Virology. 361:391-401.

16. Kawai, T., and S. Akira. 2008. Toll-like receptor and RIG-I-like receptor signaling. Ann. N. Y. Acad. Sci. 1143:1-20. doi: 10.1196/annals.1443.020.

17. Kedersha, N., G. Stoecklin, M. Ayodele, P. Yacono, J. Lykke-Andersen, M. J. Fritzler, D. Scheuner, R. J. Kaufman, D. E. Golan, and P. Anderson. 2005. Stress granules and processing bodies are dynamically linked sites of mRNP remodeling. The Journal of Cell Biology. 169:871-884. doi: 10.1083/jcb.200502088.

18. Knoops, K., M. Kikkert, S. H. E. Van Den Worm, J. C. Zevenhoven-Dobbe, Y. Van Der Meer, A. J. Koster, A. M. Mommaas, and E. J. Snijder. 2008. SARS-coronavirus replication is supported by a reticulovesicular network of modified endoplasmic reticulum. PLoS Biology. 6:1957-1974.

19. Kopek, B. G., G. Perkins, D. J. Miller, M. H. Ellisman, and P. Ahlquist. 2007. Three-dimensional analysis of a viral RNA replication complex reveals a virus-induced mini-organelle. PLoS Biol. 5:e220. doi: 10.1371/journal.pbio.0050220.

20. Kuo, L., G. J. Godeke, M. J. Raamsman, P. S. Masters, and P. J. Rottier. 2000. Retargeting of coronavirus by substitution of the spike glycoprotein ectodomain: crossing the host cell species barrier. J Virol. 74:1393-406.

21. Lai, M. M., P. R. Brayton, R. C. Armen, C. D. Patton, C. Pugh, and S. A. Stohlman. 1981. Mouse hepatitis virus A59: mRNA structure and genetic localization of the sequence divergence from hepatotropic strain MHV-3. J. Virol. 39:823-834.

22. Oostra, M., M. C. Hagemeijer, M. van Gent, C. P. Bekker, E. G. te Lintelo, P. J. Rottier, and C. A. de Haan. 2008. Topology and membrane anchoring of the coronavirus replication complex: not all hydrophobic domains of nsp3 and nsp6 are membrane spanning. J Virol. 82:12392-405.

23. Oostra, M., E. G. te Lintelo, M. Deijs, M. H. Verheije, P. J. Rottier, and C. A. de Haan. 2007. Localization and membrane topology of coronavirus nonstructural protein 4: involvement of the early secretory pathway in replication. J Virol. 81:12323-36.

24. Raaben, M., M. J. Groot Koerkamp, P. J. Rottier, and C. A. de Haan. 2007. Mouse hepatitis coronavirus replication induces host translational shutoff and mRNA decay, with concomitant formation of stress granules and processing bodies. Cell. Microbiol. 9:2218-2229. doi: 10.1111/j.1462-5822.2007.00951.x.

25. Raaben, M., M. J. Groot Koerkamp, P. J. Rottier, and C. A. de Haan. 2009. Type I interferon receptor-independent and -dependent host transcriptional responses to mouse hepatitis coronavirus infection in vivo. BMC Genomics. 10:350. doi: 10.1186/1471-2164-10-350.

26. Rasband, W. 1997-2008. ImageJ. U S National Institutes of Health, Bethesda, Maryland, USA, Http://rsbinfonihgov/ij/, 1997-2008. .

27. Reggiori, F., I. Monastyrska, M. Verheije H., T. Calì, M. Ulasli, S. Bianchi, R. Bernasconi, C. de Haan A.M., and M. Molinari. 2010. Coronaviruses Hijack the LC3-I-Positive EDEMosomes, ER-Derived Vesicles Exporting Short-Lived ERAD Regulators, for Replication. Cell Host & Microbe. 7:500.

28. Sawicki, D., T. Wang, and S. Sawicki. 2001. The RNA structures engaged in replication and transcription of the A59 strain of mouse hepatitis virus. J. Gen. Virol. 82:385-396.

29. Sawicki, S. G., and D. L. Sawicki. 1986. Coronavirus minus-strand RNA synthesis and effect of cycloheximide on coronavirus RNA synthesis. J. Virol. 57:328-334.

30. Sawicki, S. G., and D. L. Sawicki. 1995. Coronaviruses use discontinuous extension for synthesis of subgenome-length negative strands. Adv. Exp. Med. Biol. 380:499-506.

31. Sawicki, S. G., D. L. Sawicki, and S. G. Siddell. 2007. A contemporary view of coronavirus transcription. J Virol. 81:20-9.

32. Sawicki, S. G., D. L. Sawicki, D. Younker, Y. Meyer, V. Thiel, H. Stokes, and S. G. Siddell. 2005. Functional and genetic analysis of coronavirus replicase-transcriptase proteins. PLoS Pathog. 1:e39. doi: 10.1371/journal.ppat.0010039.

33. Schonborn, J., J. Oberstrass, E. Breyel, J. Tittgen, J. Schumacher, and N. Lukacs. 1991. Monoclonal antibodies to double-stranded RNA as probes of RNA structure in crude nucleic acid extracts. Nucleic Acids Res. 19:2993-3000.

34. Shi, S. T., J. J. Schiller, A. Kanjanahaluethai, S. C. Baker, J. W. Oh, and M. M. Lai. 1999. Colocalization and membrane association of murine hepatitis virus gene 1 products and De novo-synthesized viral RNA in infected cells. J Virol. 73:5957-69.

35. Sims, A. C., J. Ostermann, and M. R. Denison. 2000. Mouse Hepatitis Virus Replicase Proteins Associate with Two Distinct Populations of Intracellular Membranes. J. Virol. 74:5647-5654. doi: 10.1128/JVI.74.12.5647-5654.2000.

36. Snijder, E. J., Y. van der Meer, J. Zevenhoven-Dobbe, J. J. Onderwater, J. van der Meulen, H. K. Koerten, and A. M. Mommaas. 2006. Ultrastructure and origin of membrane vesicles associated with the severe acute respiratory syndrome coronavirus replication complex. J Virol. 80:5927-40.

37. Taguchi, F., and J. O. Fleming. 1989. Comparison of six different murine coronavirus JHM variants by monoclonal antibodies against the E2 glycoprotein. Virology. 169:233-235.

38. Ulasli, M., M. H. Verheije, C. A. de Haan, and F. Reggiori. 2010. Qualitative and quantitative ultrastructural analysis of the membrane rearrangements induced by coronavirus. Cell. Microbiol. 12:844-861. doi: 10.1111/j.1462-5822.2010.01437.x.

39. van Hemert, M. J., S. H. van den Worm, K. Knoops, A. M. Mommaas, A. E. Gorbalenya, and E. J. Snijder. 2008. SARS-coronavirus replication/transcription complexes are membrane-protected and need a host factor for activity in vitro. PLoS Pathog. 4:e1000054. doi: 10.1371/journal.ppat.1000054.

40. Verheije, M. H., M. Raaben, M. Mari, E. G. Te Lintelo, F. Reggiori, F. J. van Kuppeveld, P. J. Rottier, and C. A. de Haan. 2008. Mouse hepatitis coronavirus RNA replication depends on GBF1-mediated ARF1 activation. PLoS Pathog. 4:e1000088.

41. Verheije, M. H., M. C. Hagemeijer, M. Ulasli, F. Reggiori, P. J. M. Rottier, P. S. Masters, and C. A. M. de Haan. 2010. The coronavirus nucleocapsid protein is dynamically associated with the replication-transcription complexes. J. Virol. . doi: 10.1128/JVI.00569-10.

42. Versteeg, G. A., P. J. Bredenbeek, S. H. van den Worm, and W. J. Spaan. 2007. Group 2 coronaviruses prevent immediate early interferon induction by protection of viral RNA from host cell recognition. Virology. 361:18-26. doi: 10.1016/j.virol.2007.01.020.

43. Versteeg, G. A., O. Slobodskaya, and W. J. Spaan. 2006. Transcriptional profiling of acute cytopathic murine hepatitis virus infection in fibroblast-like cells. J. Gen. Virol. 87:1961-1975. doi: 10.1099/vir.0.81756-0.

44. Welsch, S., S. Miller, I. Romero-Brey, A. Merz, C. K. Bleck, P. Walther, S. D. Fuller, C. Antony, J. Krijnse-Locker, and R. Bartenschlager. 2009. Composition and three-dimensional architecture of the dengue virus replication and assembly sites. Cell. Host Microbe. 5:365-375. doi: 10.1016/j.chom.2009.03.007.

Chapter 7

Summarizing Discussion

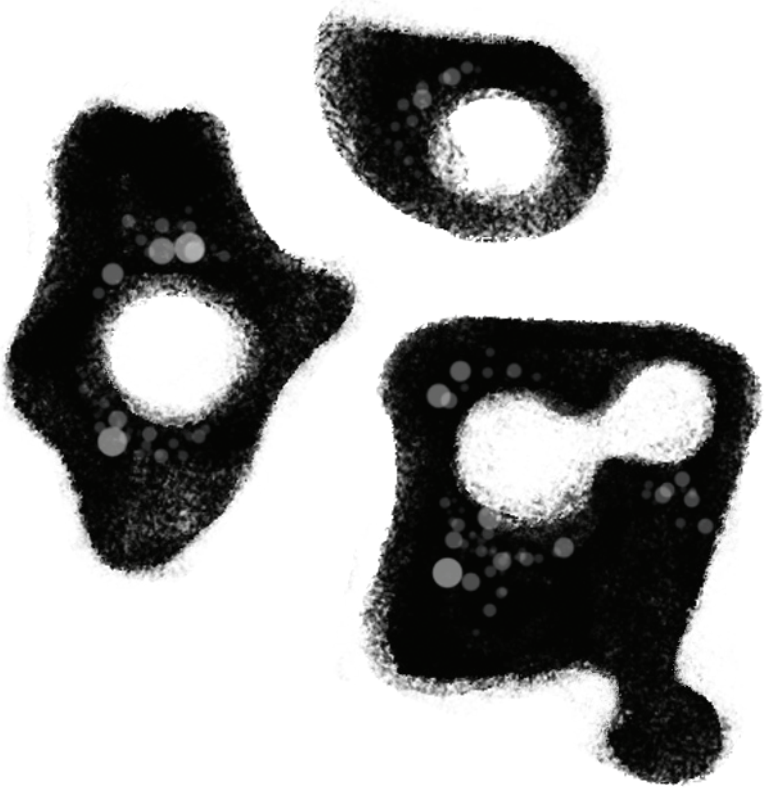

The replication of positive single-stranded RNA (+ ssRNA) viruses is intimately associated with host cellular membranes that are remodeled into organelle-like replicative structures to which the viral replication-transcription complexes (RTCs) associate. Coronaviruses (CoVs) are no exception as they induce the formation of an interconnected network of double membrane vesicles (DMVs) and convoluted membranes (CMs), i.e., the replicative structures, to both of which the nonstructural proteins (nsps) that are involved in RNA synthesis localize.

Insight into the biogenesis and functioning of these replicative structures/RTCs requires research of the properties of the individual components as well as of the complicated interplay between all constituents that make up these intricate structures. In this thesis, we have applied diverse techniques such as (co-)immunoprecipitation (coIP) analyses, confocal and electron microscopy (EM), live-cell imaging, and metabolic labeling of nascent viral RNAs in order to investigate different aspects of the CoV replicative structures and its individual components.

In this final chapter, the implications of our results will be discussed and placed in a broader perspective.

CoV-INDUCED MEMBRANE REARRANGEMENTS

Membrane topology of the CoV replicase polyproteins

CoVs encode three hydrophobic nonstructural proteins (nsps), nsp3, nsp4 and nsp6, which are hypothesized to play an important role in the biogenesis of the membranous structures associated with viral replication and in the anchoring of the RTCs to these structures. At the start of this work, detailed information on the membrane anchoring and topology of nsp3, nsp4 and nsp6 was lacking. The transmembrane domain predictions based on the multiple alignment of 27 CoV replicase polyprotein sequences presented in chapter 2, revealed an uneven number of hydrophobic domains for both nsp3 and nsp6. This prediction was peculiar as it separated the viral proteinases residing in nsp3 and nsp5 from their target sequences, implying that some of these hydrophobic domains might actually not span the membrane. Our experimental data presented in chapter 2 demonstrate that this is indeed the case. Contrary to the predictions all three transmembrane proteins have their amino terminus as well as their carboxy terminus exposed in the cytoplasm. While all four hydrophobic domains of nsp4 span the lipid bilayer, this is the case for only two of the three hydrophobic domains in nsp3 and six of the seven in nsp6. This experimentally established topology model obviously

makes more sense, as it positions all of the proteinase cleavage sites on the same side of the membrane as the viral proteinases themselves.

Whereas we were unable to determine whether the sixth or the seventh hydrophobic domain was actually membrane-spanning, Baliji *et al*. (2) showed that the seventh hydrophobic domain is most likely not crossing the lipid bilayer. The occurrence of conserved non-membrane spanning hydrophobic domains in nsp3 and nsp6, which are likely to be peripherally associated with the membrane, suggests an important function for these domains, possibly in the biogenesis of the CoV replicative structures. In this respect it is of interest to mention that the seventh hydrophobic domain of nsp6 contains putative palmitoylation sites [our own predictions and (2)]. The addition of palmitic acid to this hydrophobic domain may reinforce its peripheral membrane association.

Biogenesis of the replicative structures: protein interactions and hydrophobic domains

In chapter 5 we demonstrate that nsp3, nsp4, and nsp6 are engaged in homo- and heterotypic protein interactions and that co-expression of nsp4 with the C-terminal one-third part of nsp3 ($nsp3_C$) results in the relocalization of these proteins from the endoplasmic reticulum (ER) to the perinuclear region of the cell. Although nsp6 was not required for the observed relocalization, it was recruited to the perinuclear foci when co-expressed (unpublished results), in agreement with this protein interacting with nsp4 (chapter 5). Ultrastructural analysis of cells co-expressing nsp4 and $nsp3_C$ revealed membranous rearrangements with apposing membranes and spaghetti-like structures (unpublished results). However, these membrane rearrangements did not resemble the DMVs that have been reported for CoV-infected cells, which may not be surprising as only the C-terminal part of nsp3, which lacks a major, cytoplasmically expressed domain, was used in these co-expressions with nsp4, while the other membrane protein nsp6, was lacking entirely. Preliminary results indicate that some of the loops of nsp3 and nsp4 are crucial in the relocalization of these proteins (unpublished results). Membrane rearrangements were not observed when nsp3 of MHV and nsp4 of SARS-CoV, or *vice versa*, were co-expressed (unpublished results). While coIP and immunofluorescence assays indicate that nsp3 and nsp4 of MHV interact, this interaction could not be confirmed using the Venus protein-fragment complementation assay (PCA; chapter 5). We hypothesize that the interactions between nsp3 and nsp4 mediate some kind of "zippering" of the lipid bilayers of the ER, which ultimately leads to the formation of the DMVs.

In this model nsp3 and nsp4 interact via their luminal loops in such a way that their interaction prevents reconstitution of a functional Venus protein.

Several other studies also suggest an important role for nsp4 in the generation of the replicative structures. Although the fourth hydrophobic domain of nsp4 is dispensable, the other three transmembrane regions are required for CoV replication (69). In addition, disruption of the nsp4 glycosylation sites, which are present in the loop between the first and second hydrophobic region, leads to the formation of aberrant DMVs in which the inner and outer membranes are detached, together with an increase in number of CMs (22). Furthermore, although the topology of these proteins has not been studied in any detail, co-expression of the EAV nsp2 and nsp3 proteins (the EAV counterparts of CoV nsp3 and nsp4) in the form of a self-cleaving nsp2/3 polyprotein, resulted in the rearrangement of host cell membranes into DMVs, albeit with a morphology (68) differing from that observed in EAV-infected cells (53). Mutations of cysteine residues present in the luminal loop of EAV nsp3 resulted in altered morphologies of the DMVs, while the introduction of a *N*-glycosylation site in the loop also affected their morphology to some extent (55).

Similar to the CoVs, other + ssRNA viruses also somehow induce the membrane rearrangements that are required for their replication and transcription. For several of these viruses (co-)expression of nsps has been shown to result in membrane rearrangements similar to those observed in virus-infected cells [for reviews see (13, 14, 46)]. These proteins can be integral transmembrane proteins, examples being the NS4A proteins of Dengue virus (DENV) (45) and Kunjin virus (60) and the NS4B protein of hepatitis C virus (HCV) (18). Alternatively, they are only peripherally associated to the lipid bilayer, such as the 1a protein of brome mosaic virus (BMV) (15) and the 2C protein of poliovirus (PV) (17). Strikingly, however, also for the integral membrane proteins the occurrence of hydrophobic/amphipathic regions that do not span the lipid bilayer but are peripherally associated with membranes appears to be a common feature [chapter 2 and (41, 44, 45, 47)]. Yet another similarity, among the nsps of different + ssRNA viruses, appears to be the ability of these proteins to assemble into larger protein complexes. In chapter 5 we demonstrated that nsp3, nsp4 and nsp6 of CoVs are engaged in extensive homo- and heterotypic interactions. Such protein-protein interactions have also been reported for the nsps of other + ssRNA viruses, such as the BMV 1a protein (49, 50) and the flavivirus NS4A and NS4B proteins (42, 52).

How are the nsps of + ssRNA viruses able to induce the observed membrane rearrangements? We speculate that the similarities between the membrane-

associated nsps of different + ssRNA viruses relate to their common ability to remodel membranes. Rearrangement of host cellular membranes involves the induction of curvature in lipid bilayers. The membrane-associated viral proteins may act as multimeric scaffolds, that are able to impose curvature of the membrane protein(s) onto the lipid bilayers to which they associate, and/or act as wedges by inserting their amphipatic helices partially into one side of the bilayer [reviewed in (43, 66, 81)]. In this respect, the viral proteins may function similar to host cellular proteins known to induce membrane bending via a scaffold mechanism, as exemplified by the COPI and COPII complexes and/or via the insertion of amphipathic domains into the lipid bilayer, as has been proposed for the small GTPase Sar1, which is one of the core COPII proteins [reviewed in (43, 81)].

Replicative structures, host proteins and lipids: a largely unexplored territory

Remodeling of eukaryotic cellular membranes to generate the replicative structures is likely dependent on the combined effects of both viral and cellular proteins and probably also on the specific lipid composition of the membranes themselves. Nevertheless, only few studies have been published concerning the involvement of cellular constituents in CoV replication and the generation of the replicative structures. It is conceivable that CoVs, just like any other virus, hijack cellular pathways for their replication, consequently, adopting intrinsic properties of the utilized pathways themselves. Previous studies have demonstrated a role for several host proteins, involved in the formation of COPI and COPII coated vesicles such as Arf1, GBF1 (36, 75) and Sar1 (48), in CoV infection. Inhibition of the proteasome severely affected CoV RNA synthesis (57, 58). More recently, the LC3 protein was shown to be critically required for CoV replication, albeit independently of its known role in the cellular process of autophagy (59). MHV was proposed to hijack EDEMosomes, ER-derived vesicles involved in the transport of chaperones to lysosomes, for its replication (6, 7).

One of the difficulties associated with these studies is the complexity to discriminate whether host proteins are directly involved in the formation of the replicative structures themselves or in RNA synthesis *per se*, as inhibition of either process will result in reduced RNA synthesis, protein expression and DMV formation. To provide answers to these questions assays are needed in which the formation of replicative structures can be studied independent of viral replication. One such assay may be provided by co-expression of $nsp3_C$ with nsp4 (chapter 5), which resulted in the rearrangement of cellular membranes, although DMVs similarly to those seen in infected cells have not

been observed (unpublished results).

Recently, by using such a replication-independent assay, reticulons, which form a family of ER membrane-shaping proteins, were implicated in the formation of the BMV-induced, ER-derived spherules that are associated with viral RNA synthesis (16). Reticulons are involved in the induction of high ER membrane curvature (30, 31, 76) and for BMV seem to be required for stabilizing the spherule necks and to determine spherule diameter (16). It will be of interest to study the role of these proteins in CoV replication and in reshaping of the ER membranes by CoV nsps. Other proteins playing a role in shaping and remodeling of the ER are the atlastins and CLIMP-63 (30, 34). Also these proteins are putative candidates involved in CoV-induced membrane remodeling and would deserve to be investigated.

In addition to the role of virus and host proteins in formation of the replicative structures, lipids may also be important in this process. Dynamic alteration of the lipid composition can induce low curvature of membranes (20, 43, 66, 81), which is, however, unlikely to be sufficient to generate the organelle-like structures observed in + ssRNA virus-infected cells. It is more likely that lipids, together with lipid-modifying enzymes, contribute to the formation of the replicative structures by providing a suitable microenvironment to which the viral (and cellular) membrane shaping proteins are recruited. Even more, + ssRNA viruses may specifically hijack lipid-modifying enzymes for their own advantage (29). This is underscored by several studies, which show that inhibition of lipid synthesis by using either drugs or small interfering RNAs dramatically affects the replication of + ssRNA viruses (27-29, 54).

LIVE-CELL IMAGING OF CoV REPLICATIVE STRUCTURES

The last few decades have provided virologists with exciting new information regarding the functions and structures of individual nsps during replication and the characterization and formation of the membranous structures induced by + ssRNA viruses. These insights were obtained by classical biochemical, immunofluorescent and ultrastructural approaches. Unfortunately, one of the essential aspects that have been ignored until now is the dynamics of the (viral) proteins present at the membranous replicative structures in living cells. Such studies are important as classical approaches only provide static views of cellular processes and do not necessarily reflect the dynamics underlying virus replication in living cells. Additionally, the use of genetically encoded fluorescent proteins allows studying the localization, dynamics, kinetic properties and interactions of these proteins during replication in

a non-invasive way, i.e., without interfering with the temporal and spatial organization of these processes. The dynamic studies described in chapters 3, 4 and 5 have provided further information on the CoV replicative structures, but also on some of its individual components (nsp2, the nucleocapsid (N) protein and nsp4) that could not have been obtained using classical approaches.

Dynamics of the CoV replicative structures

The live-cell imaging data presented in chapter 3 demonstrate that the CoV replicative structures consist of two classes that demonstrate different mobilities: large structures lacking any displacement and smaller structures with relatively high saltatory mobility. We hypothesize that the smaller replicative structures correspond to individual DMVs and the larger ones to the DMV/CM assemblies as have been observed in ultrastructural studies of CoV-infected cells (35, 72). In SARS-CoV-infected cells the DMVs are confined to a reticulovesicular network (35). We therefore speculate that the small structures have not yet been 'captured' into this network. However, correlative light-electron microscopy studies will be required to solve this issue. Live-cell imaging studies of HCV- and SFV-infected cells also reported the presence of replicative structures that could be discriminated on the basis of their size and mobility. HCV induces the formation of a so-called membranous web, in which DMVs can be observed (18). Large HCV structures, probably representing membranous webs, exhibited limited movement, whereas smaller ones were mobile and could travel long distances throughout the cytoplasm (80). Semliki Forest virus (SFV)-induced vacuoles are assembled at the plasma membrane after which they are transported to modified lysosomes (38, 70). SFV-infected cells also harbor large acidic immobile perinuclear vesicles and smaller acidic cytoplasmic vesicles that showed saltatory movements. In addition to these acidic vesicles, SFV-infected cells contain a class of non-acidic highly mobile vesicles that displayed multidirectional short-distance movements. Moreover, fusion of the neutral mobile structures with the mobile acidic structures resulted in the formation of the large acidic structures (70). Such events of fusion of smaller replicative structures into larger ones have not been observed (yet) for the CoV and HCV replicative structures [chapter 3 and (80)].

The calculated velocities of the saltatory movements of the smaller nsp2-positive structures in CoV-infected cells correspond to those measured for microtubule-mediated transport. The inhibition of trafficking in the presence of a microtubule network-disturbing drug and by the observed association of these structures with microtubules confirmed the transport of the smaller

structures using microtubules (chapter 3). A role of the cytoskeleton in the movement of replicative structures has also been described for HCV, SFV, and PV (9, 19, 70, 80). Disruption of a functional microtubular network inhibited the movement of the small HCV and nascent PV replicative structures (19, 80) and the trafficking of SFV neutral vesicles to acidic organelles (70), concomitant with dispersal of these structures throughout the cytoplasm. Strikingly, inhibition of microtubule-dependent trafficking did not or only modestly affect virus replication (5, 19). In chapter 6 we demonstrate that disruption of the actin network also did not affect CoV replication much, although the replicative structures failed to accumulate in the perinuclear area. Our results (chapter 3 and chapter 5) show that the cytoskeleton is required for the perinuclear accumulation of the replicative structure rather than for replication *per se*. Additional studies are required to clarify the role of the perinuclear targeting of the CoV replicative structures during infection.

Mobility of replicative structure-associated proteins

The CoV replicase polyproteins are extensively processed by viral proteinases, resulting in the generation of sixteen nsps that collectively form the RTCs. Predicted and identified functions have been assigned to the individual nsps (for a complete overview see chapter 1) but not much is known with respect to the dynamics of the individual proteins when present at the replicative structures. In chapters 3, 4 and 5 we analyzed the dynamic properties of three replication-associated proteins, i.e., the soluble nsp2 and N proteins and the integral membrane protein nsp4, and demonstrated that these proteins display different diffusional mobilities when present at the replicative structures.

In Chapter 3 we demonstrate among others by FRAP analyses that nsp2, when expressed *in trans* was recruited to and immobilized at the RTCs. In other words, nsp2 present at the replicative structures was not exchanged by nsp2 present at other locations in the cell. Similar results have been demonstrated for other + ssRNA virus replicase-associated proteins, although the published literature on this subject is limited. Also in HCV-infected cells, NS5A-positive structures showed a static internal architecture when (part of) the NS5A fluorescent protein pool was bleached (80). When expressed individually, NS5A is highly mobile (33), similar to nsp2. Apparently, in the context of a viral infection, when other viral proteins are present, MHV nsp2 and HCV NS5A are immobilized, presumably due to protein-RNA or protein-protein interactions at the replicative structures. In agreement herewith, large-scale protein-protein interaction studies demonstrated that nsp2 of MHV and SARS-CoV is engaged in a multitude of interactions with itself, nsp3, nsp4,

nsp6, nsp7, nsp8, nsp11, nsp15 and nsp16 [(32, 51, 77) and unpublished data]. These observations are remarkable in view of the dispensability of nsp2 during CoV infection *in vitro* (25). Yet, nsp2 has to be somehow important *in vivo* as evolutionary pressure has not discarded its coding sequence from the CoV genome.

In contrast to nsp2, the structural N protein is not immobilized at the CoV replicative structures but is associated with it rather dynamically (chapter 4). This may not be surprising, as the multifunctional N protein is both involved in viral replication (1, 8, 63) and virion assembly (11). As the CoV replicative structures and virion assembly sites appear to be spatially separated, the newly synthesized genomic viral RNA needs to be transported from the replication sites to the assembly sites. The N protein presumably facilitates this transport, consistent with its dynamic association.

When expressed *in trans* in infected cells, the nsp4-GFP fusion protein was detected at the ER and the replicative structures [(48) and chapter 5]. By performing fluorescence loss in photobleaching (FLIP) experiments we demonstrated continuity between the membranes of the ER and the replicative structures that harbor nsp4, in agreement with the model that the DMVs and CMs form an interconnected network that is continuous with the ER (35). The nsp4 protein present at the different subcellular locations displayed different diffusional mobilities (chapter 5). Nsp4 present in the ER was more mobile than when present at the replicative structures. This reduced mobility may be (partly) explained by nsp4 being engaged in protein-protein interactions with the other transmembrane-containing nsps as well as with itself (chapter 5). Also the mobility of the HCV NS4B protein, which is an integral transmembrane protein as well, depends on its intracellular location. When expressed in the absence of other viral proteins, this protein is present at the ER and at so-called membrane-associated foci (MAFs) that are induced upon expression of this protein (26). Live-cell imaging (FRAP analysis) showed that NS4B present at the MAFs had a reduced mobility compared to NS4B at the ER, which was suggested to result from NS4B being engaged in different interactions when present on MAFs or the ER (26).

CoV REPLICATIVE STRUCTURES AND RNA SYNTHESIS

At the moment, perhaps one of the most enigmatic issues is the precise localization of the sites of active viral RNA synthesis. Upon infection CoVs induce a network of DMVs, which harbor dsRNA, and CMs. It is not clear, however, which of these structures are actually associated with the

biosynthesis of the CoV RNA, as the nsps localize to both structures (12, 24, 25, 35, 48, 56, 59, 65, 67, 72, 73), while the dsRNA-containing inner vesicles of the DMVs appear to be closed structures (35). To identify sites of nascent viral RNA synthesis, one has to define what actually constitutes the active viral replication complexes. Although dsRNA molecules function as intermediates of replication and transcription, their presence at certain sites *per se* does not imply (all) these structures to be actively involved in RNA synthesis. Likewise, the location of viral enzymes that are required for RNA synthesis does not need to correlate with active RTCs. Moreover, nascent RNAs are not necessarily located at their site of synthesis as they may diffuse or be transported away to other subcellular locations. In view of these considerations, sites active in RNA synthesis are expected to contain at least three components: the RNA-dependent RNA polymerase (RdRp), dsRNA intermediates active in replication/transcription and nascent viral RNA.

In chapter 6 we employed a novel method to detect and visualize newly synthesized RNA by incorporation of an alkyne-modified uridine analog, 5-ethynyl uridine (EU), onto which an azide-derivatized fluophore was coupled via a copper (I)-catalyzed cycloaddition reaction (click chemistry). Our data show that throughout the infection foci of nascent RNAs detected in MHV-infected cells colocalize with the nsp12-encoded RdRp, indicating that they correspond with sites of active coronaviral RNA synthesis. The relationship between nascent RNA and dsRNA is, however, less clear. While early in infection nascent RNAs colocalize at or adjacent to patches of dsRNA dots, this correlation is much less apparent at later times when the dsRNA dots are spread throughout the cell. Many dsRNA dots are apparently not transcriptionally active as no EU labeling was associated with them, while many foci of EU labeling did not appear to colocalize with the dsRNA dots.

Different models can be put forward to explain these observations. In one model, DMVs function as the sites of active RNA synthesis. At the later times in infection, many DMVs are no longer active, while the ones that are active may contain only little dsRNA, resulting in less apparent colocalization of dsRNA and EU labeling. In another model, DMVs are non-functional end-stage products. They are not actively involved in RNA synthesis, but rather harbor dsRNAs that are not (longer) functioning as intermediates in RNA synthesis. In this model, which is in agreement with the presumed absence of pores in these structures (35), the CMs would be the only plausible alternative for the sites of active RNA synthesis. In yet another model, DMVs may be the initial sites of active RNA synthesis, particularly early in infection, while at later times the membranes become sealed, connections are lost and

RNA synthesis shifts to the CM assemblies. Clearly, ultrastructural studies will be required, ideally (co)localizing nascent RNAs as well as the RdRp, to definitely determine the precise localization of CoV RNA synthesis.

For most other + ssRNA viruses the identification of the sites of active RNA synthesis appears less complicated. Nascent RNAs, as well as nsps, have been shown to label the spherules that are observed in BMV- (64), SFV- (38) or flock house virus (FHV)- (37) infected cells at the modified ER, lysosomes and mitochondria, respectively, indicating that these structures correspond with the sites of active RNA synthesis. Nascent RNAs were previously also shown to colocalize with dsRNA in Kunjin flavivirus-infected cells (79). Electron tomography of the membrane rearrangements observed in flavirus-infected cells revealed that the inner content of the DMVs, which contains nsps and dsRNA, are connected to the cytoplasm via a pore (23, 78), indicating that these DMVs are actually spherule-like invaginations (once) active in RNA synthesis.

FINAL REMARKS AND FUTURE DIRECTIONS

The research described in this thesis focused on the assembly and dynamics of the CoV replicative structures. Knowledge of the dynamic biological processes that underlie the formation of the RTCs and the induction of the membrane rearrangements is essential for understanding how these viruses replicate and interact with their host cells at the molecular level.

In this thesis we focused mainly on individual nsps. Yet, CoV RTCs are macromolecular structures and (in agreement with our results) engaged in multiple protein-protein interactions (32, 51, 77). Currently, the exact protein composition of the replicative structures/RTCs is not known, let alone the full arsenal of protein-protein interactions. Moreover, as indicated by our studies (chapter 5) and those of others (12, 61, 62), these structures are likely to be subject to some form of maturation, suggesting that the protein-protein interactions may change in time. Therefore, it will be of interest to confirm and extend the previously published protein-protein interactome studies that have been published for SARS-CoV (32, 51, 77), for example by investigating protein-protein interactions of other CoVs using novel (large-scale) screening approaches. Likewise, it will be of interest to get more insight into the involvement of host proteins in the formation of these structures, for example by screening for host proteins that interact with the CoV nsps or by elucidating the protein content of purified replicative structures using mass spectrometry.

It is also desirable to get more insight into the dynamic nature of the replicative structures using alternative live-cell imaging approaches. For example, photoactivatable fluorescent proteins can be used to investigate the formation of the replicative structures in real-time by 'optical pulse-labeling' in living cells, while the behavior of individual nsps associated with the RTCs can be studied by selectively 'switching-on' (sub)populations of proteins (39, 40). Furthermore, tagging of viral RNA by genetic incorporation of specific RNA sequences that bind fluorescently-tagged RNA-binding proteins (10, 21), hybridization of fluorescent 'molecular beacons' to the viral RNAs (71), or combining metabolic labeling of viral RNAs with Cu-independent click chemistry (3), will allow visualization and tracking of these ribonucleic acid species in living cells. Concomitant live-cell imaging of viral RNA and the N proteins may be used to investigate the transport of nascent RNA from the replication to the assembly sites.

Additionally, super resolution microscopy techniques, like photoactivated localization microscopy [PALM, (4)], can be applied to investigate the CoV RTCs and the membranous replicative structures at the ultrastructural level using fluorescently-tagged proteins, while EU-labeling of viral RNA in combination with correlative light-electron microscopy may provide the resolution to indisputably pinpoint the exact location of viral RNA synthesis (74).

Taken together, the research described in this thesis, in which both 'classical' molecular and biochemical virology was combined with state-of-the-art cell biological techniques, has provided new information regarding the assembly, functioning and dynamics of the CoV replicative structures. In the end, these new insights will not only provide information about basic cellular processes, but may also contribute to the development of new antiviral therapies.

REFERENCES

1. Almazan, F., C. Galan, and L. Enjuanes. 2004. The nucleoprotein is required for efficient coronavirus genome replication. J. Virol. 78:12683-12688. doi: 10.1128/JVI.78.22.12683-12688.2004.

2. Baliji, S., S. A. Cammer, B. Sobral, and S. C. Baker. 2009. Detection of nonstructural protein 6 in murine coronavirus-infected cells and analysis of the transmembrane topology by using bioinformatics and molecular approaches. J Virol. 83:6957-62.

3. Baskin, J. M., J. A. Prescher, S. T. Laughlin, N. J. Agard, P. V. Chang, I. A. Miller, A. Lo, J. A. Codelli, and C. R. Bertozzi. 2007. Copper-free click chemistry for dynamic in vivo imaging. Proceedings of the National Academy of Sciences. 104:16793-16797. doi: 10.1073/pnas.0707090104.

4. Betzig, E., G. H. Patterson, R. Sougrat, O. W. Lindwasser, S. Olenych, J. S. Bonifacino, M. W. Davidson, J. Lippincott-Schwartz, and H. F. Hess. 2006. Imaging intracellular fluorescent proteins at nanometer resolution. Science. 313:1642-1645. doi: 10.1126/science.1127344.

5. Bost, A. G., D. Venable, L. Liu, and B. A. Heinz. 2003. Cytoskeletal Requirements for Hepatitis C Virus (HCV) RNA Synthesis in the HCV Replicon Cell Culture System. J. Virol. 77:4401-4408. doi: 10.1128/JVI.77.7.4401-4408.2003.

6. Cali, T., C. Galli, S. Olivari, and M. Molinari. 2008. Segregation and rapid turnover of EDEM1 by an autophagy-like mechanism modulates standard ERAD and folding activities. Biochem. Biophys. Res. Commun. 371:405-410. doi: 10.1016/j.bbrc.2008.04.098.

7. Cali, T., O. Vanoni, and M. Molinari. 2008. The endoplasmic reticulum crossroads for newly synthesized polypeptide chains. Prog. Mol. Biol. Transl. Sci. 83:135-179. doi: 10.1016/S0079-6603(08)00604-1.

8. Compton, S. R., D. B. Rogers, K. V. Holmes, D. Fertsch, J. Remenick, and J. J. McGowan. 1987. In vitro replication of mouse hepatitis virus strain A59. J. Virol. 61:1814-1820.

9. Cui, Z., Z. Zhang, X. Zhang, J. Wen, Y. Zhou, and W. Xie. Visualizing the dynamic behavior of poliovirus plus-strand RNA in living host cells. Nucleic Acids Research. 33:3245-3252. doi: 10.1093/nar/gki629.

10. Daigle, N., and J. Ellenberg. 2007. LambdaN-GFP: an RNA reporter system for live-cell imaging. Nat. Methods. 4:633-636. doi: 10.1038/nmeth1065.

11. de Haan, C. A., and P. J. Rottier. 2005. Molecular interactions in the assembly of coronaviruses. Adv. Virus Res. 64:165-230. doi: 10.1016/S0065-3527(05)64006-7.

12. Deming, D. J., R. L. Graham, M. R. Denison, and R. S. Baric. 2007. Processing of open reading frame 1a replicase proteins nsp7 to nsp10 in murine hepatitis virus strain A59 replication. J. Virol. 81:10280-10291. doi: 10.1128/JVI.00017-07.

13. den Boon, J. A., and P. Ahlquist. 2010. Organelle-like membrane compartmentalization of positive-strand RNA virus replication factories. Annu. Rev. Microbiol. 64:241-256. doi: 10.1146/annurev.micro.112408.134012.

14. den Boon, J. A., A. Diaz, and P. Ahlquist. 2010. Cytoplasmic viral replication complexes. Cell. Host Microbe. 8:77-85. doi: 10.1016/j.chom.2010.06.010.

15. den Boon, J. A., J. Chen, and P. Ahlquist. 2001. Identification of Sequences in Brome Mosaic Virus Replicase Protein 1a That Mediate Association with Endoplasmic Reticulum Membranes. J. Virol. 75:12370-12381. doi: 10.1128/JVI.75.24.12370-12381.2001.

16. Diaz, A., X. Wang, and P. Ahlquist. 2010. Membrane-shaping host reticulon proteins play crucial roles in viral RNA replication compartment formation and function. Proceedings of the National Academy of Sciences. 107:16291-16296. doi: 10.1073/pnas.1011105107.

17. Echeverri, A. C., and A. Dasgupta. 1995. Amino Terminal Regions of Poliovirus 2C Protein Mediate Membrane Binding. Virology. 208:540-553. doi: DOI: 10.1006/viro.1995.1185.

18. Egger, D., B. Wolk, R. Gosert, L. Bianchi, H. E. Blum, D. Moradpour, and K. Bienz. 2002. Expression of hepatitis C virus proteins induces distinct membrane alterations including a candidate viral replication complex. J Virol. 76:5974-84.

19. Egger, D., and K. Bienz. 2005. Intracellular location and translocation of silent and active poliovirus replication complexes. Journal of General Virology. 86:707-718. doi: 10.1099/vir.0.80442-0.

20. Farsad, K., and P. D. Camilli. 2003. Mechanisms of membrane deformation. Curr. Opin. Cell Biol. 15:372-381. doi: DOI: 10.1016/S0955-0674(03)00073-5.

21. Fusco, D., N. Accornero, B. Lavoie, S. M. Shenoy, J. Blanchard, R. H. Singer, and E. Bertrand. 2003. Single mRNA Molecules Demonstrate Probabilistic Movement in Living Mammalian Cells. Current Biology. 13:161-167. doi: DOI: 10.1016/S0960-9822(02)01436-7.

22. Gadlage, M. J., J. S. Sparks, D. C. Beachboard, R. G. Cox, J. D. Doyle, C. C. Stobart, and M. R. Denison. 2010. Murine hepatitis virus nonstructural protein 4 regulates virus-induced membrane modifications and replication complex function. J. Virol. 84:280-290. doi: 10.1128/JVI.01772-09.

23. Gillespie, L. K., A. Hoenen, G. Morgan, and J. M. Mackenzie. 2010. The endoplasmic reticulum provides the membrane platform for biogenesis of the flavivirus replication complex. J. Virol. 84:10438-10447. doi: 10.1128/JVI.00986-10.

24. Goldsmith, C. S., K. M. Tatti, T. G. Ksiazek, P. E. Rollin, J. A. Comer, W. W. Lee, P. A. Rota, B. Bankamp, W. J. Bellini, and S. R. Zaki. 2004. Ultrastructural characterization of SARS coronavirus. Emerg. Infect. Dis. 10:320-326.

25. Graham, R. L., A. C. Sims, S. M. Brockway, R. S. Baric, and M. R. Denison. 2005. The nsp2 replicase proteins of murine hepatitis virus and severe acute respiratory syndrome coronavirus are dispensable for viral replication. J Virol. 79:13399-411.

26. Gretton, S. N., A. I. Taylor, and J. McLauchlan. 2005. Mobility of the hepatitis C virus NS4B protein on the endoplasmic reticulum membrane and membrane-associated foci. J Gen Virol. 86:1415-21.

27. Guinea, R., and L. Carrasco. 1990. Phospholipid biosynthesis and poliovirus genome replication, two coupled phenomena. EMBO J. 9:2011-2016.

28. Heaton, N. S., R. Perera, K. L. Berger, S. Khadka, D. J. LaCount, R. J. Kuhn, and G. Randall. 2010. Dengue virus nonstructural protein 3 redistributes fatty acid synthase to sites of viral replication and increases cellular fatty acid synthesis. Proceedings of the National Academy of Sciences. 107:17345-17350. doi: 10.1073/pnas.1010811107.

29. Hsu, N., O. Ilnytska, G. Belov, M. Santiana, Y. Chen, P. M. Takvorian, C. Pau, H. van der Schaar, N. Kaushik-Basu, T. Balla, C. E. Cameron, E. Ehrenfeld, F. J. M. van Kuppeveld, and N. Altan-Bonnet. 2010. Viral Reorganization of the Secretory Pathway Generates Distinct Organelles for RNA Replication. Cell. 141:799-811. doi: DOI: 10.1016/j.cell.2010.03.050.

30. Hu, J., Y. Shibata, P. P. Zhu, C. Voss, N. Rismanchi, W. A. Prinz, T. A. Rapoport, and C. Blackstone. 2009. A class of dynamin-like GTPases involved in the generation of the tubular ER network. Cell. 138:549-561. doi: 10.1016/j.cell.2009.05.025.

31. Hu, J., Y. Shibata, C. Voss, T. Shemesh, Z. Li, M. Coughlin, M. M. Kozlov, T. A. Rapoport, and W. A. Prinz. 2008. Membrane Proteins of the Endoplasmic Reticulum Induce High-Curvature Tubules. Science. 319:1247-1250. doi: 10.1126/science.1153634.

32. Imbert, I., E. J. Snijder, M. Dimitrova, J. C. Guillemot, P. Lecine, and B. Canard. 2008. The SARS-Coronavirus PLnc domain of nsp3 as a replication/transcription scaffolding protein. Virus Res. 133:136-48.

33. Jones, D. M., S. N. Gretton, J. McLauchlan, and P. Targett-Adams. 2007. Mobility analysis of an NS5A–GFP fusion protein in cells actively replicating hepatitis C virus subgenomic RNA. Journal of General Virology. 88:470-475. doi: 10.1099/vir.0.82363-0.

34. Klopfenstein, D. R., J. Klumperman, A. Lustig, R. A. Kammerer, V. Oorschot, and H. Hauri. 2001. Subdomain-Specific Localization of Climp-63 (P63) in the Endoplasmic Reticulum Is Mediated by Its Luminal α-Helical Segment. The Journal of Cell Biology. 153:1287-1300. doi: 10.1083/jcb.153.6.1287.

35. Knoops, K., M. Kikkert, S. H. E. Van Den Worm, J. C. Zevenhoven-Dobbe, Y. Van Der Meer, A. J. Koster, A. M. Mommaas, and E. J. Snijder. 2008. SARS-coronavirus replication is supported by a reticulovesicular network of modified endoplasmic reticulum. PLoS Biology. 6:1957-1974.

36. Knoops, K., C. Swett-Tapia, S. H. E. van den Worm, A. J. W. te Velthuis, A. J. Koster, A. M. Mommaas, E. J. Snijder, and M. Kikkert. 2010. Integrity of the Early Secretory Pathway Promotes, but Is Not Required for, Severe Acute Respiratory Syndrome Coronavirus RNA Synthesis and Virus-Induced Remodeling of Endoplasmic Reticulum Membranes. J. Virol. 84:833-846. doi: 10.1128/JVI.01826-09.

37. Kopek, B. G., G. Perkins, D. J. Miller, M. H. Ellisman, and P. Ahlquist. 2007. Three-dimensional analysis of a viral RNA replication complex reveals a virus-induced mini-organelle. PLoS Biol. 5:e220. doi: 10.1371/journal.pbio.0050220.

38. Kujala, P., A. Ikaheimonen, N. Ehsani, H. Vihinen, P. Auvinen, and L. Kaariainen. 2001. Biogenesis of the Semliki Forest Virus RNA Replication Complex. J. Virol. 75:3873-3884. doi: 10.1128/JVI.75.8.3873-3884.2001.

39. Lippincott-Schwartz, J., N. Altan-Bonnet, and G. H. Patterson. 2003. Photobleaching and photoactivation: following protein dynamics in living cells. Nat. Cell Biol. Suppl:S7-14.

40. Lippincott-Schwartz, J., and G. H. Patterson. 2003. Development and use of fluorescent protein markers in living cells. Science. 300:87-91.

41. Lundin, M., M. Monne, A. Widell, G. von Heijne, and M. A. A. Persson. 2003. Topology of the Membrane-Associated Hepatitis C Virus Protein NS4B. J. Virol. 77:5428-5438. doi: 10.1128/JVI.77.9.5428-5438.2003.

42. Mackenzie, J. M., A. A. Khromykh, M. K. Jones, and E. G. Westaway. 1998. Subcellular Localization and Some Biochemical Properties of the Flavivirus Kunjin Nonstructural Proteins NS2A and NS4A. Virology. 245:203-215. doi: DOI: 10.1006/viro.1998.9156.

43. McMahon, H. T., and J. L. Gallop. 2005. Membrane curvature and mechanisms of dynamic cell membrane remodelling. Nature. 438:590-596. doi: 10.1038/nature04396.

44. Miller, D. J., and P. Ahlquist. 2002. Flock House Virus RNA Polymerase Is a Transmembrane Protein with Amino-Terminal Sequences Sufficient for Mitochondrial Localization and Membrane Insertion. J. Virol. 76:9856-9867. doi: 10.1128/JVI.76.19.9856-9867.2002.

45. Miller, S., S. Kastner, J. Krijnse-Locker, S. Buhler, and R. Bartenschlager. 2007. The non-structural protein 4A of dengue virus is an integral membrane protein inducing membrane alterations in a 2K-regulated manner. J Biol Chem. 282:8873-82.

46. Miller, S., and J. Krijnse-Locker. 2008. Modification of intracellular membrane structures for virus replication. Nat Rev Microbiol. 6:363-74.

47. Miller, S., S. Sparacio, and R. Bartenschlager. 2006. Subcellular Localization and Membrane Topology of the Dengue Virus Type 2 Non-structural Protein 4B. Journal of Biological Chemistry. 281:8854-8863. doi: 10.1074/jbc.M512697200.

48. Oostra, M., E. G. te Lintelo, M. Deijs, M. H. Verheije, P. J. Rottier, and C. A. de Haan. 2007. Localization and membrane topology of coronavirus nonstructural protein 4: involvement of the early secretory pathway in replication. J Virol. 81:12323-36.

49. O'Reilly, E., J. Paul, and C. Kao. 1997. Analysis of the interaction of viral RNA replication proteins by using the yeast two-hybrid assay. J. Virol. 71:7526-7532.

50. O'Reilly, E. K., Z. Wang, R. French, and C. C. Kao. 1998. Interactions between the Structural Domains of the RNA Replication Proteins of Plant-Infecting RNA Viruses. J. Virol. 72:7160-7169.

51. Pan, J., X. Peng, Y. Gao, Z. Li, X. Lu, Y. Chen, M. Ishaq, D. Liu, M. L. DeDiego, L. Enjuanes, and D. Guo. 2008. Genome-wide analysis of protein-protein interactions and involvement of viral proteins in SARS-CoV replication. PLoS ONE. 3:.

52. Paul, D., I. Romero-Brey, J. Gouttenoire, S. Stoitsova, J. Krijnse-Locker, D. Moradpour, and R. Bartenschlager. 2011. NS4B Self-Interaction through Conserved C-Terminal Elements Is Required for the Establishment of Functional Hepatitis C Virus Replication Complexes. J. Virol. 85:6963-6976. doi: 10.1128/JVI.00502-11.

53. Pedersen, K. W., Y. van der Meer, N. Roos, and E. J. Snijder. 1999. Open reading frame 1a-encoded subunits of the arterivirus replicase induce endoplasmic reticulum-derived double-membrane vesicles which carry the viral replication complex. J. Virol. 73:2016-2026.

54. Perez, L., R. Guinea, and L. Carrasco. 1991. Synthesis of Semliki Forest virus RNA requires continuous lipid synthesis. Virology. 183:74-82. doi: DOI: 10.1016/0042-6822(91)90119-V.

55. Posthuma, C. C., K. W. Pedersen, Z. Lu, R. G. Joosten, N. Roos, J. C. Zevenhoven-Dobbe, and E. J. Snijder. 2008. Formation of the arterivirus replication/transcription complex: a key role for nonstructural protein 3 in the remodeling of intracellular membranes. J Virol. 82:4480-91.

56. Prentice, E., J. McAuliffe, X. Lu, K. Subbarao, and M. R. Denison. 2004. Identification and characterization of severe acute respiratory syndrome coronavirus replicase proteins. J Virol. 78:9977-86.

57. Raaben, M., G. C. M. Grinwis, P. J. M. Rottier, and C. A. M. de Haan. 2010. The Proteasome Inhibitor Velcade Enhances rather than Reduces Disease in Mouse Hepatitis Coronavirus-Infected Mice. J. Virol. 84:7880-7885. doi: 10.1128/JVI.00486-10.

58. Raaben, M., C. C. Posthuma, M. H. Verheije, E. G. te Lintelo, M. Kikkert, J. W. Drijfhout, E. J. Snijder, P. J. M. Rottier, and C. A. M. de Haan. 2010. The Ubiquitin-Proteasome System Plays an Important Role during Various Stages of the Coronavirus Infection Cycle. J. Virol. 84:7869-7879. doi: 10.1128/JVI.00485-10.

59. Reggiori, F., I. Monastyrska, M. Verheije H., T. Calì, M. Ulasli, S. Bianchi, R. Bernasconi, C. de Haan A.M., and M. Molinari. 2010. Coronaviruses Hijack the LC3-I-Positive EDEMosomes, ER-Derived Vesicles Exporting Short-Lived ERAD Regulators, for Replication. Cell Host & Microbe. 7:500.

60. Roosendaal, J., E. G. Westaway, A. Khromykh, and J. M. Mackenzie. 2006. Regulated Cleavages at the West Nile Virus NS4A-2K-NS4B Junctions Play a Major Role in Rearranging Cytoplasmic Membranes and Golgi Trafficking of the NS4A Protein. J. Virol. 80:4623-4632. doi: 10.1128/JVI.80.9.4623-4632.2006.

61. Sawicki, S. G., and D. L. Sawicki. 1986. Coronavirus minus-strand RNA synthesis and effect of cycloheximide on coronavirus RNA synthesis. J. Virol. 57:328-334.

62. Sawicki, S. G., D. L. Sawicki, D. Younker, Y. Meyer, V. Thiel, H. Stokes, and S. G. Siddell. 2005. Functional and genetic analysis of coronavirus replicase-transcriptase proteins. PLoS Pathog. 1:e39. doi: 10.1371/journal.ppat.0010039.

63. Schelle, B., N. Karl, B. Ludewig, S. G. Siddell, and V. Thiel. 2005. Selective replication of coronavirus genomes that express nucleocapsid protein. J. Virol. 79:6620-6630. doi: 10.1128/JVI.79.11.6620-6630.2005.

64. Schwartz, M., J. Chen, M. Janda, M. Sullivan, J. den Boon, and P. Ahlquist. 2002. A Positive-Strand RNA Virus Replication Complex Parallels Form and Function of Retrovirus Capsids. Mol. Cell. 9:505-514. doi: DOI: 10.1016/S1097-2765(02)00474-4.

65. Shi, S. T., J. J. Schiller, A. Kanjanahaluethai, S. C. Baker, J. W. Oh, and M. M. Lai. 1999. Colocalization and membrane association of murine hepatitis virus gene 1 products and De novo-synthesized viral RNA in infected cells. J Virol. 73:5957-69.

66. Shibata, Y., J. Hu, M. M. Kozlov, and T. A. Rapoport. 2009. Mechanisms Shaping the Membranes of Cellular Organelles. Annu. Rev. Cell Dev. Biol. 25:329-354. doi: 10.1146/annurev.cellbio.042308.113324. http://dx.doi.org/10.1146/annurev.cellbio.042308.113324.

67. Snijder, E. J., Y. van der Meer, J. Zevenhoven-Dobbe, J. J. Onderwater, J. van der Meulen, H. K. Koerten, and A. M. Mommaas. 2006. Ultrastructure and origin of membrane vesicles associated with the severe acute respiratory syndrome coronavirus replication complex. J Virol. 80:5927-40.

68. Snijder, E. J., H. van Tol, N. Roos, and K. W. Pedersen. 2001. Non-structural proteins 2 and 3 interact to modify host cell membranes during the formation of the arterivirus replication complex. J Gen Virol. 82:985-94.

69. Sparks, J. S., X. Lu, and M. R. Denison. 2007. Genetic analysis of Murine hepatitis virus nsp4 in virus replication. J Virol. 81:12554-63.

70. Spuul, P., G. Balistreri, L. Kaariainen, and T. Ahola. 2010. Phosphatidylinositol 3-Kinase-, Actin-, and Microtubule-Dependent Transport of Semliki Forest Virus Replication Complexes from the Plasma Membrane to Modified Lysosomes. J. Virol. 84:7543-7557. doi: 10.1128/JVI.00477-10.

71. Tyagi, S., and F. R. Kramer. 1996. Molecular beacons: probes that fluoresce upon hybridization. Nat. Biotechnol. 14:303-308. doi: 10.1038/nbt0396-303.

72. Ulasli, M., M. H. Verheije, C. A. de Haan, and F. Reggiori. 2010. Qualitative and quantitative ultrastructural analysis of the membrane rearrangements induced by coronavirus. Cell. Microbiol. 12:844-861. doi: 10.1111/j.1462-5822.2010.01437.x.

73. van der Meer, Y., E. J. Snijder, J. C. Dobbe, S. Schleich, M. R. Denison, W. J. Spaan, and J. K. Locker. 1999. Localization of mouse hepatitis virus nonstructural proteins and RNA synthesis indicates a role for late endosomes in viral replication. J. Virol. 73:7641-7657.

74. van Rijnsoever, C., V. Oorschot, and J. Klumperman. 2008. Correlative light-electron microscopy (CLEM) combining live-cell imaging and immunolabeling of ultrathin cryosections. Nat. Methods. 5:973-980. doi: 10.1038/nmeth.1263.

75. Verheije, M. H., M. Raaben, M. Mari, E. G. Te Lintelo, F. Reggiori, F. J. van Kuppeveld, P. J. Rottier, and C. A. de Haan. 2008. Mouse hepatitis coronavirus RNA replication depends on GBF1-mediated ARF1 activation. PLoS Pathog. 4:e1000088.

76. Voeltz, G. K., W. A. Prinz, Y. Shibata, J. M. Rist, and T. A. Rapoport. 2006. A class of membrane proteins shaping the tubular endoplasmic reticulum. Cell. 124:573-586. doi: 10.1016/j.cell.2005.11.047.

77. von Brunn, A., C. Teepe, J. C. Simpson, R. Pepperkok, C. C. Friedel, R. Zimmer, R. Roberts, R. Baric, and J. Haas. 2007. Analysis of intraviral protein-protein interactions of the SARS coronavirus ORFeome. PLoS ONE. 2:.

78. Welsch, S., S. Miller, I. Romero-Brey, A. Merz, C. K. Bleck, P. Walther, S. D. Fuller, C. Antony, J. Krijnse-Locker, and R. Bartenschlager. 2009. Composition and three-dimensional architecture of the dengue virus replication and assembly sites. Cell. Host Microbe. 5:365-375. doi: 10.1016/j.chom.2009.03.007.

79. Westaway, E. G., A. A. Khromykh, and J. M. Mackenzie. 1999. Nascent Flavivirus RNA Colocalizedin Situwith Double-Stranded RNA in Stable Replication Complexes. Virology. 258:108-117. doi: DOI: 10.1006/viro.1999.9683.

80. Wolk, B., B. Buchele, D. Moradpour, and C. M. Rice. 2008. A dynamic view of hepatitis C virus replication complexes. J Virol. 82:10519-31.

81. Zimmerberg, J., and M. M. Kozlov. 2006. How proteins produce cellular membrane curvature. Nat. Rev. Mol. Cell Biol. 7:9-19. doi: 10.1038/nrm1784.

Nederlandse Samenvatting

Virussen (Latijn voor vergif) zijn zeer kleine ziekteverwekkers voor zowel mens als dier. Het zijn obligaat intracellulaire parasieten die volledig afhankelijk zijn van de geïnfecteerde gastheercel om zichzelf te reproduceren. Ze bestaan uit (cellulaire) eiwitten, nucleïnezuren, lipiden en koolhydraten. Van alle verschillende soorten virussen komen degenen die als erfelijk materiaal een enkelstrengs positief RNA (+ ssRNA) genoom bevatten het meest in de natuur voor. Tot deze klasse van virussen behoren relevante humane virussen, waaronder het poliovirus, het hepatitis C virus en het 'severe acute respiratory syndrome' (SARS)-coronavirus.

Coronavirussen (CoVs) zijn + ssRNA virussen die tot de familie van de *Coronaviridae* in de orde van de *Nidovirales* behoren. Vanuit een historisch oogpunt zijn het belangrijke ziekteverwekkers die verantwoordelijk zijn voor luchtweg- en darminfecties in vee en huisdieren. In het algemeen veroorzaken humane CoVs vooral milde luchtweginfecties zoals ordinaire verkoudheden. Echter, in 2002-2003 was er een ernstige uitbraak van het dodelijke SARS-CoV wat duidelijk maakte dat CoVs ook levensbedreigende infectieziekten in mensen kunnen veroorzaken.

Het CoV viruspartikel bezit een lipide omhulsel (envelop) waarin zich drie structurele membraan eiwitten bevinden: het membraan (M) eiwit, het envelop (E) eiwit en het 'spike' (S) eiwit. Het viruspartikel bevat het virale genomische RNA dat met het nucleocapside (N) eiwit gezamenlijk het ribonucleoprotein (RNP) complex vormt. Het lineaire CoV genoom is extreem groot (~26 – 32 kb) voor een + ssRNA virus en bevat genetische informatie voor zowel *replicatie* (de synthese van genomisch RNA) als *transcriptie* (de productie van subgenoom mRNA). Tevens bevat het virale genoom een 5' 'cap' structuur en is het 3' gepolyadenyleerd waardoor het op cellulair mRNA lijkt en direct door de machinerie van de gastheer kan worden getransleerd. Translatie van de twee 5' open leesramen (ORFs) ORF1a en ORF1b resulteert in twee grote multi-eiwitten die door virale proteinases in 16 kleinere eiwitten worden geknipt, de zogenaamde niet-structurele eiwitten (nsps). Deze nsps bevatten enzymatische activiteiten; onder andere proteinase activiteit (nsp3 en nsp5), RNA-afhankelijke RNA polymerase activiteit (nsp8 en nsp12), voorspelde en bewezen RNA-modificerende functies (nsp13-nsp16) en activiteiten die de aangeboren antivirale immuunrespons onderdrukken (nsp1 en nsp3). Tezamen met het structurele N eiwit, en tot nu toe nog onbekende gastheer eiwitten, vormen deze 16 nsps de CoV replicatie-transcriptie complexen (RTCs).

Een karakteristiek kenmerk voor + ssRNA virussen in het algemeen is de reorganisatie van cellulaire membranen in gespecialiseerde membraan compartimenten welke betrokken zijn bij de synthese van viraal RNA.

CoVs zijn geen uitzondering op deze regel. De meest prominente membraanbevattende structuren in CoV-geïnfecteerde cellen zijn blaasjes van ongeveer 200 tot 350 nm in grootte bestaande uit een dubbele lipide bilaag, de zogenaamde 'double-membrane vesicles' (DMVs). Tussen de DMVs bevinden zich reticulaire 'convoluted membranes' (CMs). Tezamen worden deze membraan structuren, die zich bevinden in de perinucleaire regio van geïnfecteerde cellen, de *replicatie structuren* genoemd. De replicatie structuren worden gevormd van membranen van het endoplasmatisch reticulum (ER), zijn fysiek met elkaar verbonden en vormen een continue netwerk van membranen. In het algemeen wordt aangenomen dat CoV RNA synthese plaatsvindt aan deze replicatie structuren.

Er is nog weinig bekend over de vorming van de CoV replicatie structuren, het functioneren van de nsps tijdens de assemblage van de RTCs en de replicatie structuren, de membraanverankering van de RTCs en de precieze lokalisatie van de virale RNA synthese. Het onderzoek beschreven in dit proefschrift richt zich specifiek op (i) de mechanismen die ten grondslag liggen aan de vorming van de replicatie structuren, (ii) de interacties en dynamiek van eiwitten behorende tot de replicatie structuren en (iii) het ontrafelen van de exacte locatie van CoV RNA synthese. In onze studies werd het prototype muizen hepatitis virus (MHV) als model CoV gebruikt.

Drie van de 16 nsps bevatten transmembraan domeinen en functioneren waarschijnlijk als integraal membraan eiwitten die verantwoordelijk zijn voor de vorming van de replicatie structuren en de verankering van de RTCs daaraan. Om meer inzicht te krijgen in de rol van deze eiwitten met betrekking tot de vorming van de replicatie structuren, hebben we in hoofdstuk 2 de topologie van nsp3, nsp4 en nsp6 bestudeerd, voor zowel MHV-A59 als het SARS-CoV. Voor beide virussen bevinden de amino- en carboxy-termini van nsp3, nsp4 en nsp6 zich in het cytoplasma. Nsp3, nsp4 en nsp6 blijken respectievelijk twee, vier en zes transmembraan domeinen te bevatten. Bovendien bezitten nsp3 en nsp6 beiden hydrofobe domeinen die niet door de lipide bilaag heen gaan. De aanwezigheid van zulke hydrofobe, waarschijnlijk perifeer aan het membraan geassocieerde domeinen, komt vaker voor bij + ssRNA virussen en deze spelen waarschijnlijk een belangrijke rol in de vorming van de de virale replicatie structuren.

Om een beter inzicht in de dynamiek van de CoV replicatie structuren en de individuele componenten van de RTCs (nsp2, nsp4 en het N eiwit) te krijgen hebben we met behulp van fluorescentie microscopie fluorescerende versies van deze eiwitten in levende cellen bestudeerd (hoofdstukken 3 t/m 5). Onze studies in hoofdstuk 3 laten zien dat er in principe twee typen

CoV replicatie structuren bestaan: (i) grote statische structuren en (ii) kleine structuren met een hoge beweeglijkheid. Deze kleine structuren bewegen door de cel door gebruik te maken van de microtubuli. We veronderstellen dat de kleine mobiele structuren overeenkomen met individuele DMVs en de grote statische structuren met de assemblages van DMV/CMs. Het nsp2 eiwit, wanneer geëxpreseerd in niet-geïnfecteerde cellen, is zeer mobiel. Echter, in geïnfecteerde cellen, wanneer het aanwezig is in de replicatie structuren, is het eiwit onbeweeglijk. Een verklaring voor deze observatie is waarschijnlijk dat het nsp2 eiwit verschillende eiwit-eiwit interacties aangaat wanneer het een onderdeel van de RTCs is.

Het N eiwit is een structureel eiwit dat een belangrijke rol speelt tijdens de assemblage van het coronavirion, maar ook tijdens de replicatie van het virale genoom. Onder meer om deze reden hebben wij de dynamiek van dit eiwit bestudeerd (hoofdstuk 4). Onze data laten zien dat in tegenstelling tot nsp2 het N eiwit dynamisch is geassocieerd met de replicatie structuren. Dit lijkt logisch omdat het N eiwit een multifunctioneel eiwit is dat vermoedelijk een belangrijke rol speelt in het transport van nieuw gesynthetiseerd RNA van de plaats van replicatie naar de plaats van assemblage. Waarschijnlijk is deze dynamiek van het N eiwit een vereiste om deze taak te kunnen vervullen tijdens de CoV levenscyclus.

Het integraal transmembraan eiwit nsp4 speelt waarschijnlijk een belangrijke rol bij de vorming van de CoV replicatie structuren. In hoofdstuk 5 focussen we op de dynamiek en eiwit-eiwit interacties van nsp4. Expressie van nsp4 in geïnfecteerde cellen leidt tot een tweeledige subcellulaire lokalisatie van dit eiwit in zowel het ER als de replicatie structuren. Dit gegeven maakte het mogelijk om met behulp van microscopische technieken vast te stellen dat er continuïteit tussen beide membraan compartimenten bestaat. Dit resultaat komt overeen met het eerder beschreven continue membraan netwerk dat geobserveerd werd in SARS-CoV-geïnfecteerde cellen door Eric Snijder en zijn medewerkers in Leiden. De mobiliteit van nsp4 hangt af van de subcellulaire lokalisatie van dit eiwit. Wanneer het aanwezig is in de membranen van het ER is het mobieler dan wanneer het aanwezig is bij de replicatie structuren. Dit verschil in mobiliteit komt waarschijnlijk doordat nsp4 in de replicatie structuren niet alleen eiwit-eiwit interacties aangaat met zichzelf, maar ook met de andere transmembraan eiwitten nsp3 en nsp6. Co-expressie van het gedeelte van nsp3 dat de hydrofobe domeinen bevat met nsp4 bleek zelfs te resulteren in een herlokalisatie van deze twee eiwitten van het ER naar de perinucleaire regio van de cel. We denken dat de interactie tussen nsp3 en nsp4 essentieel is in de vorming van de DMVs en/of de CMs.

Het reorganiseren van cellulaire membranen in de speciale compartimenten dient maar één specifiek doel: het synthetiseren van nieuw viraal RNA. Ook CoV RNA synthese vindt plaats aan/bij de replicatie structuren. Echter, of dit de DMVs en/of de CMs zijn is nog niet bekend. De nsps zijn op beide membraan structuren aanwezig, maar dubbelstrengs (ds)RNA, waarvan gedacht wordt dat het overeenkomt met intermediairen in de RNA synthese, is alleen maar aangetroffen in de DMVs. Momenteel wordt de locatie van dsRNA in geïnfecteerde cellen gezien als een goede indicatie voor de locatie van actieve RNA synthese. De DMVs lijken echter gesloten structuren te zijn. Er zijn geen poriën waargenomen die de inhoud van de DMVs met het cytoplasma verbinden, waardoor het maar de vraag is of CoV RNA synthese plaats vindt op dezelfde locatie als waar het dsRNA zich bevindt. In hoofdstuk 6 hebben we een nieuwe techniek, waarbij gebruik gemaakt wordt van zogenaamde klik chemie, toegepast om nieuw gesynthetiseerd viraal RNA in geïnfecteerde cellen te visualiseren. Vroeg in de infectie is er een duidelijke correlatie tussen nieuw gesynthetiseerd RNA en dsRNA. Later in de infectie is deze correlatie veel minder duidelijk. Deze resultaten laten zien dat dsRNA geen goede indicator is voor de plek van actieve RNA synthese en suggereren dat de replicatie structuren en/of de RTCs 'rijpen' gedurende de infectie. Tijdens de gehele duur van de infectiecyclus is er wel een sterke correlatie tussen de lokalisatie van het nieuw gesynthetiseerde RNA en het RNA-afhankelijke RNA polymerase bevattende nsp12. RNA synthese vindt dus hoogstwaarschijnlijk plaats daar waar deze twee colokaliseren.

Samenvattend kunnen we stellen dat het onderzoek beschreven in dit proefschrift ons fundamentele inzicht in de assemblage, dynamiek en functioneren van de replicatie structuren van + ssRNA virussen in het algemeen en van CoVs in het bijzonder heeft vergroot. Het gebruik van vernieuwende technieken zoals 'live-cell imaging' en RNA detectie met behulp van 'klik chemie' heeft hier in belangrijke mate aan bijgedragen.

Dankwoord

Dit is waarschijnlijk het meest lastigste hoofdstuk om te schrijven, omdat (in tegenstelling tot de rest van het proefschrift) zo goed als iedereen het zal lezen en je natuurlijk niemand (onbedoeld) wilt vergeten in je dankbetuigingen. Als ik per ongeluk toch mensen ben vergeten, mijn welgemeende excuses, er is geen opzet in het spel. Graag wil ik van de gelegenheid gebruik maken om enkele personen in het bijzonder te bedanken. Ik zal proberen het kort te houden.

Allereerst wil ik mijn promotor en co-promotor bedanken. Beste Peter, bedankt voor alle hulp tijdens mijn promotietraject. Ik heb de afgelopen jaren zeer veel van je geleerd en zal deze kennis optimaal benutten in mijn verdere wetenschappelijke carrière. Beste Xander, ik vond het geweldig om samen met jou de afgelopen jaren onderzoek te doen en heb op wetenschappelijk gebied zeer veel van je geleerd. Jouw enthousiasme en gedrevenheid voor de wetenschap werken zeer motiverend, maar bovenal waardeer ik je betrokkenheid bij het onderzoek. Heel erg bedankt daarvoor! Ik hoop dat ik met jullie beiden contact zal houden in de toekomst.

Mijn 'oude' kamergenootjes van kamer 514 op de 5e verdieping van het Androclus gebouw wil ik ook graag bedanken. Eddie, ik vond het heel gezellig om met jou op dezelfde kamer te zitten en samen te werken. Bedankt voor alle experimentele bijdragen die je hebt geleverd aan sommige artikelen. Hela, oftewel Hélène, bedankt voor de gezelligheid op onze 'oude' kamer en de fijne samenwerking. Ik zal onze live-cell imaging experimenten in het UMC nooit vergeten. Ik ben er trots op dat dit heeft geresulteerd in twee prachtige artikelen voor ons beiden.

Natuurlijk mag ik de (oud)leden van de "coronavirus replicatie groep" niet vergeten (twee ervan heb ik hierboven al genoemd). Iryna, je bent een top collega om mee samen te werken, alleen jammer dat we nooit zijn toegekomen aan het daadwerkelijke live-cell imagen. Misschien kunnen we dit nog in de laatste maanden na mijn promotie doen? Annelotte, jij ook hartstikke bedankt voor al het harde (pipetteer)werk en gezelligheid. Ik weet zeker dat dit tot een mooie publicatie zal leiden waar we samen als auteurs op zullen staan!

Onze "collaborators" van de afdeling celbiologie van het UMC, Mustafa en Fulvio. Mustafa, hartelijk dank voor alle tijd en moeite die jij hebt gestopt in het maken van de mooie EM plaatjes. Fulvio, onze maandelijkse werkdiscussies waren altijd zeer productief en ik heb hier zeer veel van geleerd.

Monique, Matthijs, Mijke, Martijn, Matthijn en Robbert, ofwel de M-en (en Robbert). Jullie zijn mijn (ex)-AIO collega's waar ik het meest mee ben opgetrokken. Jullie zorgden voor een fantastische sfeer die het plezierig maakte om op het lab te werken en die tijd zal ik de rest van mijn leven niet

meer vergeten. Sommige van jullie zijn uit het onderzoek gegaan, anderen zijn erin gebleven of nog bezig met promoveren, desalniettemin hoop ik dat we elkaar nog regelmatig zullen zien en/of spreken in de toekomst!

Willem, Pepijn en Esther, jullie hebben de Virologie afdeling al verlaten, maar waren er wel toen ik AIO was. Hartstikke bedankt voor alle gezelligheid en hulp zowel binnenin als buiten het lab. We houden contact!

Ik wil ook graag mijn nieuwe kamergenoten/AIO's Christine, Ole en Qiushi bedanken voor de gezelligheid en de vele wetenschappelijke discussies die op kamer 514 worden gevoerd. Christine, heel erg bedankt voor het doorlezen van mijn proefschrift op fouten! Heel veel succes met jullie promotietraject, ik weet zeker dat het succesvol zal zijn en er mooie publicaties uit voort zullen komen!

In mijn promotieonderzoek heb ik veel microscopische technieken gebruikt. Helaas ging dit niet altijd even soepel en had ik af en toe hulp nodig van ervaren microscopisten. Bij deze wil ik dan ook Richard, Esther en Corlinda bedanken voor alle hulp met betrekking tot de microscopie-gerelateerde zaken.

Tijdens de jaren dat ik AIO was heb ik enkele Bachelor en Master studenten mogen begeleiden. Ik wil vooral Arjan, Indra, Marieke en Boaz bedanken voor al het harde en belangrijke pipetteerwerk dat zij tijdens hun stages hebben verzet.

Bij deze wil ik ook alle andere collega's van de afdeling Virologie bedanken. Allereerst de 'oude' rotten van de afdeling: Berend Jan, Raoul, Herman en Erik. Jullie wetenschappelijke input werd zeer gewaardeerd. De 'harde kern' van de afdeling: Nancy en Arno. Beiden zorgen jullie ervoor dat veel zaken draaiende blijven op de afdeling zonder dat veel mensen zich dat eigenlijk realiseren. Marleen, Wen, Alan, Martine, Ivy en Inge Marie. De meeste van onze gesprekken waren in de koffiekamer maar dat maakte ze zeker niet minder gezellig (en belangrijk!). De 'nieuwe aanwinsten': Mandy en Marleen. Ik ken jullie nog maar kort, maar jullie zijn gezellige collega's. Veel succes en plezier op de afdeling.

Tot slot wil ik naast collega's van het werk ook vrienden en familie bedanken. Het hebben van goede vrienden die begrijpen wat het inhoudt om te promoveren (het werken van onregelmatige tijden en het maken van lange dagen) en daar begrip voor tonen is zeer belangrijk. Matthijs, Loek, Joery, Teun en Emiel, bedankt! Menno, jouw vriendschap is heel belangrijk voor mij. Ik ben blij dat mijn beste vriend straks tijdens mijn verdediging achter mij staat als paranimf. Mijn lieve kleine tweelingzusje Xenia. Ik vind het fantastisch dat ook jij mijn paranimf wilt zijn en me zal bijstaan tijdens mijn

verdediging. Mijn grote broer, Rouven. Jij bent geweldig! Altijd sta je voor mij klaar als er wat is, zelfs voor de meest onbenullige dingen. Ik vind het jammer dat ik niet drie paranimfen mag hebben, maar ik ben blij dat je het niet erg vind dat ons zusje deze keer de honneurs waarneemt bij mijn verdediging.

Als allerlaatste wil ik mijn lieve ouders bedanken. Mama en papa, jullie zijn zeer belangrijk in mijn leven. Ik ben jullie enorm dankbaar dat jullie mij alle kansen hebben geboden om dit te bereiken en om te doen wat ik echt leuk vind. Zonder jullie steun en liefde was me dit nooit gelukt. Ik hou van jullie!

Marne Hagemeijer

Utrecht, September 2011

Curriculum Vitae

Marne Casper Hagemeijer werd op 29 juni 1983 geboren te 's-Gravenhage. Het atheneum diploma werd behaald in 2001 aan het Huygens Lyceum te Voorburg. In hetzelfde jaar startte hij met de Bachelor-opleiding Scheikunde aan de Universiteit Utrecht. De propedeuse werd in 2002 behaald en het Bachelor diploma in 2004. Tijdens de Bachelor-opleiding verschoof zijn interesse meer richting de Immunologie en Infectieziekten wat resulteerde in de start van de Master-opleiding "Immunity and Infection". Tijdens deze fase van zijn Universitaire opleiding liep hij allereerst stage bij de afdeling Pathologie in het Universitair Medisch Centrum Utrecht, onder leiding van dr. R.A. de Weger. Deze stage resulteerde in zijn eerste wetenschappelijke artikel "T cells in Cardiac Allograft Vasculopathy Are Skewed to Memory Th-1 Cells in the Presence of a Distinct Th-2 Population", waarvoor hem de "Novartis Transplantation Grant 2009" werd toegekend. Een tweede onderzoekstage werd gelopen bij de afdeling Virologie, Departement Infectieziekten en Immunologie, van de Faculteit Diergeneeskunde aan de Universiteit Utrecht onder leiding van dr. M. Oostra. Begin 2007 werd de Master-opleiding succesvol afgerond en het promotie onderzoek, zoals beschreven in dit proefschrift, gestart onder begeleiding van prof. dr. P.J.M. Rottier en dr. C.A.M. de Haan.

List of Publications

1. **Mobility and interactions of coronavirus nonstructural protein 4.**
   Hagemeijer M.C., Ulasli M., Vonk A.M., Reggiori F., Rottier P.J., de Haan C.A.
   J Virol. 2011 May;85(9):4572-7. Epub 2011 Feb 23.

2. **The coronavirus nucleocapsid protein is dynamically associated with the replication-transcription complexes.**
   Verheije M.H.*, Hagemeijer M.C.*, Ulasli M., Reggiori F., Rottier P.J., Masters P.S., de Haan C.A.
   J Virol. 2010 Nov;84(21):11575-9. Epub 2010 Aug 25.

3. **Dynamics of coronavirus replication-transcription complexes.**
   Hagemeijer M.C.*, Verheije M.H.*, Ulasli M., Shaltiël I.A., de Vries L.A., Reggiori F., Rottier P.J., de Haan C.A.
   J Virol. 2010 Feb;84(4):2134-49. Epub 2009 Dec 9.

4. **Topology and membrane anchoring of the coronavirus replication complex: not all hydrophobic domains of nsp3 and nsp6 are membrane spanning.**
   Oostra M., Hagemeijer M.C., van Gent M., Bekker C.P., te Lintelo E.G., Rottier P.J., de Haan C.A.
   J Virol. 2008 Dec;82(24):12392-405. Epub 2008 Oct 8.

5. **T cells in cardiac allograft vasculopathy are skewed to memory Th-1 cells in the presence of a distinct Th-2 population.**
   Hagemeijer M.C., van Oosterhout M.F., van Wichen D.F., van Kuik J., Siera-de Koning E., Gmelig Meyling F.H., Schipper M.E., de Jonge N., de Weger R.A.
   Am J Transplant. 2008 May;8(5):1040-50.

   * equal contribution